MASS TRANSPORT OF LARGE MOLECULES IN ZEOLITES

A Dissertation Presented

by

FERNÃO DOMINGOS DE MONTENEGRO BAPTISTA MALHEIRO DE MAGALHÃES

Submitted to the Graduate School of the
University of Massachusetts Amherst in partial fulfillment
of the requirements for the degree of

DOCTOR OF PHILOSOPHY

September 1997

Chemical Engineering

MASS TRANSPORT OF LARGE MOLECULES IN ZEOLITES

A Dissertation Presented

by

FERNÃO DOMINGOS DE MONTENEGRO BAPTISTA MALHEIRO DE MAGALHÃES

Approved as to style and content by:

W.C. Conner, Chair

R.L. Laurence, Member

J.L. Ragle, Member

M.F. Doherty, Department Head
Chemical Engineering

ACKNOWLEDGMENTS

I would like to thank both my advisors, Professors Conner and Laurence, for their support and guidance. Curt kept me on track along these years, helping me in giving this work a consistent scientific basis and unified structure. Bob gave me not only priceless research advice, but also an example to follow, as someone remarkable both as a scientist and as a person. It was an enriching experience to work with both of them.

I would also like to thank professor Ragle for accepting become part of the dissertation committee and for his input to this thesis.

Also special thanks to those who were patient enough to be my housemates: Ioannis, Takis and Cesar.

And to all those I've met in these United States of America: thanks for everything and sorry for anything. You turned this Ph.D. into a very enjoyable personal adventure. I wanted to write many names here, but some would have to be left out and I don't like to grade friendships.

And to my good old friends back in Portugal: thanks for having me back.

ABSTRACT

MASS TRANSPORT OF LARGE MOLECULES IN ZEOLITES

SEPTEMBER 1997

FERNÃO DOMINGOS DE MONTENEGRO BAPTISTA MALHEIRO DE MAGALHÃES, LICENCIADO, FACULDADE DE ENGENHARIA DA UNIVERSIDADE DO PORTO

Ph.D., UNIVERSITY OF MASSACHUSETTS AMHERST

Directed by:
Professor William C. Conner and Professor Robert L. Laurence

Mass transport in zeolitic materials has been the object of extensive research in the last several decades. Many ambiguities and unanswered questions still subsist. In order to obtain a more complete understanding of the phenomena involved, we conducted a careful and consistent study of different adsorbate/adsorbent systems.

The work has been approached on three levels, roughly corresponding to three different physical scales.

First, mass transport in a bed of zeolite particles is analyzed. The importance of transport in the bulk-gas phase relative to intra-crystalline diffusion is discussed. A simple heterogeneous transport model is presented in order to illustrate these concerns. The validity of the model was tested in the simulation of a set of ^{129}Xe NMR experiments for the benzene/ZSM-5 system.

In the second part, attention is focused on transport in a single zeolite particle exhibiting a surface resistance. The diffusion of *n*-paraffins in zeolite T is studied. A strategy for separation of the internal and external mass transfer resistance parameters is

developed, based on the temporal moments of the gravimetric sorption data. Both resistances are strongly dependent on zeolite occupancy. The external resistance is the controlling process at low loadings, while at high loadings mass transfer is diffusion-controlled. No evidence was found of the "window effect" reported by Gorring for the intra-crystalline diffusivities in this system.

Finally, intra-crystalline diffusion alone is addressed. A simultaneous thermal analyzer was used to study the diffusion of cyclohexane and several alkyl-cyclohexanes in silicalite. Heats of sorption as well as diffusion coefficients can be estimated from these experiments. Zero length chromatography was also used for some of the adsorbates. The following trend in diffusion rates was observed: *trans*-1,4-dimethylcyclohexane >> methylcyclohexane > cyclohexane > ethylcyclohexane, *cis*-1,4-dimethylcyclohexane. A comprehensive interpretation of the experimental results is presented, using basic qualitative arguments of Transition State Theory. Entropic effects may play a significant role in this system.

TABLE OF CONTENTS

LIST OF TABLES

LIST OF FIGURES

CHAPTER 1

INTRODUCTION

The extraordinary importance of zeolites to modern industry, in areas like selective catalysis or sorptive separation, is undeniable. During the last decades the scientific community has developed a significant effort to study and to clarify several aspects related to these materials: structural characterization, catalyzed reaction kinetics, mass transport, etc. The peculiar characteristics of the zeolitic structures, with near-molecular dimensions of the pores, are the basis for important attributes like shape selectivity. They are also responsible for a special diffusion regime that P. Weisz [1973] coined as *configurational diffusion.* This designation is certainly ambiguous and restrictive, but it recognizes the unique character of the mass transport in these materials.

Many aspects of mass transport in zeolites are not yet completely understood (see, for example, the review by Wei [1994]). The main objective of this work is to attain a better understanding of some of these phenomena. This is achieved by developing theoretical and experimental tools that address the specificity of each problem, always keeping in mind the global coherence and consistence of the study.

Transport in zeolites is unique in many aspects. Some examples: the uniformity of pore sizes, the near molecular dimensions of the pores, the well defined periodicity of the pore network. But it is not only the intra-crystalline diffusion that is addressed in this work. Other transport phenomena often coexist in practical applications, and have a determinant influence on global mass transport. Some of these effects are analyzed, like

the significance of surface barriers or transport through the gas-phase in a bed of zeolite particles.

Different adsorbate/zeolite systems are studied. Attention is focused on "large" adsorbates. This designation is used to describe those molecules that have one or more characteristic dimensions (cross-sectional diameter, chain length, etc.) close to some characteristic dimension of the zeolitic framework (channel or cage diameters, framework periodicity length, etc.).

This dissertation is organized as follows. Chapter 2 reviews some essential concepts and approaches associated with the study of diffusion in zeolites, as well as some of the prior experimental and theoretical work.

The following chapters discuss different aspects of the mass transport problem, starting, in Chapter 3, with the analysis of heterogeneous transport in a bed of zeolite crystallites. The analysis is illustrated by some results of ^{129}Xe NMR experiments performed with the system benzene/Silicalite.

Chapter 4 focuses on transport at a single particle scale, addressing the problem of a "surface barrier" generating a resistance additional to intra-crystalline diffusion. The particular system under study is *n*-paraffins in zeolite T. The original motivation for this study was to re-examine Gorring's results on the "window effect" [Gorring, 1973]. However, the study ended with broader implications.

Finally, in Chapter 5, diffusion in the zeolite framework alone is analyzed, and some of the factors that may affect it are discussed. The experimental work concerned the diffusion of cyclohexane and alkyl-cyclohexanes in Silicalite.

The major conclusions are summarized in Chapter 6.

Appendix A deals in some detail with some applications of Transition State Theory to diffusion in zeolites, as a complement to the simple notions introduced in Chapter 5. Brownian Motion theory, and its application to the description of diffusion in a periodic potential, is described in Appendix B. This is based on the work of Nitsche and Wei [1991], motivated by Gorring's results on the "window effect". The possibility of the DRIFTS technique adding further insights on some of the phenomena analyzed in this work is described in Appendix C. Appendix D focuses on mathematical modeling of transport on chromatographic-type systems, as a possible basis for the theoretical treatment in future work.

CHAPTER 2

BACKGROUND

2.1 Fundamental Concepts

Two distinguishable diffusion phenomena are commonly identified in the literature: transport diffusion and self-diffusion†. Since these designations will be used in the present work, it is important to define clearly both concepts, as well as the diffusion coefficients (experimentally measurable) that characterize them:

- *Transport diffusion* results from the presence of a concentration gradient. A net flux of molecules exists. A formal definition of the transport diffusivity, D, may be given by Fick's First Law (for diffusion of a single species):

$$J = - D \nabla c \tag{2.1}$$

  where J is the diffusant's molar flux relative to the molar-average velocity, c is the concentration and x is the diffusion coordinate. The diffusivity is measured by macroscopic methods.

- *Self-diffusion* is originates from Brownian molecular motion in the absence of a concentration gradient. There is no net flux since the system is under

---

† The specific terms "transport" and "self" diffusion are generally employed by the research groups associated to Kärger and Ruthven. Other researchers may designate the same phenomena in other ways (*c.f.* Riekert, 1970; Kärger and Ruthven, 1989, 1992; Tsikoyannis and Wei, 1990a; Krishna, 1990).

equilibrium conditions. The diffusivity is measured either by measuring the migration rate of a tagged fraction of the diffusing molecules or by determining the mean square displacement associated to the trajectories of a large number of diffusing molecules. The self-diffusivity, D^*, can then be defined in two equivalent ways:

$$J^* = - D^* \nabla c^* \tag{2.2}$$

(c^* is the concentration of tagged molecules) or, from random walk theory for one dimensional diffusion:

$$\langle z^2(t) \rangle = 2D^* t \tag{2.3}$$

where $\langle z^2(t) \rangle$ is the mean square displacement.

The molar fluxes J, J^* and the diffusion coefficients D, D^* are only completely defined after a unambiguous *frame of reference* is established. The molar flux (relative to fixed coordinates) of component j in a n-component mixture is traditionally defined as (see [Bird, Stewart and Lightfoot, 1960]):

$$N_j = J_j + x_j \sum_i^n N_i \tag{2.4}$$

where J_j is the diffusional flux of component j relative to the molar bulk flow and $x_j \sum_i^n N_i$ is the flux associated to the bulk motion of the fluid. As noted by Krishna [1990], in the particular case of surface diffusion (or, more generally, diffusion in a microporous solid) where the diffusing molecules occupy fixed sites in the solid's structure, one obtains:

$$N_j = J_j + x_j \sum_i^{n+1} N_i \qquad \text{sorbed species: } 1,\ldots,n \quad \text{vacancy: } n+1 \tag{2.5}$$

This way our system will always correspond to *equimolar counter-diffusion,* $\sum_{i}^{n+1} N_i = 0$, since the "vacancy flux" balances the fluxes of the sorbed species. Thus, for transport diffusion of one single species A, one obtains $N_A = -N_{vac}$ and thus:

$$N_A = J_A + x_A (N_A + N_{vac}) = J_A \tag{2.6}$$

where J_A is given by Equation 2.1. In self-diffusion one can further notice that $N_A + N_A^* = 0$ and $N_{vac} = 0$. Thus:

$$N_A^* = J_A^* + x_A^* (N_A^* + N_A^* + N_{vac}) = J_A^* \tag{2.7}$$

and J_A^* is given by Equation 2.2. One therefore concludes that the molar fluxes J_A and J_A^* are always relative to fixed coordinates (associated with the solid lattice). Of course that this approach is only strictly valid when there is a "one to one" correspondence between molecules and vacancies. The consistency of the treatment, must be maintained when a molecule adsorbs on more than one site in the solid framework and undergoes segmental motion (this might be the case of a linear alkane, for instance). In this case the "vacancy" must be defined as the total number of adsorption sites occupied by the molecule and the diffusion coefficient is related to the motion of the molecular center of mass.

2.2 Kinetic Theory

More than half a century ago Barrer [1941], developed the first kinetic model for zeolitic diffusion, which he approached as a variant of atomic diffusion in solids. The zeolite crystals, he says, "have channels in the lattice which are sufficiently wide for ions or neutral molecules to diffuse through the structure". In his cubic lattice model

each atom moves a distance d (mean free path) in one of the 6 possible directions when diffusing. This jump can occur only if the atom, with a vibration frequency in the lattice of ν, acquires the necessary energy, E. The final expression obtained for the diffusion coefficient† in Fick's law is:

$$D = d^2 \frac{1}{6}(1-\theta) \frac{1}{(f-1)!} \left(\frac{E}{RT}\right)^{f-1} \nu_0 \exp\left(-\frac{E}{RT}\right) \qquad (2.8)$$

Based on the empirical reasoning that an atom can only jump in a particular direction if the neighboring site is not occupied, the factor $(1-\theta)$ (fraction of vacant sites) was introduced as a correction for D. f is the number of degrees of freedom that contribute to the accumulation of activation energy.

Riekert [1970, 1971] developed a more consistent approach based on simple arguments. He tried to describe the dependence of self and transport diffusivities on lattice occupancy. Consider two planes perpendicular to the direction of diffusion (x) with area A and at a distance δ from each other. One is concerned with transport diffusion of a single species. There are n_1 particles on plane 1 and n_2 in plane 2. the total number of sites in each plane is m. A particle can only jump from a site in plane 1 to a neighboring site in plane 2 if this is unoccupied. This way the average frequency of *successful* jumps will be proportional to $\nu(1-n_2/m)$, where ν is the jumping frequency. The net flow rate from plane 1 into plane 2 is then given by:

---

† In this section, as well as in most of this work, if not stated otherwise, we refer to the transport diffusivity measured by uptake rate experiments as simply diffusion coefficient or diffusivity.

$$\dot{n} = n_1 \nu \left(1 - \frac{n_2}{m}\right) - n_2 \nu \left(1 - \frac{n_1}{m}\right) = \nu (n_1 - n_2) \tag{2.9}$$

and the flux is:

$$J = \frac{\dot{n}}{A} = \nu \delta^2 \frac{n_1 - n_2}{\delta^2 A} = - \nu \delta^2 \frac{dc}{dx} \tag{2.10}$$

Note that, since this work deals with diffusion of a single species, the subscripts in the variables N, J , D or c are usually omited.

By comparison with Fick's law, one obtains for the transport diffusion coefficient:

$$D = \nu \delta^2 \tag{2.11}$$

The analysis of self-diffusion is, however, slightly different. Since there is no total concentration gradient, the occupancy is the same on both planes, 1 and 2. Thus:

$$\dot{n} = n_1^* \nu (1 - \theta) - n_2^* \nu (1 - \theta) = \nu (1 - \theta) (n_1 - n_2) \tag{2.12}$$

where n_1^* is the number of labeled particles in plane 1 and θ is the occupancy. Now the flux is given by:

$$J = \frac{\dot{n}^*}{A} = - \nu (1 - \theta) \delta^2 \frac{dc^*}{dx} \tag{2.13}$$

and the self-diffusion coefficient is dependent on the total occupancy:

$$D^* = \nu (1 - \theta) \delta^2 \tag{2.14}$$

Barrer and Jost [1949] proposed a correction for the Fickian transport diffusivity based in the concept that the true driving force for diffusion is the gradient of chemical potential instead of concentration. Some minor refinements were later introduced by Ash and Barrer [1967]. The molar flux, J. is given by:

$$J = - Bc \frac{\partial \mu}{\partial x} \tag{2.15}$$

where μ is the chemical potential of the diffusing species and $Bc = L$ is the phenomenological coefficient of irreversible thermodynamics. B is the intrinsic mobility of the species. Assuming ideal vapor phase, 2.2 can be rewritten as:

$$J = - BRT \frac{d\ln(a)}{d\ln(c)} \frac{\partial c}{\partial x} = - BRT \frac{d\ln(p)}{d\ln(c)} \frac{\partial c}{\partial x} \tag{2.16}$$

where a is the activity of the adsorbed species and p the partial pressure in the bulk gas phase. Thus, the Fickian diffusivity, D, is given by:

$$D(c) = BRT \frac{d\ln(p)}{d\ln(c)} = D_{corr} \frac{d\ln(p)}{d\ln(c)} \tag{2.17}$$

$D_{corr} = BRT$ is the *"corrected" diffusivity*. Relationship 2.17 is actually the *Darken equation*, originally derived for interdiffusion of two alloys. If under the operating conditions the Henry's law is obeyed then p is directly proportional to c and $D = D_{corr}$. More consideration of the practical importance of the Darken equation will be given in the next section.

Krishna [1990], in a very consistent approach, identified the corrected diffusivity in Equation 2.17, D_{corr}, with the "Stefan-Maxwell diffusivity". The Stefan-Maxwell equations for a mixture of n species diffusing in a microporous solid can be written as:

$$\frac{c_i}{RT}\ \mathrm{grad}(\mu_i)_{T,P} = \sum_{j=1}^{n+1} \frac{c_i\ N_j - c_j\ N_i}{c_t\ \mathbb{D}_{ij}} \tag{2.18}$$

where θ_i is the fractional coverage of component I, c_t is the total concentration of adsorbed species and $\mathbb{D}_{ij}$ is the Stefan-Maxwell diffusivity for binary counter diffusion of the pair i-j. The vacant sites are assumed as the $(n+1)^{th}$ component (see previous section). The left hand side of the previous equation can be rewritten in terms of the gradients of the fractional coverage:

$$\frac{c_i}{RT}\ \mathrm{grad}(\mu_i)_{T,P} = c_i \sum_{j=1}^{n} \frac{\partial \mu_i}{\partial c_j} \frac{dc_j}{dx} = c_i \sum_{j=1}^{n} \frac{1}{c_j} \frac{\partial \ln(p_i)}{\partial \ln(c_j)} \frac{dc_j}{dx} \tag{2.19}$$

where once again the gas mixture was assumed ideal. In the case of diffusion of a single species (A) we get from Equations 2.18 and 2.19:

$$N_A = J_A = -\ \mathbb{D}_{Av} \frac{\partial \ln(p_A)}{\partial \ln(c_A)} \frac{dc_A}{dx} \tag{2.20}$$

$\mathbb{D}_{Av}$ is the coefficient of counter-diffusion for the pair species A - vacancy. The author refers the possibility of $\mathbb{D}_{Av}$ having a weak dependence on the occupancy. He suggests that this can be described by the Vignes relation:

$$\mathbb{D}_{Av} = (\mathbb{D}^{0}_{Av})^{1-\theta_A}\ (\mathbb{D}^{1}_{Av})^{\theta_A} \tag{2.21}$$

where $\mathbb{D}^{0}_{Av}$ and $\mathbb{D}^{1}_{Av}$ are the coefficients at zero and full coverage, repectivelly.

Palekar and Rajadhyaksha [1985] used a Monte-Carlo approach to simulate one and two component diffusion in a model of parallel and non-intersecting channels with uniformly distributed sites. The adsorbed molecules (maximum one per site) are

activated ν times per second to overcome the potential barrier imposed to the transport process (jump between adjacent sites). Molecules cannot pass each other during the jumps. An extension of the previous analysis to a two-dimensional model was made by Aust et al. [1989]. They considered different situations in the simulation: variable number of molecules per site; the molecules can/cannot pass each other between sites; variable number of molecules that may leave the site at one time; the molecules have/do not have to leave the site if the first jump attempt is unsuccessful.

Wei and co-workers [Theodorou and Wei, 1983; Qureshi and Wei, 1990; Tsikoyiannis and Wei, 1991a] applied the theory of Markov pure jump processes in the modeling of zeolitic diffusion. They made the following assumptions for the transport mechanism:

- the movement of molecules takes place by a series of activated jumps between adjacent sites;
- each jump event is generated by an independent Poisson process;
- if the neighboring site randomly selected for the jump destination is already occupied, then the molecule remains where it is and another molecule is selected.

The Markovian formalism allows the consideration of bombardment of the lattice by gas molecules, diffusive motion and unimolecular reaction as a sequence of events that are continuous in time, but discrete in space. Tsikoyiannis and Wei showed that the model follows a Langmuir type isotherm and a Fickian law for diffusional transport. The introduction of weak interparticle interactions (attractive or repulsive) changed the occupancy dependence of diffusivity (see next section).

In recent work, Xiao and Wei [1992a] proposed an interesting modification, giving particular importance to the modeling of the molecule-zeolite and molecule-

molecule interactions. Their approach takes into account the recent concepts of molecular behavior inside zeolites based on experimental observations:

a) In ZSM-5 bulky molecules (aromatics, branched paraffins) are located at the channel intersections, while smaller molecules stay in the channels.

b) Nonpolar molecules rotate as freely as if in a liquid phase when above room temperature. At very low temperatures the freedom of rotation decreases as the molecules become more attached to the surface.

c) Polar molecules, with specific interactions with the sites (water, alcohol), are strongly adsorbed in the sites, and vibrate with the lattice.

d) Molecule-lattice interactions are the dominant factor at low concentrations. At high concentrations the molecule-molecule interactions become important.

The molecular transport in zeolites at low occupancy is then considered to be bounded by two extreme cases (in terms of molecule-zeolite interactions), described by the following two models:

Gas translation model: the molecule-zeolite interactions are weak. The molecules retain their gaseous characteristics but the movement between "sites" (in this case "equilibrium positions" would be more appropriate term) is restricted by the energy barrier imposed by the zeolite's physical structure. The potential field is represented by a flat bottom well.

Solid vibration model: the zeolite framework interacts strongly with the molecules, making them lose their gaseous identity. The molecules vibrate with the host lattice before accumulating enough energy to jump to a neighboring site. The potential field is that of a harmonic oscillator.

2.3 Concentration dependence

Several researchers have observed and attempted to explain different dependences of zeolitic diffusivities on sorbate concentration. Xiao and Wei [1992b] identified four types of characteristic behavior in works previously published:

Type I: the apparent diffusivity, D, increases monotonically with increasing concentration, c.

Type II: D is independent of c.

Type III: D decreases monotonically with c.

Type IV: D decreases and then increases with c.

Ruthven and Lee [1981] pointed out that some observations considered of type III and IV may actually reflect transport controlled by heat transfer and diffusion in the bed.

Riekert [1970, 1971] derived a single-component diffusion coefficient independent of occupancy (see Equation 2.11). He suggested, however, that an alternative model containing different types of sites would give rise to a concentration dependence of the diffusivity. In one simple case, the lattice is assumed to consist of sites "type A" with pockets of sites "type B". Migration between pockets is not possible. Molecules move via type A sites, and are locally distributed between type A and B sites. If the migration along A sites is rate-determining, then an equilibrium between molecules adsorbed in the two sites is established and the following relationship can be derived:

$$D(c) = D_{A0} \frac{dc_A}{dc} \tag{2.22}$$

where c_A is the concentration of molecules in A sites, c is the total concentration and D_A is the diffusivity based on the gradient of c_A. Since the sites may have different adsorption characteristics, $\frac{dc_A}{dc}$, and thus D(c) may increase or decrease with total concentration.

Kutner [1981] also obtained theoretically a diffusion coefficient independent on occupancy, for a lattice gas of non-interacting particles. He added a qualitative argument to this result. Assuming a local concentration gradient in the lattice, there will be two opposing fluxes: from the more dense to the less dense region and the opposite. The net flux is the difference. At greater occupancies the particles will be hindered in their motion by the surrounding particles, resulting in smaller fluxes. However, both fluxes are reduced equally, and thus the net result remains unchanged.

The diffusivity correction mentioned previously (Darken equation 2.17) has been used to correlate experimental data with relative success, giving a corrected diffusivity, D_{corr}, that is essentially concentration-independent. Such is the case of the results of Ruthven and co-workers [Ruthven and Loughlin, 1971a, 1971b; Ruthven et al., 1973; Yucel and Ruthven, 1980; Karger and Ruthven, 1981; Ruthven et al., 1982; Kumar et al., 1982; Ruthven, 1992] and by other researchers (see [Ruthven, 1984a] for a review of previous works; [Shah et al., 1988]; [Tsikoyiannis and Wei, 1991b]). Systems in which D_{corr} is still concentration dependent have also been reported [Choudary, 1986]. According to Ash and Barrer's approach (see Section 2.2), since $D_{corr} = BRT$ and the mobility, B, is, in principle, concentration-dependent, one may expect that D_{corr} will not be constant, in particular at higher concentrations [Ruthven, 1984b]. This dependence must, however, be small compared to the correction factor $\frac{d\ln(p)}{d\ln(c)}$. This derivative is

determined from the adsorption isotherm. For a Langmuir type isotherm Equation 2.17 will give:

$$D(\theta) = \frac{D_{corr}}{1-\theta} \qquad \text{with } \theta = \frac{c}{c_{sat}} \tag{2.23}$$

which implies an increase of the apparent diffusivity with concentration.

Ruthven and Loughlin [1971] proposed the use of an isotherm derived from the Dubinin-Polanyi theory, valid in the vicinity of saturation:

$$\theta = 1 - (\alpha\, \Delta G)^2 \tag{2.24}$$

where:

$$\Delta G = RT \ln\left(\frac{p}{p_{sat}}\right) = \text{adsorption potential} \tag{2.25}$$

In this case 2.17 gives:

$$D(\theta) = \frac{D_{corr}}{2RT\alpha} \frac{\theta}{\sqrt{1-\theta}} \tag{2.26}$$

Barrer [1971] derived expressions for $D(\theta)$ for other types of isotherms.

Notice that, as pointed out by Xiao and Wei [1992a], the Darken equation 2.17 is based only on conceptual formalisms of irreversible thermodynamics, and does not involve a detailed description of the diffusion mechanism. These authors contend that this equation should be considered only as a correlation tool for experimental data without any predictive value.

The Monte-Carlo simulations of Palekar and Rajadhyaksha [1985] showed a concentration dependence of the diffusion coefficient consistent with Equation 2.23. The subsequent work of Aust et al. [1989] considered several scenarios for the Monte Carlo simulations:

a) Varying the maximum number of particles per cage:

- for a maximum of one particle per cage the following relationship was found:

$$D(c) = D_{corr} \exp(k\,\theta) \tag{2.27}$$

- for two molecules the relationship had the form:

$$D(c) = \frac{D_{corr}}{(1-\theta)^{k'}} \tag{2.28}$$

- no simple relationship was found for more than two molecules per cage.

b) Particles can pass each other in a "window" (channel between sites):

- with up to three particles per cage the following expression seems to be accurate:

$$D(c) = \frac{\alpha}{1-\theta} \tag{2.29}$$

c) More than one particle may leave the cage at a time:

- A relationship of the form of Equation 2.29 seems to apply, but the results show a large scattering.

d) Particles need not leave the cage in a single step (i.e., a particle stays in its present site if the first jump attempt is unsuccessful, even if other free jump directions are available):

- D(c) almost does not depend on occupancy.

Notice that when the computed values of D(c) were corrected using Equation 2.29, a trend of decreasing diffusivity with increasing occupancy was observed in all the cases.

Tsikoyiannis and Wei [1991a] developed a model that put some emphasis on the importance of interparticle interactions. When these were absent, their model predicted a concentration-independent diffusivity. The situation changed when soft nearest neighbor interactions were considered. Attractive interactions resulted in an increase in the diffusivity with occupancy and the converse with repulsive interactions. This result is counterintuitive. It implies that at higher fixed occupancy the diffusivity increases as we add attractive molecular interactions to the system. The opposite should be expected, since the attraction forces must partly inhibit the molecular tendency to leave denser regions, while in the areas of lower density the molecular random walks are more or less unperturbed. We consider that this situation is due to a misconception in the formulation of the model. A brief discussion of this problem follows.

These authors defined the potential energy profile of a particle in the lattice without interactions (besides the hard interactions due to exclusion of double occupancy) in the following way:

1) The energy of the particle is infinite when it is located at an already occupied site (exclusion of double occupancy).

2) The energy of the particle located at an empty site is Φ_S (independent of the environment).

3) The energy of the particle at the transition region between two sites (at the height of the potential barrier) is Φ_T (also independent of the environment).

The activation energy for diffusion is then $E_a = \Phi_T - \Phi_S$ ($\Phi_T > \Phi_S > 0$).

For the lattice with both hard and soft interactions:

1) Same as (1) above.

2) The energy of the particle located at an empty site depends on the local environment and is $\Phi_S + n\,\Phi_{SS}$, where n is the number of neighboring adsorbed particles and Φ_{SS} is the interaction energy. $\Phi_{SS} < 0$ (> 0) for attractive (repulsive) interactions.

3) The energy of the particle at the transition region between two sites is $\Phi_T + n\,\Phi_{TS}$, where Φ_{TS} is the interaction energy between two particle, one located at a site and the other at the transition region. $\Phi_{TS} < 0$ (> 0) for attractive (repulsive) interactions.

E_a will now depend also on the local environment. The jumping rate of a molecule from site i to site i+1 is proportional to $\exp(-E_a/kT)$. Let us analyze the two possible local configurations for an one-dimensional lattice (assume *attractive* interactions) shown in Figure 2.1.

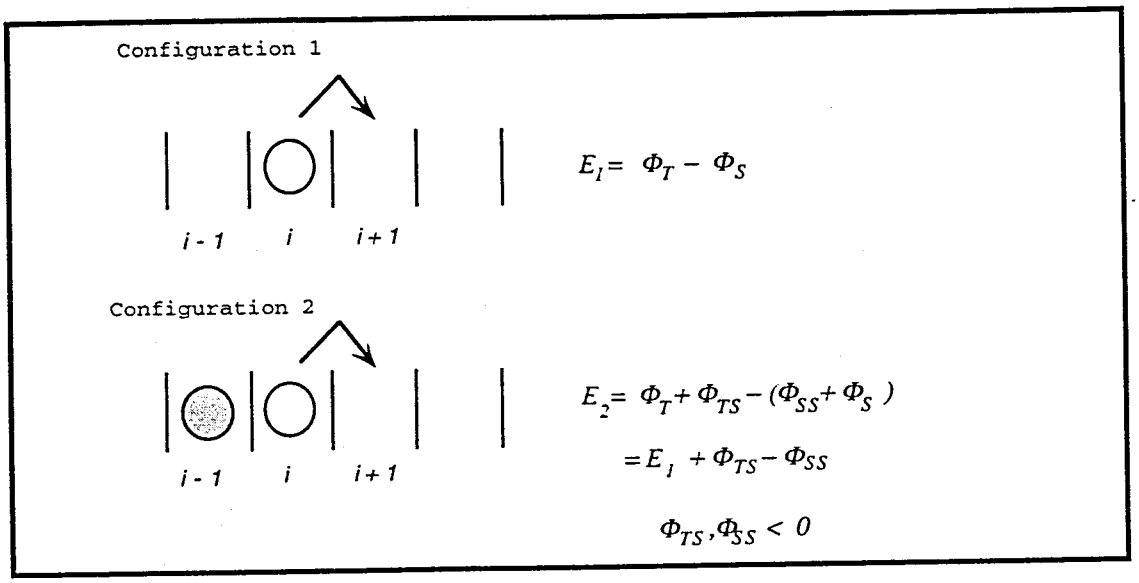

Figure 2.1 Activated jump configurations from the model by Tsikoyiannis and Wei.

The model assumes that the energy of the molecule in the transition region is reduced by Φ_{TS} when another molecule is in a neighboring site, independently of its relative location. This way, depending on the relative value of Φ_{TS} and Φ_{SS}, the activation energy for configuration 2, E_2, may be higher or lower than the one for configuration 1, E_1. In other words, the test particle in site i may actually have a higher probability to leave the site in configuration 2 if $|\Phi_{TS}| > |\Phi_{SS}|$, even though it is subjected to the attractive action of the particle in site i-1. As a consequence of this, the increase of the diffusivity with occupancy is erroneously attributed to attractive interactions with $|\Phi_{TS}| > |\Phi_{SS}|$. Indeed, when using the model to describe experimental results for diffusion of benzene, toluene and p-xylene in HZSM-5 [Tsykoyiannis and Wei, 1991b] the best fit was obtained for $\Phi_{TS} < 0$ and $\Phi_{SS} = 0$! The error lies in the fact that the transition state between i and i+1 is being assumed to possess lower potential energy when there is a neighboring particle either in i-1 or i+2. The position of

the neighboring particle in relation to the direction of the jump should have been considered in the analysis.

A more consistent approach was given by Xiao and Wei [1992a]. They used the same mathematical tools for the development of the lattice model but the molecular interactions are described in a different way. The hard sphere repulsion, which excluded double occupancy, is substituted by a repulsive interaction between molecules located at the same site. This implies that the molecule's activation energy decreases ΔE if another molecule is present in the site. Notice, however, that interactions between molecules at different sites are assumed negligible. An expression for the dependence of the apparent diffusion coefficient on occupancy was derived:

$$D(\theta) = D_{corr}\, e^{\theta(2)w}\left[1 + w\theta(1 - \theta)\frac{\partial\theta(2)}{\partial\theta}\right] \tag{2.30}$$

where $\theta(2)$ is the probability of finding two and only two molecules at a site, which is related to the total occupancy, θ, and the parameter w, the nondimensionalized energy change due to molecular interactions ($w = \Delta E/RT$) by:

$$\theta(2) = \frac{\sqrt{[1 - 2\theta(1 - e^{-w})]^2 + 4e^{-w}(1 - e^{-w})\theta^2} - [1 - 2\theta(1 - e^{-w})]}{2(1 - e^{-w})} \tag{2.31}$$

Note that now $\theta = 1$ corresponds adsorption of two molecules in all available sites. Equation 2.31 implies an increase of $D(\theta)$ with θ when the soft interactions are considered ($w > 0$). This effect becomes more accentuated as w increases. An expression for the adsorption isotherm was also derived:

$$\frac{p}{\nu} = \frac{e^{\theta(2)w}\,\theta}{1-\theta} \tag{2.32}$$

where p is the bombardment rate from the gas phase into the lattice (proportional to the gas pressure) and ν is the jump frequency. From this the Langmuir parameter, K, can be obtained:

$$K = \frac{\theta}{p(1-\theta)} = \nu^{-1}\, e^{-\theta(2)w} \tag{2.33}$$

K is then seen to decrease with θ at high occupancy. This happens with a sharp change of slope around $\theta = 0.5$, suggesting a "phase transition" from a single-occupancy to a double-occupancy distribution in the lattice.

Xiao and Wei [1992b] applied their model to the diffusion of benzene in ZSM-5 as follows: At occupancies lower than 4 molecules/unit cell there will be one or less molecules of benzene per cage. Interactions between molecules in adjacent cages are negligible due the relative long length of the channels between them. At higher concentrations molecules would start to reside also at the channels (double occupancy at the cage is prohibited due to strong intermolecular repulsions). The resulting soft repulsions between nearby molecules give rise to an increase of the molecular potential and a consequent decrease of the activation energy. Note that the proposed locations of the benzene molecule in the zeolitic framework are in agreement with the reported by Mentzen, based on the analysis of X-ray diffraction and calorimetric data [Mentzen, 1987; Sacerdote, Bosselet and Mentzen, 1990].

The model was also applied to diffusion of heptane in zeolite 5A, but now double occupancy in the cage was allowed due to its large size. The model seems to

describe the experimental data with some discrepancy, but the general trends are reasonably predicted. We observed that Darken equation seems to give a better fit for the experimental results than Equation 2.31 specially at high occupancy (Figure 2.2). As noted by the authors, the exclusion of the interactions between molecules at different sites and the effect of the molecule-molecule interactions on the molecule-site interactions from the model's formulation might be critical at high concentrations.

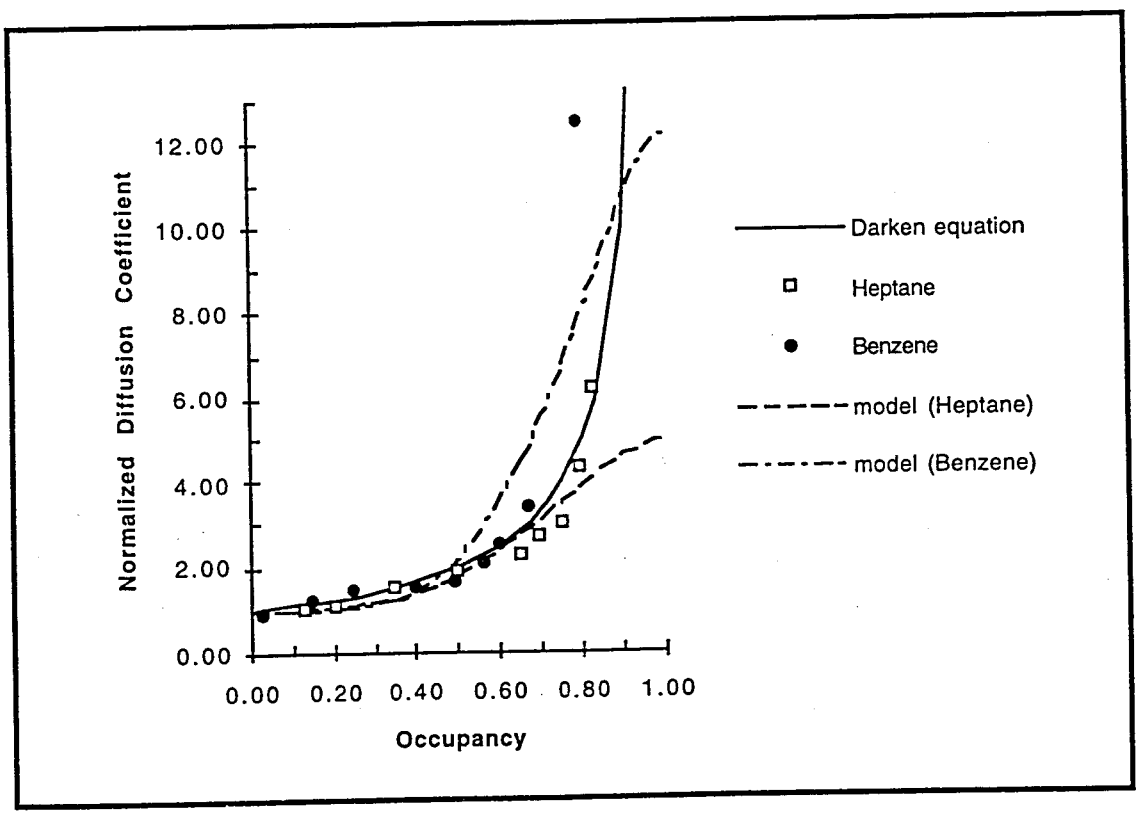

Figure 2.2 Experimental and theoretical results obtained by Xiao and Wei [1992b] for diffusion of heptane in 5A and benzene in ZSM-5.

2.4 Activation Energies and Molecular Size/Geometry Effects

Zeolitic diffusion is an activated process and the temperature dependence may be correlated by an Eyring type equation:

$$D_{corr} = D_0 e^{-E/RT} \tag{2.34}$$

where D_{corr} is the corrected diffusivity and D_0 is the pre-exponential factor and E the activation energy. The values of E are generally different from the enthalpies of desorption [Riekert, 1970], indicating that the molecular transport between sites involves a transition state that is not equivalent to a free gas state. The pre-exponential factor is usually assumed to be proportional to a vibration frequency and the squared distance between adjacent sites [Riekert, 1970; Barrer, 1971; Chihara et al., 1978].

It is intuitive that the activation energy will depend strongly on the ratio between the dimensions of the molecules and the zeolitic channels. Ruthven [1984b] reports an increase of E with the van der Waals radius of several n-paraffins (C_2 to C_{10}) in 4A and 5A zeolites. He recognizes, however, that other parameters, such as the molecular shape must also be considered, since long linear molecules, like linear paraffins, may diffuse through the lattice more easily than shorter but bulkier molecules, like isobutane or cyclohexane.

Paravar and Hayhurst [1983] determined the activation energies of *n*-butane and *i*-butane in Silicalite: 3.3 and 5.6 Kcal/mol respectively. *N*-butane had the highest diffusivity. The kinetic diameter of the first molecule is 4.3 Å while for the second is 5.0 Å, much closer to the Silicalite's pore diameter (5.2 to 5.8 Å). Paravar (referred by Ruthven, 1984a) observed a decrease of diffusivity with chain length for diffusion of *n*-alkanes (C_2 to C_5).

Nayak and Moffat [1987] measured the diffusivities of several aromatic hydrocarbons (benzene, toluene, xylene, mesitylene and *m*-diethylbenzene) on three heteropoly oxometalates. They report a decrease of diffusivity with increasing size and molecular weight. They also analyzed the diffusion of some *n*-alcohols (C_2 to C_6) in heteropoly oxometalates and ZSM-5 [Nayak and Moffat, 1988]. Once again the diffusivity decreased with chain-length.

Chon and Park [1988] found an almost linear increase of the activation energy with increasing chain length of monosubstituted *n*-alkylcyclohexanes. The diffusion coefficients, however, showed a more complex trend, which will be analyzed in detail in Chapter 5.

Xiao and Wei [1992a; 1992b] developed a simple model for the estimation of activation energies. In essence the activation energy is assumed to be the difference between the potentials of the molecule at the channel and at the cage. The potentials are computed as the sum of Lennard-Jones potentials corresponding to the interactions between the molecule and the framework atoms. In the cage, the molecule is modeled as a sphere in a concentric sphere (the cage). In the channel, the molecule is described as a circle in a concentric circle. The diameter of the molecular circle is given by the molecule's minimum cross-sectional diameter. Even though this is a very simplified model, the results are in general agreement with the experimental evidence.

In order to explain qualitatively the importance of configuration and flexibility relatively to size effects in sorption/diffusion of bulky molecules, Choudhary and co-workers [1989; 1990; 1992] proposed the *"shuttlecock-shuttlebox" model.* The penetration and diffusion of a molecule in the zeolite pore structure is compared to the insertion and movement of a shuttlecock in a shuttlebox. A bulky molecule will be able to penetrate into the channel only when it has an orientation in which its compression to

the size of the channel is relatively easy. Thus the probability of penetration is proportional to the product between the probabilities of assuming the most favorable configuration(s) among all the possible ones and of possessing the necessary minimum energy for complete penetration. This translates in a mass transfer resistance at the zeolite crystal surface. Once inside, the molecule will diffuse only in the direction that offers less resistance to the movement of the compressed groups. Reorientation may occur if the zeolite possesses cages larger in diameter than the channels, allowing for free molecular rotation. The authors used the model to predict the relative penetrability and diffusivity of several different sorbates in ZSM-5 and Silicalites. The results are in good agreement with the experimental observations.

Derouane and co-workers [1987a; 1987b; 1988a; 1988b] studied the surface curvature effects on the interactions between diffusing molecule and the zeolitic framework. They introduced the curious concepts of *floating molecule* and *creep diffusion*. They note that a molecule inside a cylindrical pore will always assume a lower potential (higher stabilization) in a position close to the walls unless the molecular dimensions closely match those of the channel and then the molecule will have its equilibrium position at the center of the pore (floating molecule). The smaller molecules are assumed to diffuse in a "hopping" process, moving from the wall to the center of the pore and then to another site at the wall. In this they have to overcome the "sticking" force that attracts them to the wall. The "floating molecule", however, moves through the pore without "hopping". This implies a higher mobility (*supermobility*) of the molecule inside the zeolite. There is no experimental evidence of this supermobility effect [Vigné-Maeder and Amrani, 1993]. The diffusion of chain molecules is described as a crawling motion originated by the movement of chain segments while the whole molecule sticks to the wall (*creeping motion*). It is interesting to note the possibility of

drawing a parallel with the "reptation" theory for diffusion of polymeric chains [de Gennes, 1979].

Recently Garcia and Weisz [1990: 1993] proposed a simplified mechanistic model for diffusion in zeolites with interesting implications in terms of the significance of the experimentally estimated activation energies. They argue that, at any one time, only a fraction of the molecules inside the zeolite participates in the stochastic motion process. This is not analogous to the two phase adsorption mechanism for macroporous solids (gaseous - moving - and adsorbed - stationary - phases). Their theoretical development is presented next, in a somewhat modified formulation, in order to improve clarity and conciseness.

The concentration of molecules in the moving and immobilized phases, in a certain location inside the zeolite, are given by c_m and c_i respectively. The two species are assumed to be in dynamic equilibrium:

$$c_i = K_{im}\, c_m \tag{2.35}$$

For this system, Fick's second law must be written as:

$$\frac{\partial(c_m+c_i)}{\partial t} = \frac{\partial}{\partial x}\left(D_m \frac{\partial c_m}{\partial x}\right) \tag{2.36}$$

or, if D_m can be assumed constant in the operation interval:

$$\frac{\partial(c_m+c_i)}{\partial t} = D_m \frac{\partial^2 c_m}{\partial x^2} \tag{2.37}$$

This equation can be rewritten as:

$$\frac{\partial c_m}{\partial t} = \frac{D_m}{1+K_{im}} \frac{\partial^2 c_m}{\partial x^2} \tag{2.38}$$

Note that $1/(1+K_{im})$ corresponds to the ratio "h/m" in the original paper [Garcia and Weisz, 1990]. Equation 2.38 implies then that the diffusivity measured by a transient method, like gravimetric uptake or chromatography, is actually an apparent diffusivity, related to the real stochastic parameter by:

$$D_{app} = \frac{D_m}{1+K_{im}} \tag{2.39}$$

D_{app} and D_m will coincide only when $K_{im} \rightarrow 0$ ($C_i \rightarrow 0$). An important consequence is that D_{app} will show an "activation energy" that is different from the "true" activation energy associated with D_m:

$$E_{a,app} = E_a + |\Delta H_{im}| \tag{2.40}$$

where ΔH_{im} is the enthalpic energy difference between the immobilized and mobile states. This value being significant, the computed $E_{a,app}$ would be larger than the true value.

Using a frequency response technique, Rees and co-workers [Shen et al., 1990; Shen and Rees, 1991] found evidence of an interesting phenomena in the diffusion of C_4 hydrocarbons in Silicalite. The transient sorption of 2-butyne could not be described in terms of a single diffusion coefficient, contrary to *n*-butane. The authors suggested that 2-butyne (a stiff molecule) goes through a slow molecular reorientation process after sorption, in order to achieve a denser packing of the adsorbed phase. This process is faster for the more flexible molecule of *n*-butane, and thus only the diffusion-controlled sorption is detected.

2.5 Window Effect

The designation "window effect" was introduced by Gorring [1973] to describe a peculiar dependence of the measured uptake diffusion coefficient on the chain length of linear paraffins in zeolite T. Gorring's results were never reproduced by other researchers and there is no report of a similar effect occurring in other systems. A short description of this effect and its interpretations (either by Gorring or others) is presented next.

Gorring's measurements (shown in Figures 2.3 and 2.4) demonstrate that the diffusivities of n-paraffins have a minimum value for *n*-octane, followed by a maximum for dodecane, the difference between the two extrema being of two orders of magnitude. In his explanation of this phenomenon, Gorring first recognized that diffusion in zeolite T (an intergrowth of offretite and erionite regions) is controlled by the small channels in the erionite regions (Figure 2.5). After analysis of the chain length of the paraffins and some geometric considerations, he concluded that molecules smaller than *n*-octane fit entirely inside erionite's cages. Inside the cage, the molecule resides in a deep potential well (the narrow eight membered rings - "windows" - that connect the cages give rise to a significant repulsion to the chain movement). The diffusivity decrease between C_3 and C_8 was attributed to molecular weight effects. Larger molecules, however, do not fit inside the cage, and have to extend through the eight membered rings. Therefore, they are not 'trapped' in the cage's potential well, and must have a larger diffusivity. The fraction of the molecular length located outside the cage increases between C_9 and C_{12}. This would explain the diffusivity increase in this interval. C_{12} extends entirely through a unit cell, between the extremes of the eight membered rings. One may then think that dodecane corresponds to a critical point and molecular weight and steric effects may take over for larger molecules.

Gorring also noted that the observed diffusivity dependence on the chain length can be used to justify the unexpected product distribution obtained from the catalytic cracking of n-C_{23} over H-erionite reported by Chen and co-workers [Chen et al., 1969].

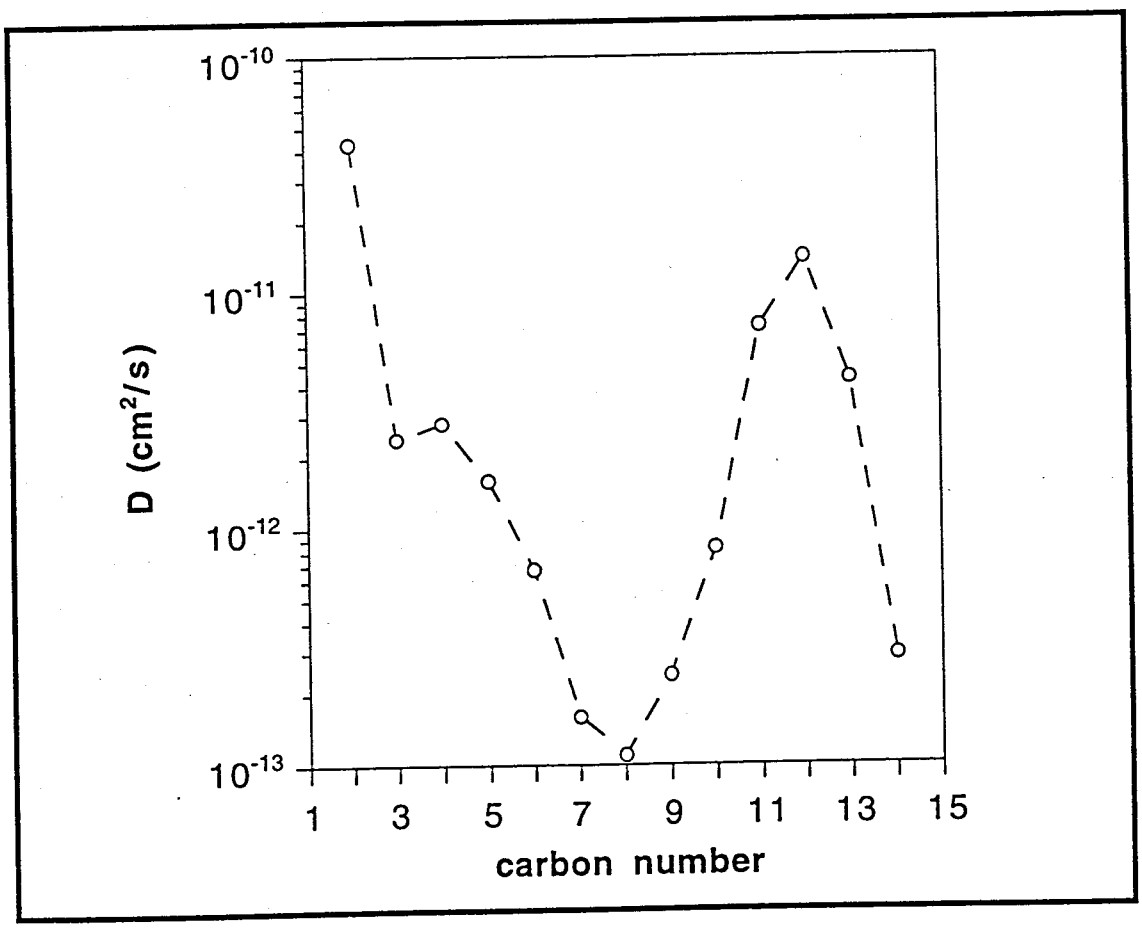

Figure 2.3 Diffusivities of n-paraffins in zeolite T at 300°C as a function of the molecule's carbon number [Gorring, 1973].

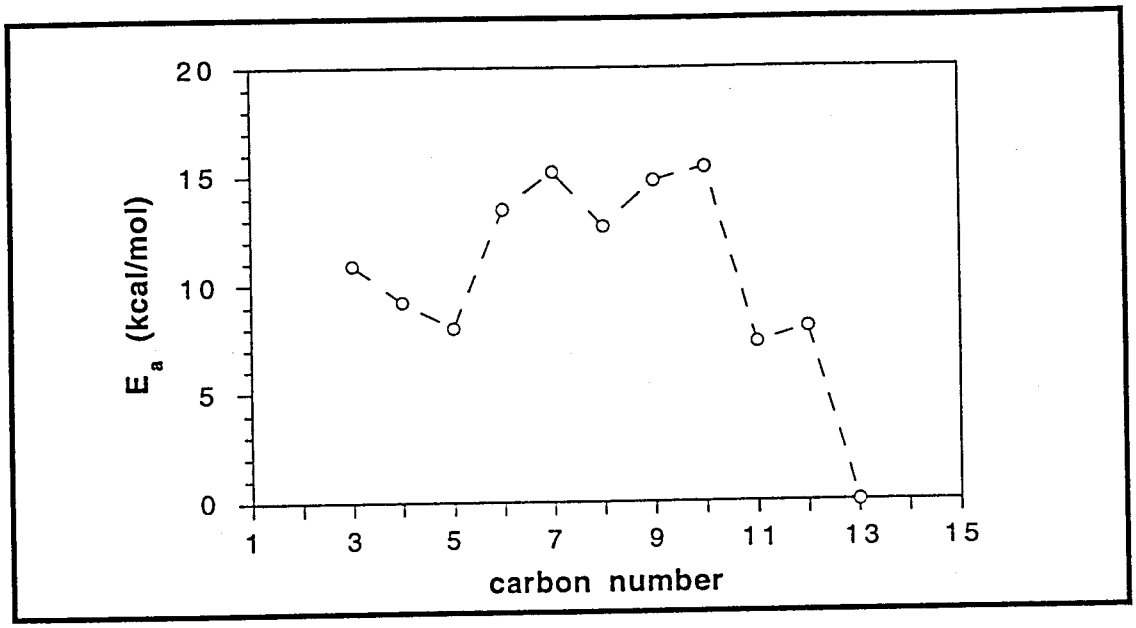

Figure 2.4 Activation energies for diffusion of *n*-paraffins in zeolite T [Gorring, 1973].

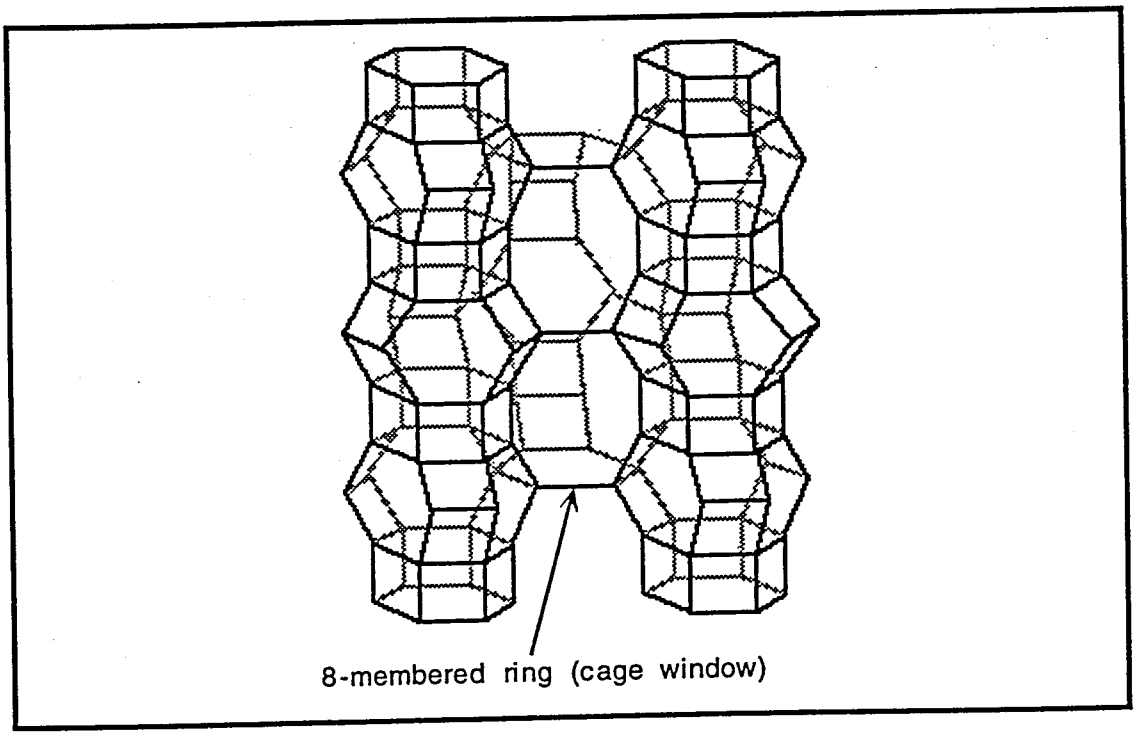

Figure 2.5 Structure of the Erionite's framework (reproduced from ZeoFile, by J.M. Newsam and M.M.J. Treacy, 1992).

The window effect was later discussed by Ruckenstein and Lee [1976]. They summarized Gorring's intricate considerations in a more general, but still qualitative fashion. They considered a molecule moving along a linear periodic potential (associated to the succession of channels and cages in a zeolite pore). The period of this potential, L, coincides with the period of the zeolite's framework. A molecule with length equal to L (or an integer multiple of L) will assume a potential that is independent of its position along the one-dimensional pore. Since there are no energetic barriers to overcome, the diffusion process will show no activation energy. This molecule would then exhibit the faster diffusion rate. This would be the case of dodecane in the erionite system. Smaller and longer molecules will be subjected to energetic potential barriers, and thus will have lower diffusivities. Ruckenstein and Lee termed this effect 'resonant diffusion'.

More recently, a quantitative approach was developed by Nitsche and Wei [1991]. They described the diffusion of linear paraffins in erionite also as an one-dimensional process, in which the molecule (modeled as a rigid rod) moves along a periodic potential, which they have quantified by first specifying the interactions between the molecule's segments and the zeolite's framework. The energy barriers that the entire molecule must overcome can then be computed. As in the previous analysis, molecules with length multiple of the potential's period show zero activation energy. The authors in addition have adopted a Brownian motion model to describe the relationship between the diffusion coefficient and the periodic potential acting on the molecule. The results obtained fit Gorring's data relatively well. It is interesting to analyze in some detail these authors' approach. This is done in Appendix B.

It is intriguing that there are no reports of similar effects occuring in other systems. One would expect that frameworks characterized by periodic sequences of

tight channels and relatively wide cages (like chabazite or 5A) would satisfy the conditions for the existence of such phenomena. The extensive work performed by Ruthven and co-workers on the diffusion of linear paraffins in zeolites 5A, Silicalite and NaX [Ruthven and Eic, 1988; Vavlitis et al., 1981] shows no evidence of an window effect.

2.6 Transition State Theory

The principles of transition state theory (or theory of rate processes), as developed by Eyring [Glasstone, Laidler and Eyring, 1941] were first applied to diffusion in zeolites by Ruthven and Derrah [1972]. The general statistical thermodynamic basis for the analogy between activated diffusion and the Eyring theory was decribed by Hill [1986]. The zeolite's cages are assumed to be the positions of lower potential for the diffusing molecules. Diffusion occurs when the molecules move to an adjacent cage by passing through a window (channel). Due to repulsion forces there may be an appreciable energy barrier associated with this process. For systems in which these assumptions are valid, the diffusion process may be considered as a rate process involving a transition state (the passage through the window). The development of the statistical thermodynamic model can lead to interesting results that include, for instance, rotational partitioning effects. Other references to this model can be found in later works [Ruthven et al., 1973; Ruthven and Doetsch, 1975; Kärger et al., 1980]. The recent work of Xiao and Wei [1992a] also included a similar approach. A more detailed description of the theory and its applications will be given in Appendix A.

2.7 Extraneous Mass Transfer Resistances and Surface Bariers

The limiting mass transfer process in an assemblage of zeolite particles may be other than intra-crystalline diffusion. Diffusion inside macropores (in case of pelleted zeolites) or along the bed void space may sometimes play a significant role, as will be discussed in Chapter 3. In addition, it has been often suggested that "surface barriers" (a mass transfer resistance located at the zeolite crystal surface) also affect the transport process in some zeolite/adsorbate systems. This hypothesis has been investigated to some extent in the last two decades and will be briefly reviewed here. Its importanced for the present study will become clear in Chapter 4.

Kondis and Dranoff [1971] obtained uptake curves for adsorption and desorption of ethane in 4A zeolite of slightly sigmoidal shape, This is contrary to the expected initial linear dependence of the fractional uptake on $\sqrt{t}$ [Crank, 1975]. Bülow and co-workers also reported sigmoidal uptake curves for sorption of *n*-hexane in MgA [Bülow et al., 1980] and *n*-decane in NaMgA [Bülow et al., 1982]. These observations were attributed to a particle surface resistance. In particular, there is evidence that the development of this resistance in zeolite A systems is related to the severity of the hydrothermal pretreatment of the samples [Bülow et al., 1980, 1982, 1985; Kondis and Dranoff, 1971]. It has been suggested that this is due to an effect similar to the one observed in zeolite HY [Breck, 1974a]: Al is removed from the framework by hydrolysis at high temperature, and, consequently, the frameworks' unit cell dimensions are reduced, giving rise to narrower pore openings. Additional evidence relative to the existence and nature of surface barriers in zeolite 5A systems has been provided by N.M.R. experiments (*e.g.*, see Kärger et al. [1981, 1987, 1988]).

In addition to this framework-structure related resistance, other possibilities have been discussed in the literature [Bülow, 1991]. We list here the more pertinent hypotheses:

i) Conformational barrier [Bülow et al., 1980]. In order to diffuse into the crystal, a molecule may have to undergo a change in conformation. In the case of a linear paraffin diffusing into a small channel system like 5A, the molecule must pass from a coiled conformation (the more stable in the gas phase) into a more elongated one, through rotations of the chain segments. The activation step associated with this transformation may induce an extra-crystalline transport barrier. Experimental evidence of this phenomenon is not conclusive.

ii) Evaporation barrier [Barrer, 1987]. During desorption, molecules must acquire enough energy in order to escape the interactions with the framework. If this desorption energy is higher than the activation energy for intra-crystalline diffusion, an evaporation barrier is present at the crystal surface. There is no experimental evidence of this effect [Kärger and Ruthven, 1989].

iii) Thermal barrier [Bülow and Struve, 1984]. If the heat of adsorption is not efficiently dissipated from the crystal interface, the local temperature may increase, causing the sorbate concentration to decrease and thus delaying the adsorption uptake. It was shown that this effect is significant in the adsorption of benzene by NaX zeolite.

iv) Nonequilibrium barrier [Micke et al., 1994]. Adsorption at the surface may not be an instantaneous equilibrium process. The particular kinetics of the process may give rise to an apparent surface barrier. A model assuming Langmuir kinetics at the crystal surface did fit the experimental results well for the system *p*-ethyl-toluene/ZSM-5.

2.8 Heats of Sorption

Some confusion and inconsistency can be found in the published results of heats of sorption for different adsorbate/zeolite systems, measured either isostericaly or

calorimetrically. However, a few works deserve some attention, since they advance some interesting hypotheses.

Thamm [1987a; 1987b; 1988] has studied calorimetrically the sorption of different molecules on Silicalite and ZSM-5 materials. Some adsorbates showed heats of sorption that vary with loading in a complicated manner. The heats of molecules like benzene, toluene and ethylbenzene present an initial plateau at low loadings, followed by a local minimum and a step increase to the highest values at moderate loadings. Thamm has interpreted this in terms of adsorption site heterogeneity and sorbate-sorbate interactions. At low loadings, the molecules are located at the zigzag channels (the energetically higher sites) and sorbate-sorbate interactions are impossible due to the distances between molecules. As loading increases, the maximum capacity of these sites is reached. Occupancy of the less energetic sites (the straight channels or the intersections) takes place, causing the heats of sorption to decrease. However, at a certain point, the loading will be high enough so that inter-molecular interactions (molecular associations) become significant, and the heats rise. Other sorbates, like *n*-alkanes, do not exhibit this adsorption heterogeneity. Adsorbate-adsorbate interactions start at low loadings, and the heats of sorption rise progressively and monotonicaly with loading, as the interactions increase. Interestingly, *p*-xylene seems to show a behavior intermediate between these two cases.

Talu and co-workers [Talu, Guo and Hayhurst, 1989; Guo, Talu and Hayhurst, 1989; Li and Talu, 1993] have developed a different interpretation for the kind of behavior described before. Their discussion also involves the notion of structural heterogeneity of the zeolite, but with a different approach. The authors recall that adsorption equilibria is controlled by the Gibbs free energy:

$$\Delta G = \Delta H - T\Delta S \tag{2.41}$$

It is usually assumed that the more energetic sites (higher $|\Delta H|$) are occupied first. However, this may not be true in the case microporous heterogeneous adsorbents, since the entropic term in 2.41 may play a determining role. In the case of Silicalite, the zigzag channels may be the most energetic sites, but they also imply the higher mobility restrictions to the sorbed molecules (higher $|\Delta S|$). Therefore, depending on the temperature, the entropic term may oppose the effect of the enthalpic term, and less energetic sites may be filled first. This would account for the step changes from low to high heats of adsorption measured for many adsorbates.

2.9 Experimental Measurement of Diffusion Coefficients

Several methods are available for measurement of transport diffusivities. Some of the more commonly found in the literature are briefly described next. A good review is given by Kärger and Ruthven [1992].

Transient uptake rate. This class of unsteady state methods involves several variations. In one of the simplest, the zeolite sample is equilibrated with a gas (single component or mixture) in a vessel of fixed volume. The evolution of the sample's weight with time is monitored by a highly sensitive balance. This data is then fitted to the appropriate mathematical model allowing for the computation of the diffusivity [Crank, 1975]. In a variation of this method, the sample is in contact with a flowing carrier gas in which a step change in the concentration of adsorbable component is introduced. The measurements can be performed in other ways in addition to gravimetrically. In a fixed volume system, the pressure of the gas-phase may be

measured. Alternatively, the pressure is maintained constant and the sorption uptake is determined volumetrically.

Frequency response. A variation of the uptake rate experiments employs a periodic perturbation of the system volume instead of the conventional step change in ambient conditions. This method is useful in the analyzes of fast processes since heat and mass transfer resistances can be controlled more easily.

Concentration Pulse (or Step) Chromatography. A nonadsorbable carrier gas is flowed continuously through a column packed with zeolite particles (single or bound crystals). A pulse of diffusing component is injected at the column inlet and the response peak is recorded and analyzed. The injected pulse must be small in order to guarantee that the adsorption obeys a linear pressure versus amount adsorbed relationship. More comments on this method will be made in chapter 3.

Zero Length Chromatography. In ZLC a small sample of zeolite particles is initially equilibrated with a flow of constant (small) sorbate concentration and then purged with an pure inert gas. The effluent desorption curve is recorded and analyzed. Axial dispersion effects can be eliminated with this method and thus the dispersion of the response peak is due only to particle mass transfer resistances.

Permeability. The flux of gas through a plug of sample is measured under steady-state conditions. Even though the method is quite simple, it is limited by the fact that the permeability rather than the diffusivity is measured and the relationship between both may be difficult to establish. Also measurements with samples which comprise microporous particles that must be pressed or bound together in some manner to form the plug are complicated by the difficulty in separating inter- from intra-particle transport.

Wicke-Kallenbach. This steady-state method is similar to the previous one but now the pressure is kept identical in both sides of the sample and the diffusion process is driven by a constant concentration gradient of diffusant. A transient version of this method has also been developed.

CHAPTER 3

HETEROGENEOUS MASS TRANSPORT IN ZEOLITE BEDS: TRANSPORT OF BENZENE IN ZSM-5

3.1 Introduction

The problem of mass transport through a bed of microporous particles with high adsorption capacity (like zeolites) contains subtle aspects that may not be initially evident. Proper analysis of the individual contributions of the gas and solid-phase transport is essential for the study of many practical systems. The recent ^{129}Xe NMR work on the transport of benzene in zeolite beds performed by Fraissard's research group [Springuel-Huet et al., 1996] supplies very useful information towards the understanding of these phenomena. Here those experiments are analyzed in greater detail, obtaining new insight into the significance of the results.

A clearer picture of the competing effects of intra- and inter-particle transport may be developed from a simple model describing mass transfer in an bed of porous particles. This will also admit a more fruitful discussion of the experimental NMR data. Before detailing the mathematical aspects, however, some general observations will be made.

In a system consisting of a bed of particles with a monodisperse porous structure, the time constant for intra-particle transport may be immediately identified as:

$$\tau_i = \frac{\lambda_i^2}{D_i} \tag{3.1}$$

where D_i is the diffusivity of the adsorbate inside the particle and λ_i the particle's characteristic length. One may associate a similar time constant with the transport in the inter-particle gas-phase:

$$\tau_g = \frac{L^2}{D_g} \tag{3.2}$$

where L is the bed length and D_g the adsorbate diffusivity in the bulk gas, corrected with the bed's tortuosity factor. Though it might be tempting, to compare directly τ_i and τ_g in order to determine which is the controlling transport process is incorrect. The gas-phase transport in this system is not described by τ_g alone. This becomes evident if one considers the simplified case of negligible intra-particle resistance. The mass balance for the gas-phase is then:

$$\frac{\partial c}{\partial t} = \varepsilon_b D_g \frac{\partial^2 c}{\partial x^2} - (1-\varepsilon_b)\frac{\partial q}{\partial t} \tag{3.3}$$

where c is the concentration in the gas-phase and q the concentration in the particle (adsorbed phase). ε_b is the bed's porosity. Presuming operation in the Henry's law region of the adsorption isotherm (q = Kc) Equation 3.3 becomes:

$$\frac{\partial c}{\partial t} = \frac{D_g}{\frac{1}{\varepsilon_b} + \frac{1-\varepsilon_b}{\varepsilon_b} K}\frac{\partial^2 c}{\partial x^2} \approx \frac{D_g}{\frac{1-\varepsilon_b}{\varepsilon_b} K}\frac{\partial^2 c}{\partial x^2} \tag{3.4}$$

where K is assumed to be large. Evidently, the true time constant characterizing transport through the gas-phase is then:

$$\tau_{bed} = \frac{1-\varepsilon_b}{\varepsilon_b} K \frac{L^2}{D_g} = \frac{1-\varepsilon_b}{\varepsilon_b} K \tau_g \qquad (3.5)$$

Any conclusion relative to the limiting transport process must be driven from the comparison of τ_i and τ_{bed}. The high adsorptive capacity of microporous solids like zeolites (large K) may often counteract the effect of the low intra-crystalline diffusivity (D_i) and lead to otherwise unexpected bed mass transfer limitations. This is not clearly addressed in the literature, and errors can sometimes be found in studies of such systems (*e.g.* Chmelka et al. [1990]).

The significance of Equation 3.5 is certainly not new. The concept of *long range-diffusion* developed by Kärger [Kärger and Ruthven, 1992; Springuel-Huet et al., 1996] in the perspective of self-diffusion in a bed of microporous particles leads to an identical result. Ruckenstein, Anathan and Youngquist [1971] also correctly identified the role of the adsorption constant K in their detailed analysis of an equivalent problem: the competing effects of macro- and micropore transport resistances on a bidisperse particle.

To complete the analysis, one should mention another possible mass transport scenario: the existence of an adsorption front. When the adsorption isotherm is very steep or the gas-phase concentration sufficiently large, the isotherm can be assumed as rectangular:

$$c = 0 \rightarrow q = 0$$

$$c > 0 \rightarrow q = q_{sat} \qquad (3.6)$$

where q_{sat} is the saturation concentration in the solid phase. As a consequence, a concentration front will propagate along the bed in the solid-phase. The time

dependence of the position of the front, l_f, can be obtained from a simple mass balance, following a shrinking-core model:

$$(1-\varepsilon_b)\, q_{sat} \frac{dl_f}{dt} = -\varepsilon_b D_g \left(\frac{\partial c}{\partial x}\right)_{x=l_f} = \varepsilon_b D_g \frac{c_0}{l_f} \tag{3.7}$$

where pseudo steady state was assumed for the concentration of adsorbate in the gas-phase (with $c = c_0$ at the entrance of the bed). From this equation, one can compute the time necessary for the front to reach the end of the bed ($l_f = L$):

$$\tau_{bed} = \frac{1-\varepsilon_b}{\varepsilon_b} \frac{q_{sat}}{2c_0} \frac{L^2}{D_g} = \frac{1-\varepsilon_b}{\varepsilon_b} \frac{q_{sat}}{2c_0} \tau_g \tag{3.8}$$

This time constant is formally similar to the one in Equation 3.5. The factor 2 in the denominator (absent in Equation 3.5) is a simple consequence of the slightly different strategies used to solve the two cases. The time constant in Equation 3.5 corresponds to full equilibration of the system, *i.e.* concentration in the gas-phase is c_0 throughout the bed. Equation 3.8, on the other hand, corresponds to the time when the concentration front in the solid reaches the end of the bed. At this point there is a linear (pseudo steady-state) concentration profile in the gas phase with $c = c_0$ at one end and $c = 0$ at the other (average concentration in the gas is $c_0/2$). Since the time necessary to reach this profile is half of the full equilibration time, a factor of 2 appears in the denominator of Equation 3.8.

It must be noted that information on the existence of a concentration front can only be inferred from the analysis of the adsorption isotherm and the operation conditions. Comparison of time constants is meaningless in this case.

3.2 Model Development

A more detailed study of this heterogeneous transport problem can be undertaken with the aid of a simple mathematical model. An introductory general case will be discussed first. Subsequently, the model will be applied to the description of the experimental ^{129}Xe NMR data.

Consider the simple case of a bed of microporous particles exposed to a constant concentration of adsorbate in the gas phase. In order to simplify the mathematical treatment (and in particular to avoid the use of particle geometry-dependent coordinates for the solid phase transport), this system is described by segregating the gas and solid phases (Figure 3.1).

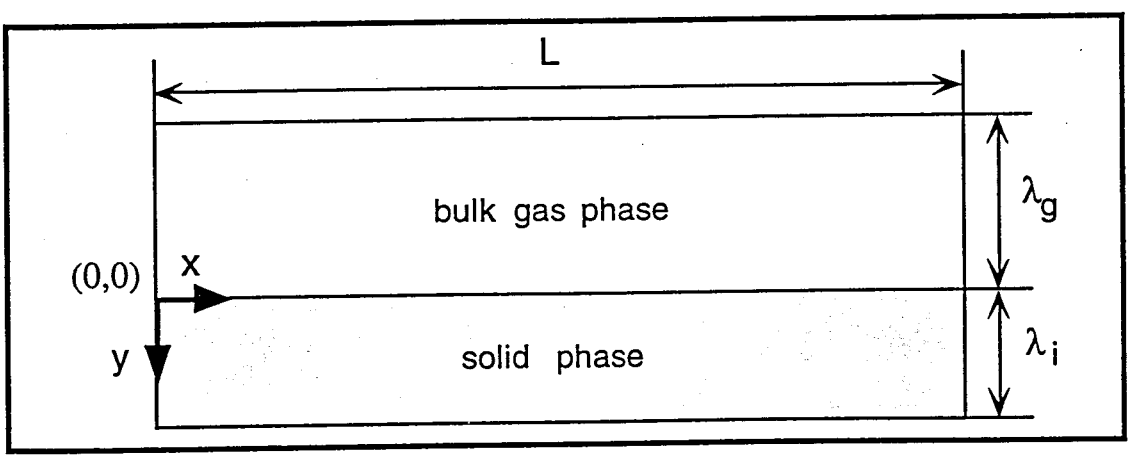

Figure 3.1 Model representation of an adsorbent particle bed.

Molecular transport in the solid takes place along the y direction, and in the gas phase (along the bed) in the x direction. It is further assumed that the operating conditions are within the Henry's law region of the adsorption isotherm and that the diffusivity in the solid is invariant with concentration. The normalized mass balance for the gas phase is:

$$\frac{\partial C}{\partial t} = \frac{1}{\tau_g}\frac{\partial^2 C}{\partial X^2} + \frac{\lambda_i}{\lambda_g}\frac{1}{\tau_i} K \left(\frac{\partial Q}{\partial Y}\right)_{Y=0} \tag{3.9}$$

and for the solid phase:

$$\frac{\partial Q}{\partial t} = \frac{1}{\tau_i}\frac{\partial^2 Q}{\partial Y^2} \tag{3.10}$$

The following normalized variables have been used: $C = c/c_0$, $Q = q/q_0$, $X = x/L$, $Y = y/\lambda_i$,. The model's parameters are: $\tau_g = L^2/D_g$, $\tau_i = \lambda_i^2/D_i$ and $K = q/c$ (Henry's law constant). The thickness ratio λ_i/λ_g is related to the porosity of the bed:

$$\frac{\lambda_i}{\lambda_g} = \frac{1-\varepsilon_t}{\varepsilon_b} \tag{3.11}$$

The boundary conditions are:

$$t = 0 \rightarrow C = 0,\ Q = 0$$

$$X = 0 \rightarrow C = 1 \qquad X = 1 \rightarrow \frac{\partial C}{\partial X} = 0$$

$$Y = 0 \rightarrow Q = C \qquad Y = 1 \rightarrow \frac{\partial Q}{\partial Y} = 0 \tag{3.12}$$

This set of differential equations is easily solved in the Laplace domain, and the result may be numerically inverted into the time domain.

The behavior of the system is characterized by the parameter R_{ig}:

$$R_{ig} = \frac{\tau_{bed}}{\tau_i} = \frac{1-\varepsilon_b}{\varepsilon_b} \frac{K\ \tau_g}{\tau_i} \qquad (3.13)$$

This is the ratio between the time scales for transport in the gas and solid phases. $R_{ig} << 1$ implies that solid-phase transport is the controlling process, and the opposite for $R_{ig} >> 1$.

Figure 3.2 shows the gas and solid-phase concentration profiles obtained for the following set of parameters: $\tau_g = 1$, $\tau_i = 10^4$, $K = 10^2$. $R_{ig} = 0.01$ in this case. The concentration in the gas phase, C(X), becomes uniform very rapidly (Figure 3.2a). The average concentration in the solid, $Q_{avg}(X)$, is also uniform along the bed, but rises only gradually. The concentration profiles inside the solid-phase (shown in Figure 3.2b for X=1) have a significant gradient. Equilibrium is reached when t approaches τ_i. That the profile actually equilibrates only for $t = 2\tau_i$ is simply a feature of the slab geometry adopted for the solid-phase diffusion model [Crank, 1975].

If one makes $K = 10^4$ then $R_{ig} = 1$ and the rate of gas and solid-phase transport are identical. The concentration gradients in the gas are now significant during the entire process (Figure 3.3a), while in the solid (Figure 3.3b) the gradients are less pronounced than in the previous case ($R_{ig} = 0.01$). In addition, it takes slightly longer for equilibrium to be attained.

Finally, if $K = 10^6$ ($R_{ig} = 100$), diffusion through the gas-phase controls the global process. Equilibrium is reached only for $t = (1-\varepsilon_b)/\varepsilon_b\ K\ \tau_g = R_{ig}\ \tau_i$ (Figure 3.4a). Concentration profiles in the solid are flat (Figure 3.4b).

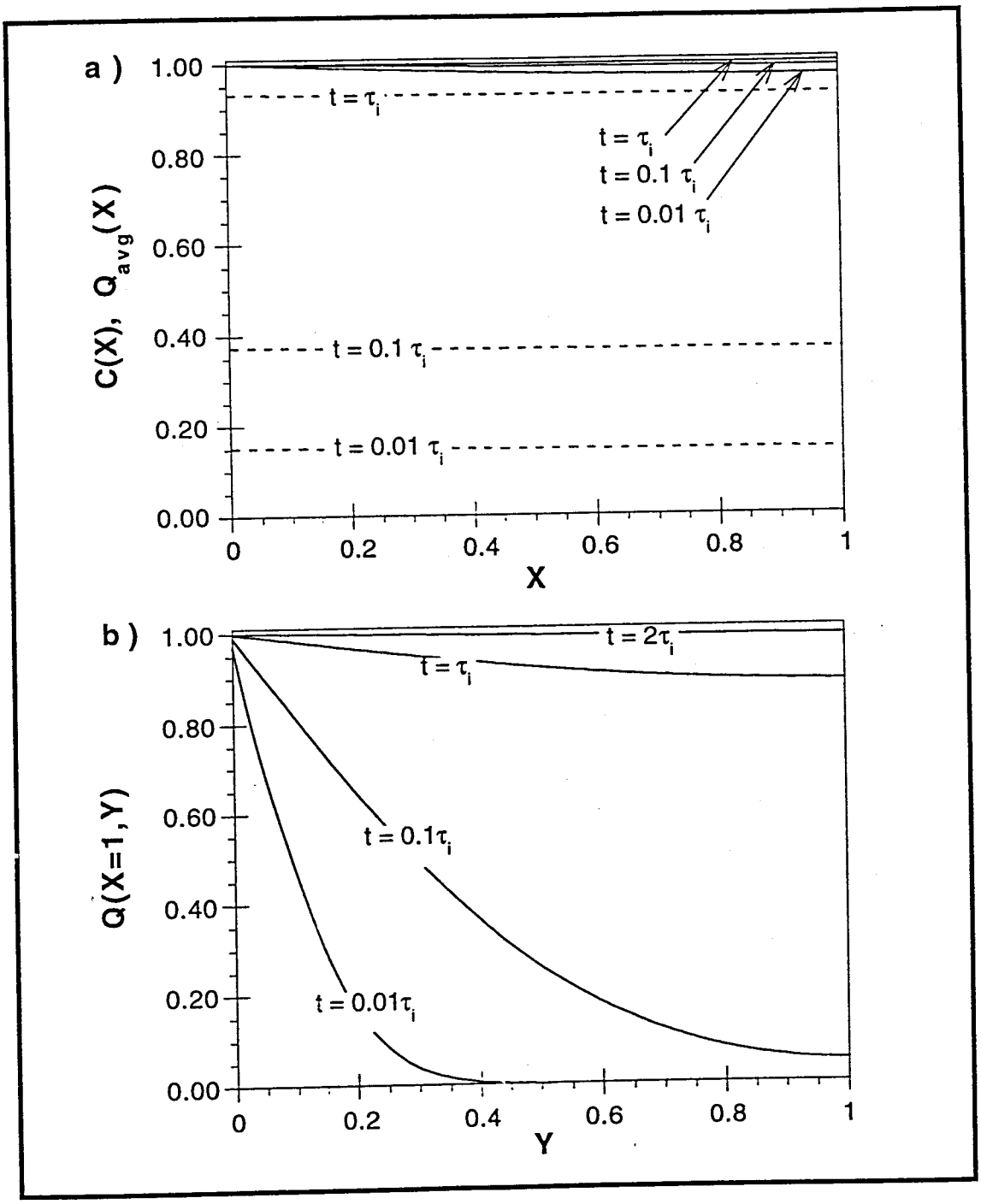

Figure 3.2 Concentration profiles computed for $\tau_g = 1$, $\tau_i = 10^4$, $K = 10^2$ ($R_{ig} = 0.01$). a) profiles along direction X: C(X) is the concentration in the gas-phase (solid line), $Q_{avg}(X)$ is the average concentration in solid-phase (dashed line). b) Profiles along Y direction: Q(X=1, Y) is the concentration in the solid-phase at X=1.

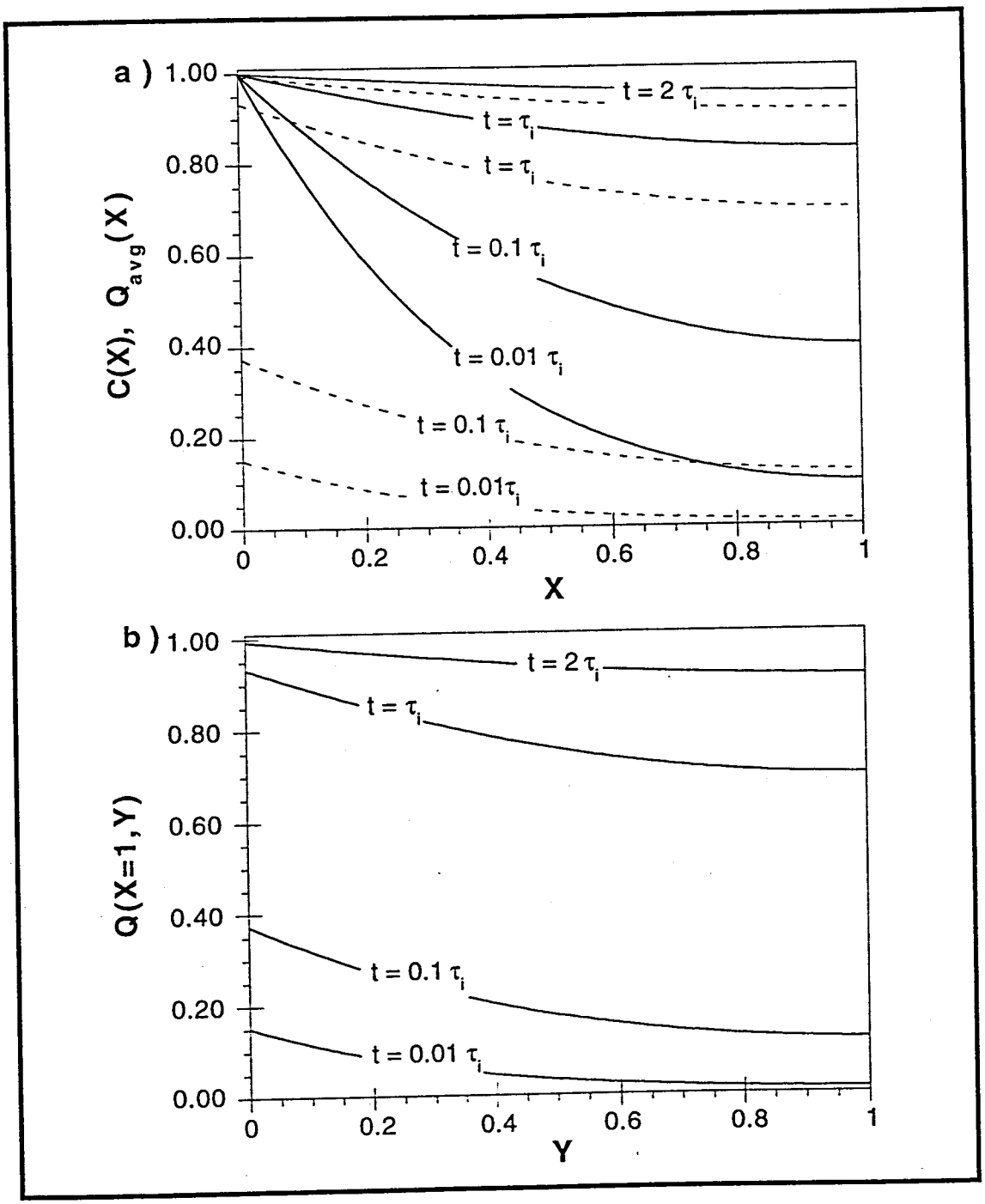

Figure 3.3 Concentration profiles computed for $\tau_g = 1$, $\tau_i = 10^4$, $K = 10^4$ ($R_{ig} = 1$). Legend for a) and b) as in Figure 3.2.

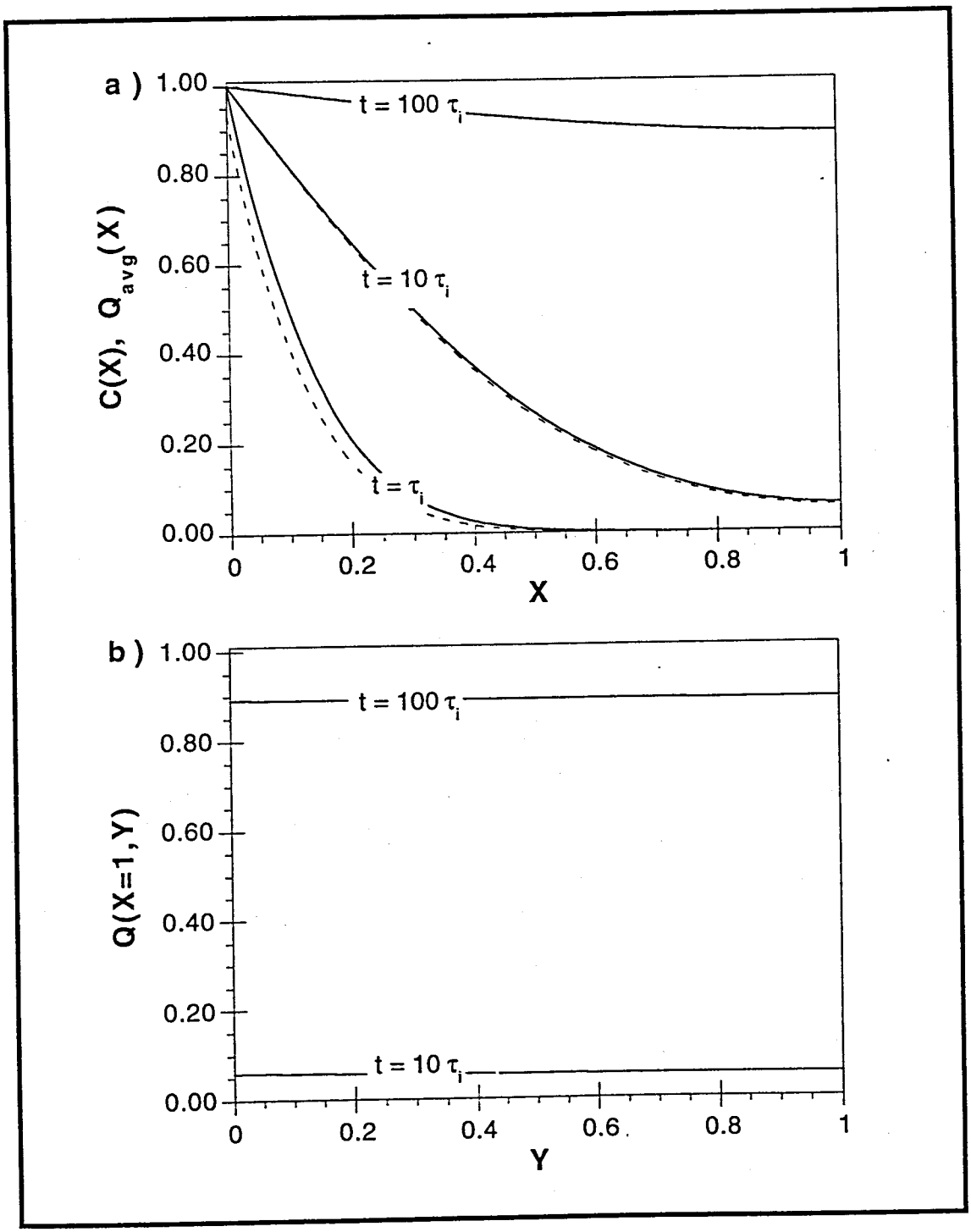

Figure 3.4 Concentration profiles computed for $\tau_g = 1$, $\tau_i = 10^4$, $K = 10^6$ ($R_{ig} = 100$). Legend for a) and b) as in Figure 3.2.

3.3 Experimental Evidence: ^{129}Xe NMR Studies

3.3.1 Background on the Technique

The ^{129}Xe NMR technique has proven to be successful in the characterization of microporous solids. A particularly interesting application involves probing the intra-crystalline adsorbate concentration distribution [Fraissard and Ito, 1988] [Kärger et al., 1992]. The basic phenomenology involves the dependence of the chemical shift of xenon's NMR spectra upon the concentration of a co-adsorbed species. For example, a propagating concentration wavefront of the co-adsorbed species in a particle bed would produce a ^{129}Xe NMR spectrum consisting of two narrow bands (one corresponding to the region of the bed with ^{129}Xe and co-adsorbent and another to the region with only ^{129}Xe). On the other hand, if there is no sharp discontinuity in the co-adsorbate distribution, then a single broad band would be observed.

In reality, not only the chemical shift in the spectrum is affected by the presence of the co-adsorbed species [Kärger et al., 1992]. The peak-width often increases with increasing co-adsorbate concentration. In the case of benzene, this is due to the magnetic dipolar interaction between its protons and the xenon molecules. In addition, the line intensity decreases with increasing co-adsorbate concentration. This is a simple consequence of the decrease in the concentration of adsorbed ^{129}Xe when another species competes for adsorption sites.

3.3.2 Experimental Results for Transport of Benzene in a Bed of ZSM-5 Crystallites

The recent experiments of Fraissard and coworkers show how this technique can provide information on the adsorbate distribution over a bed of zeolite particles. A detailed description of the experimental setup and procedures can be found elsewhere [Springuel-Huet et al., 1996]. Only a brief description of each experiment is given here. The bed consisted of ZSM-5 crystallites, 2/3 being spheres 30 μm in diameter and the rest had dimensions: 30×30×100 μm^3. The adsorbate employed was benzene except for the experiment of type D, described below. Schematic experiments of the arrangements employed in each experiment are shown in Figure 3.5.

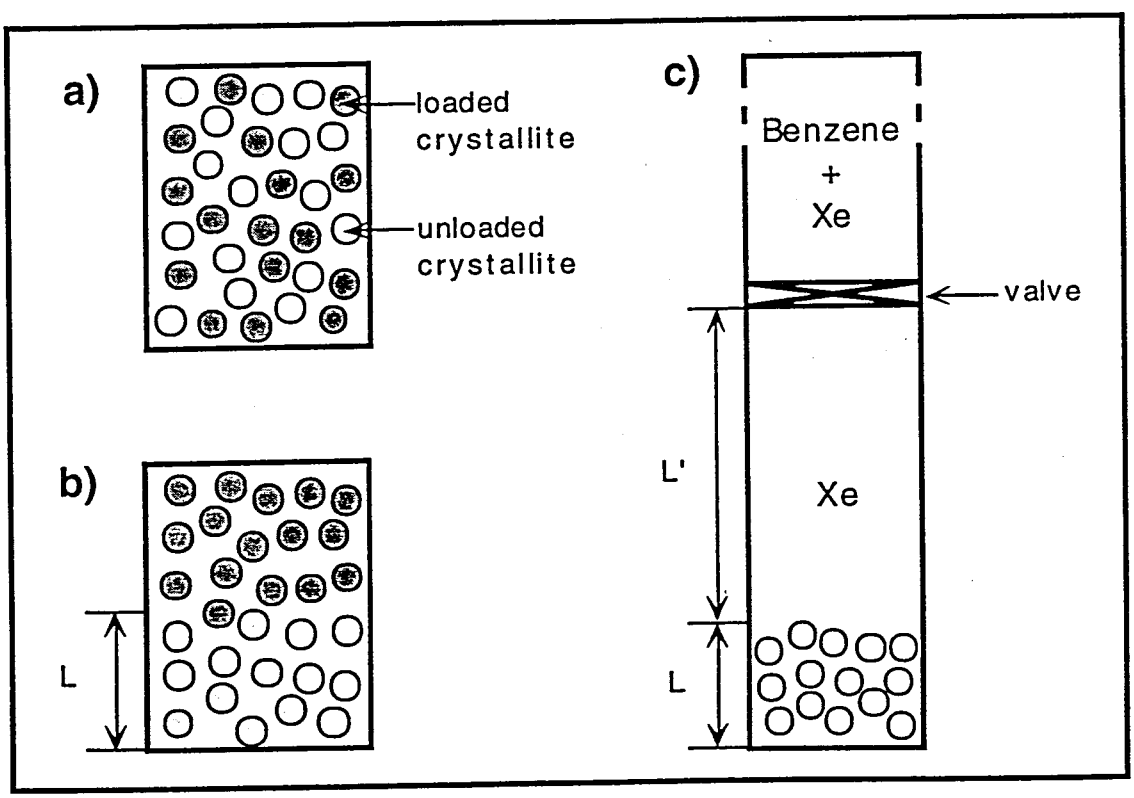

Figure 3.5 Schematic representation of the bed arrangements in experiments a) A, b) B and c) C.

Experiment A: adsorption/desorption in a well mixed bed of "loaded" and "unloaded" crystallites (Figure 3.5a). The "loaded" particles were equilibrated under a benzene and xenon atmosphere so that the final benzene loading is 6 molecules/unit cell. Subsequently these were well mixed with an identical amount of "unloaded" particles in the NMR ampoule (under a Xe atmosphere), immediately before the beginning of the experiment. The NMR spectra were collected at different times, until equilibrium was attained (spectra remained invariant with time). The results are shown in Figure 3.6.

Experiment B: adsorption/desorption in a segregated bed of "loaded" and "unloaded" crystallites (Figure 3.5b). The "loaded" particles (6 molecules/uc) were carefully layered over the "unloaded" zeolite in the ampoule, without mixing. Each layer was about 5mm deep. The NMR spectra obtained are shown in Figure 3.7.

Experiment C: adsorption from the gas phase into a bed of "unloaded" crystallites (Figure 3.5c). The "unloaded" particles were placed in a special ampoule divided in two sections separated by a valve. The zeolite lay in the bottom of the lower section, filled with Xe. The upper section contained Xe and a known amount of benzene. The valve was opened at the beginning of the experiment, allowing the benzene to diffuse into the lower section. The final equilibrium concentration of benzene in the zeolite was 6 molecules/uc. The thickness of the bed was about 8 mm. The length of the tube between the bed and the valve was 20 cm. The corresponding results are shown in Figure 3.8.

Experiment D: adsorption of n-hexane from the gas phase into a bed of "unloaded" crystallites. Same procedure as in experiment C, but *n*-hexane was used instead of benzene. The corresponding NMR spectra are shown in Figure 3.9.

All experiments were performed at 300 K and under a xenon pressure of 31.6 kPa

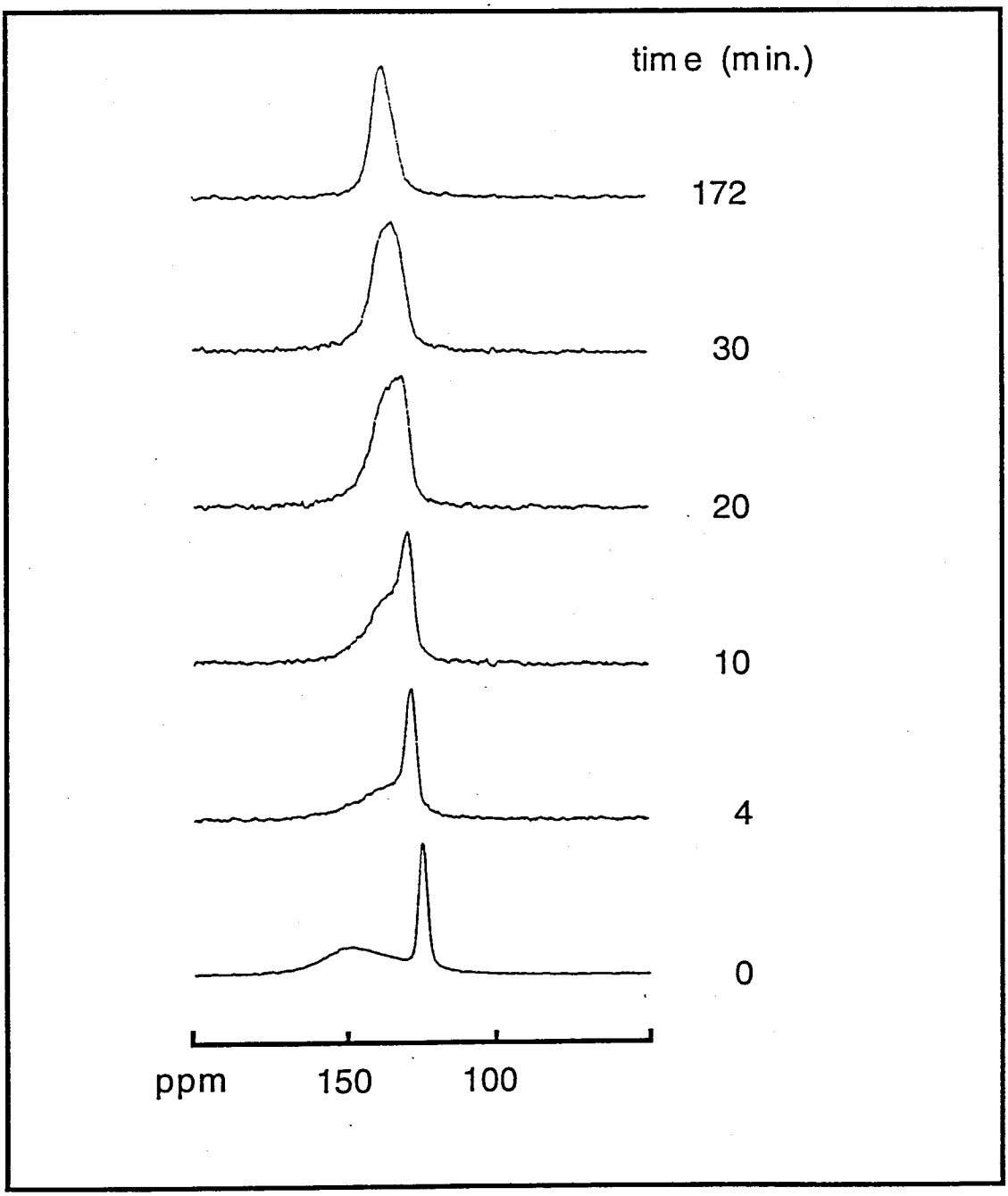

Figure 3.6 Experimental NMR data obtained in experiment A.

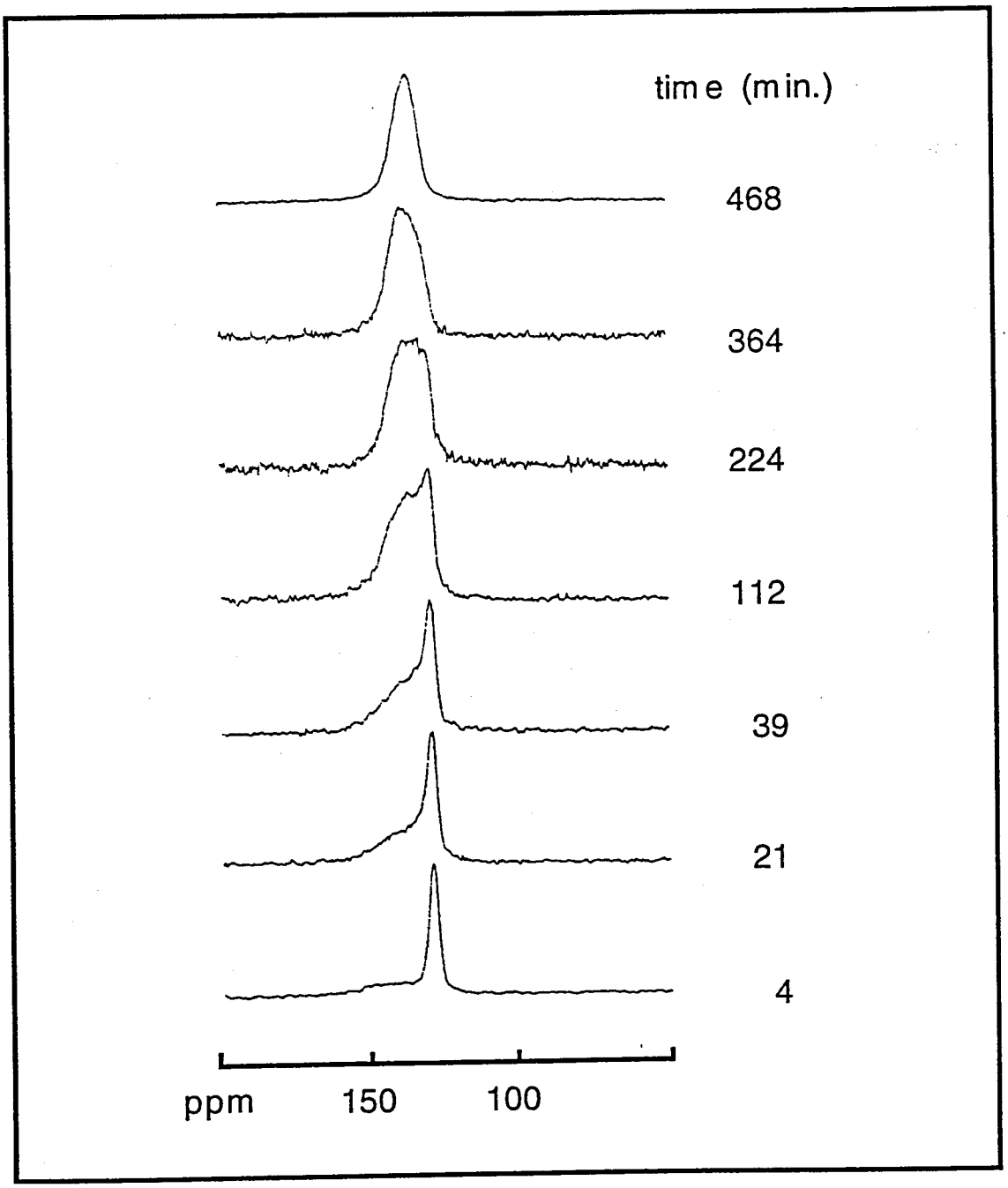

Figure 3.7 Experimental NMR data obtained in experiment B.

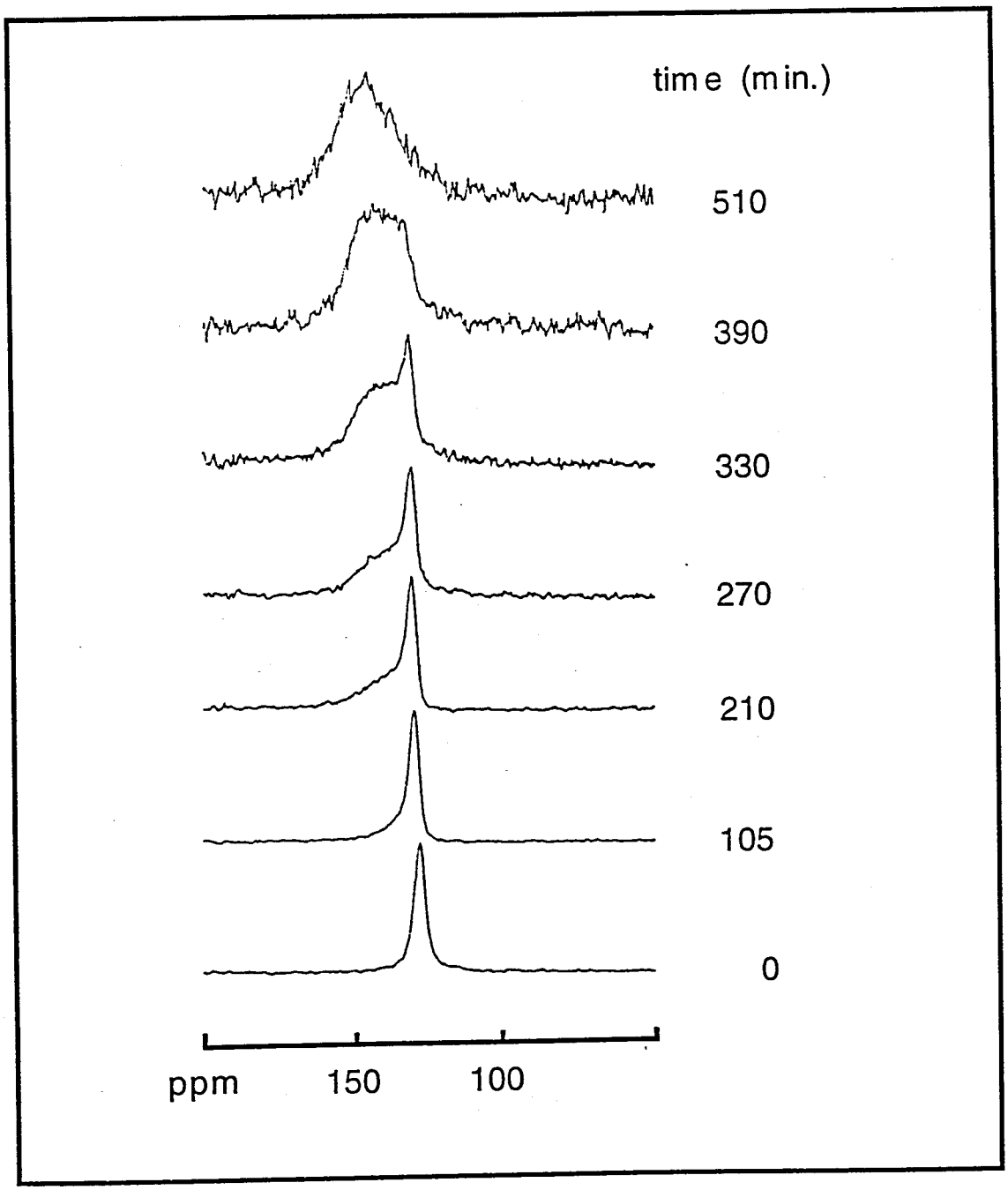

Figure 3.8 Experimental NMR data obtained in experiment C.

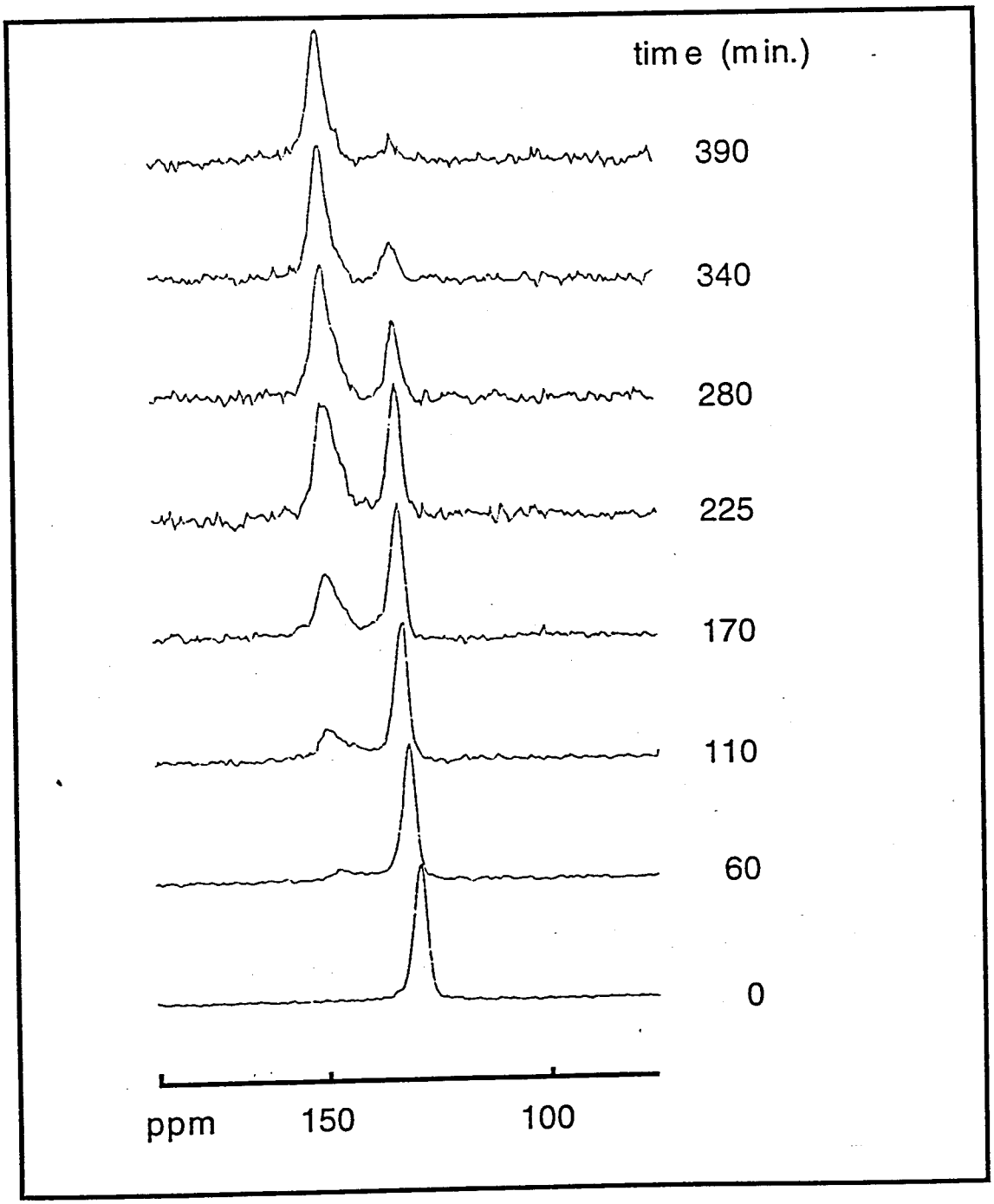

Figure 3.9 Experimental NMR data obtained in experiment D.

3.4 Model Application to Experimental Data

Let's begin with a model of experiment B, since experiments A and C can be understood as particular cases of B. The two segregated beds are schematized in Figure 3.10.

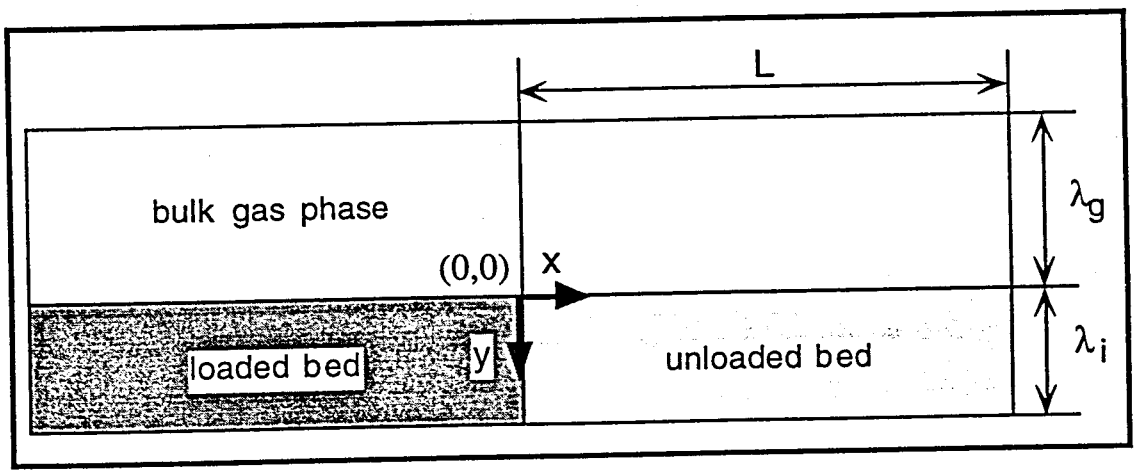

Figure 3.10 Model depiction of experiment B.

Intra-crystalline diffusion occurs along the y direction and gas-phase diffusion along the x direction. The material balances for the gas and solid-phase in both beds are given by Equations 3.9 and 3.10 with boundary conditions:

$$t = 0, -1 < X < 0 \rightarrow C = 1, Q = 1$$

$$t = 0, \ 0 < X < 1 \rightarrow C = 0, Q = 0$$

$$C(X=0^-) = C(X=0^+) \ ; \ \left(\frac{\partial C}{\partial X}\right)_{X=0^-} = \left(\frac{\partial C}{\partial X}\right)_{X=0^+}$$

$$Y = 0 \rightarrow Q = C \ ; \ Y = 1 \rightarrow \frac{\partial Q}{\partial Y} = 0 \qquad (3.14)$$

In experiment A, because the crystallites are well mixed, transport in the gas phase occurs along a much shorter distance, between two neighboring "loaded" and "unloaded" particles. The model can be defined equivalently, but the characteristic length L is now of the order of a particle diameter, and the two "beds" actually represent two neighboring crystallites.

Experiment C involves diffusion of benzene along a distance L' before reaching the "unloaded" bed. The material balance for this region ($-L' < x < 0$ or $-\lambda < X < 0$, with $\lambda = L'/L$) is simply:

$$\frac{\partial C}{\partial t} = \frac{1}{\tau_g'} \frac{\partial^2 C}{\partial X^2} \qquad (3.15)$$

Equations 3.9 and 3.10 apply again to the bed section, modeled as in Figure 3.1 ($0 < x < L$ or $0 < X < 1$). The boundary conditions are:

$$t = 0 \rightarrow C = 0,\ Q = 0$$

$$X = -\lambda \rightarrow C = 1 \qquad (\lambda = L'/L)$$

$$C(X=0^-) = C(X=0^+)\ ;\ \left(\frac{\partial C}{\partial X}\right)_{X=0^-} = \left(\frac{\partial C}{\partial X}\right)_{X=0^+}$$

$$Y = 0 \rightarrow Q = C\ ;\ Y = 1 \rightarrow \frac{\partial Q}{\partial Y} = 0 \qquad (3.16)$$

The simulated concentration profiles can be used to generate theoretical NMR spectra. This allows for a closer comparison between the model results and the experimental NMR data. The NMR signal of ^{129}Xe, $I(\omega,c)$, can be related to the

adsorbate concentration, c, by a simple Lorentzian, in which the line shift and the line intensity are a linear function of concentration [Kärger et al., 1992]. For any given time t, the NMR spectrum is computed from the solid phase concentration profile by using a weighed mean:

$$I(\omega,t) = \int I(\omega,c)\,\frac{1}{\lambda_i}\,\frac{\partial y(c,t)}{\partial c}\,dc \qquad (3.17)$$

where y(c,t) is an implicit function obtained from c(y,t). If the concentration profiles change along the bed, a global spectrum can be obtained by averaging a number of local spectra computed for equidistant points in the bed. It must be noted that the goal is not to reproduce the experimental data exactly, but simply to obtain a good agreement in relation to the experimental time scales and to the main features of the spectra.

The parameters of the model can be easily estimated. In experiment A, there is an intimate contact between the "loaded" and "unloaded" particles. Transport in the gas-phase occurs along a very short length, between neighboring particles. It seems then valid to presume that the limiting process is intra-crystalline diffusion, and therefore identify τ_i with the equilibration time of the NMR spectrum. In this way, one obtains $\tau_i \approx 1.0\times10^4$ s, and, from Equation 3.1, $D_i = 2.2\times10^{-14}$ m^2/s (for an equivalent particle diameter of 30 μm). This is in very good agreement with literature data on benzene diffusion in ZSM-5 at room temperature [Zikánová et al., 1987; Beschmann et al., 1987].

D_g can be estimated for the binary diffusion of benzene in xenon [Reid et al., 1987]:

$$D_g = \frac{1}{\xi}\frac{0.00266\ T^{3/2}}{P\ M_{AB}^{1/2}\ \sigma_{AB}\ \Omega_D} \approx 2\times10^{-5}\ m^2/s \qquad (3.18)$$

($\xi \approx 1/\varepsilon_b = 1/0.8$ is the bed tortuosity factor). The value of τ_g will depend, of course, on the bed arrangement in each experiment as discussed before. The values of the parameters estimated for the three experiments are summarized in Table 3.1.

The Henry's law constant, K, was estimated to be in the order of 10^5, based on the known experimental equilibrium conditions [Springuel-Huet et al., 1996].

Table 3.1 Estimated model parameters.

	K	τ_i	τ_g	R_{ig}
Experiment A	10^5	1.0×10^4 s	4.5×10^{-5} s ($L \approx 30\times10^{-6}$ m)	1×10^{-4}
Experiment B			1.2 s ($L = 5\times10^{-3}$ m)	3
Experiment C			3.2 s ($L = 8\times10^{-3}$ m)	8

3.5 Simulation Results and Discussion

In experiment A, $R_{ig} << 1$ (see Table 3.1) and thus only intra-crystalline transport contributes to the time scale of the transport process. The concentration profiles in the initially "unloaded" solid-phase are shown in Figure 3.11 (the profiles for the "loaded" solid would be given by 1-Q(Y)).

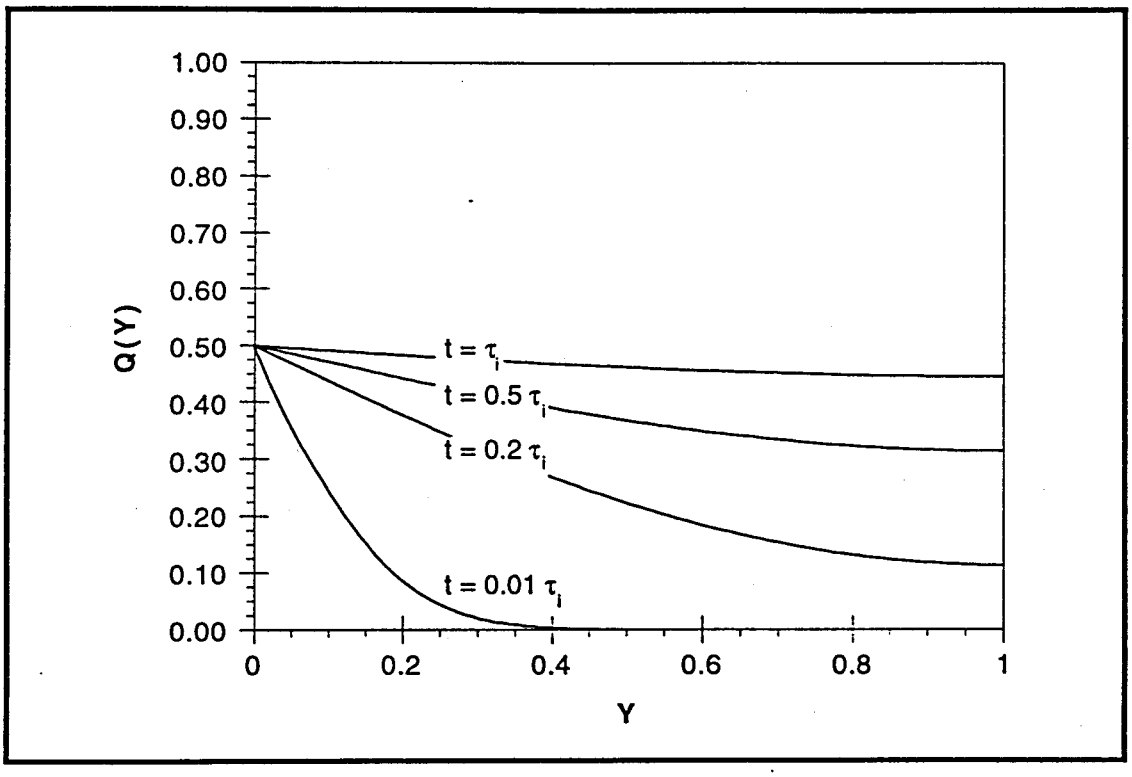

Figure 3.11 Simulated solid-phase concentration profiles for experiment A.

Equilibrium is attained for a time approximated by τ_i. The simulated NMR spectra are shown in Figure 3.12. The general time-dependent features of the experimental spectra (see Figure 3.6) are well reproduced. Initially two peaks are visible: one, of higher intensity, at lower chemical shift, corresponding to the signal from the xenon molecules in the "unloaded" particles, and a less intense one at higher chemical shift generated by the xenon in the "loaded" particles. The two peaks coalesce as the concentration field gradually homogenizes throughout the entire bed. The spectra equilibrates for $t = \tau_i$, justifying the assumption previously made when estimating this time constant. Notice that even though the experimental data show peak broadening with increasing benzene concentration, this effect was not included in our simulated spectra.

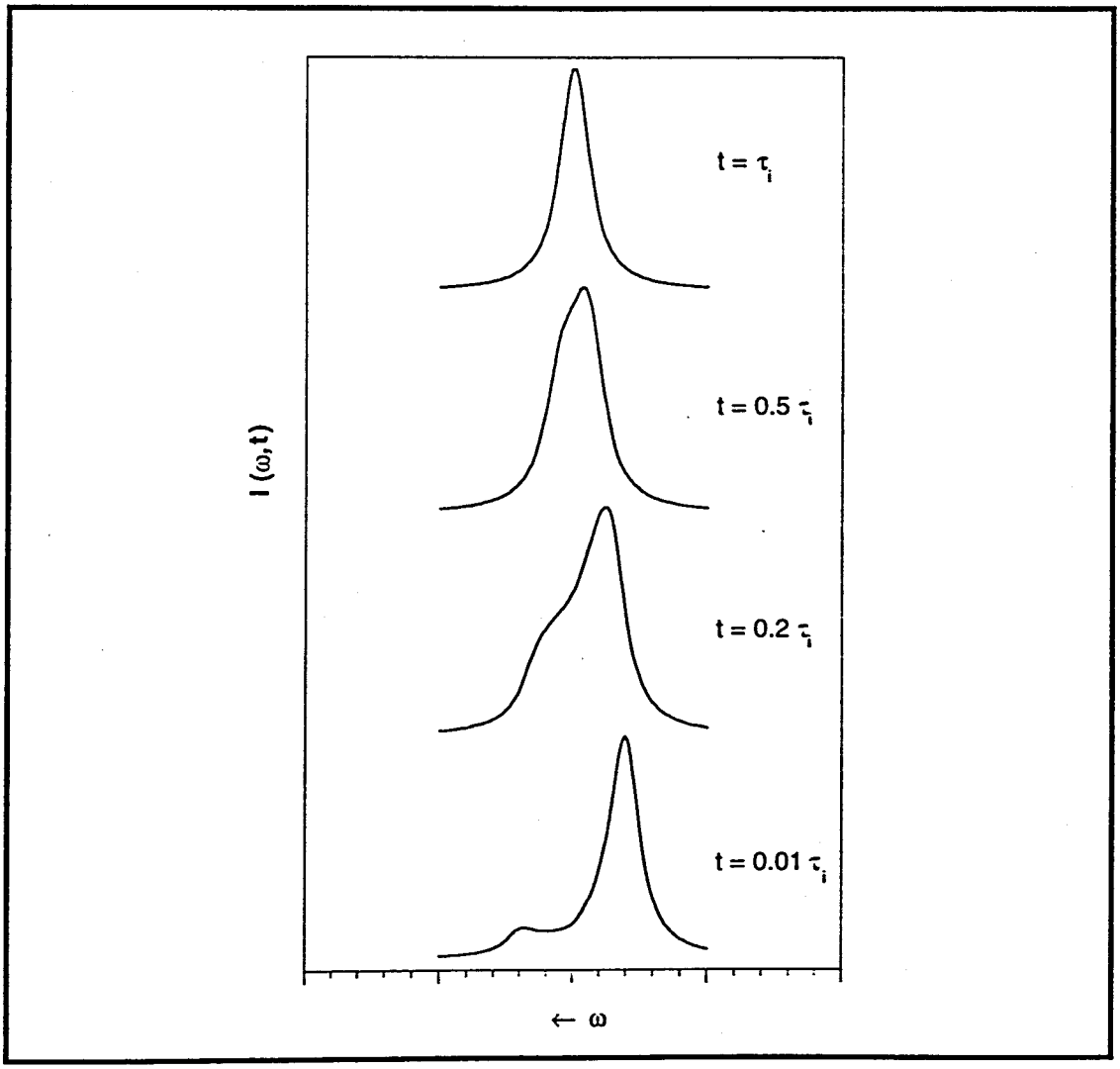

Figure 3.12 Simulated NMR spectra for experiment A.

The effect of segregating the "loaded" and "unloaded" particles (experiment B) is clearly seen in Figure 3.13.

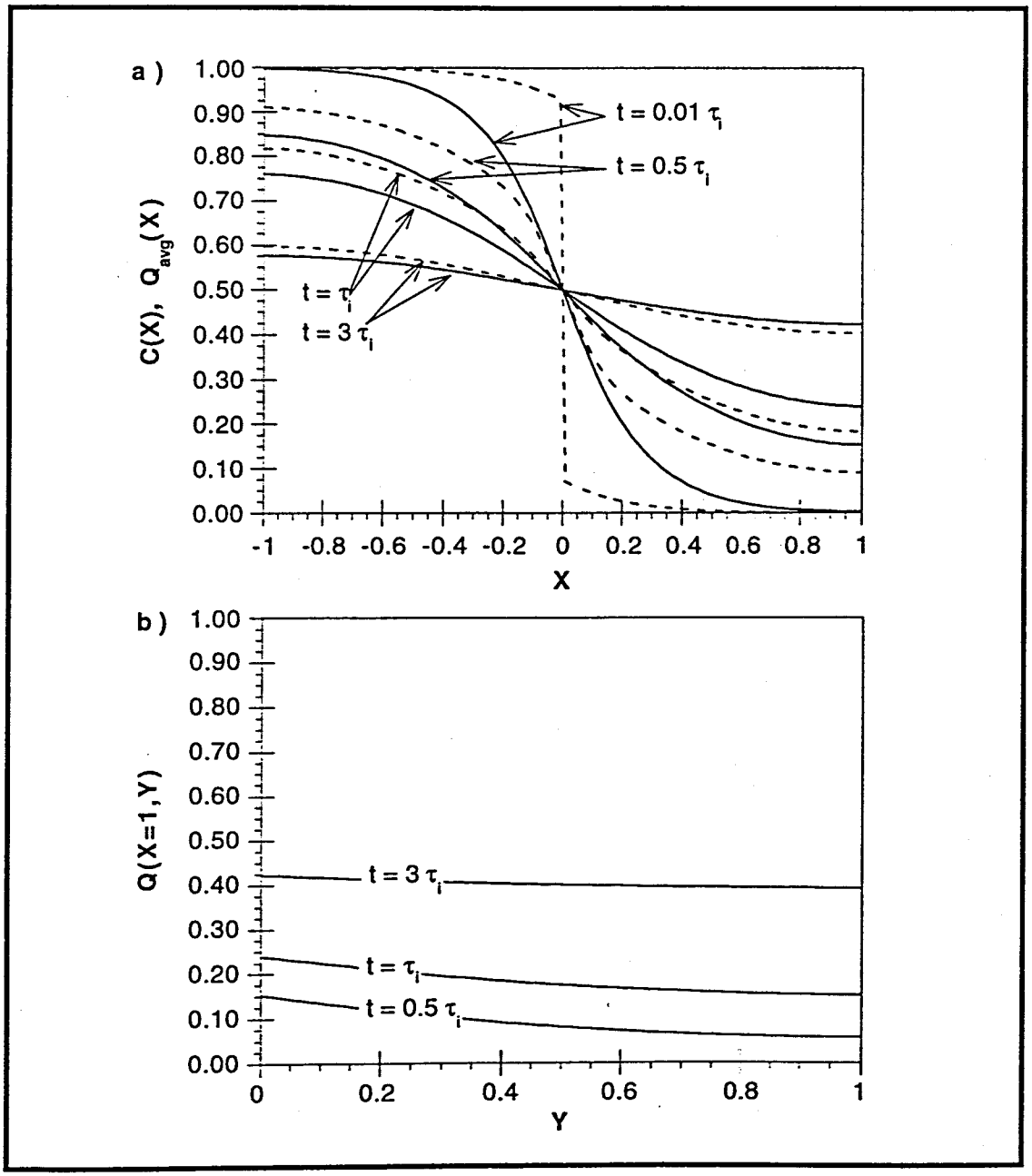

Figure 3.13 Simulated concentration profiles for experiment B. Legend as in Figure 3.2.

Concentration gradients in the gas phase are significant during the entire process. The average concentration in the solid also changes appreciably along the bed. On the other hand, the local solid-phase concentration gradients (at X = 1) are not very steep (Figure 3.13b). The computed NMR spectra is shown in Figure 3.14. The equilibration time is approximately $3\tau_i$, definitely higher than before. This is in good agreement with the experimental results (Figure 3.7).

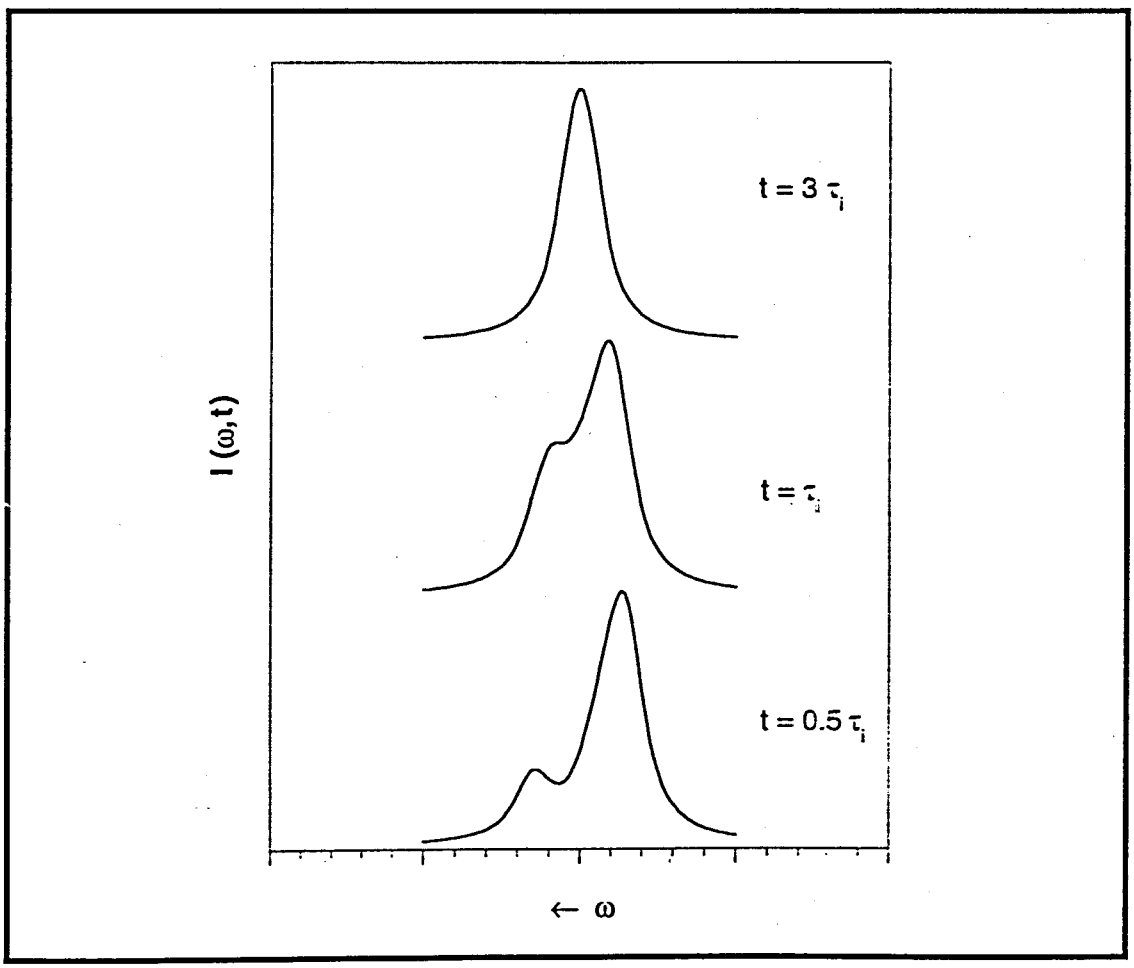

Figure 3.14 Simulated NMR spectra for experiment B.

In experiment C the adsorbate is assumed to diffuse along a length L', before reaching the "unloaded" bed. It may seem obvious to associate a time constant $\tau_g' = (L')^2/D_g'$ (D_g' differs from D_g in that it does not include the tortuosity factor ξ) with this initial diffusion process, and argue that its sole effect will be to delay the global transport by τ_g'. This approach is, however, incorrect. It is essentially the same error made considering the transport in the bed in terms of τ_i and τ_g alone, ignoring the effect of the solid's high adsorptive capacity. The simulation results (Figure 3.15) show clearly what actually happens in this case. The benzene concentration in the gas right above the bed (at X = 0) rises very slowly. Transport is actually limited by the supply of benzene across the length L'. The total equilibration time is greater than $100\tau_i$! The concentration profiles in the solid and in the gas-phase within the bed remain practically flat throughout the entire process.

These results, however, do not agree with the experimental data. The NMR spectra in Figure 3.8 equilibrates after about 510 min. ($\approx 3\tau_i$), far before the theoretical value of $100\tau_i$. The fact that operation conditions may be beyond the Henry's law region and that benzene's intra-crystalline diffusivity may increase significantly with concentration [Xiao and Wei, 1992] does not seem sufficient to explain this discrepancy. Besides, the latter effect would be unimportant if intra-crystalline resistance is not the controlling process. In addition, the simulated and experimental results differ in a more subtle way. The simulations show that the concentration in the solid-phase is uniform throughout all the bed, at any given time. Consequently, the NMR spectra should consist of *one single peak*, gradually shifting towards higher chemical shift, as concentration in the bed rises. The experimental spectra, however,

show clearly a peak at low chemical shift that persists during a significant portion of the process, and coexists with an increasing "bump" at higher ω. Only at longer times the spectra coalesces into a single peak. This is an indication of non-uniform adsorbed-phase concentration along the bed. The explanation for this inconsistency became clear after the experimental procedure was analyzed more closely.

After pretreatment of the zeolite sample, the ampoule was filled with xenon at a known pressure (31.6 kPa). The section of the ampoule above the valve (without sample) was then frozen with liquid nitrogen and a known amount of benzene was introduced. After the system is allowed to return to room temperature, the valve was open and benzene penetrated the lower section (containing the sample). This procedure guarantees that the xenon pressure will be the same on both sections, but the total pressure on the upper section would be higher due to the additional presence of benzene. The pressure ratio in the two sections is estimated as being about 1.4.

As a consequence, there is a significant bulk flow of adsorbate into the lower section, in addition to the desired molecular diffusion. The time necessary for the concentration to become uniform in the space above the bed must then be only a few seconds. The model must then be redefined, assuming $L' = 0$ and constant adsorbate concentration at $X = 0$. The new results are shown in Figure 3.16. Now the average solid-phase concentration ($Q_{avg}(X)$) varies significantly along the bed in the initial stages of the process. Figure 3.17 shows the corresponding NMR spectra. Similarly to the experimental data, initially there is a peak at low chemical shift that gradually broadens towards higher chemical shift. Closer to equilibrium, only a single approximately symmetrical peak is visible. The equilibration time in the simulations is still higher than the experimental value, but the difference can now be reasonably interpreted in terms of non-linearity of the isotherm and possible convection into part of the bed's void space.

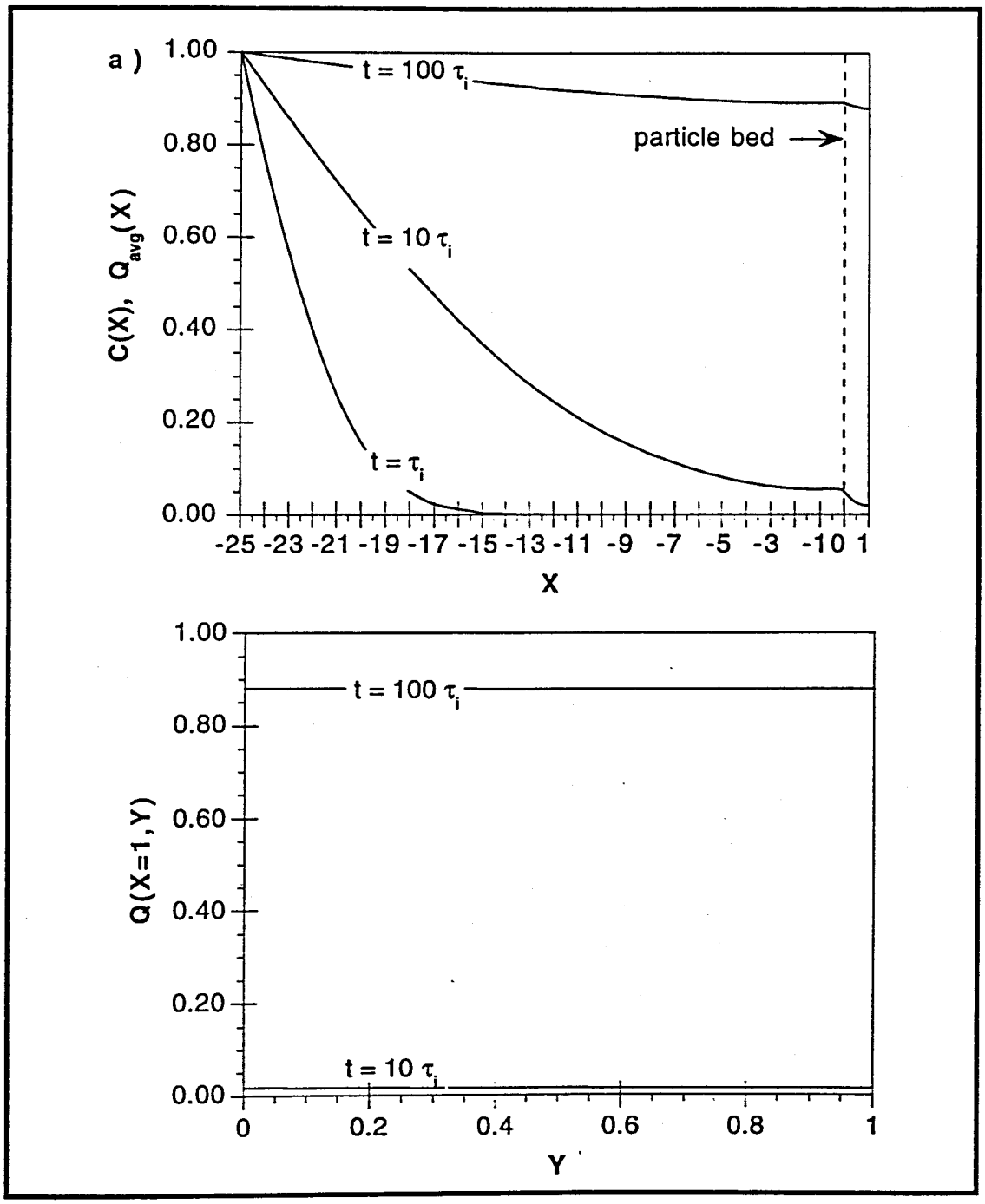

Figure 3.15 Simulated gas-phase concentration profiles for experiment C, with L' = 20 cm. a) $-25 < X < 0$ corresponds to the region above the bed; $0 < X < 1$ corresponds the bed. b) Profiles in the bed region only.

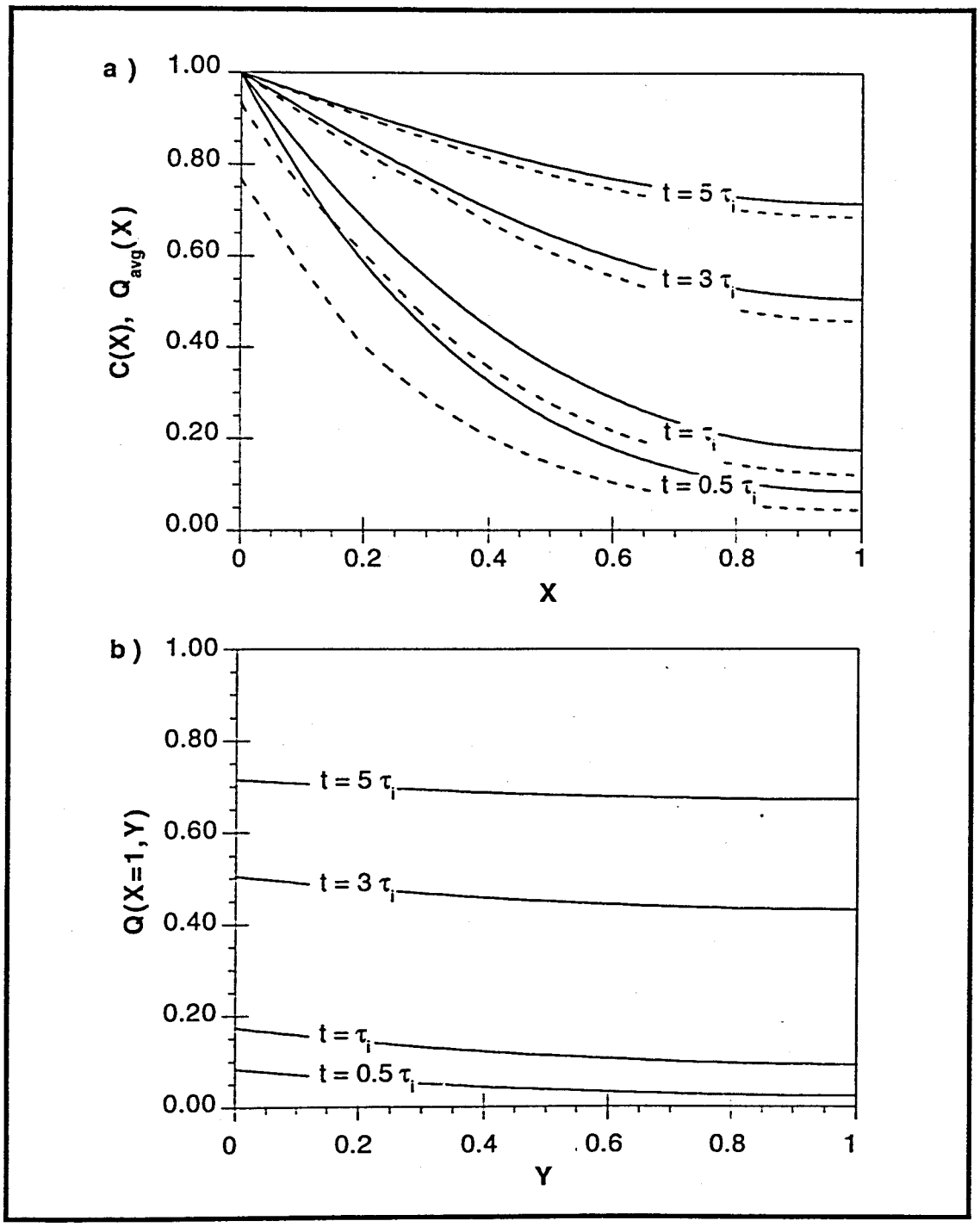

Figure 3.16 Simulated gas and solid-phase concentration profiles for experiment C, with L' = 0. Legend defined as in Figure 3.2.

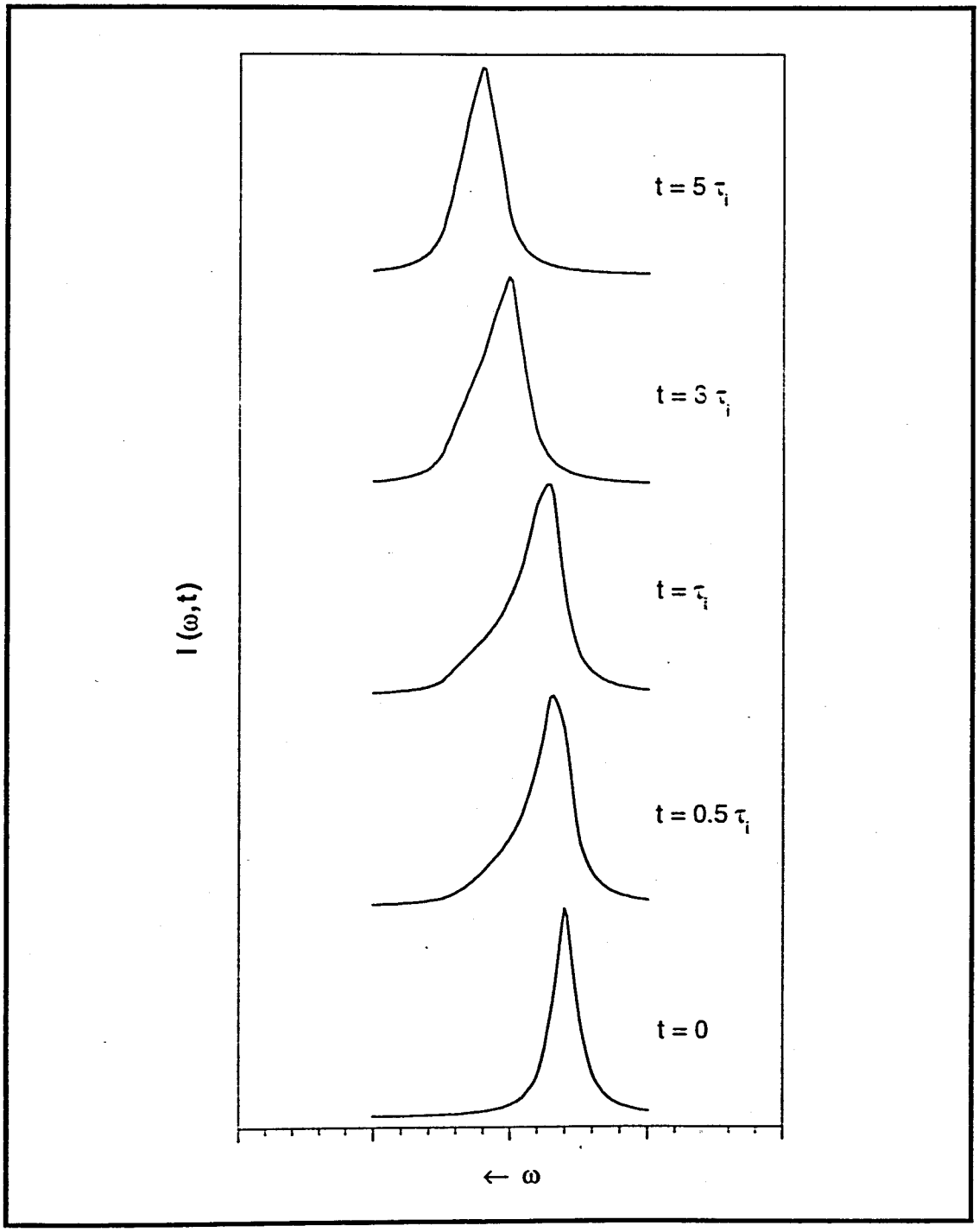

Figure 3.17 Simulated NMR spectra for experiment C.

Experiment D illustrates the case when a concentration front is formed in the adsorbed phase, as discussed in the introduction (Equation 3.7). Since *n*-hexane is adsorbed more strongly in ZSM-5, the solid becomes saturated practically as soon as it is contacted by adsorbate in the gas-phase. The NMR spectra is very characteristic (Figure 3.9): two individual peaks coexist during the entire experiment, at the two chemical shifts corresponding to the saturated and unsaturated portions of the bed. The relative intensities of the peaks change as the front progresses, until only the peak at higher chemical shift remains.

3.6 Conclusions

In order to present an accurate analysis of mass transport in a bed of microporous particles with high adsorption capacity, a simple mathematical model was developed, giving a clear semi-quantitative picture of the process and identifying the significant parameters. Other phenomena, like a surface barrier to mass transfer, can easily be included.

The model provides a qualitative agreement with ^{129}Xe NMR data obtained for adsorption of benzene in a bed of ZSM-5 crystals. The results show how important the transport along the bed (in the extra-crystalline space) might be, even in a small scale system.

Finally, the ^{129}Xe NMR technique itself has been shown to be a powerful tool for the study of transport studies in zeolite systems. Critical information, both qualitative and quantitative, can be obtained from the careful analysis of NMR spectra.

CHAPTER 4

SYSTEMS WITH SURFACE RESISTANCE: TRANSPORT OF *N*-PARAFFINS IN ZEOLITE T

4.1 Introduction

In this chapter the mass transport of some *n*-paraffins in zeolite T is studied using gravimetric sorption/desorption. Investigation of the existence of the "window effect", as reported by Gorring [1973] for this system, was the original goal. Despite the attention and discussion given to this phenomena in the literature [Wei, 1973; Froment and Bischoff, 1990; Wei, 1994], no work has been published confirming Gorring's data. However, evidence of non-diffusional mass transfer (surface barrier) prompted an unconventional analysis of the experimental data. A review of Gorring's work and subsequent studies on the "window effect" is presented in section 2.5. A summary of the existing work concerning surface barriers is given in section 2.7.

The theoretical approach for the study of this system is presented next. It involves modeling of mass transfer and strategies for parameter estimation from experimental data. This is followed by the experimental measurements and respective treatment and discussion.

4.2 Theory

4.2.1 Mathematical Model for a System with External Resistance

The structural relationship between the synthetic zeolite Linde T and the natural zeolites offretite and erionite was elucidated by Bennett and Gard [1967]. They proposed that zeolite T is a disordered intergrowth of erionite and offretite, the latter being the predominant phase. The erionite regions form thin layers within the offretite matrix. They may be viewed as defects in the framework. Fault-free offretite is a typical large pore zeolite like Linde X or Y. Straight pores, formed by circular 12-membered ring apertures (6.7 Å in diameter [Meier and Olson, 1992]), establish a favorable route for diffusion of both linear and cyclical molecules. The erionite intergrowths, as noted by Gorring [1973] and Chen [1972], are bottlenecks in offretite's large pore framework. Diffusion through the erionite regions is possible only through 8-membered rings (3.6×5.1 Å in diameter [Meier and Olson, 1992]) in a zig-zag path. Only linear paraffins are able to pass through apertures with such small dimensions [Barrer and Peterson, 1964; Xiao and Wei, 1992]. This picture suggests that intra-crystalline transport of a linear paraffin in zeolite T can be described by a simple two-resistances-in-series model [Nitsche and Wei, 1991].

$$\frac{1}{D_z} = \frac{\phi_{eri}}{D_{eri}} + \frac{1-\phi_{eri}}{D_{off}} \tag{4.1}$$

One assumes the erionite's resistance term to be dominant. The diffusivity of heptane, in a 8-membered ring system (*e.g.*, zeolite 5A) is 4 orders of magnitude lower than in a 12-membered system (*e.g.*, zeolite X) [Kärger and Ruthven, 1992]. The total volume fraction of erionite in the crystal, ϕ_{eri}, is typically quite small (2-5%) [Chen,

1972; Gorring, 1973]. This may affect the relative importance of the erionite's resistance term in Equation 4.1.

One assumes that the intra-crystalline transport can be described by the diffusion equation. The transport is characterized by an effective diffusion coefficient, D_z, describing diffusion in the two constituent regions. The material balance takes the form:

$$D_z\left(\frac{\partial^2\bar{q}(r,t)}{\partial r^2} + \frac{2}{r}\frac{\partial\bar{q}(r,t)}{\partial r}\right) = \frac{\partial\bar{q}(r,t)}{\partial t} \tag{4.2}$$

with boundary conditions:

$$t = 0 \Rightarrow \bar{q}(r,0) = 0 \tag{4.3}$$

$$r = 0 \Rightarrow \frac{\partial\bar{q}(r,t)}{\partial r}\Big|_{r=0} = 0 \tag{4.4}$$

$$r = R \Rightarrow \bar{q}(R,t) = K\,\bar{C}_i(t) \tag{4.5}$$

$\bar{q}$ and $\bar{C}_i$ are displacement variables:

$$\bar{q}(r,t) = q(r,t) - q(r,0) \tag{4.6}$$

$$\bar{C}_i(t) = C_i(t) - C_i(0) \tag{4.7}$$

The effective diffusivity D_z is assumed constant over the concentration range corresponding to each adsorption (or desorption) step. Furthermore, it is asssumed that K, in Equation 4.5, may be approximated by the local slope of the adsorption isotherm:

$$K(\theta_m) = \frac{\bar{q}(R,t)}{\bar{C}_i(t)} \sim \frac{d(q_{eq})}{d(C_{b,eq})} \Bigg|_{\theta_m} \tag{4.8}$$

where θ_m is the mean fractional occupancy for the corresponding step:

$$\theta_m = \frac{1}{2}\frac{m_0 + m_\infty}{m_{max}} \tag{4.9}$$

(from here on, the subscript will be omitted from θ_m). The approximation in Equation 4.8 is valid only if the step is sufficiently small, enabling the assumption that the isotherm may be assumed as linear over that concentration range. This can be critical at intermediate occupancies, where the isotherm shows the greatest curvature.

Our measured transient uptake curves show a distinct sigmoidal shape. Two other features were added to the model in order to account for this: external resistance to mass transfer, and a non-ideal step in the bulk-gas adsorbate concentration. The external resistance is considered in two alternative formulations (see Figure 4.1): a) the resistance is located in the external gas-phase; and b) the resistance is located in the particle's surface.

The resistance in a) may be associated with a stagnant gas-phase film surrounding the particle or with an ineffective gas-phase mixing between the free stream and the particle bed. The specific nature of these resistances shall not be detailed any

further. It is assumed that they can be expressed in terms of mass transfer coefficients (k_f and k_s, respectively).

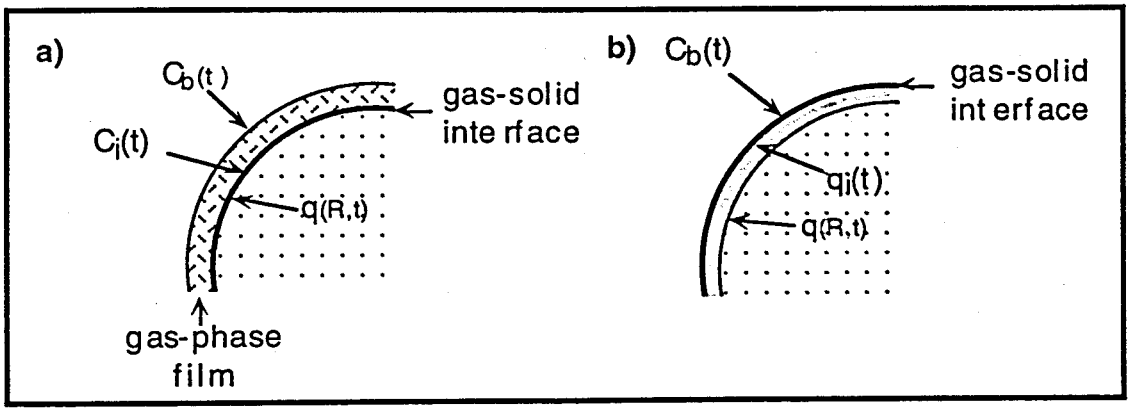

Figure 4.1 Schematic representation of the two formulations for the external resistance: a) external gas-phase resistance; b) particle surface resistance.

The corresponding mass balances are:

$$D_z \left.\frac{\partial \bar{q}(r,t)}{\partial r}\right|_{r=R} = k_f (\bar{C}_b(t) - \bar{C}_i(t)) \tag{4.10}$$

and:

$$D_z \left.\frac{\partial \bar{q}(r,t)}{\partial r}\right|_{r=R} = k_s (\bar{q}_i(t) - \bar{q}(R,t)) \tag{4.11}$$

where:

$$\bar{C}_b(t) = C_b(t) - C_b(0) \tag{4.12}$$

$$\bar{q}_i(t) = q_i(t) - q_i(0) \tag{4.13}$$

The subscript $_i$ denotes concentration at the gas-phase/particle-surface interface. Notice that when considering case b) (Equation 4.11), boundary condition 4.5 takes the form:

$$r = R \Rightarrow \bar{q}_i(R,t) = K \bar{C}_b(t) \tag{4.14}$$

Finally, the bulk gas phase concentration, $\bar{C}_b$, is allowed to be time-dependent. This enables the model to account for the response time of the mass flow controllers, mixing, axial dispersion, parabolic velocity profile, etc. The time-dependence of changes in concentration is probably sigmoidal in shape and can be approximated by the following expression (see Figure 4.2):

$$\bar{C}_b(t) = H(t - \tau_{c1}) \left\{ 1 - \exp\left[- \frac{1}{\tau_{c2}} (t - \tau_{c1}) \right] \right\} \Delta C_b \tag{4.15}$$

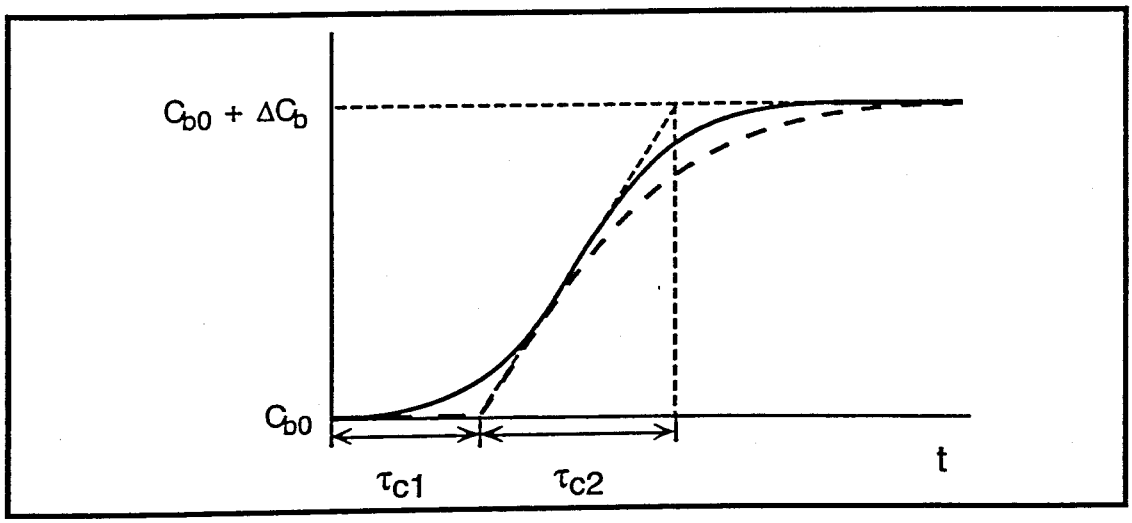

Figure 4.2 Representation of a non-ideal step in the gas-phase concentration, C_b.

The set of three equations that defines the problem (Equations 4.2, 4.10 or 4.11, and 4.15) can be solved after transformation into the Laplace domain. The intra-crystalline mass balance becomes (the "~" over the variables designates their Laplace transform) :

$$D_z\left(\frac{\partial^2\tilde{q}(r,s)}{\partial r^2} + \frac{2}{r}\frac{\partial\tilde{q}(r,s)}{\partial r}\right) = s\,\tilde{q}(r,s) \tag{4.16}$$

$$r = 0 \Rightarrow \left.\frac{\partial\tilde{q}(r,s)}{\partial r}\right|_{r=0} = 0 \tag{4.17}$$

$$r = R \Rightarrow \tilde{q}(R,s) = K\,\tilde{C}_i(s) \quad \text{or} \quad \tilde{q}(R,s) = K\,\tilde{C}_b(s) \tag{4.18}$$

The external resistance:

$$D_z \left.\frac{\partial\tilde{q}(r,s)}{\partial r}\right|_{r=R} = k_f\,(\tilde{C}_b(s) - \tilde{C}_i(s)) \tag{4.19}$$

or:

$$D_z \left.\frac{\partial\tilde{q}(r,s)}{\partial r}\right|_{r=R} = k_S\,(\tilde{q}_i(s) - \tilde{q}(R,s)\,) \tag{4.20}$$

And the gas-phase adsorbate concentration:

$$\tilde{C}_b(s) = \frac{\Delta C_b \exp(-\tau_{c1}\,s)}{s(\tau_{c2}\,s + 1)} \tag{4.21}$$

Equation 4.16 is a modified spherical Bessel's equation, whose solution may be expressed in terms of hyperbolic functions [Abramowitz and Stegun, 1965]. The final expression of $\tilde{q}(r,s)$ is lengthy and is not presented here.

The mean concentration inside the particle, $\bar{Q}(t)$, can be obtained from the concentration profile $\bar{q}(r,t)$ using the following relationship:

$$\frac{4}{3}\pi R^3 \frac{d\,\bar{Q}(t)}{dt} = 4\pi R^2 D_z \left.\frac{\partial \bar{q}(r,t)}{\partial r}\right|_{r=R} \tag{4.22}$$

or, in the Laplace domain:

$$\tilde{Q}(s) = \frac{1}{s}\frac{3}{R} D_z \left.\frac{\partial \tilde{q}(r,s)}{\partial r}\right|_{r=R} \tag{4.23}$$

The resulting expression is, in terms of fractional uptake $f(t) = (m-m_0)/(m_\infty-m_0)$ $= \bar{Q}(t)/K\Delta C_b$:

$$\tilde{f}(s) = \frac{3\exp(-\tau_{c1}\,s)}{(\tau_{c2}\,s+1)\,s\sqrt{s\,\tau_{diff}}\left\{\left[\coth\left(\sqrt{s\,\tau_{diff}}\right) - \left(\sqrt{s\,\tau_{diff}}\right)^{-1}\right]^{-1} + \frac{\sqrt{s\,\tau_{diff}}}{Bi_m}\right\}} \tag{4.24}$$

where τ_{diff} is the time constant for intra-crystalline diffusion:

$$\tau_{diff} = \frac{R^2}{D_z} \tag{4.25}$$

Bi_m is the Biot number for mass transfer. This is defined as:

$$Bi_m = \frac{k_f R}{D_z K} \tag{4.26}$$

when the external mass transfer resistance is associated with a gas-phase resistance (Equation 4.10); or as:

$$Bi_m = \frac{k_s R}{D_z} \tag{4.27}$$

when the resistance is at the particle's external surface (Equation 4.11). Bi_m is related to the ratio between the intra-crystalline diffusion and external resistance time constants.

Analytical solutions in the time domain were obtained by Crank for the separate problems of intra-crystalline diffusion with time-dependent bulk gas phase concentration and intra-crystalline diffusion with external gas-film resistance [Crank, 1975].

Fractional uptake versus time solutions can be obtained by numerically inverting Equation 4.24 into the time domain. The *IMSL* routine *INLAP* was used for this purpose. Some uptake curves are shown in Figure 4.3. Curve (1), obtained for $Bi_m \rightarrow \infty$, corresponds to intra-crystalline diffusion control. In this case, the first portion of the curve is linear with $t^{1/2}$ for small times. From the corresponding slope one can compute the diffusion coefficient D_z directly [Crank, 1975]. This fact (usually referred to as '$\sqrt{t}$ law') is the basis for the traditional treatment of transient uptake experiments. This does not hold, however, when a significant external resistance or non-ideal gas-bulk concentration step is present, since the uptake curves become increasingly sigmoidal in

shape as the Biot number decreases (see Equation 4.26 or 4.27), or as τ_{c1} and τ_{c2} increase.

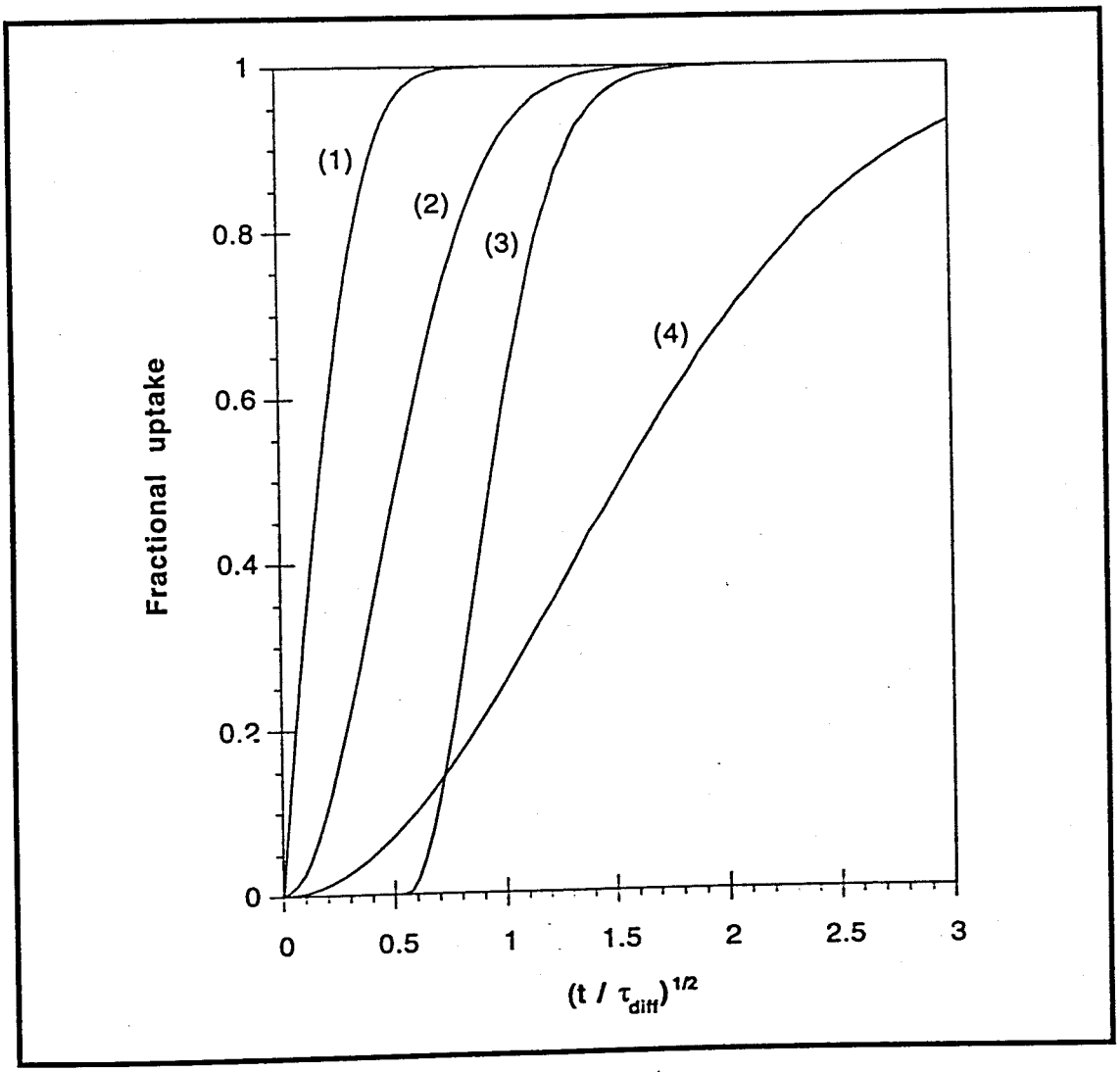

Figure 4.3 Uptake curves obtained by numerical inversion of equation 4.24. The numbers on the curves correspond to the following parameters: (1) $Bi_m \rightarrow \infty$, $\tau_{c1}/\tau_{diff} = 0$, $\tau_{c2}/\tau_{diff} = 0$; (2) $Bi_m = 1$, $\tau_{c1}/\tau_{diff} = 0$, $\tau_{c2}/\tau_{diff} = 0$; (3) $Bi_m = 1$, $\tau_{c1}/\tau_{diff} = 0.3$, $\tau_{c2}/\tau_{diff} = 0.3$; (4) $Bi_m = 0.1$, $\tau_{c1}/\tau_{diff} = 0$, $\tau_{c2}/\tau_{diff} = 0$.

It is also interesting to analyze the limiting case of external resistance control ($D_z \rightarrow \infty$). The only necessary material balance is (for gas-phase resistance):

$$\frac{d\bar{q}}{dt} = \frac{3k_f}{R}(\bar{C}_b - \bar{C}_i) = \frac{3k_f}{R}\left(\frac{\bar{q}_\infty}{K} - \frac{\bar{q}}{K}\right) \tag{4.28}$$

Equation 4.28 can be solved, in terms of the fractional uptake, $f = (m-m_0)/(m_\infty-m_0)$, to yield:

$$\ln(1-f) = -\frac{3k_f}{RK}\,t \tag{4.29}$$

When the resistance is at the surface of the crystal one would obtain:

$$\ln(1-f) = -\frac{3k_s}{R}\,t \tag{4.30}$$

This scenario is a particular case of the complete model, since, when $D_z \rightarrow \infty$, Equation 4.24 becomes the Laplace transform of Equation 4.29 (or 4.30), depending on the definition of Bi_m). Both Equations 4.29 and 4.30 show a linear time-dependence of ln(1-f). This result is commonly described as the criterion for identifying an external gas film or surface resistance control [Kärger and Ruthven, 1992a; Riekert, 1989]. However, this is a necessary but not sufficient condition that external transport is the dominant resistance in the mass transfer process. To show this, plots of log(1-f) versus time are shown in Figure 4.4, for different values of Bi_m. Curves (3) and (4) are both essentially linear. However, curve (3), with $Bi_m = 1$, does not yet correspond to pure external resistance control. This can be seen by comparing curve (3) to the plot of Equation 4.29 (or 4.30) - dashed line on Figure 4.4 - using the relationship:

$$\frac{k_f}{RK} = \frac{Bi_m}{\tau_{diff}} \quad \text{or} \quad \frac{k_s}{R} = \frac{Bi_m}{\tau_{diff}} \tag{4.31}$$

The two plots are only coincident for small values of Bi_m (curve (4)).

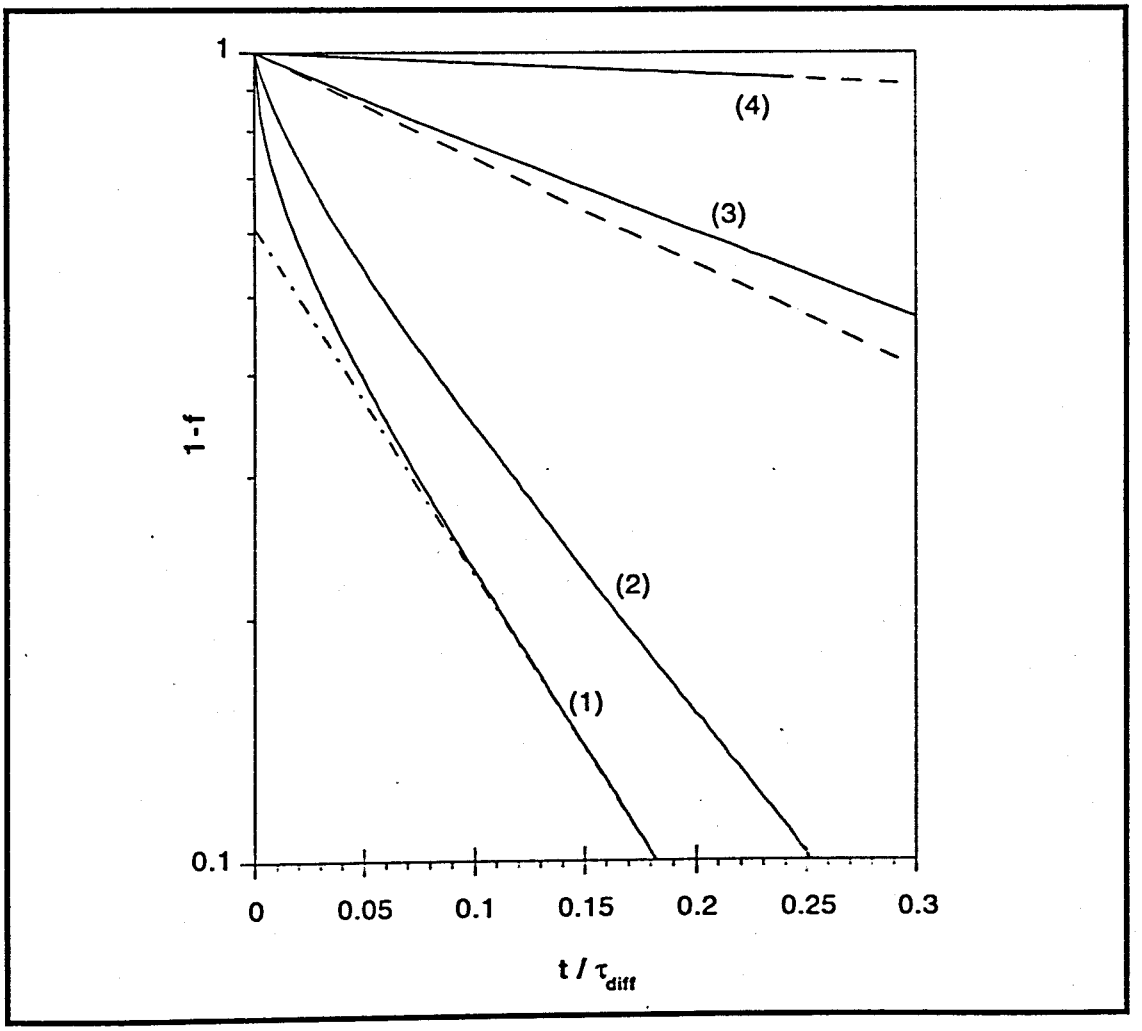

Figure 4.4 Uptake curves obtained by numerical inversion of equation 4.24. $\tau_{c1} = \tau_{c2} = 0$ for all curves. The numbers on the curves correspond to the following values of Bi_m: (1) $Bi_m \rightarrow \infty$; (2) $Bi_m = 10$; (3) $Bi_m = 1$; (4) $Bi_m = 0.1$. The dashed lines are plots of $\ln(1-f) = -3\,t\,(B_{im}/\tau_{diff})$ for the conditions of curves (3) and (4). The dashed-dotted line is the plot of equation 4.32 for the conditions of curve (1).

When the transport process is diffusion-controlled (curve (1) in Figure 4.4), the long-time portion of the curve may be approximated by [Kärger and Ruthven, 1992b]:

$$\ln(1-f) = \ln\left(\frac{6}{\pi^2}\right) - \frac{D_z \pi^2}{R^2} t \qquad (4.32)$$

Thus, D_z can be estimated from the slope of the linear region of the curve (dotted-dashed line in Figure 4.4).

The effect of a delay in the gas concentration step on the log(1-f) versus t curves is shown on Figure 4.5. For small values of τ_{c1}, the curve is essentially shifted to the right, without significant change in slope. As the delay increases, however, the slope at long times is somewhat affected.

4.2.2 Parameter Fitting Using Temporal Moments

The use of the statistical moments obtained from the transient uptake data in the analysis of transport properties was first suggested by Kocirik and Zikánová [1970; 1974]. Their objective was to study the individual contributions to the transport process of the macro and micro-porous regions in a bidisperse material. Dubinin and co-workers [Dubinin et al., 1975] developed the method further, for biporous adsorbents. Kärger and co-workers [Kärger et al., 1982] suggested that measurements of the temporal moments for samples of varying particle radius could be used to identify the limiting process in the kinetic process.

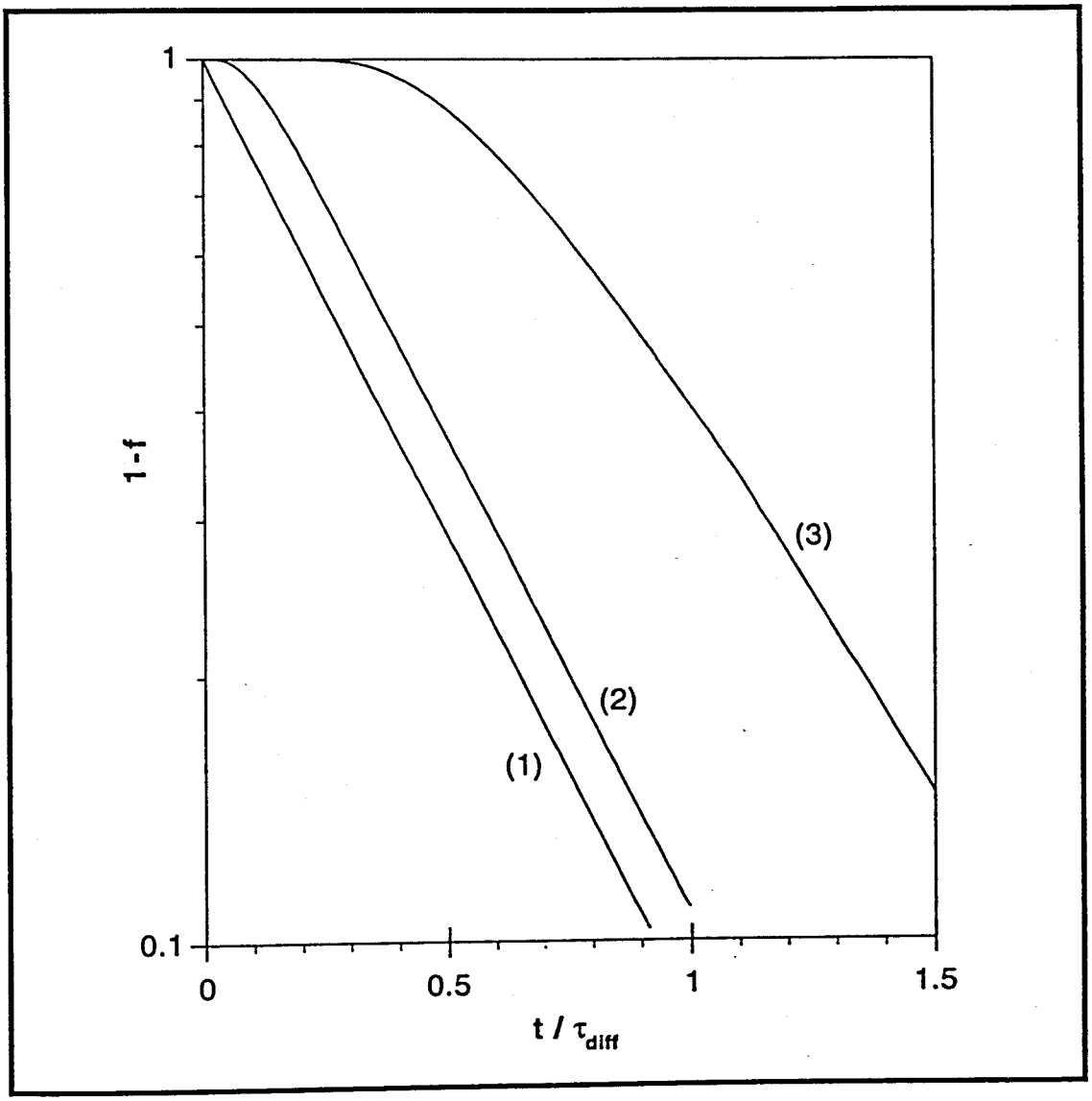

Figure 4.5 Uptake curves obtained by numerical inversion of equation 4.24. $Bi_m = 1$ and $\tau_{c2} = 0$ for all curves. The numbers on the curves correspond to the following values of τ_{c1}: (1) $\tau_{c1}/\tau_{diff} = 0$; (2) $\tau_{c1}/\tau_{diff} = 0.05$; (3) $\tau_{c1}/\tau_{diff} = 0.3$.

The moments are computed in relation to the first time derivative of the fractional uptake, f(t). An analytical expression for the k^{th} moment can be obtained from the Laplace transform $\bar{f}(s)$ (see Equation 4.24):

$$M_k = \int_0^\infty t^k \frac{df}{dt} dt = (-1)^k \lim_{s\to 0} \frac{d^k}{ds^k}\left(L\left\{\frac{df}{dt}\right\}\right) = (-1)^k \lim_{s\to 0} \frac{d^k}{ds^k}(s\bar{f}(s)) \quad (4.33)$$

This way, the following expressions can be derived for the first and second moments:

$$M_1 = (\tau_{c1} + \tau_{c2}) + \frac{\tau_{diff}}{15} + \frac{\tau_{diff}}{3\,Bi_m} \quad (4.34)$$

$$\frac{M_2}{2} = \left(\tau_{c1}^2 + \tau_{c1}\,\tau_{c2} + \frac{\tau_{c2}^2}{2}\right) + (\tau_{c1} + \tau_{c2})\,\tau_{diff}\left(\frac{1}{15} + \frac{1}{3\,Bi_m}\right) +$$

$$+ \tau_{diff}^2\left(\frac{2}{315} + \frac{2}{45\,Bi_m} + \frac{1}{9\,Bi_m^2}\right) \quad (4.35)$$

Equation 4.34, with $(\tau_{c1} + \tau_{c2}) = 0$, is equivalent to the expression derived by Kärger for the mean intracrystalline life time in a N.M.R. tracer desorption experiment [Kärger, 1982].

One does not have to evaluate the time derivatives in order to compute the moments from experimental data, since it can be shown that:

$$M_k = k \int_0^\infty t^{k-1}\,(1 - f(t))\,dt \quad (4.36)$$

Note that the first moment is simply the area under the 1-f(t) curve.

4.2.3 Parameter Fitting in the Fourier Domain

The initial estimates of the model 's parameters (τ_{diff}, Bi_m, τ_{c1}, τ_{c2}) obtained from the experimental moments can, in principle, be improved using the fitting in the Fourier domain. This has been applied successfully to the estimation of diffusion coefficients in a two-parameter model of chromatographic column with a polymer-coated capillary [Arnould and Laurence, 1989]. The Fourier transform of the model can be obtained from Equation 4.24 since:

$$\hat{g}(k) = \frac{1}{t_\infty}\int_0^{t_\infty} g(t)\exp\left(-\frac{i\pi kt}{t_\infty}\right)dt = \frac{1}{t_\infty}\tilde{g}(s) \quad \text{with } s = \frac{i\pi k}{t_\infty} \qquad (4.37)$$

where:

$$g(t) = 1 - f(t) \quad \text{and} \quad \tilde{g}(s) = L\{g(t)\} = \left(\frac{1}{s} - \tilde{f}(s)\right) \qquad (4.38)$$

The Fourier transform of the experimental uptake curve (more precisely, of 1-f(t)) is first computed, and then the difference between this and the theoretical transform minimized. This optimization is based on a least-squares criterion, since, according to Parseval's theorem, this criterion is equivalent in the time and Fourier domains. The objective function is then:

$$F_{obj} = \int_0^\infty \{[Re_{exp}(\omega) - Re_{theo}(\omega)]^2 + [Im_{exp}(\omega) - Im_{theo}(\omega)]^2\}d\omega \qquad (4.39)$$

where Re(ω) and Im(ω) are, respectively, the real and imaginary parts of the experimental or theoretical transforms. The parameter values computed from the statistical moments are used as initial estimates. A modified Levenberg-Marquardt algorithm (IMSL routine BCLSF) was used for the fitting.

This problem shows, however, some particular features that seriously restrict the applicability of the technique. This is exemplified in Figure 4.6. A 'true solution' corresponding to $\tau_{diff} = 100$, $Bi_m = 1$, and $\tau_{c1} = \tau_{c2} = 0$ was assumed. The objective function, F_{obj}, was then mapped for different values of the optimization parameters τ_{diff} and Bi_m (τ_{c1} and τ_{c2} were kept constant to simplify the analysis). F_{obj} is zero for the true solution and greater than zero elsewhere. In an ideal problem, the optimization surface would be a sharply defined well converging to the true solution (the absolute minimum). Figure 4.6 indicates that our problem is far from ideal. The response surface forms a 'canyon'. Its floor is relatively wide and has a very flat gradient towards the true solution. The consequences are obvious: noisy experimental data cause the floor of the canyon to be unavoidably uneven, creating local minima. Finding the 'true solution' becomes practically impossible.

More optimization parameters make the task even more difficult. Indeed, a similar problem exists the optimization surface defined by parameters τ_{diff} and τ_{c1}. Figure 4.7 shows another 'canyon', along which the local minima will appear.

The canyon's base, projected on the τ_{diff} - Bi_m plane in Figure 4.6, appears to follow Equation 4.34 with M_1 equal to the first moment of the true solution (40 seconds) (see curve on the upper graph of Figure 4.6). An infinite set of values of τ_{diff} and Bi_m, correlated by Equation 4.34, generate uptake curves with the same first moment and an almost identical image in the Fourier domain as the true solution.

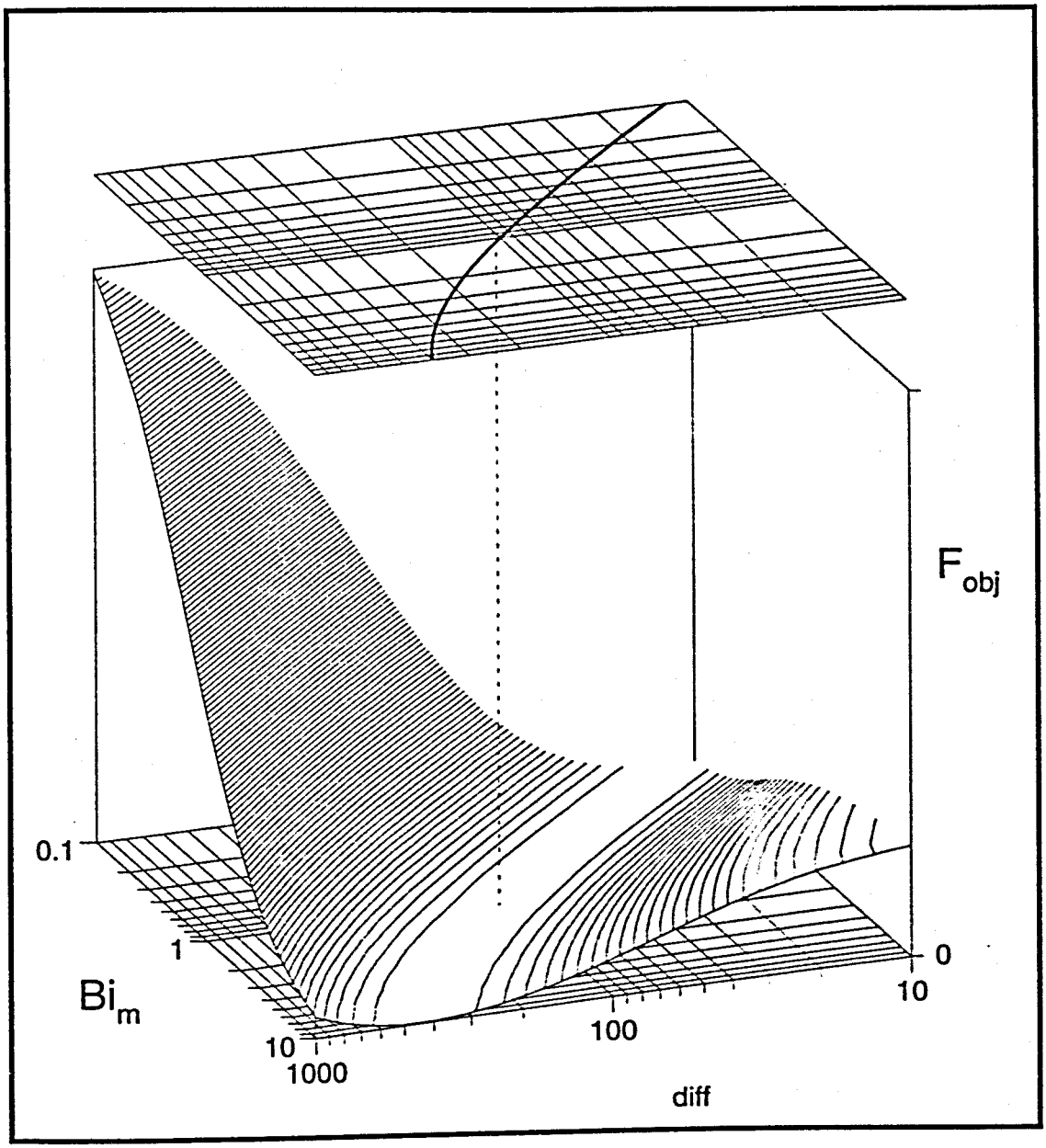

Figure 4.6 Optimization surface for the 'true solution': $\tau_{diff} = 100$ s, $Bi_m = 1$, and $\tau_{c1} = \tau_{c2} = 0$ s. Curve on the upper graph is defined by equation (34) with $M_1 = 40$ s and $\tau_{c1} = \tau_{c2} = 0$ s.

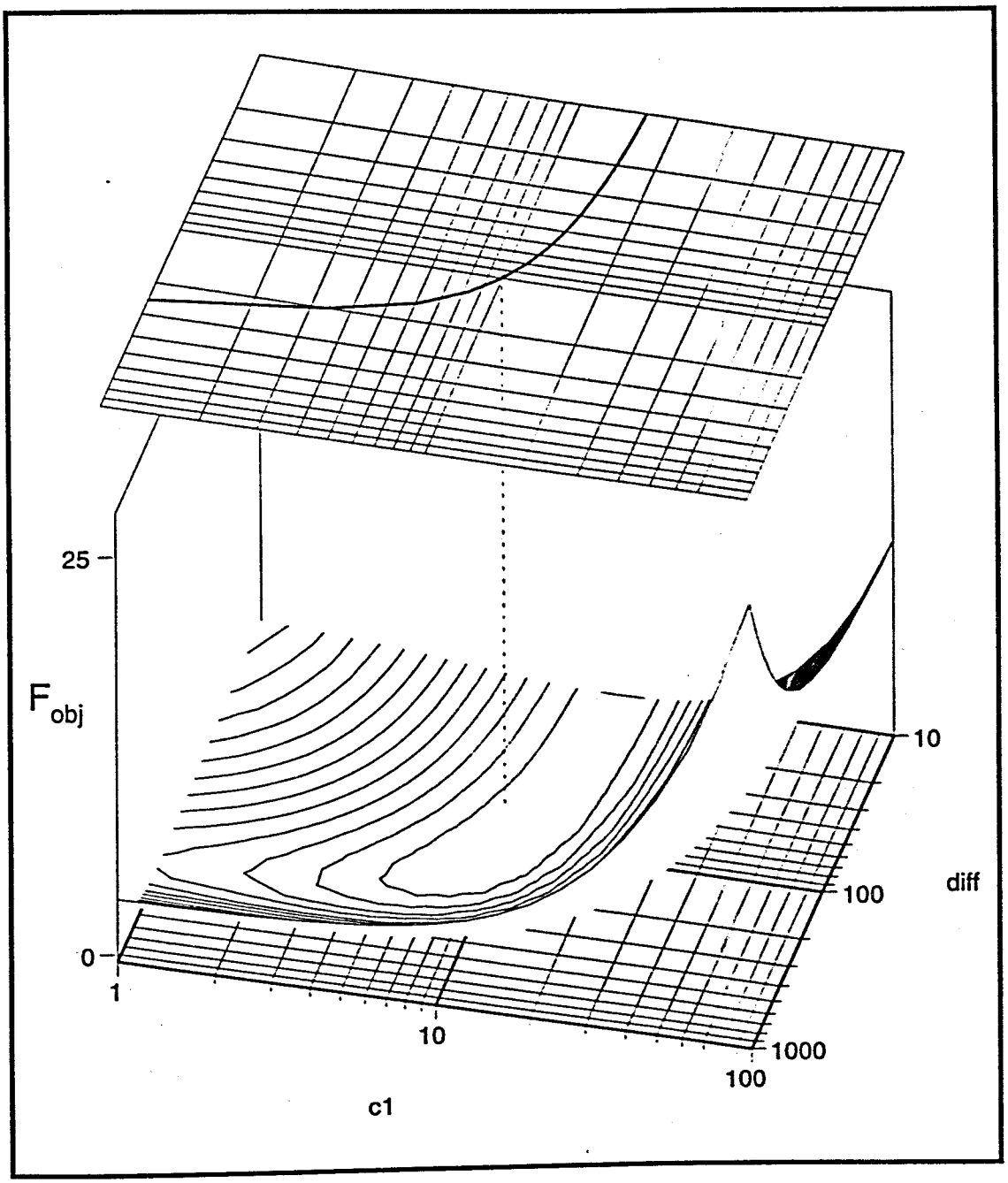

Figure 4.7 Optimization surface for the 'true solution': $\tau_{diff} = 100$ s, $\tau_{c1} = 10$, $Bi_m = \infty$ and $\tau_{c2} = 0$ s. Curve on the upper graph is defined by equation 4.34 with $M_1 = 140$ s and $Bi_m = \infty$, $\tau_{c2} = 0$ s.

This observation can be rationalized when the equations for the temporal moments (4.34 and 4.35) are analyzed more closely. Some manipulation yields the following relationships:

$$\text{when } \tau_{c1} = \tau_{c2} = 0: \quad \frac{M_2}{2} = M_1^2 + \frac{3}{1575}\tau_{diff}^2 \tag{4.40}$$

$$\text{when } Bi_m = \infty, \tau_{c2} = 0: \quad \frac{M_2}{2} = M_1^2 - \frac{2}{15}\tau_{diff}\tau_{c1} + \frac{3}{1575}\tau_{diff}^2 \tag{4.41}$$

For low values of τ_{diff}, Equation 4.40 becomes $M_2 = 2\,M_1^2$. The second moment dependends only on the first moment. Therefore, Equation 4.40 cannot be used with 4.34 in order to compute the two parameters, τ_{diff} and Bi_m. These are then correlated by the equation of the first moment (4.34). The same happens in Equation 4.41 when both τ_{diff} and τ_{c1} have low values.

The difficulties predicted by these observations were confirmed when working with experimental data. Depending on the initial estimates, numerous sets of parameters can be obtained from the fitting of a single uptake curve, and it was impossible to identify the true optimum solution. Parameter estimation in the Fourier domain is therefore essentially useless in the analysis of this problem.

4.3 Experimental

4.3.1 Materials

The zeolite T samples used in this work were prepared by A. W. Peters at W. R. Grace. The final composition was similar to Gorring's: alumina 16.0%, silica 70.5%, potassium 13.3%, sodium 0.2%.

Electron micrographs revealed that the zeolite particles had an ellipsoidal shape (about 1.6 μm in length and 0.8 μm in width). An average equivalent sphere diameter of 1.13 μm was assumed.

Prior to use, the samples were calcined in air at 450 °C for 24 hr and outgassed at 400 °C and 10^{-5} Torr for 12 hr. Heating rates were kept low to avoid possible thermal stress effects on the framework.

4.3.2 Apparatus

The experimental setup is shown in Figure 4.8. A Cahn 2000 electrobalance was used for the weight measurements. The sample (20 to 30 mg) was placed in a aluminum weighing pan (~ 1 cm in diameter) inside a vertical glass column (~ 2.1 cm in diameter). Helium (the carrier gas) was introduced from below. The glass column was wrapped in heating tape and insulated. A Eurotherm temperature controller, connected to a thermocouple located immediately below the sample pan, regulated the temperature within 1°C. To guarantee saturation, two bubblers in series were used to introduce the adsorbate. Molecular sieve was used to adsorb water eventually dissolved in the liquid.

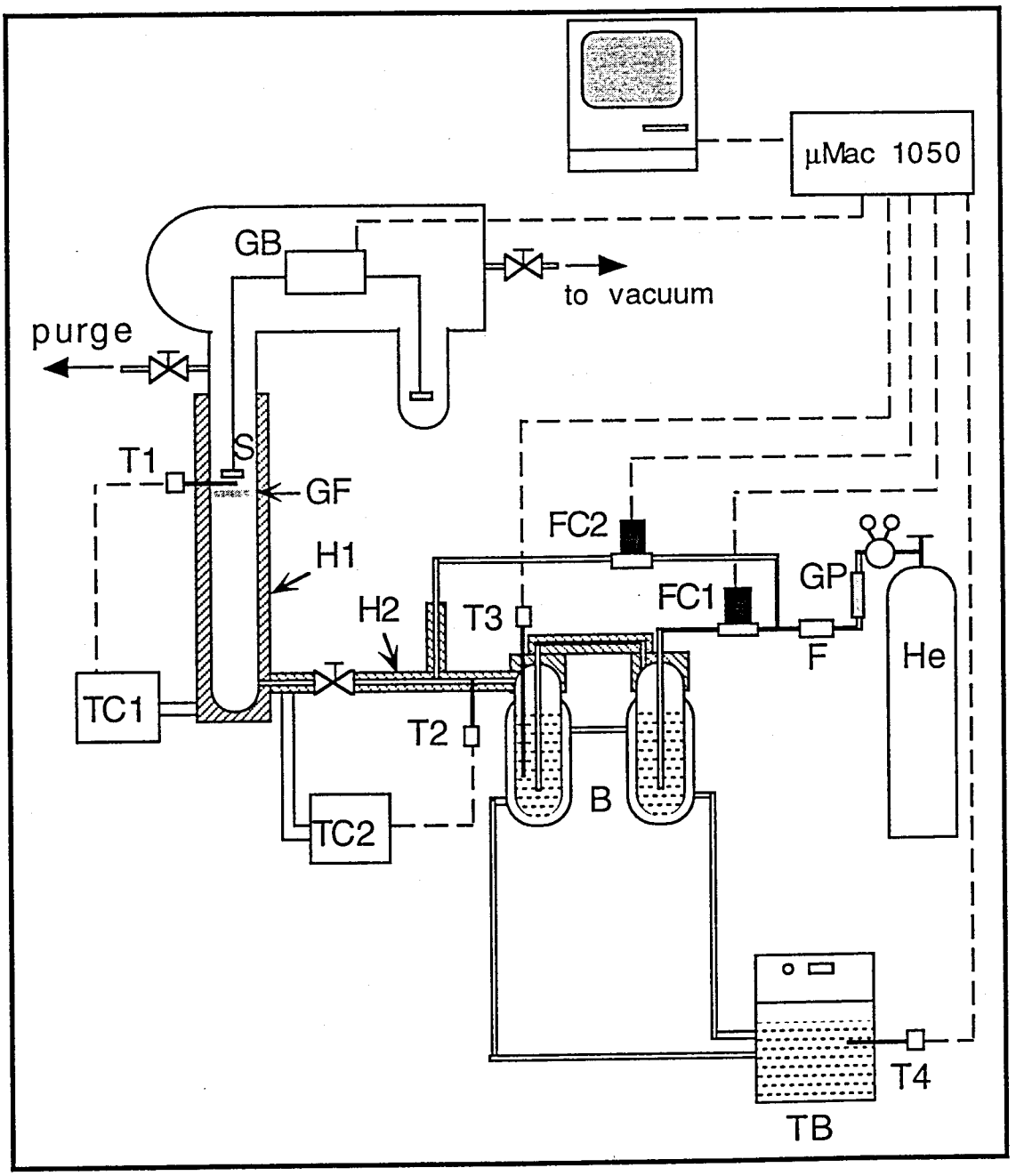

Figure 4.8 Schematic representation of the experimental apparatus. Legend: B - jacketed sorbate bubblers; F - filter; FC1, FC2 - mass flow controlers; GB - microgravimetric balance; GF - glass frit; H1, H2 - heated regions; GP - gas purifier; T1, T2, T3, T4 - thermocouples; TB - thermostatic bath; TC1, TC2 - temperature controlers; S - sample pan.

A Haake thermal bath circulated heating/cooling fluid through the bubblers' external jackets. The stream of helium plus adsorbate coming from the bubblers was then diluted with a stream of pure helium. The flow rates of both streams were regulated by two Tylan mass flow controllers. Setting the temperature in the bubblers and the ratio between the two gas streams flow rates allowed control of the adsorbate concentration in the gas over the sample. To guarantee saturation of the bubblers stream, this flow rate was never greater than to 20 cm^3/min. The total gas flow rate going through the sample was always 100 cm^3/min.

Data acquisition was performed with an Azonix μMac 1050 unit connected to a Macintosh SE computer. Besides the transient weight measurements, the output and set points of the mass flow controllers were also monitored.

4.4 Results and Discussion

Experimental studies were performed with *n*-Heptane, *n*-Nonane and *n*-Dodecane. The results obtained and the corresponding analysis are presented next. For each adsorbent, the text is divided into discussion of sorption isotherms and transient mass transfer measurements.

4.4.1 *n*-Heptane

4.4.1.1 Isotherms

The sorption isotherms were obtained gravimetically at three different temperatures (200, 250 and 300 °C). These are shown in Figure 4.9. Since an explicit mathematical expression of the local slope of the isotherm, K, is necessary in the

analysis of the transient uptake data, the data was fitted with simple equations for the isotherms. The best results were obtained by adding an interaction factor, β, to the Langmuir isotherm [Barrer, 1971]:

$$p = \frac{\theta\, e^{\beta\theta}}{\alpha\,(1 - \theta)} \qquad (4.40)$$

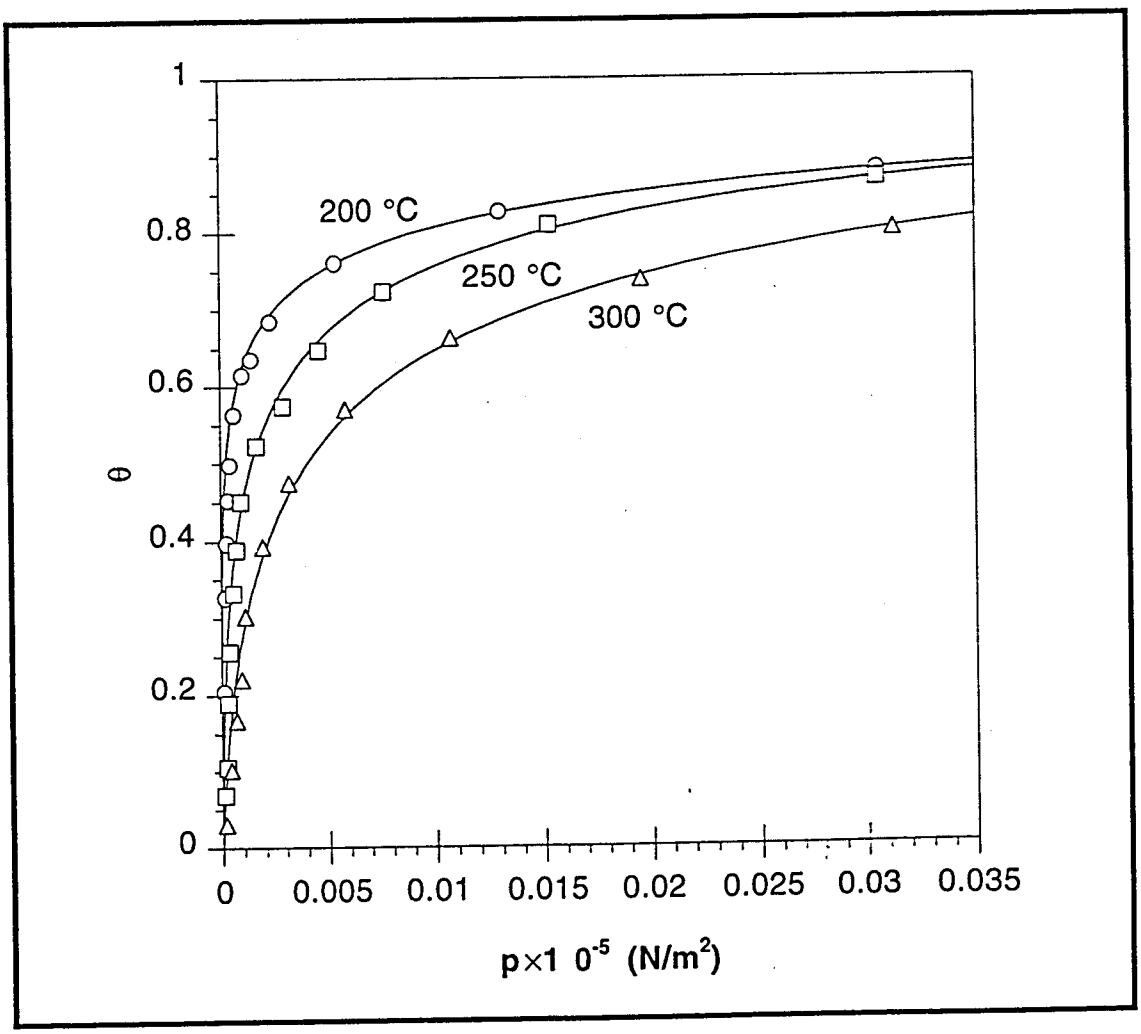

Figure 4.9 Isotherms for n-heptane sorption. The curves correspond to the fits of Equation 4.40 to the experimental data.

The parameter β can be interpreted as an interaction parameter: $\beta > 0$ implies repulsion between adsorbed molecules and $\beta < 0$ attraction. Equation 4.40 becomes the Langmuir isotherm when $\beta = 0$. One is not, however, concerned with a detailed analysis of the physical significance or accuracy of this model. As mentioned before, our only purpose is to obtain a simple analytical expression for K. This has the form:

$$K(\theta) \sim \frac{d(q_{eq})}{d(C_{b,eq})}\Big|_{\theta} = \left(\frac{R_g T\, d_z\, m_{max}}{M_w\, m_{sample}}\right)\frac{d\theta}{dp} =$$

$$= \left(\frac{R_g T\, d_z\, m_{max}}{M_w\, m_{sample}}\right)\frac{\alpha\,(1-\theta)^2}{e^{\beta\theta}\,(1 + \beta\theta - \beta\theta^2)} \qquad (4.41)$$

A value of d_z (the framework density) = 1.50 g/cm^3 for zeolite T was obtained from Breck [1974b].

The values computed for parameters α and β are shown in Table 4.1.

Table 4.1 Parameters α and β obtained from fitting Equation 4.40 to experimental sorption isotherms of *n*-heptane.

Temperature (°C)	α ((N/m^2)$^{-1}$)	β
200	1.82	7.52
250	3.41×10^{-2}	3.16
300	3.89×10^{-3}	1.46

4.4.1.2 Transient Mass Transfer

Each adsorption (or desorption) step was assumed isothermal, given the use of helium as carrier gas and the small amounts of sample employed. Furthermore, no significant change in the uptake data was detected by changing sample size.

One important aspect in these experiments is the step size. The change in adsorbate loading in each adsorption or desorption step should be small enough to guarantee the validity of the assumptions of constant local diffusivity and local isotherm linearity. If the step is too small, though, the base line noise may affect the measurements. One can usually find the correct operation conditions by successively decreasing the step size until the uptake curves become essentially invariant. Also, agreement between adsorption and desorption curves can be used as a criterion. Garg and Ruthven [1972] have shown that, in a system where intra-crystalline diffusion is concentration-dependent, adsorption and desorption curves will show an apparent diffusion coefficient higher than the true value. The discrepancy is stronger for the adsorption curves, and increases drastically with increasing step size. The magnitude of this effect should depend on the particular type of the isotherm. In general, it was found in this work that consistency between adsorption and desorption curves could be obtained with step changes in the sorbed amount not greater than about 8% of the maximum loading.

A mass spectrometry analysis of the effluent during desorption showed no evidence of hydrocarbon cracking at the higher temperatures. The good reproducibility of the measurements and visual inspection of the samples after use indicated that coking was not significant.

The analysis of the transient data was based on the temporal moments of the uptake curves. The first moment was computed, as described previously (Equation

4.33), for different occupancy levels. The results were fit to the theoretical model (Equation 4.34) assuming four possible cases:

Model (I): The intra-crystalline diffusivity, D_z, is concentration-dependent. The relationship between D_z and θ (the mean occupancy for each adsorption, or desorption, step) is obtained from the Darken equation:

$$D_z(\theta) = D_{z0} \frac{d \ln(p)}{d \ln(q)} \Bigg|_{\theta} \tag{4.43}$$

This equation has been widely used to describe the concentration dependence of the diffusivity measured in different zeolite systems [Ruthven and Loughlin, 1971; Ruthven et al., 1973; Vavlitis et al., 1981]. D_{z0} is commonly designated as the "corrected diffusivity" (generally identified with the self-diffusivity) and its weak concentration-dependence may be neglected in this kind of measurements [Ruthven, 1984].

The derivative in Equation 4.43 is obtained from the adsorption isotherm. Thus, from 4.40 one obtains:

$$D_z = D_{z0}\left(\frac{1}{1-\theta} + \beta\,\theta\right) \tag{4.44}$$

In addition, gas-phase mass transfer resistance is assumed, and consequently $K(\theta)$ must be evaluated from Equation 4.41.

After substitution, Equation 4.34 becomes:

$$M_1 = (\tau_{c1} + \tau_{c2}) + \frac{1}{15}\frac{R^2}{D_{z0}}\frac{1}{\frac{1}{1-\theta} + \beta\,\theta} + \frac{1}{3}\frac{R}{k_f}\,K(\theta) \qquad (4.45)$$

The fitting parameters in the model are D_{z0} and k_f. $(\tau_{c1} + \tau_{c2})$ is estimated by direct extrapolation from the experimental data for $\theta \rightarrow 1$.

Model (II): D_z is again concentration-dependent, but now the more simple relationship is assumed:

$$D_z = D_{z0}\frac{1}{1-\theta} \qquad (4.46)$$

This result can be obtained from Equation 4.43 in the case of an ideal Langmuir isotherm ($\beta = 0$). Even though the isotherms described in this work are not ideal, it is important to test the relationship of Equation 4.46, since this is actually the form of the dependence commonly described in the literature.

In relation to the external mass transfer resistance, the assumptions are the same as in model I. The final expression for M_1 is then:

$$M_1 = (\tau_{c1} + \tau_{c2}) + \frac{1}{15}\frac{R^2}{D_{z0}}(1 - \theta) + \frac{1}{3}\frac{R}{k_f}\,K(\theta) \qquad (4.47)$$

Once again, the fitting parameters are D_{z0} and k_f. $(\tau_{c1} + \tau_{c2})$ is estimated by direct extrapolation from the experimental data for $\theta \rightarrow 1$.

Model (III): D_z is not concentration-dependent. The variation of M_1 with occupancy is given only by the external gas-film resistance term:

$$M_1 = C + \frac{1}{3}\frac{R}{k_f} K(\theta) \tag{4.48}$$

where $C = (\tau_{c1} + \tau_{c2}) + \frac{1}{15}\frac{R^2}{D_z}$. C and k_f are the fitting parameters.

Model (IV): D_z is concentration-dependent, according to Equation 4.44. The external resistance is now assumed to be at the particle surface, and is represented by k_s (invariant with loading). The corresponding term is therefore independent of θ:

$$M_1 = C + \frac{1}{15}\frac{R^2}{D_{z0}} \frac{1}{\frac{1}{1-\theta} + \beta\,\theta} \tag{4.49}$$

where $C = (\tau_{c1} + \tau_{c2}) + \frac{1}{3}\frac{R}{k_s}$. C and D_{z0} are the parameters to estimate. Note that k_s is, so far, assumed as concentration-independent. The validity of this hypothesis will be discussed later.

Model (V): D_z is concentration dependent, according to Equation 4.44. The external resistance is associated to nonequilibrium sorption conditions at the surface. Micke and co-workers [Micke et al., 1994] used Langmuir kinetics to model this phenomena. Their model leads to a pseudo surface barrier at the particle surface, with k_s being concentration dependent (Equation 4.50).

$$k_s = k_a\, p + k_d = k_a \frac{\theta\, e^{\beta\theta}}{\alpha\ (1 - \theta)} + k_d \tag{4.50}$$

M_1 is then given by:

$$M_1 = (\tau_{c1} + \tau_{c2}) + \frac{1}{15}\frac{R^2}{D_{z0}}\frac{1}{\frac{1}{1-\theta} + \beta\,\theta} + \frac{1}{3}\frac{R}{k_a \frac{\theta\, e^{\beta\theta}}{\alpha\,(1-\theta)} + k_d} \qquad (4.51)$$

The fitting parameters are D_{z0}, k_a and k_d.

One critical assumption is present in all these formulations. As discussed above, intra-crystalline mass transport should be controlled by the erionite regions. Thus, the concentration dependence of D_z should be established in terms of the occupancy in these regions. However, only the total occupancy, θ, is known. One has, therefore, to assume uniform coverage of the entire framework for each step. The consequences of this assumption will be discussed later.

Experimental values of M_1 as a function of $(1-\theta)$ are plotted in Figures 4.10 to 4.12 for adsorption and desorption steps of heptane at 200, 250 and 300 °C. The "best fits" of the models previously described are also shown (model (IV) is shown only in Figure 4.11). A least-squares criteria was employed for these evaluations. It must be noted firstly that the moments computed from adsorption and desorption steps are in good agreement. This was also confirmed by comparing the shape of the adsorption and desorption curves. Since one expects the moments computed from desorption steps to be closer to the "true" value, only these were used for the parameter estimation.

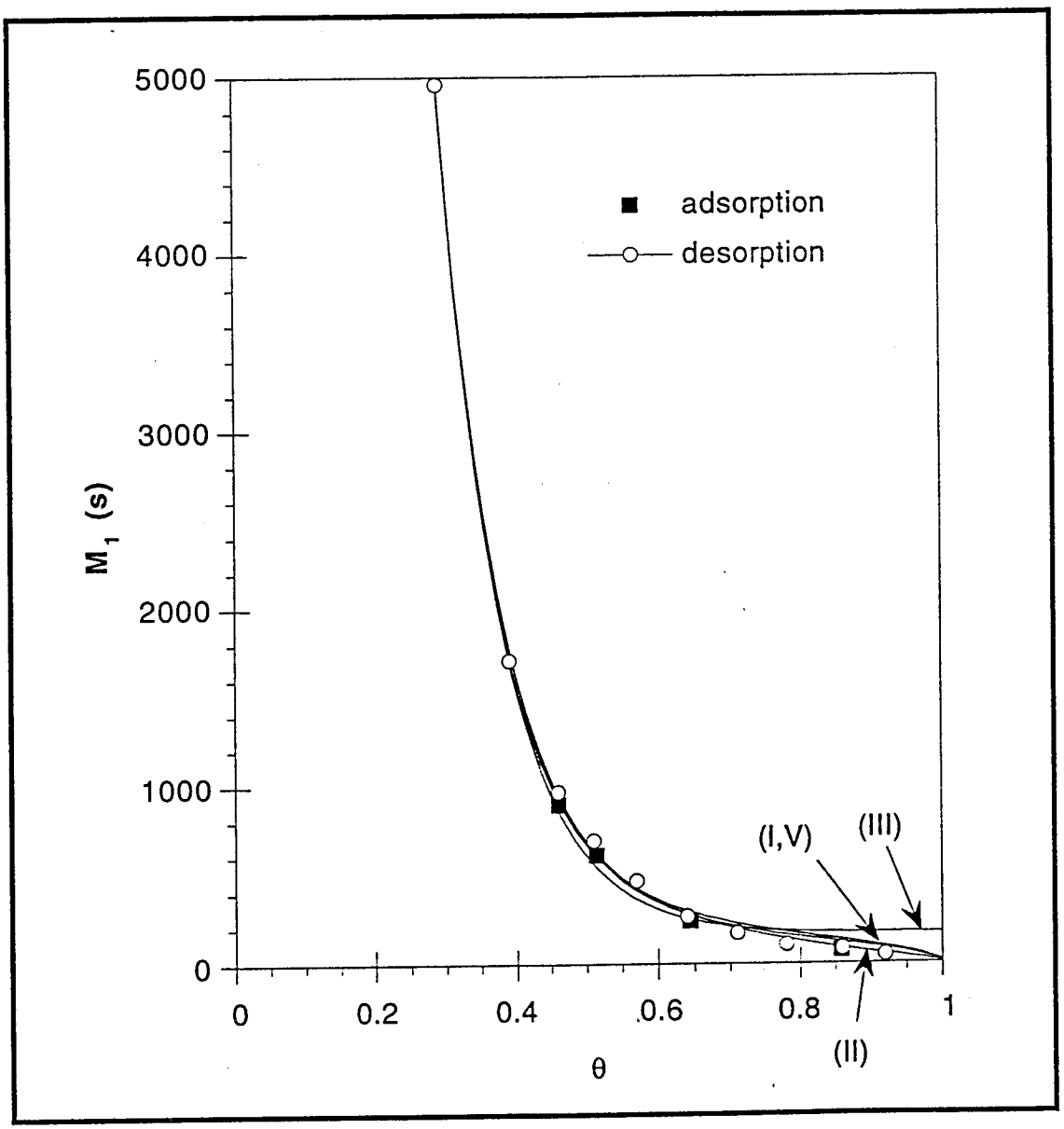

Figure 4.10 First moment data computed from heptane adsorption and desorption at 200 °C. The roman numeral on each line designates the model.

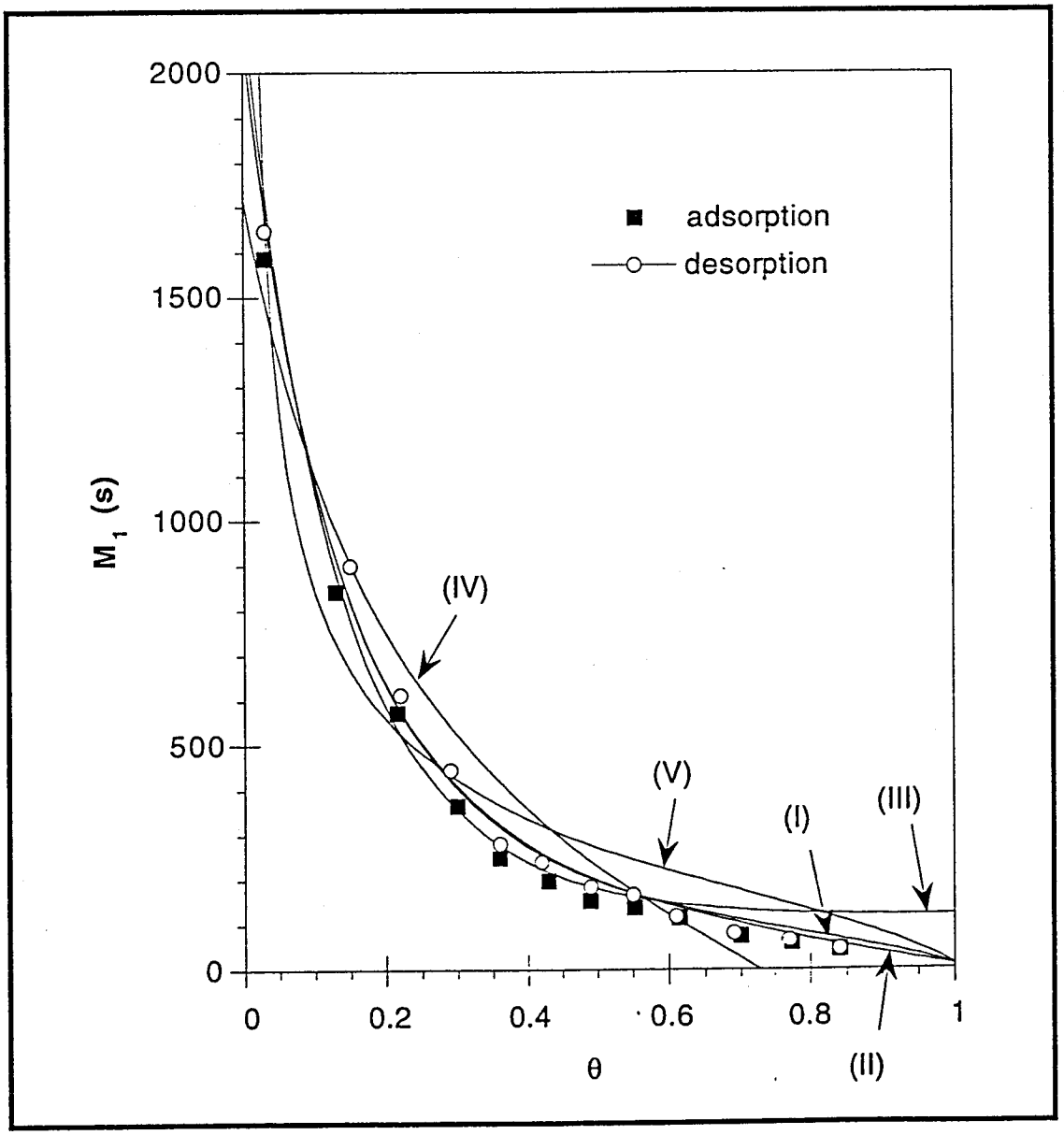

Figure 4.11 First moment data computed from heptane adsorption and desorption at 250 °C. The roman numeral on each line designates the model.

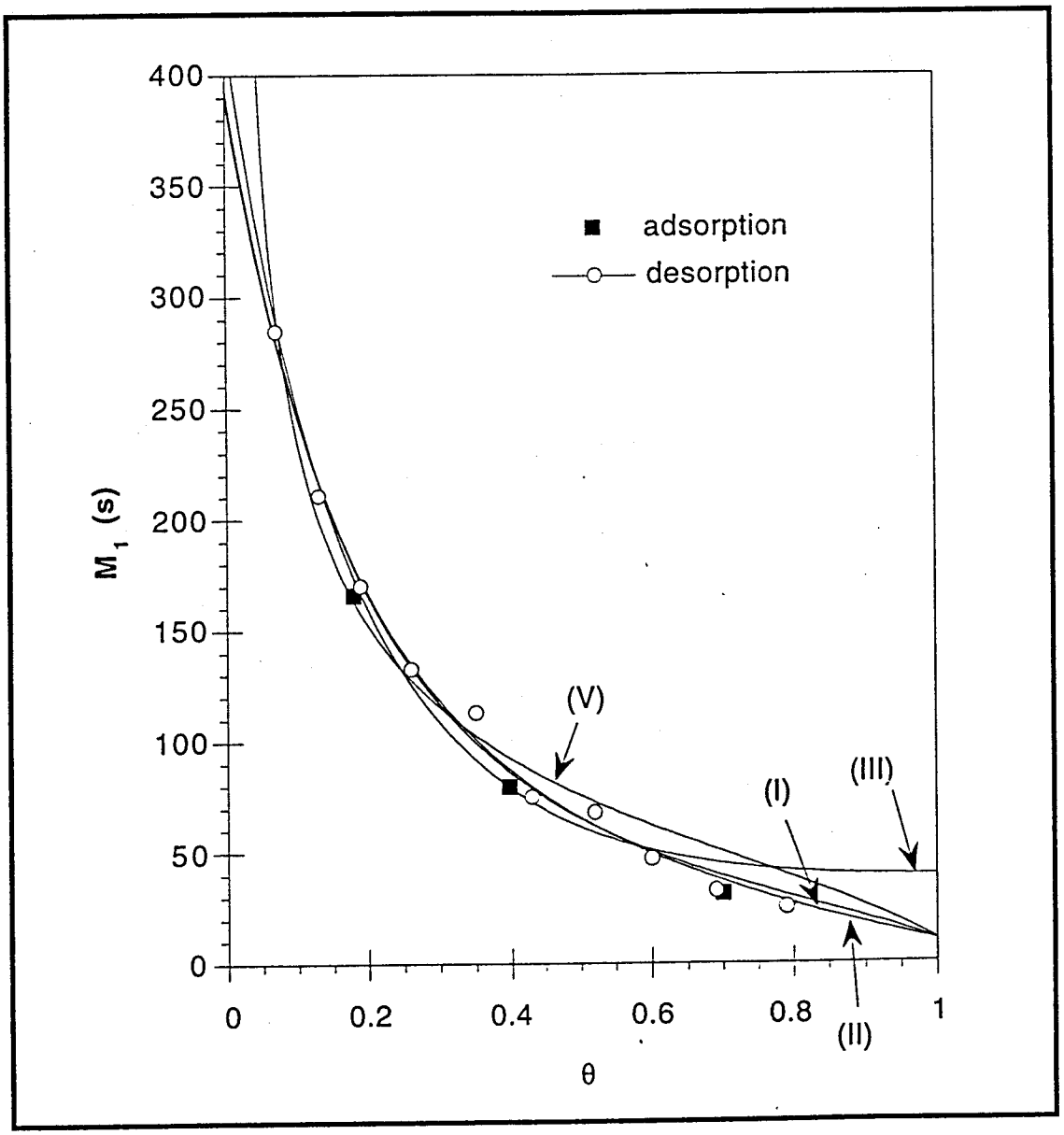

Figure 4.12 First moment data computed from heptane adsorption and desorption at 300 °C. The roman numeral on each line designates the model.

It was assumed that $(\tau_{c1} + \tau_{c2}) = 10$ s. This value was obtained from rough extrapolation of the data points at all temperatures for $\theta \rightarrow 1$ (the point at which the time constants for the other processes should vanish). The contribution of the non-ideal gas-phase concentration step to the dynamics of the global transport process is therefore relatively insignificant. This was verified by observing that no significant change in the uptake curves occurred when the measurements were performed at different carrier gas flow rates. In addition, reproducible results were also obtained with different amounts of sample, indicating that transport in the gas-phase along the bed and in the unmixed region above it is not limitant, and therefore reinforcing the idea that we are in presence of a surface barrier effect.

It is immediately clear that only models (I) and (II) fit the data properly over the entire range of occupancies and temperatures. Model (V) fits the data only at the lower temperature (200 °C). The values of the parameters D_{z0} and k_f corresponding to the fits of models (I) and (II) are shown in Table 4.2.

Table 4.2 Parameters D_{z0} and k_f obtained from fitting models (I) and (II) to experimental values of M_1 for heptane.

Temperature (°C)	model (I)		model (II)	
	D_{z0} (cm^2/s)	k_f (cm/s)	D_{z0} (cm^2/s)	k_f (cm/s)
200	1.41×10^{-13}	4.41×10^{-4}	3.82×10^{-13}	4.40×10^{-4}
250	4.41×10^{-13}	1.09×10^{-3}	7.54×10^{-13}	9.46×10^{-4}
300	1.71×10^{-12}	1.30×10^{-3}	2.75×10^{-12}	1.12×10^{-3}

The values obtained for D_{z0} and k_f were then used in Equation 4.35 to compute the second moment, and the results compared to the experimental values of M_2 (see Figures 4.13 - 4.15). The agreement is quite good, considering the expected larger error in the computation of M_2 from experimental data. Once again, only models (I) and (II) seem to describe the trend of the experimental data for all θ. Model (II), actually, seems to give the best fits. Model (III) does not even reproduce the trend of the experimental data. Model (V) does not give satisfactory results at the two higher temperatures.

The activation energies corresponding to the intra-crystalline and external resistance coefficients can then be estimated, even though we are aware of the limited precision involved in a computation based on only three temperatures. The corresponding Arrhenius plots are shown in Figures 4.16 and 4.17.

The values of E_a determined by Gorring for *n*-heptane are also shown in Figure 4.16. His diffusivities are about one order of magnitude lower than the values obtained in this work. The activation energies obtained from the estimates of models (I) and (II) (see Table 4.3) are 11% and 30%, respectively, lower than Gorring's.

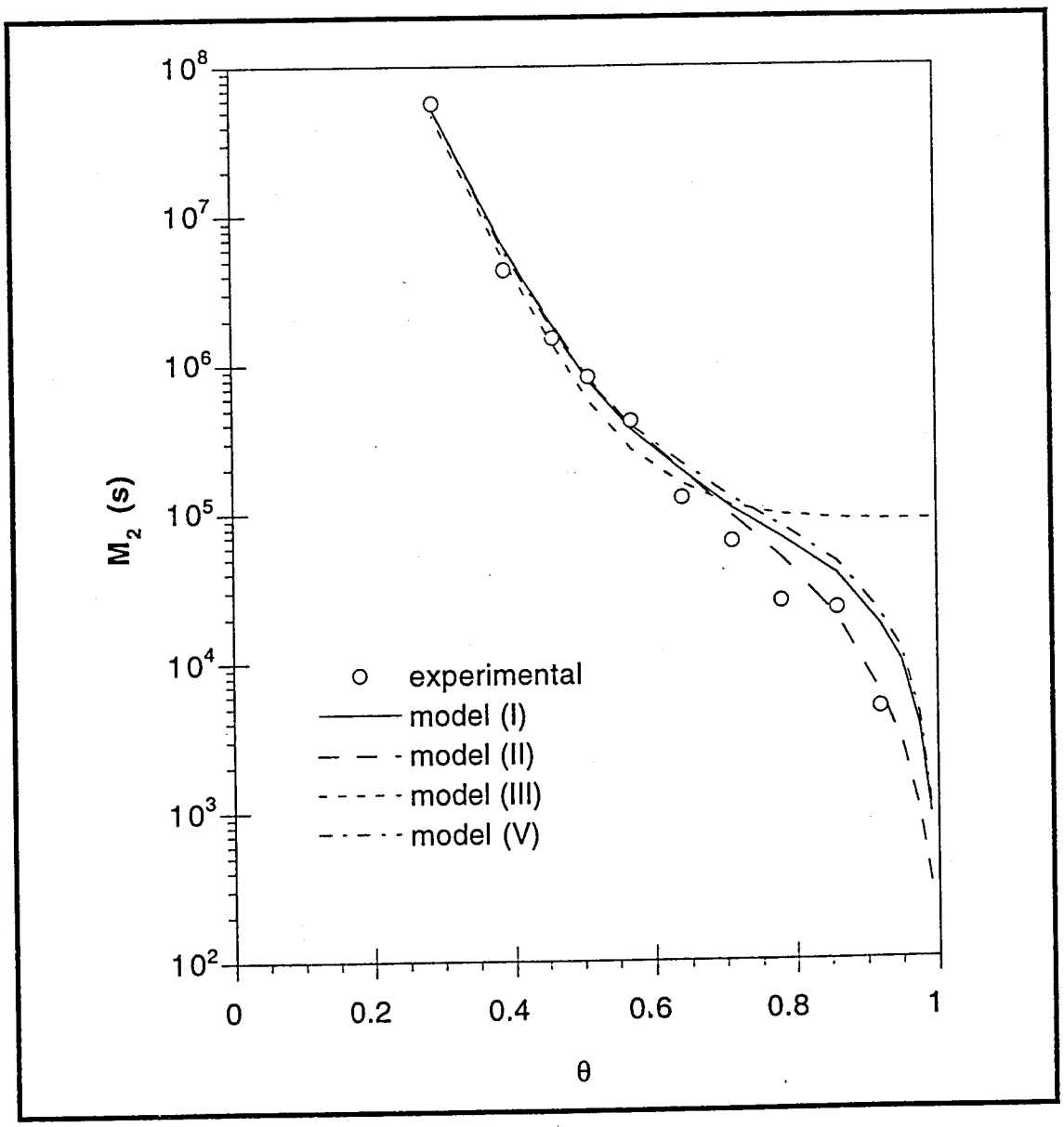

Figure 4.13 Second moment data computed from heptane desorption at 200 °C. The values from the models were computed using the parameters determined from the fittings of the first moment.

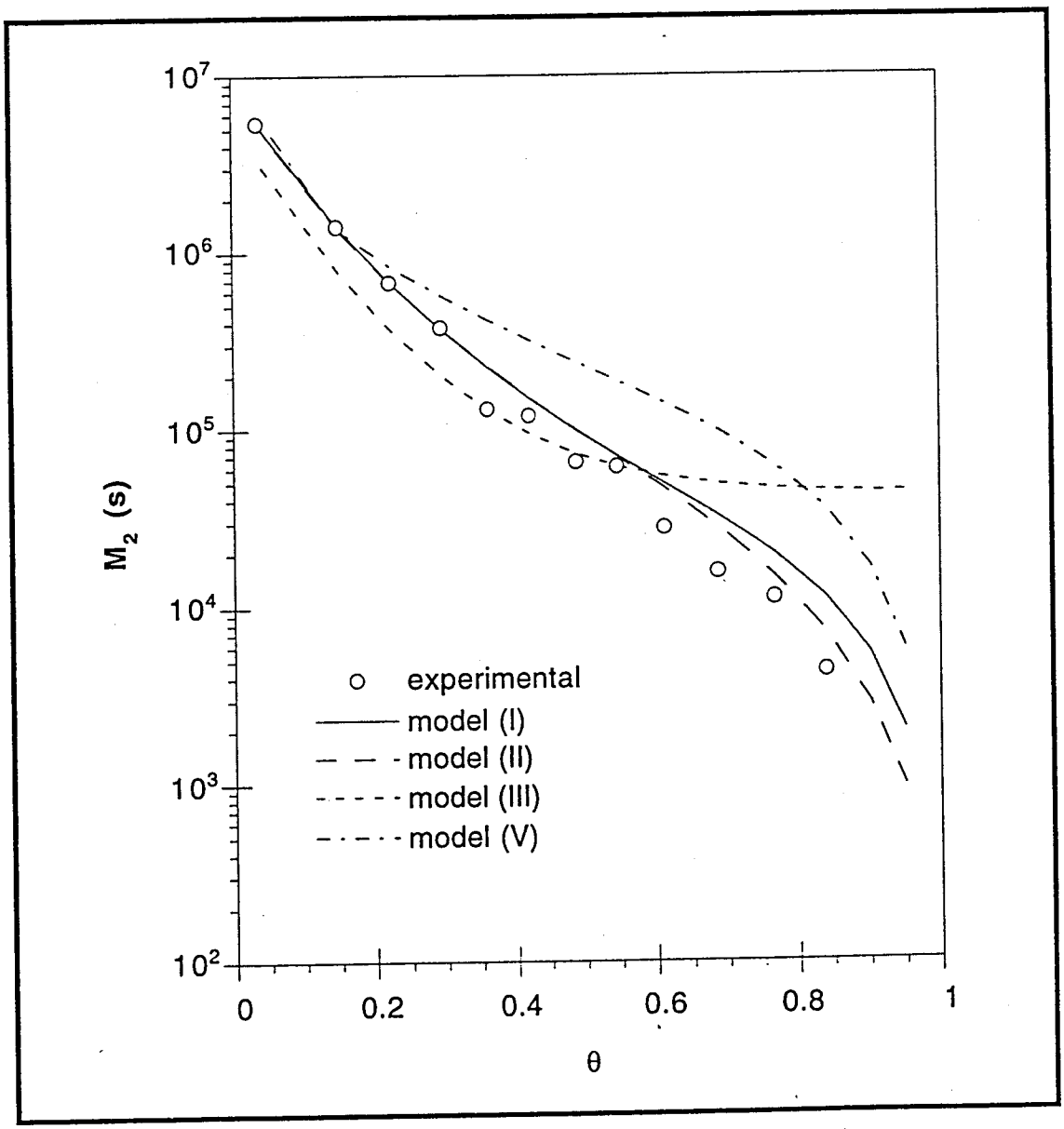

Figure 4.14 Second moment data computed from heptane desorption at 250 °C. The values from the models were computed using the parameters determined from the fittings of the first moment.

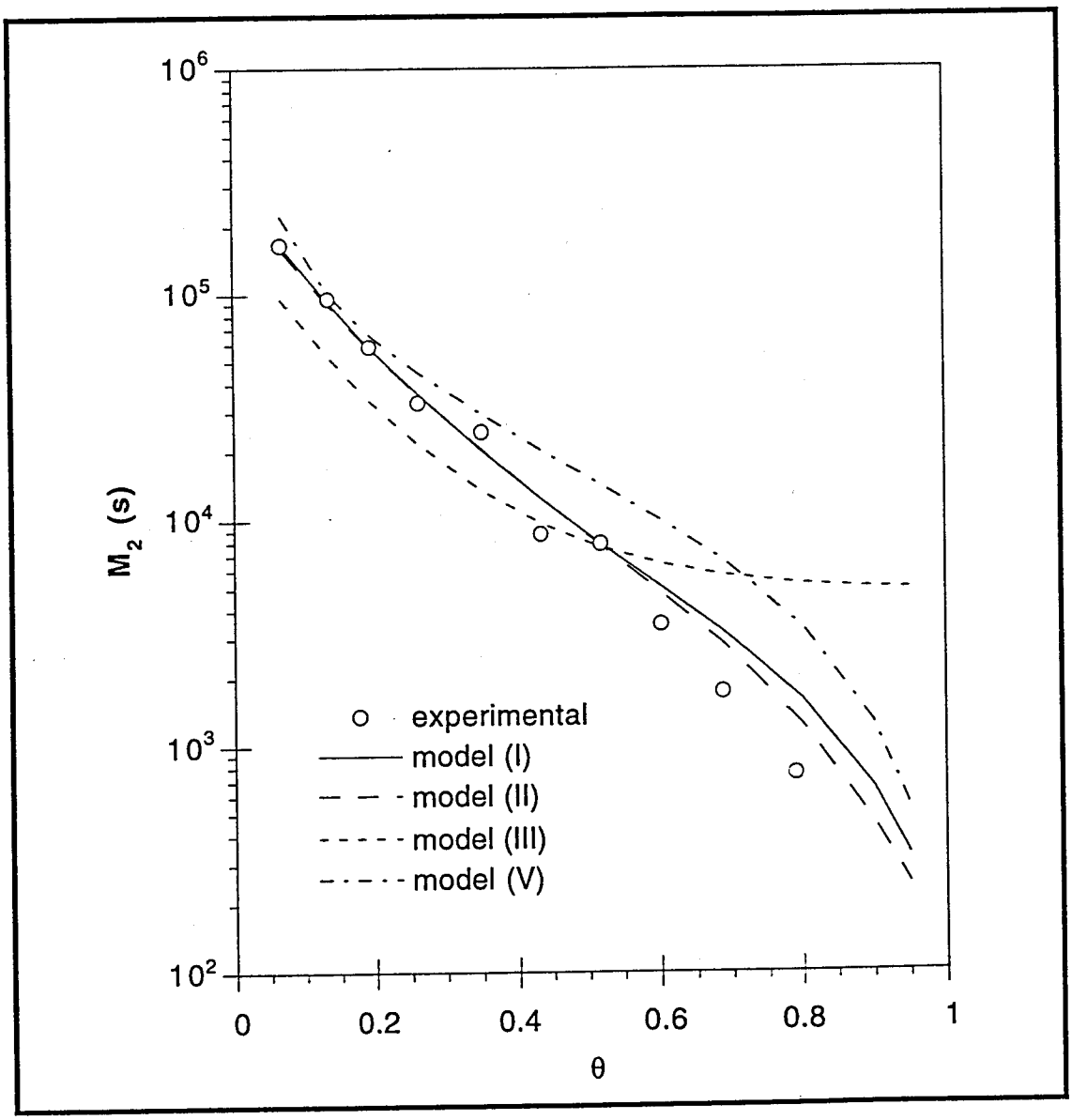

Figure 4.15 Second moment data computed from heptane desorption at 300 °C. The values from the models were computed using the parameters determined from the fittings of the first moment.

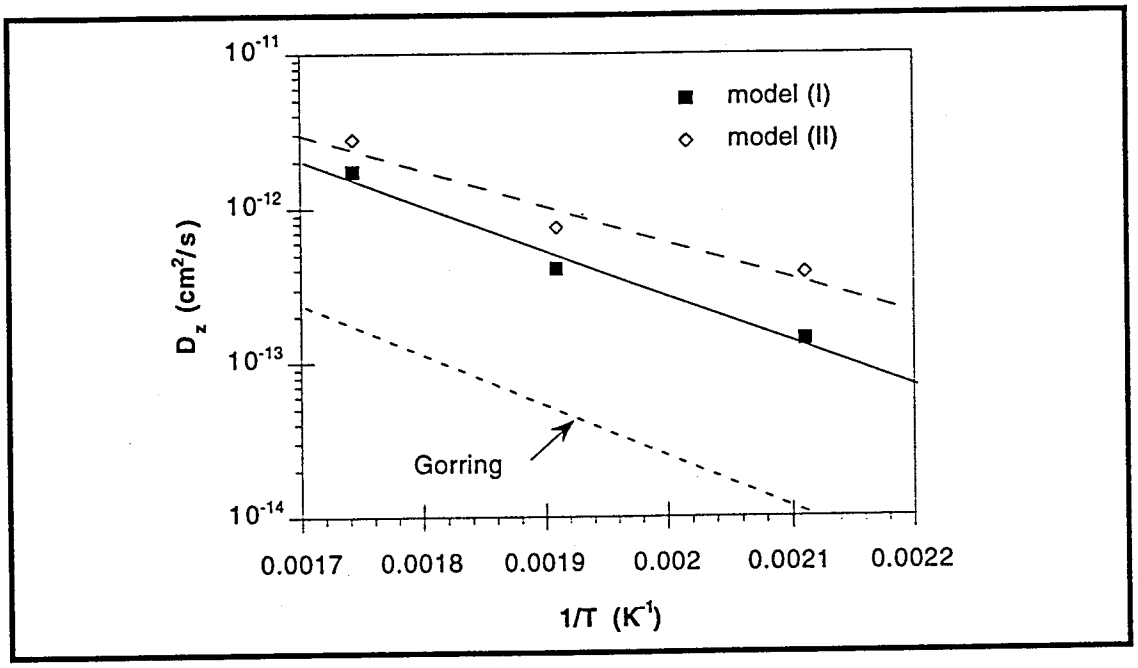

Figure 4.16 Arrhenius plots for diffusion coefficients of n-heptane obtained from models (I) and (II). Gorring's result is also shown.

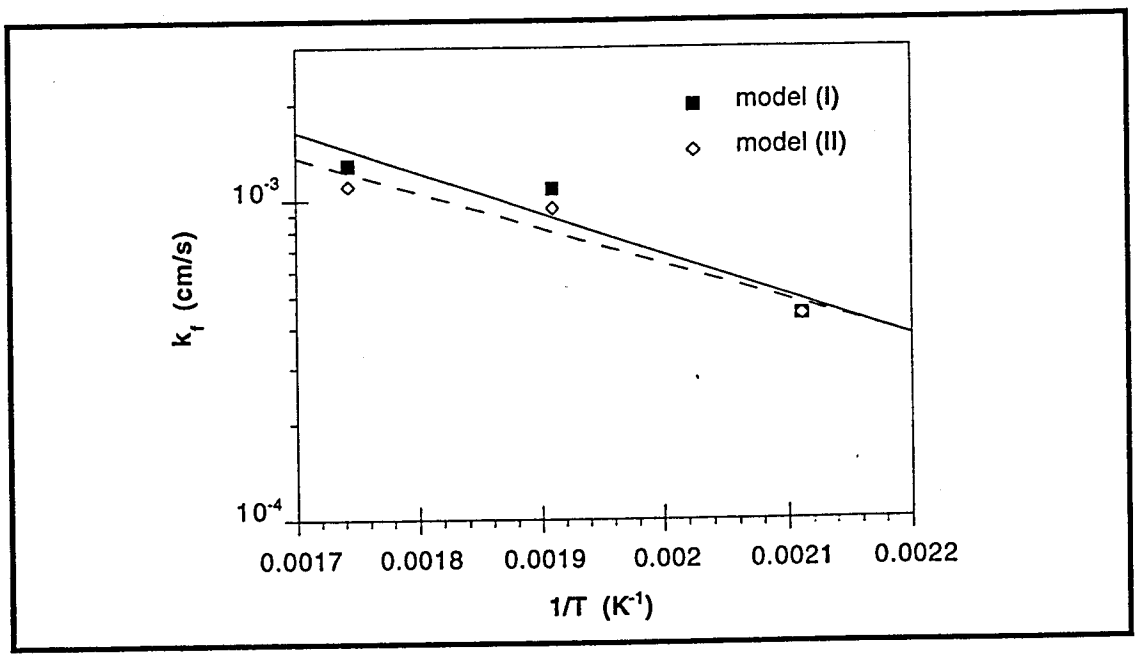

Figure 4.17 Arrhenius plots for external mass transfer resistance coefficients of n-heptane obtained from models (I) and (II).

Table 4.3 Activation energies, E_a, and pre-exponential factors, A, for D_z and k_f computed from models (I) and (II) and from Gorring's results [Gorring, 1973].

	D_{z0}		k_f	
	E_a (kJ/mol)	A (cm^2/s)	E_a (kJ/mol)	A (cm^2/s)
model (I)	56.3	2.03×10^{-7}	24.7	2.56×10^{-1}
model (II)	44.3	2.58×10^{-8}	21.3	1.07×10^{-1}
Gorring	63.6	1.20×10^{-7}		

Analysis of the individual contributions of the intra-crystalline diffusion and external gas-film resistance terms to the first moment is shown in Figure 4.18, for model (I) (similar results can be obtained for model (II)). At low occupancies, both terms are large, but the external resistance is the most important. As occupancy increases, both terms decrease. The external resistance term, however, decreases more sharply, due to the strong dependence of $K(\theta)$ on concentration. The diffusion term does not decrease as rapidly, and becomes the major contribution to M_1 at high occupancy.

An alternative way to perform this analysis is by computing Bi_m as a function of occupancy (Equation 4.26) using the assumptions and estimated parameters of model (I). An example is shown in Figure 4.19. At low occupancies, Bi_m is quite low, reflecting the importance of the external resistance's contribution. As θ increases, Bi_m increases rapidly, and the intra-crystalline diffusion becomes the controlling process.

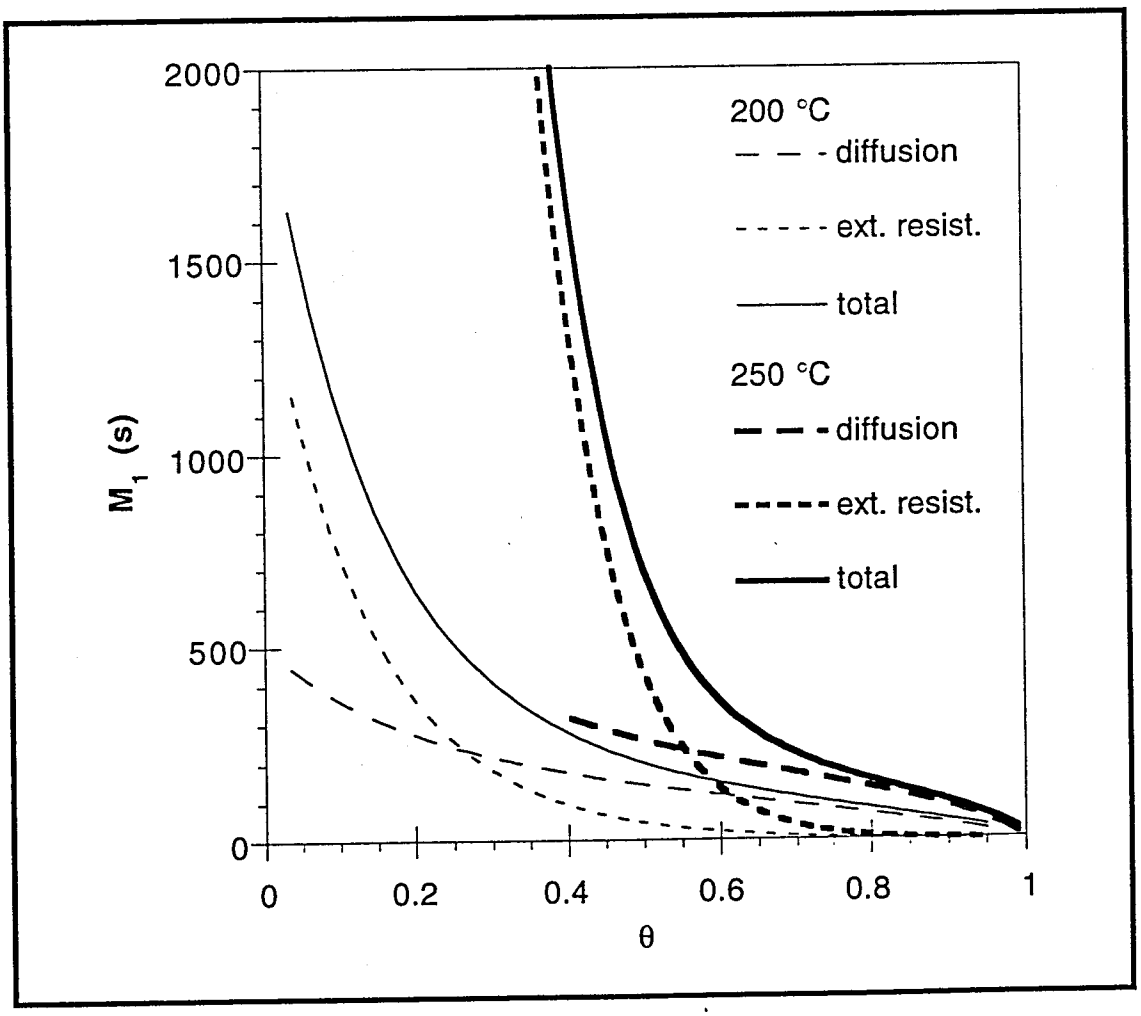

Figure 4.18 Contributions of the diffusion and external resistance terms to the first moment computed by model (I).

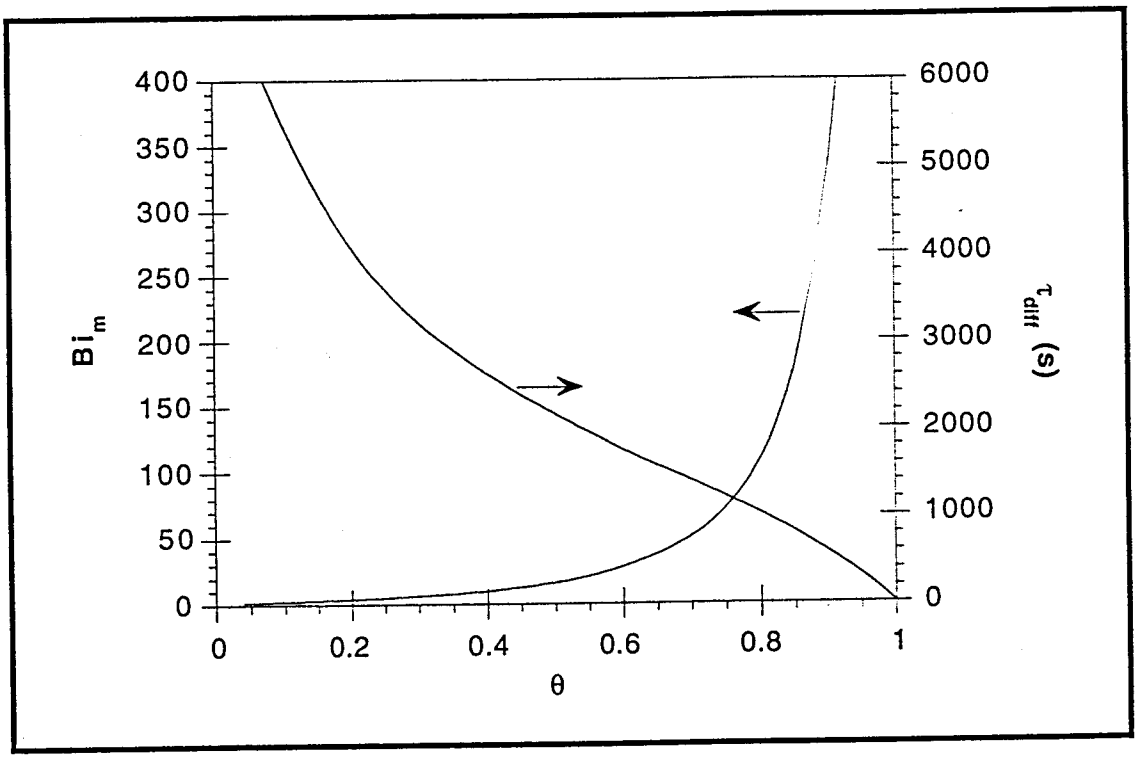

Figure 4.19 Values of Bi_m and τ_{diff} corresponding to the fit of model (I) to heptane desorption at 250 °C.

In order to see how well the model can reproduce the uptake curves in the entire range of occupancies, values of τ_{diff} and Bi_m computed from the moments were used as initial guesses in the Fourier domain fitting of the uptake curves. A few examples of the resulting optimized curves are shown in Figure 4.20 as f vs. $\sqrt{t}$, and in Figure 4.21 as log(1-f) vs. t. As discussed earlier in this work, the optimized values of the parameters cannot be trusted as "best" solutions, since the fitting procedure is strongly affected by local minima. The only purpose of the results shown is to prove that the model can reproduce the experimental uptake data. Note that the optimized parameters follow the same trend as previously discussed: low Bi_m at low θ, much higher Bi_m at higher occupancies.

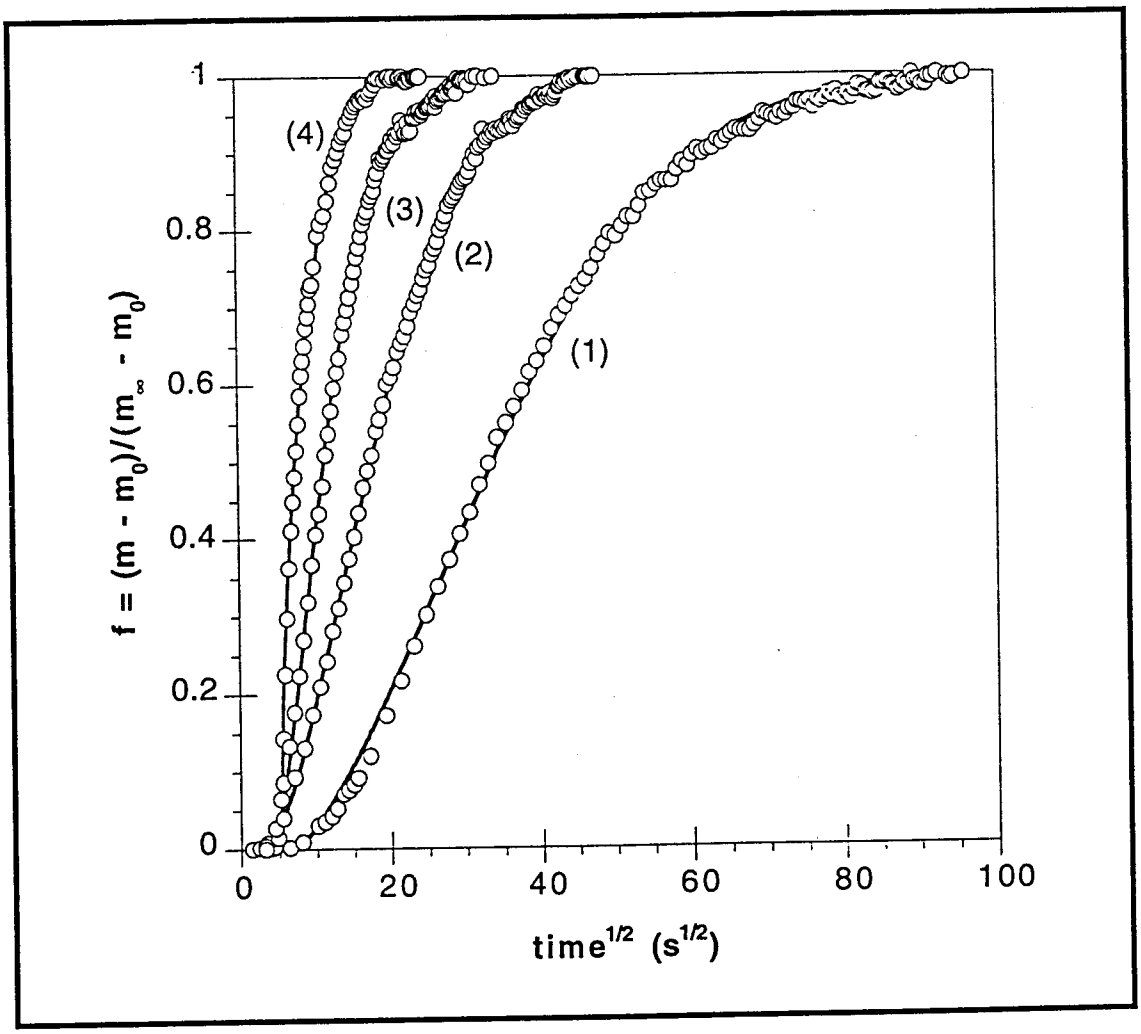

Figure 4.20 Experimental desorption curves for heptane at 250 °C, compared to theoretical curves obtained from Fourier domain fitting. The numbers on the curves designate the following optimized parameters: (1) $\theta = 0.04$, $\tau_{diff} = 9.21\times10^3$, $Bi_m = 1.22$; (2) $\theta = 0.29$, $\tau_{diff} = 2.28\times10^3$, $Bi_m = 2.76$; (3) $\theta = 0.49$, $\tau_{diff} = 1.88\times10^3$, $Bi_m = 18.9$; (4) $\theta = 0.69$, $\tau_{diff} = 7.53\times10^2$, $Bi_m = 54.7$;

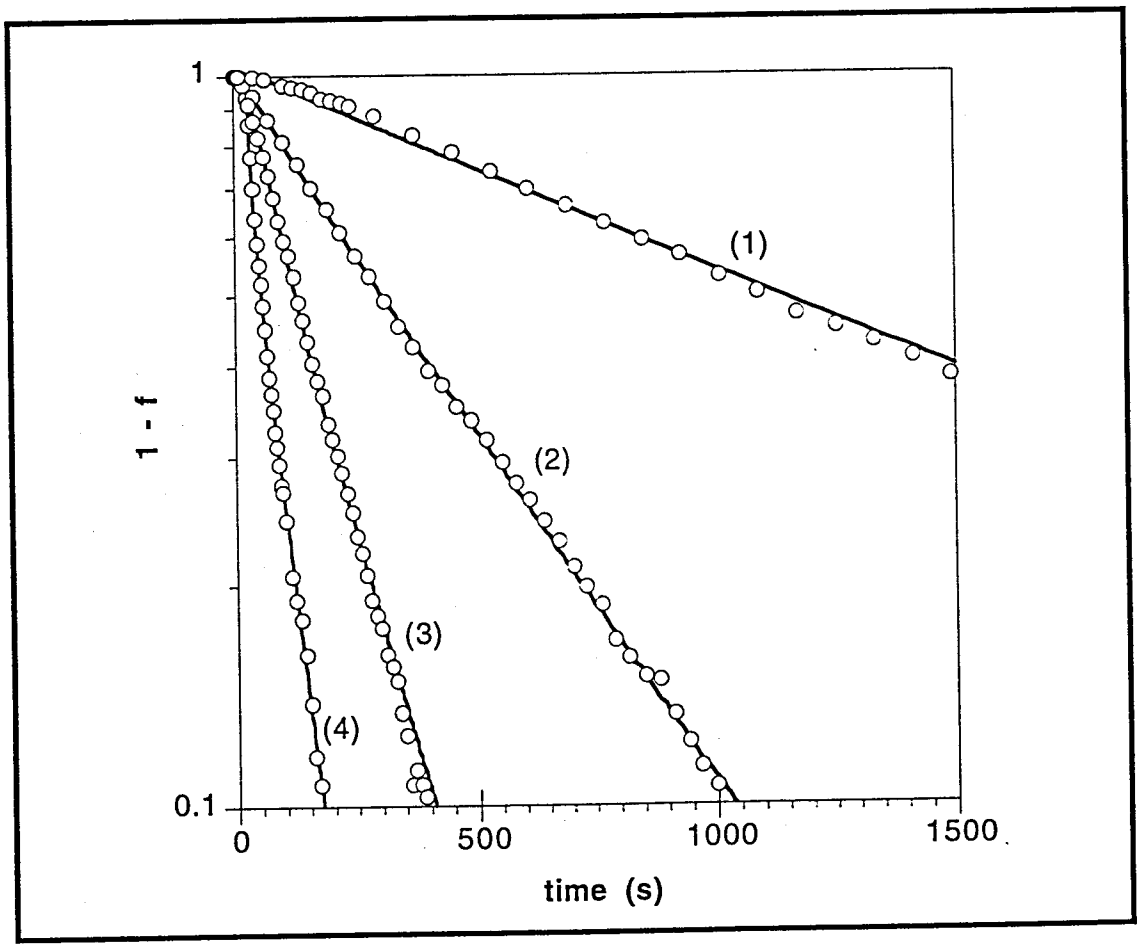

Figure 4.21 Experimental desorption curves for heptane at 250 °C, compared to theoretical curves obtained from Fourier domain fitting. The numbers on the curves designate the same parameters as in figure 4.16.

So far in the present discussion, it has been found that the experimental results are well described only by the models involving the gas-phase resistance formulation (models (I) or (II)). However, an inconsistency becomes in the computed values of k_f, the gas film mass transfer coefficient. Indeed, from Table 4.2, k_f is around 10^{-3} cm/s. This value is very low for this type of resistance. Molecular diffusion of *n*-heptane in helium is about 0.92 cm^2/s (estimated from [Reid et al., 1987]). Considering a stagnant film of gas around the zeolite particle (Sh = 2), one would have:

$$k_f = \frac{Sh\ D_m}{2\ R} = 3.2\times10^4 \text{ cm/s} \qquad (4.52)$$

If one assumes Knudsen diffusion in the inter-crystalline space, then the gas-phase diffusivity would be $D_k \sim 10^{-4}$ cm^2/s (for an inter-crystalline pore radius of 1 μm). Using the same relationship as in Equation 4.52, k_f would now be in the order of 1 cm/s, which is still too large. These results lead us to consider that the transport resistance is associated with a framework-related surface barrier (constrictions of the pore entrances). However, it has been shown that model (IV) fails completely in describing the measured data (see Figure 4.11). The analysis of the values of k_f seems to indicate that the resistance mechanism that is more complex than initially presumed. However, the mathematical formulation of the model is still valid. Further verification of its consistency will be given below.

It may be interesting to analyze in more detail the association of the local slope of the isotherm to a gas-phase resistance model, since this is the essential difference between the formulations of the gas-phase and particle-surface resistance models. This can be better understood with the help of a simple schematic representation of the concentration profiles involved (Figure 4.22). Consider a gas-phase resistance (Figure 4.22a). Initially, the concentration in the bulk gas is C_{b0} and inside the particle is q_0. During an adsorption step so that the final intra-particle concentration becomes q_∞, then the outside gas concentration must be increased to $C_{b\infty}$. Assuming local linearity of the isotherm:

$$(C_{b\infty} - C_{b0}) = \frac{1}{K}\,(q_\infty - q_0) \qquad (4.53)$$

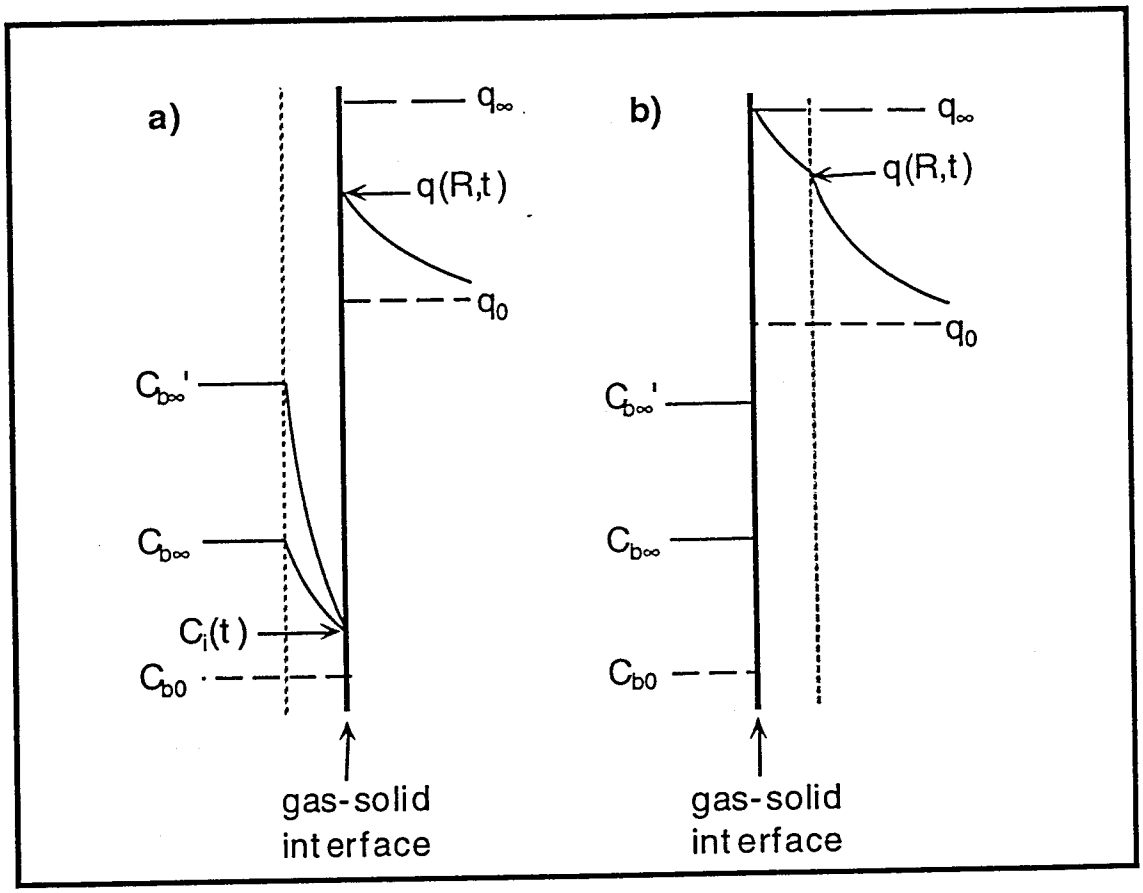

Figure 4.22 Concentration profiles when extra-crystalline mass transfer resistance is located at a) external gas-phase, b) particle surface.

During this adsorption step, the concentration in the gas phase at the interface will be $C_i(t)$, in equilibrium with q(R,t) - the concentration at the particle surface. The driving force for mass transfer across the gas film is proportional to $(C_{b\infty} - C_i(t))$. For a similar adsorption step (final concentration inside the particle is q_∞) but with a lower value for the local slope of the isotherm ($K' < K$), the concentration in the bulk gas phase would have been obtained from:

$$(C_{b\infty}' - C_{b0}) = \frac{1}{K'} (q_\infty - q_0) > (C_{b\infty} - C_{b0}) \qquad (4.54)$$

In other words, the concentration step in the gas phase ($C_{b\infty}' - C_{b0}$) would have to be higher than before. As a consequence, the driving force across the gas film would also have been higher (see Figure), implying faster mass transfer through the film. In the case of a particle surface resistance (Figure 4.22b), the driving force is located in the surface of the solid, and does not depend on $C_{b\infty}$ (and thus on K).

Some critical assumptions associated with the previous models deserve also some attention. Relationships between D_z and θ, the total occupancy in the particle, were described in Equations 4.44 and 4.46. However, as pointed out before, D_z should be related to the occupancy in the erionite regions only. It can be argued that, if this deviates significantly from θ, the suggested forms for $D_z(\theta)$ would not be valid; a corrected relationship might admit a better fit of model (IV) to the data. But whatever formulation is chosen for the variation of D_z with loading, a surface resistance model would still be intrinsically incompatible with the experimental results. Recall that such model implies that $K(\theta)$ does not appear in the definition of Bi_m:

$$Bi_m = \frac{k_s R}{D_z} \tag{4.27}$$

This way, the dependence of Bi_m on loading is given only by D_z (k_s is, so far, assumed independent of θ). Since M_1 decreases by several orders magnitude with loading, the diffusivity will have to increase also by orders of magnitude. Consequently, Bi_m at low loadings must be significantly larger than at high loadings. This is incompatible with the observed shape of the uptake curves. In Figure 4.23 a few examples are shown for uptake at 200 and 250 °C and different loadings. The slopes increase with occupancy because D_z increases. But the critical observation is that the

curves corresponding to higher occupancies show some curvature. This is characteristic of diffusion controlled transport (high Bi_m). At lower occupancies, on the other hand, the curves are essentially linear, clearly indicating stronger extra-crystalline resistance (lower Bi_m). These observations are totally compatible with the previous analysis of models (I) and (II). Indeed, for a gas-phase resistance:

$$Bi_m = \frac{k_f R}{D_z K} \tag{4.26}$$

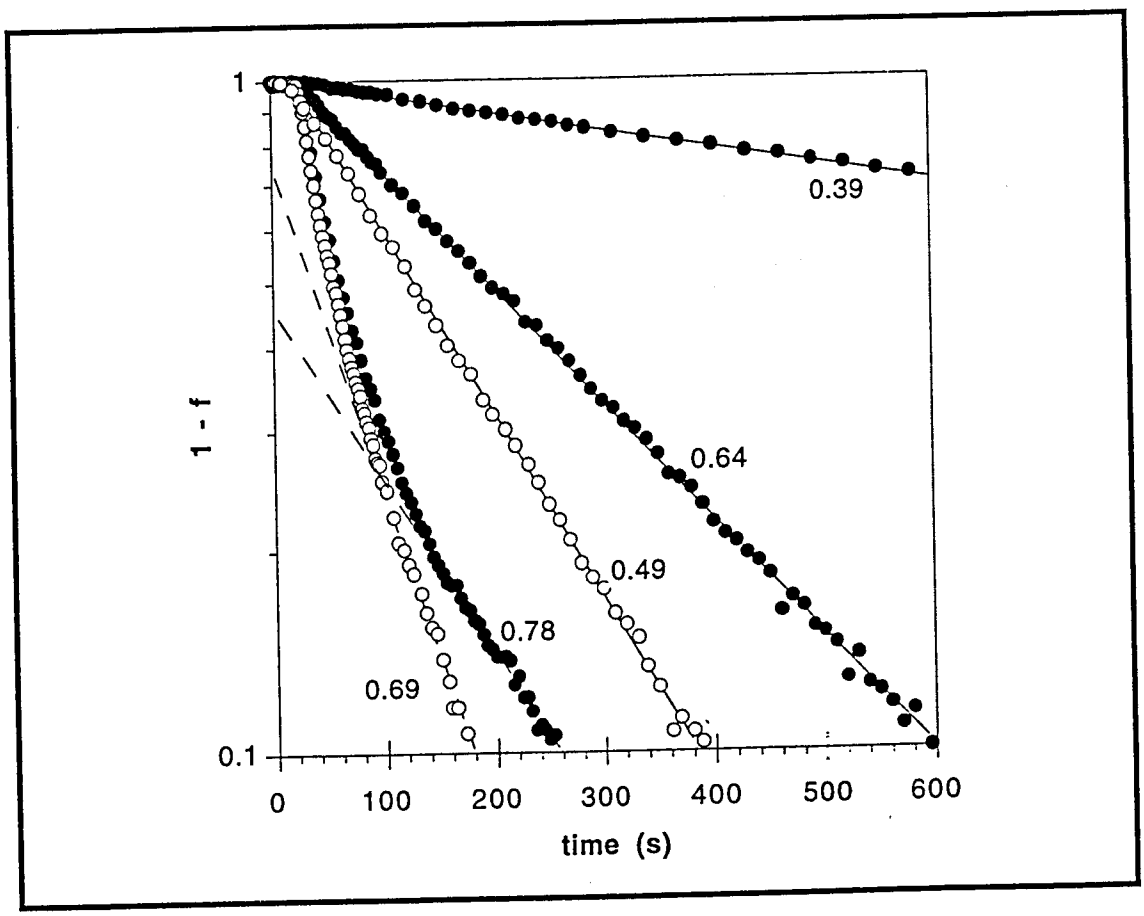

Figure 4.23 Uptake curves for n-heptane desorption. The numbers on the curves correspond to the mean occupancy of the desorption step, θ. Full circles: 200 °C; empty circles: 250 °C.

The increase of D_z is overcome by the stronger dependence of K on occupancy. As a result, Bi_m increases with θ. This shows that the consistency of the gas-phase resistance model with the results is not limited to the temporal moments data.

Note that a new element may be introduced in the discussion of the surface-resistance model if k_s were to depend on occupancy. Since the nature of the surface resistance is unknown, discussion of this aspect is very restricted. If the surface barrier is structural, then k_s may change with occupancy in a way similar to D_z. On the other hand, as shown by model (V), a loading-dependent k_s may result from nonequilibrium sorption at the surface. This model did not, however, fit the data as well as models (I) and (II).

Another test of the consistency of the results obtained with the gas-phase resistance model is to compare these to values of k_f computed from the slope of ln(1-f) vs. time plots, for the lower-occupancy curves. As pointed out earlier, the values of k_f computed directly from the plots will coincide with the "true" coefficients only when the external resistance controls the mass transfer process. If both external resistance and intra-crystalline diffusion are important, the plots will still be linear, but the computed k_f will be lower than the true value (see Figure 4.3). Some results are shown in Table 4.4. Equation 4.28 was used to calculate k_f, with $K(\theta)$ computed from Equation 4.41. Calculated values of k_s, from Equation 4.29, are also shown in Table 4.4. As expected, the computed values of k_f are somewhat lower than the models' estimates (Table 4.2). The agreement is still quite good, though, in particular at lower occupancies (when the contribution from the external resistance is higher) and for model (II). The particularly good agreement obtained at 200 °C would be expected, since it is at this temperature that

the external resistance (at low loadings) more strongly dominates the diffusional term (see Figure 4.18).

Table 4.4 Values of k_f and k_s computed from Equations 4.29 and 4.30, respectively. The relative differences between these values of k_f and the estimates from models (I) and (II) are also shown.

Temperature (°C)	θ	kf (cm/s)	kf - kf(I)	kf - kf(II)	ks (cm/s)
200	0.29	4.41×10-4	0 %	0.2 %	4.00×10-9
	0.39	3.75×10-4	15 %	15 %	1.12×10-8
250	0.04	7.87×10-4	28 %	17 %	1.18×10-8
	0.15	6.18×10-4	43 %	35 %	2.15×10-8
300	0.07	8.91×10-4	31 %	20 %	7.33×10-8
	0.14	8.25×10-4	36 %	26 %	1.00×10-7

It is interesting to note that Bülow and co-workers [Bülow et al., 1980] estimated values of k_s between 10^{-5} and 10^{-7} cm/s for sorption of *n*-hexane on MgA zeolite in the same temperature range, applying a model equivalent to Equation 4.29 to low occupancy data.

Values of D_{z0} can also be estimated directly from the uptake data. As previously discussed, the higher occupancy curves reflect a diffusion-controlled transport. In these conditions, $D_z(\theta)$ can be estimated from the linear portion of the uptake curves (corresponding to long times), according to Equation 4.32. D_{z0} can then be obtained

from Equations 4.44 or 4.46. Values estimated in this way agreed within 5 to 30% with the results from the first moment fittings. This again supports the validity of the model.

4.4.2 *n*-Nonane

4.4.2.1 Isotherms

The sorption isotherms obtained for *n*-nonane are shown in Figure 4.24. The computed parameters, from the fitting of Equation 4.40, are shown in Table 4.5. These curves are steeper in the lower occupancy regions than the ones for *n*-heptane.

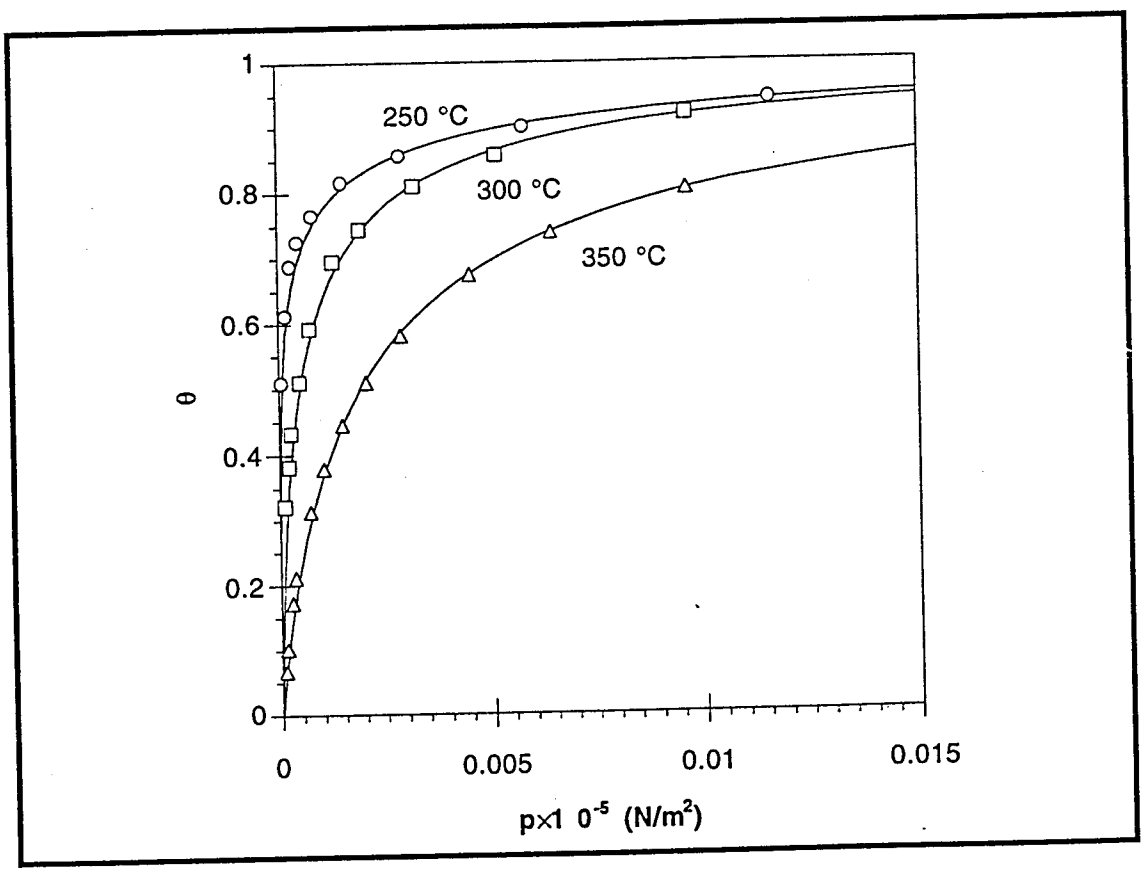

Figure 4.24 Isotherms for n-nonane sorption. The curves correspond to the fits of Equation (4.40) to the experimental data.

Table 4.5 Parameters α and β obtained from fitting Equation 4.40 to experimental sorption data of *n*-nonane.

Temperature (°C)	α $((N/m^2)^{-1})$	β
250	1.83	5.19
300	4.00×10^{-2}	1.34
350	7.19×10^{-3}	0.651

4.4.2.2 Transient Mass Transfer

The analysis of the mass transfer dynamics for *n*-nonane was done in the same way as for *n*-heptane. Plots of the first moment of the uptake curves, as a function of occupancy, and the corresponding fits of the models are shown in Figures 4.25 to 4.27. Model (I) and (II) give once again the best fits. Model (V) is acceptable only at the lower temperature (250 °C).

The computed values of D_{z0} and k_f obtained from models (I) and (II) are shown in Table 4.6. Once again, it was assumed $(\tau_{c1} + \tau_{c2}) = 10$ s. An example of the comparison between the values of the second moments computed from these parameters and the experimental results can be seen in Figures 4.28 to 4.30.

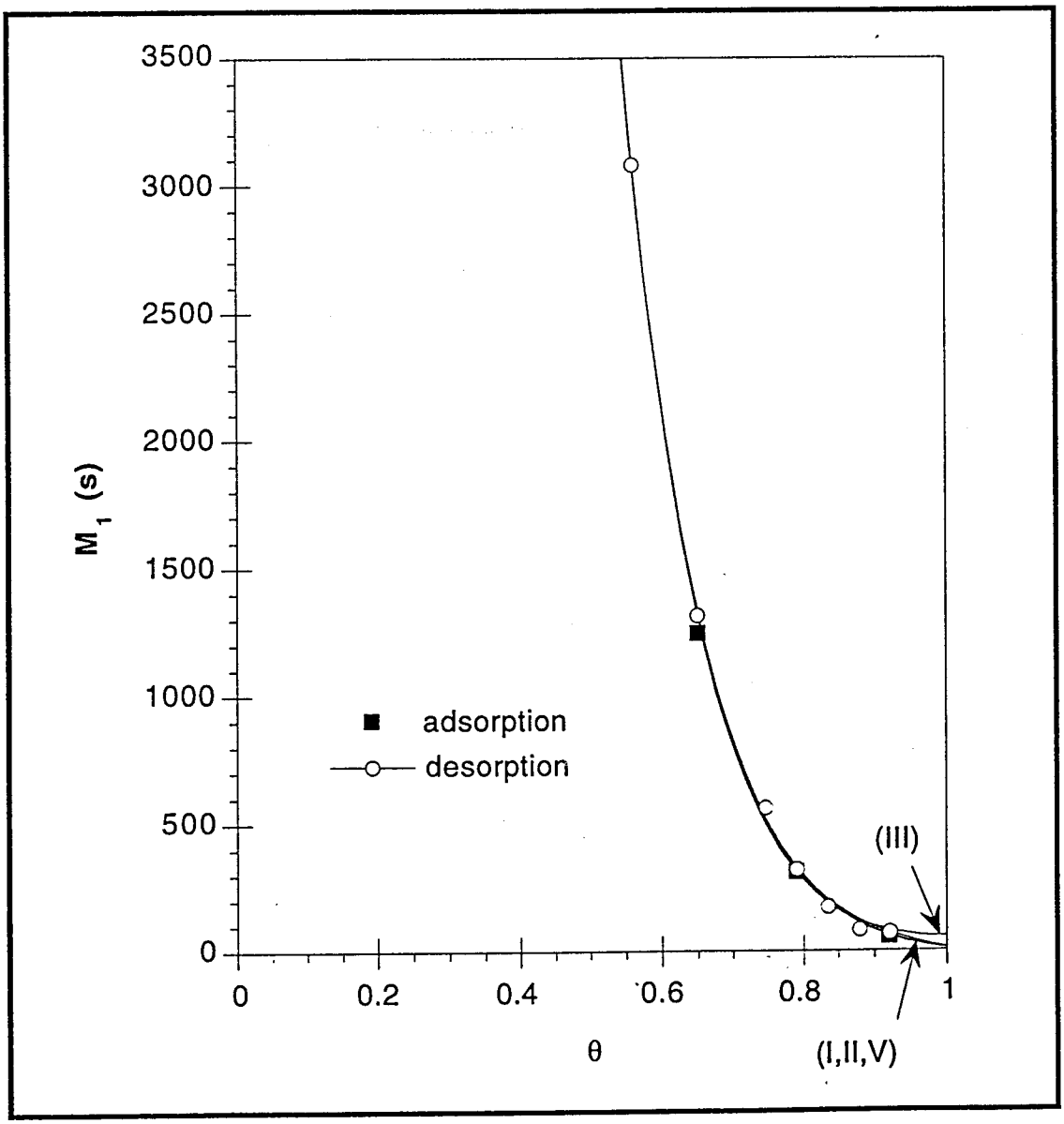

Figure 4.25 First moment data computed from nonane adsorption and desorption at 250 °C. The roman numeral on each line designates the model.

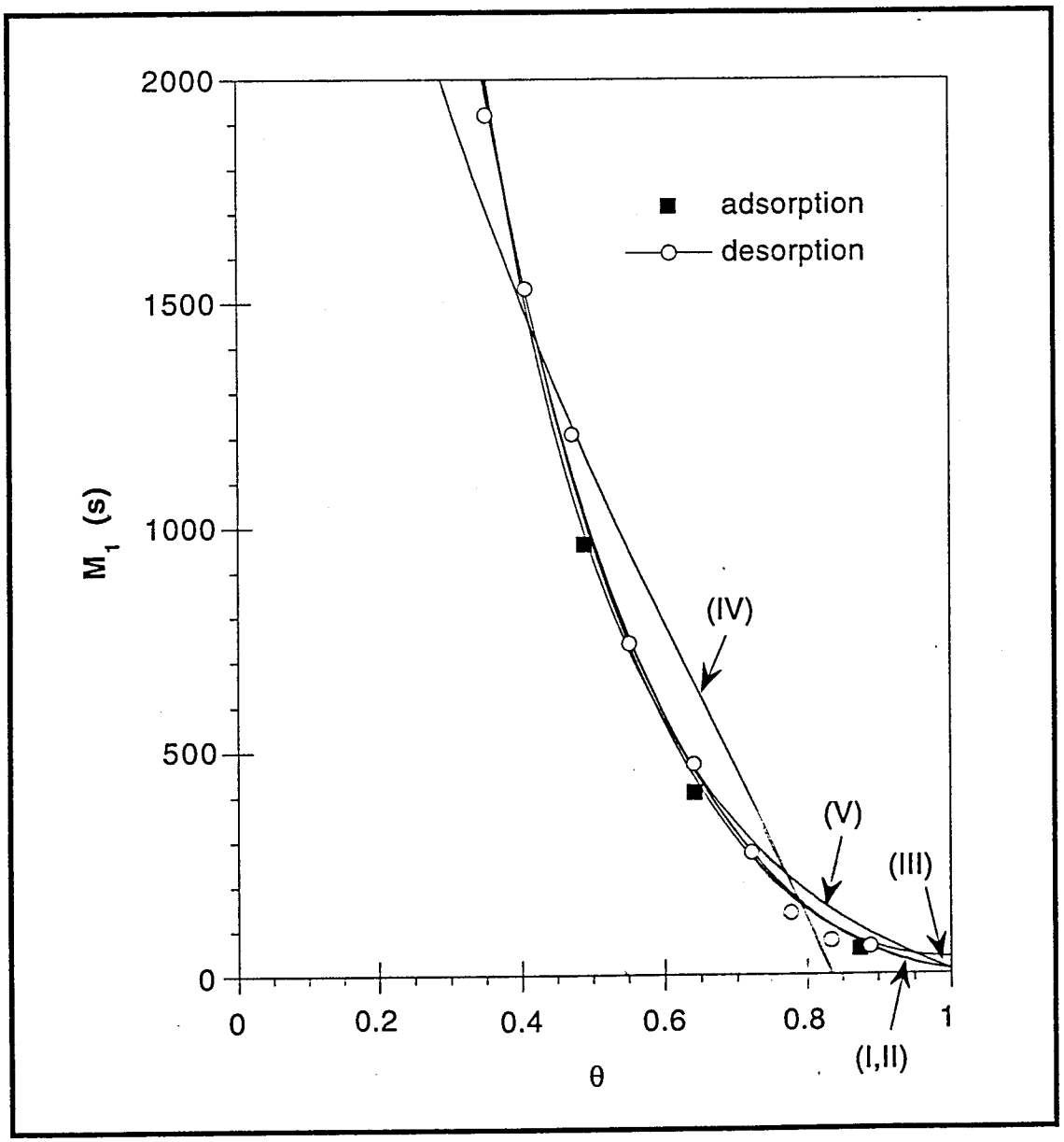

Figure 4.26 First moment data computed from nonane adsorption and desorption at 300 °C. The roman numeral on each line designates the model.

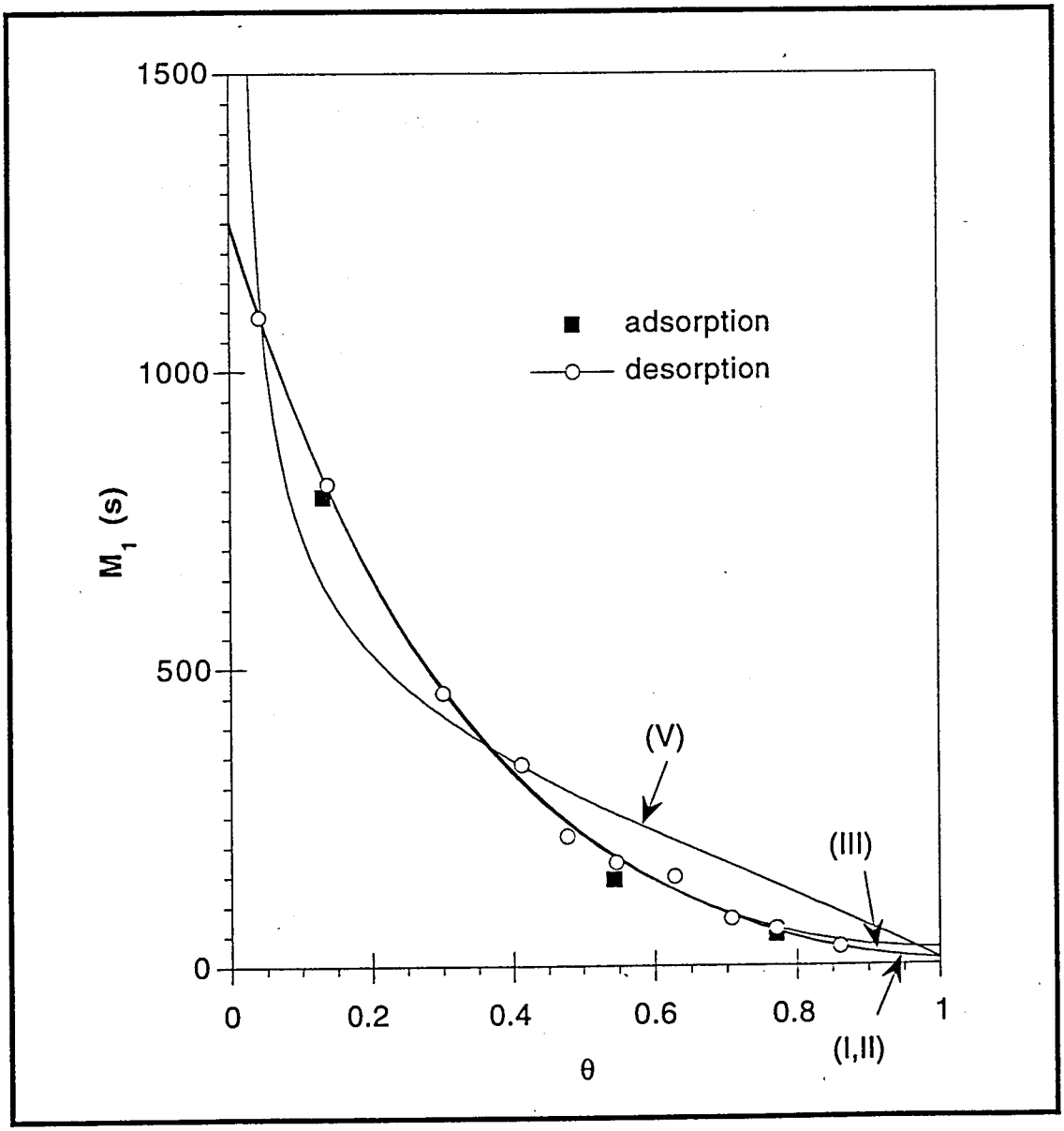

Figure 4.27 First moment data computed from nonane adsorption and desorption at 350 °C. The roman numeral on each line designates the model.

Table 4.6 Parameters D_{z0} and k_f obtained from fitting models (I) and (II) to experimental values of M_1 for *n*-nonane.

Temperature (°C)	model (I)		model (II)	
	D_{z0} (cm²/s)	k_f (cm/s)	D_{z0} (cm²/s)	k_f (cm/s)
250	3.18×10^{-13}	1.52×10^{-4}	6.64×10^{-13}	1.53×10^{-4}
300	8.98×10^{-13}	2.27×10^{-4}	1.07×10^{-12}	2.29×10^{-4}
350	2.49×10^{-12}	3.22×10^{-4}	3.07×10^{-12}	3.18×10^{-4}

The computed values of D_{z0} and k_f obtained from models (I) and (II) are shown in Table 4.6. Once again, it was assumed $(\tau_{c1} + \tau_{c2}) = 10$ s. An example of the comparison between the values of the second moments computed from these parameters and the experimental results can be seen in Figures 4.28 to 4.30.

As a first observation, one notes that the plots of models (I) and (II) are now indistinguishable, with both describing well the measured data. This is due to the smaller (in relation to heptane's) relative contribution of the diffusional resistance term to the moments. Recall that the two models differ only in the form of this term. The ratio of the external and diffusional resistance terms in Equation 4.45 for heptane and nonane at 250 °C is shown in Figure 4.31. It is clear that the external resistance term largely overcomes the diffusional term at low occupancies.

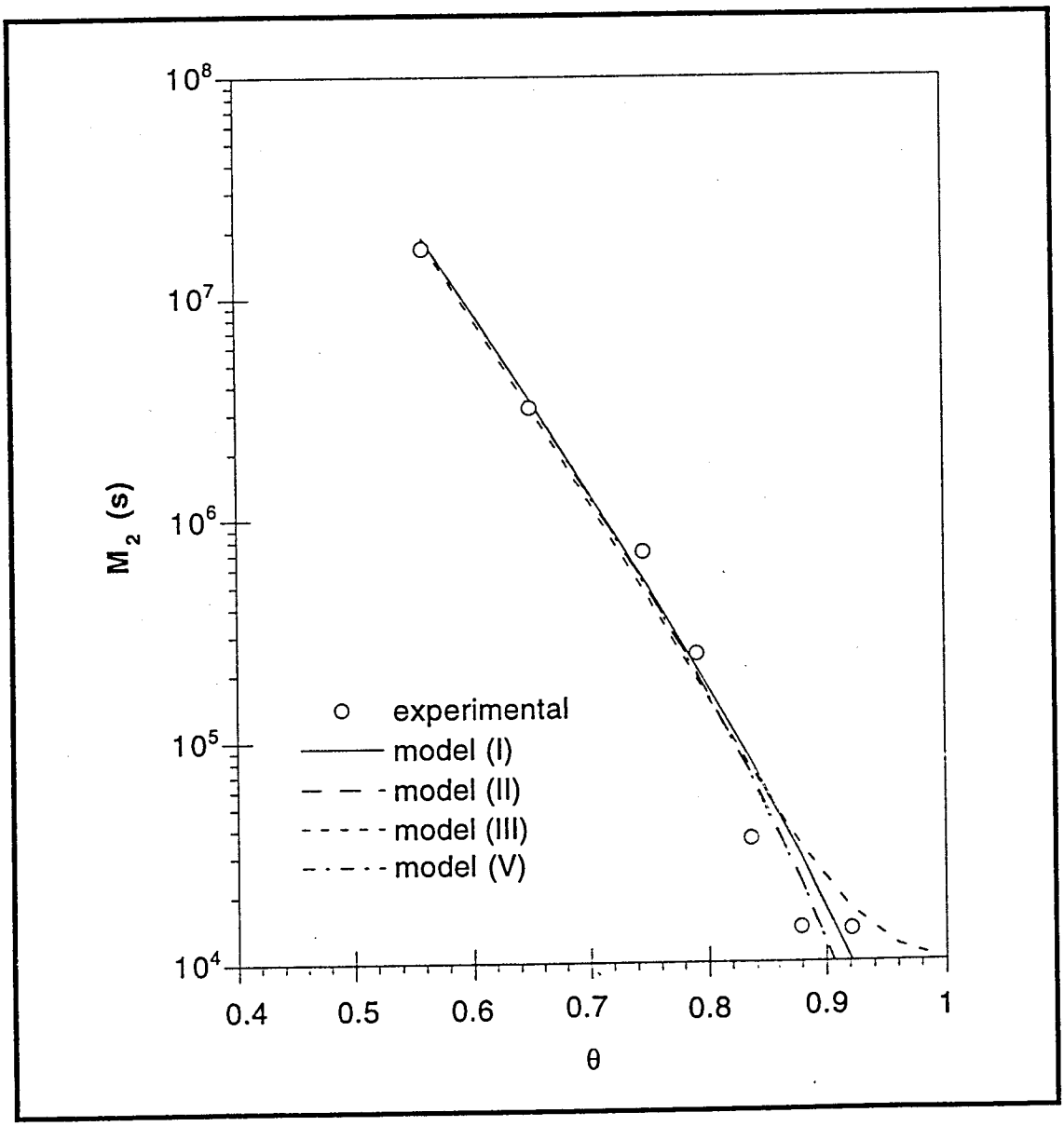

Figure 4.28 Second moment data computed from nonane desorption at 250 °C. The values from the models were computed using the parameters determined from the fittings of the first moment. The curves for models (I) and (II) are practically coincident.

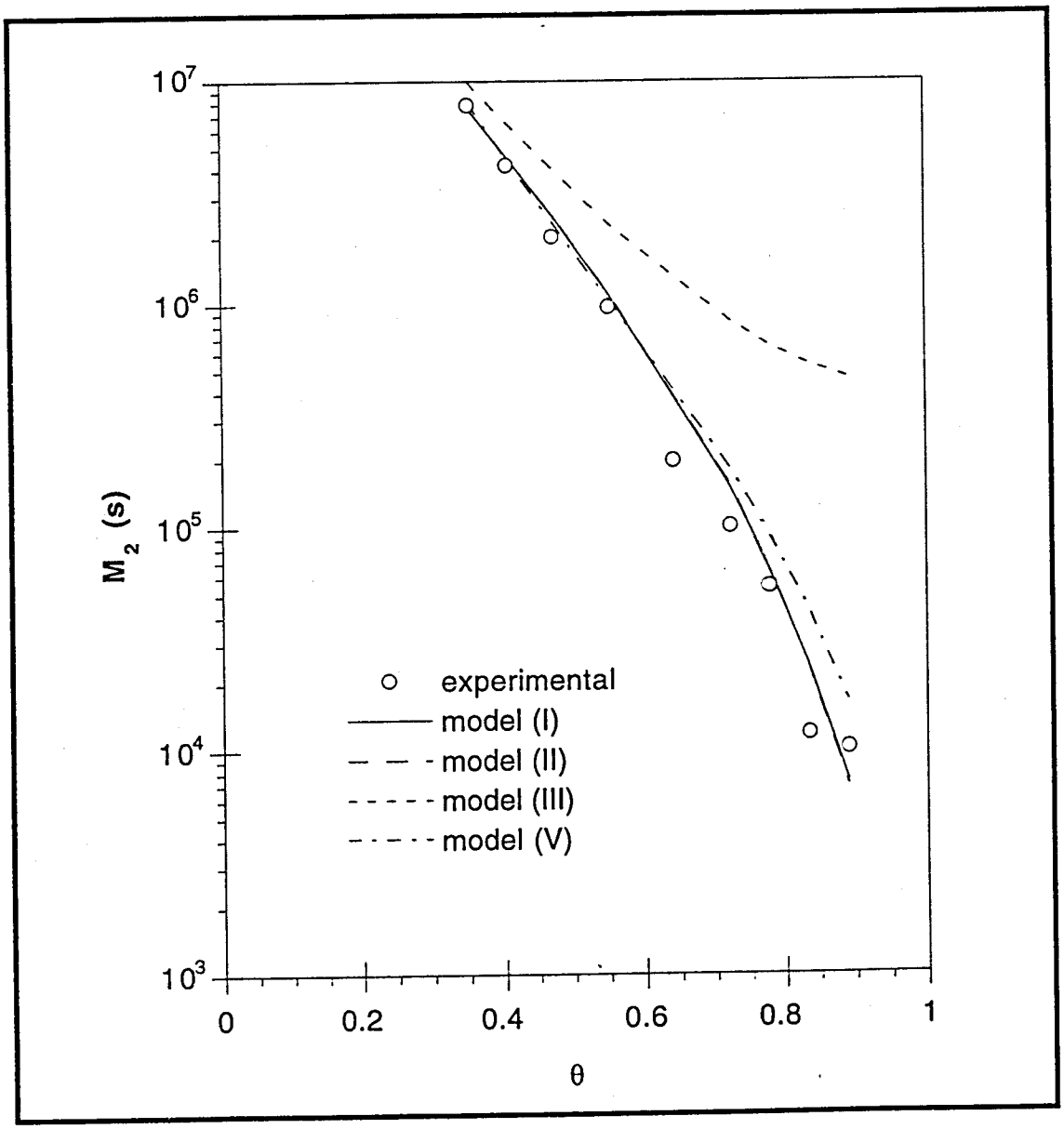

Figure 4.29 Second moment data computed from nonane desorption at 300 °C. The values from the models were computed using the parameters determined from the fittings of the first moment. The curves for models (I) and (II) are practically coincident.

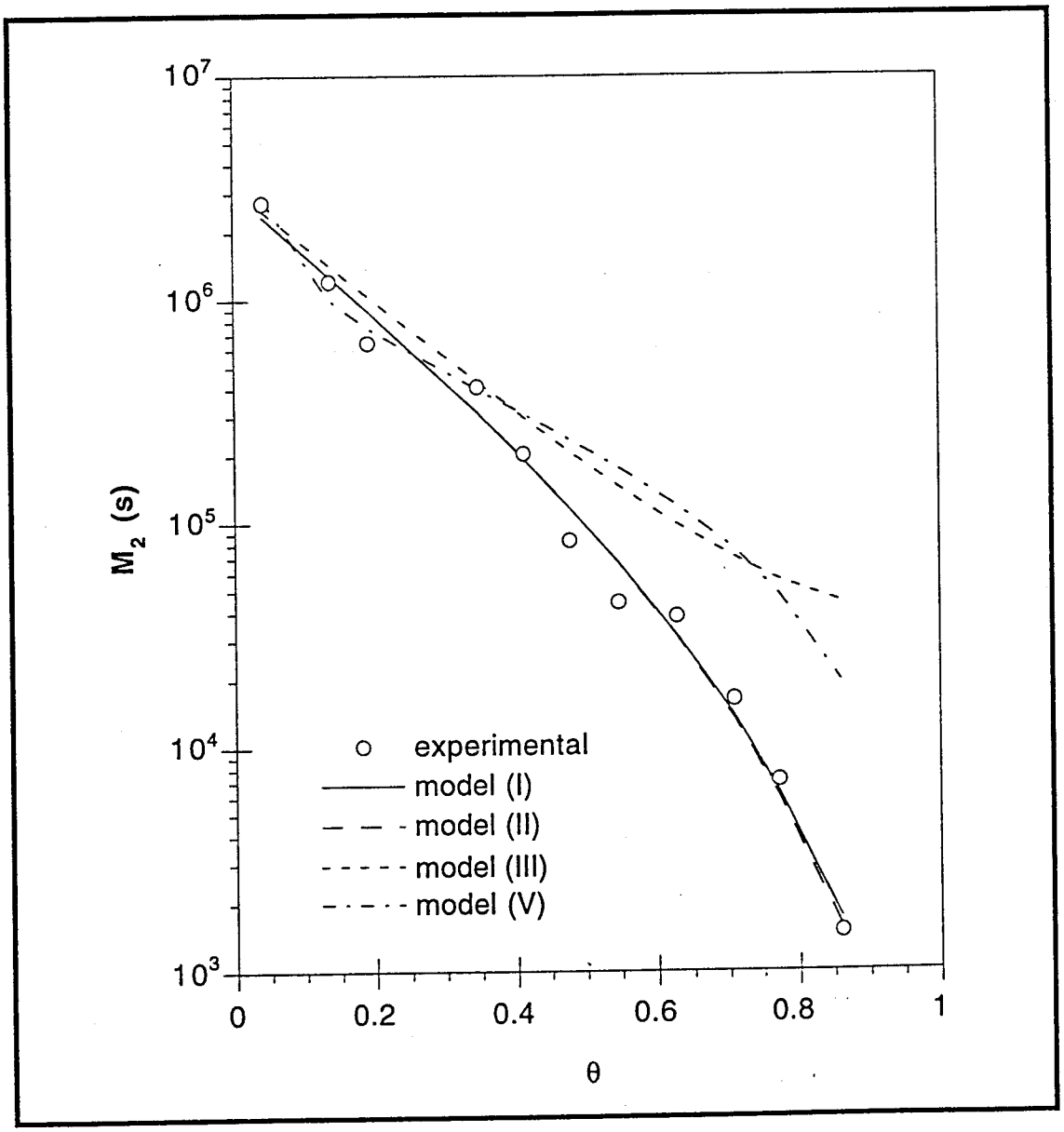

Figure 4.30 Second moment data computed from *n*-nonane desorption at 350 °C. The values from the models were computed using the parameters determined from the fittings of the first moment.

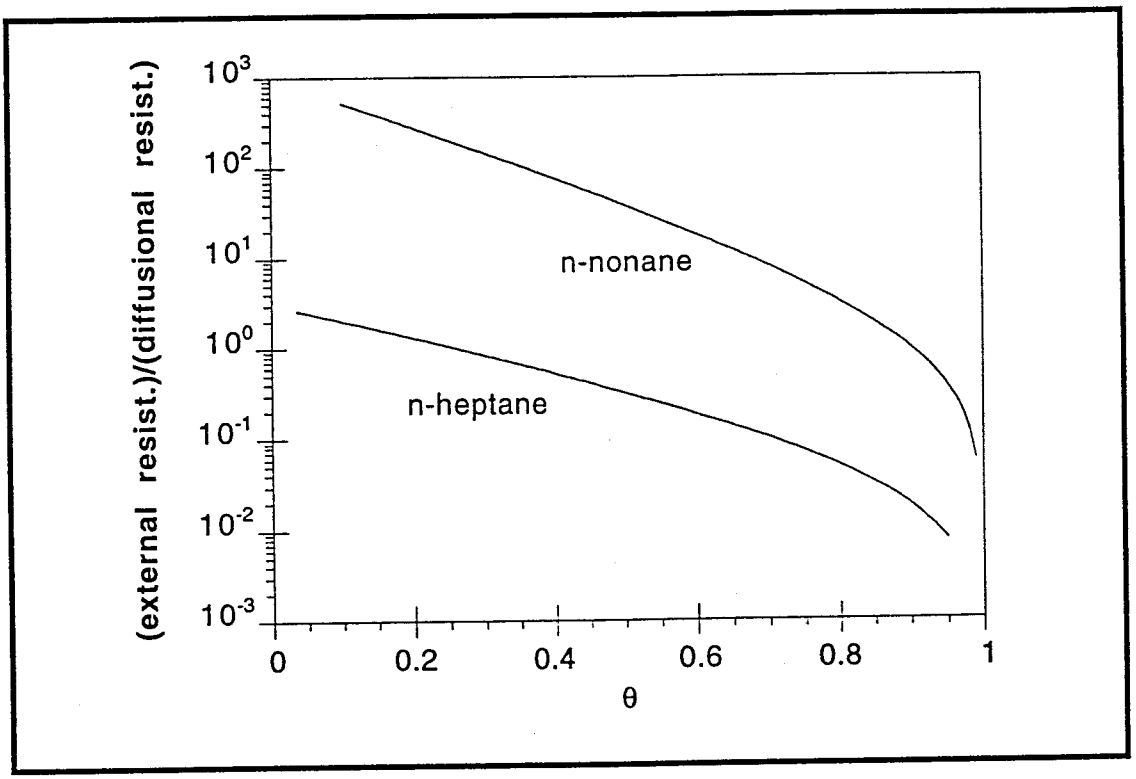

Figure 4.31 Ratio between the external resistance and diffusional resistance terms in the expression of the first moment - model (I).

It is striking that the first moments measured at low occupancies are much larger for nonane, at the same temperatures. According to models (I) and (II), this is a consequence of the larger external resistance term, due to the lower values of k_f (cf. Tables 4.2 and 4.6) and higher initial slopes of the isotherms. The diffusional term, even though it is also higher for nonane (cf. D_{z0} in Tables 4.2 and 4.4), does not contribute significantly for the first moment, as seen in Figure 4.31.

The analysis of the shape of the uptake curves leads to the same results as for heptane: at high occupancies the log(1-f) vs. t plots are concave upwards, characteristic of diffusion control; while at low occupancies the plots are linear, indicating that external resistance is dominant (see Figure 4.32).

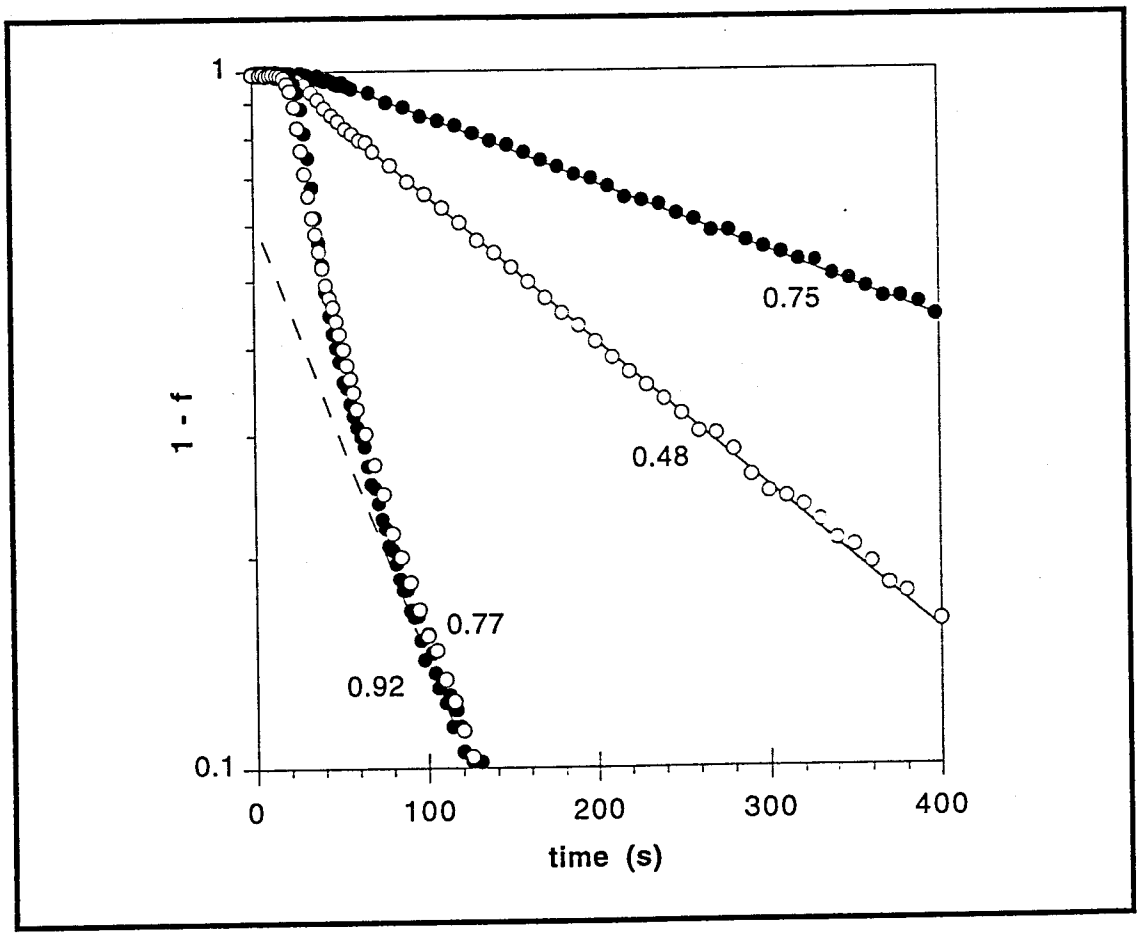

Figure 4.32 Uptake curves for *n*-nonane desorption. The numbers on the curves correspond to the mean occupancy of the desorption step, θ. Full circles: 250 °C; empty circles: 300 °C.

Values of k_s and k_f were also computed directly from the experimental ln(1-f) vs. t plots at lower occupancies, according to Equations 4.28 and 4.29. The results are shown in Table 4.7. The agreement between the values of k_f computed in this way and obtained from models (I) and (II) is very good. Notice that this is true even at the higher temperatures. For heptane, the discrepancy increased with temperature. One would expect this to happen, since for nonane the external resistance is largely dominant in the entire range of temperatures analyzed. For heptane, however, the two resistances were

closer at higher temperatures, and there would be a larger error in estimating k_f directly from the uptake curves.

Table 4.7 Values of k_f and k_s computed from Equations 4.29 and 4.30, respectively, for *n*-nonane. The relative differences between these values of k_f and the estimates from models (I) and (II) are also shown.

Temperature (°C)	θ	k_f (cm/s)	$k_f - k_f$(I)	$k_f - k_f$(II)	k_s (cm/s)
250	0.56	1.41×10^{-4}	7 %	7 %	5.89×10^{-9}
	0.65	1.33×10^{-4}	12 %	12 %	1.34×10^{-8}
300	0.35	2.09×10^{-4}	8%	9%	9.33×10^{-9}
	0.41	1.88×10^{-4}	17%	18%	1.09×10^{-8}
350	0.041	3.00×10^{-4}	7 %	6 %	1.74×10^{-8}
	0.14	2.58×10^{-4}	20 %	19 %	2.06×10^{-8}

Also, as with *n*-heptane, D_{z0} can be estimated from the slopes of the long-time portion of the higher occupancy curves. The results were within 30% of the first moment fitting estimates.

The computed activation energies and pre-exponential factors are shown in Table 4.8. The corresponding Arrhenius plots are shown in Figures 4.33 and 4.34. The activation energies for both D_{z0} and k_f are practically identical for heptane and nonane. The pre-exponential factors show more significant differences, and are lower for nonane.

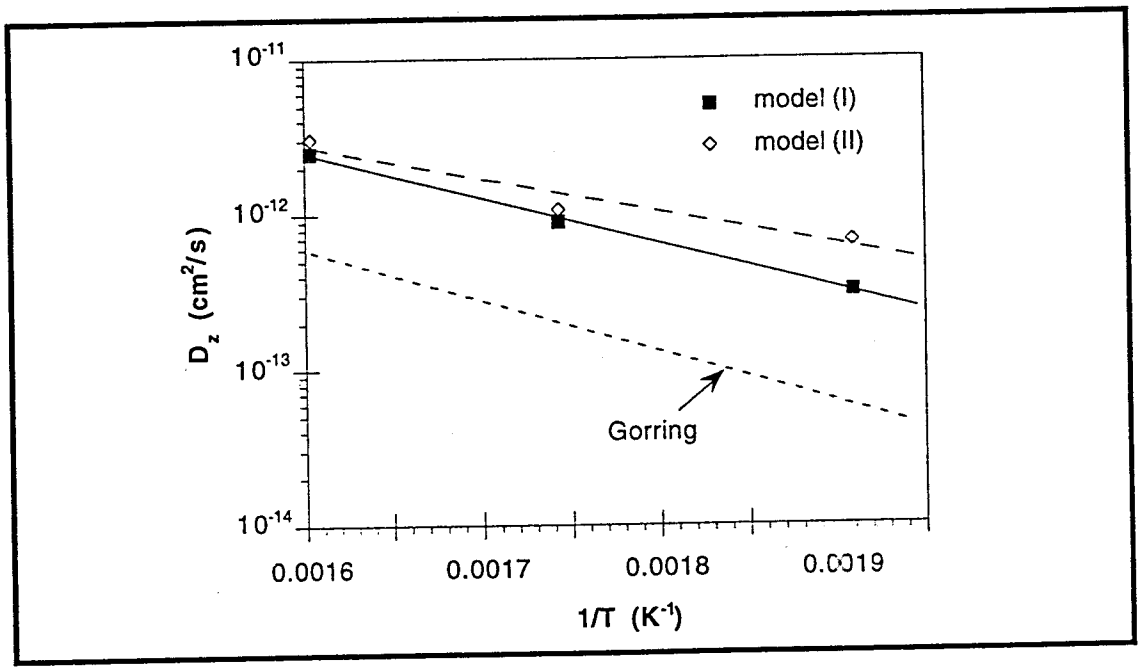

Figure 4.33 Arrhenius plots for diffusion coefficients of n-nonane obtained from models (I) and (II). Gorring's result is also shown.

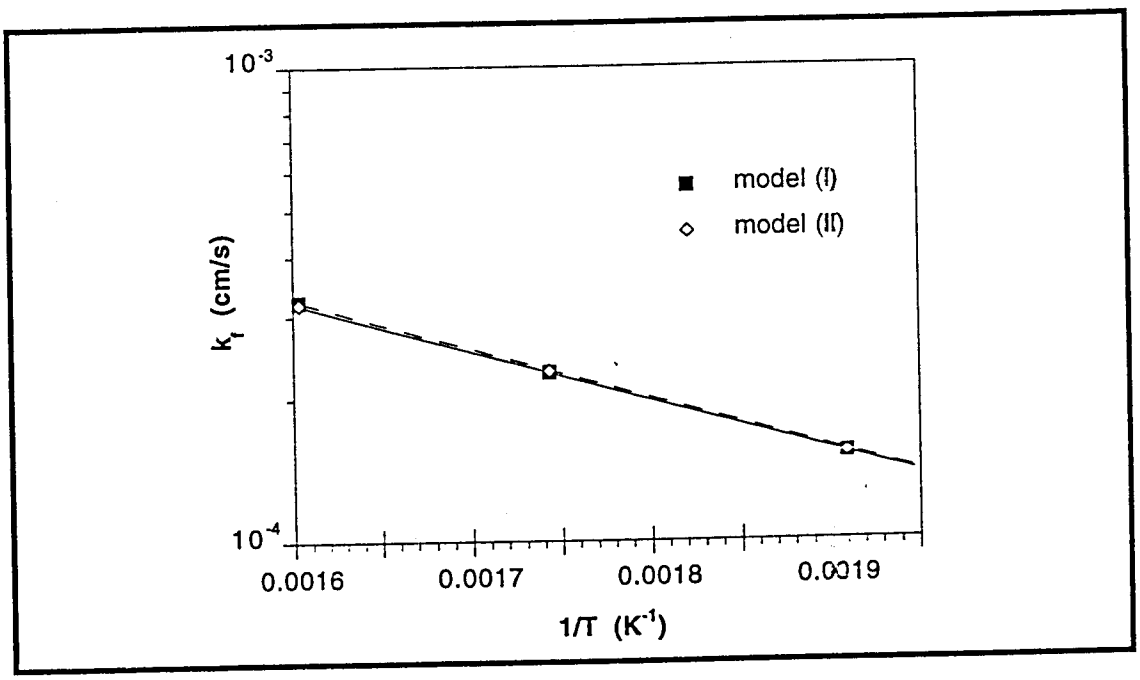

Figure 4.34 Arrhenius plots for external resistance coefficients of n-nonane obtained from models (I) and (II).

Table 4.8 Activation energies, E_a, and pre-exponential factors, A, for D_z and k_f computed from models (I) and (II) and from Gorring's results [Gorring, 1973] for *n*-nonane.

	D_{z0}		k_f	
	E_a (kJ/mol)	A (cm^2/s)	E_a (kJ/mol)	A (cm^2/s)
model (I)	55.8	1.13×10^{-7}	19.9	1.48×10^{-2}
model (II)	41.0	7.36×10^{-9}	19.9	1.47×10^{-2}
Gorring	62.0	8.50×10^{-8}		

4.4.3 *n*-Dodecane

The low volatility of *n*-dodecane resulted in adsorbate condensation in the sample hanging wire and in some internal glass walls, at high gas-phase concentrations, Consequently, adequate control of the gas-phase concentration steps and measurements at high occupancies were not possible. Therefore, reliable data for the statistical moments analysis could not be obtained with this adsorbate. However, since parameter estimation directly from the uptake curves had proven reasonably accurate in the two previous cases, this approach was used in order to obtain estimates for D_{z0} and k_f. Uptake curves at high enough concentration could be measured in order to obtain the characteristic curve shape indicative of diffusion control. From these, a diffusivity of $D_{z0} \sim 1\times10^{-13}$ cm^2/s at 300 °C was estimated. From the low occupancy curves a value of $k_f \sim 4\times10^{-5}$ cm/s was calculated, at the same temperature.

Some first moment data at low occupancy is shown in Figure 4.35. It is striking how much longer the time constant is for transport of *n*-dodecane. This is a consequence of the lower k_f and the steeper isotherm (and, thus, larger $K(\theta)$).

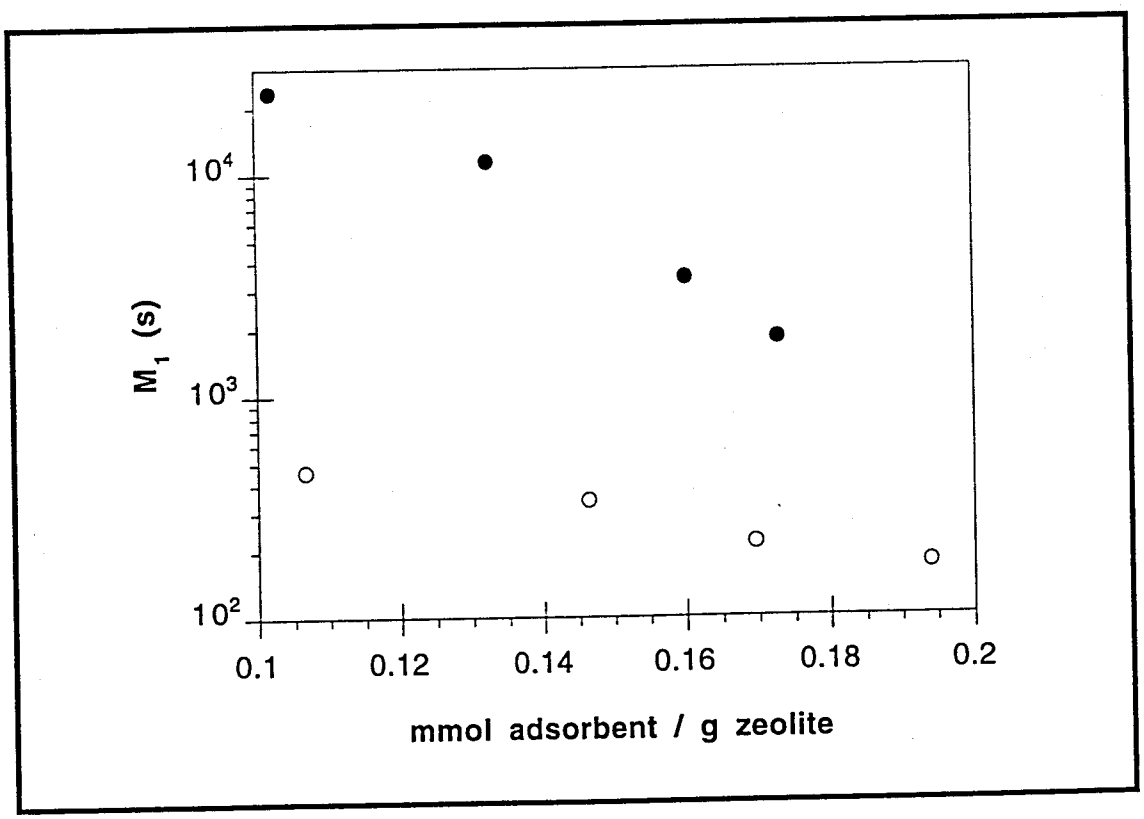

Figure 4.35 First moment data obtained for n-dodecane at 400 °C (full circles). Data for n-nonane at 350 °C (empty circles) is also shown for comparison.

It is essential to recall that the original objective of the present work is the study of the existence of the window effect. The major feature of the Gorring data consisted in the 100-fold increase of diffusivity relative *n*-heptane or *n*-nonane. Our estimates indicate that D_{z0} for *n*-dodecane is definitely not higher than for the other two species. Indeed diffusion coefficients at 300°C of 1.71×10^{-12} - 2.75×10^{-12} cm^2/s (depending on whether Equation 4.44 or 4.46 was used) were calculated for *n*-heptane, and of

8.98×10^{-13} - 1.07×10^{-12} cm^2/s for *n*-nonane. On the other hand, the diffusivity estimated for *n*-dodecane was 1×10^{-13} cm^2/s.

4.5 Conclusions

Non-diffusional transport significantly affects the mass transfer of *n*-paraffins in the sample of zeolite T studied. It was shown that a model involving intra-crystalline diffusion (occupancy-dependent) and external (non-diffusional) mass transfer resistance (dependent on the local slope of the sorption isotherm) describes well the first and second moment data. The transport parameters estimated from the first moment data are consistent with the observed shape of the uptake curves and with the values estimated directly from the curves. At low loadings, mass transfer is strongly limited by the external resistance. Closer to saturation, however, the process becomes controlled by intracrystalline diffusion.

The low magnitude of the values computed for the external resistance mass transfer coefficient, k_f, and its relatively high activation energy, indicate that this process may be associated with transport within the solid phase, *i.e.*, at the particle surface. The theories of thermal, evaporation or conformational barriers are not compatible with the good agreement observed between the adsorption and desorption data. The hypothesis of a "surface barrier" being due to framework modifications at the crystal surface, as reported in the literature for hydrothermally pretreated samples of zeolite A [Bülow et al., 1982], does not, by itself, justify the verified importance of the local slope of the isotherm in the description of the experimental results. Entropic effects involved in the adsorption/desorption at the surface may be important. The nonequilibrium sorption model did not fit satisfactorily all the data. It did, however,

show the same qualitative trends as our results and also involves a loading-dependent external resistance term.

No evidence of the existence of an window effect was found. The estimated diffusional parameters, D_{z0}, decrease continuously with chain length, contrary to Gorring's results. The activation energy for diffusion, however, is similar for *n*-heptane and *n*-nonane (about 48 kJ/mol). This agrees with Ruthven's observations for *n*-paraffin diffusion in zeolites 5A, silicalite and NaX [Ruthven and Eic, 1988; Vavlitis et al., 1981]: after initially increasing with chain length, activation energies become essentially constant above a certain carbon number; on the other hand, the pre-exponential factors decrease continuously. Barrer [1983], based on similar results obtained by Kärger with NMR experiments in NaX [Kärger et al., 1980], suggested that this behavior is due to segmental diffusion of the chain. This effect is attributed to the segmental rotation of part of a linear molecule about a C-C bound, resulting in changes in the center of mass of the molecule without necessarily involving simultaneous translation of all parts of the chain. If the mechanism involves segments of approximately constant size above a certain chain-length then the activation energy becomes almost constant. Also, since for a longer chain more diffusion unit steps are necessary for migration of the entire molecule between sites, the pre-exponential factor must decrease with chain length. The magnitudes of the estimated values of the diffusional activation energy and diffusion coefficients are characteristic of a small-pore zeolite (cf. reference [Kärger and Ruthven, 1992c]), which supports the assumption that intra-crystalline transport is limited by the erionite phase.

In relation to the non-diffusional resistance parameter, kf, the activation energy is again similar for *n*-heptane and *n*-nonane (about 22 kJ/mol). The fact that, despite this, k_f decreases significantly with chain length (note that its pre-exponential factor is an

order of magnitude lower for nonane than for *n*-heptane), may indicate that chain length dependent entropic effects are involved in the transport through the external barrier.

Since Gorring did not show plots of the uptake curves, it is not possible to analyze the possibility of non-diffusional effects (sigmoidal curves) in his data. Also, Gorring states that the diffusion coefficient does not vary significantly with concentration up to 80% of the saturation loading. Above 80% saturation diffusivities were said to decline. This is in strong disagreement with the results of this work, since a very pronounced decrease of the transport time constants (*i.e.*, an increase in diffusivity) was observed with increasing occupancy. It is not possible to conclude whether these discrepancies are due to differences in the nature or treatment of the samples, or to deficiencies in Gorring's experimental procedure. Aspects such as heat dissipation, mass transfer resistance in the sample bed (Gorring reports using 5.38 g of sample!), sorbate condensation in components of the balance, or sample modifications (*e.g.*, coking) throughout the studies (it is reported that the same sample was used in all experiments) may have affected his results.

The approach developed in this work for isolating intra-crystalline and external mass transfer resistances provides a good description of the experimental data, and leads to consistent results. The method is based on the analysis of the occupancy dependence of the temporal moments of the transient uptake curves and a simple mass transfer model.

CHAPTER 5

SOME DETERMINANT FACTORS IN INTRA-CRYSTALLINE DIFFUSION: DIFFUSION OF CYCLOHEXANE AND ALKYL-CYCLOHEXANES IN SILICALITE

5.1 Introduction

The diffusion of cyclohexane in silicalite is a particularly interesting case of mass transport in zeolites, considering the large dimensions of the molecule relative to the diameter of micropores. The studies of Chon and Park [1988] on this system revealed some interesting results. Methylcyclohexane diffused somewhat faster than cyclohexane and higher alkyl-cyclohexanes. Even more puzzling, *trans*-1,4-dimethylcyclohexane had a diffusion coefficient two orders of magnitude higher than any of the other molecules studied. The existence of an "window effect" [Gorring, 1973] (see Section 2.5) was suggested as an explanation for the higher diffusivity of methylcyclohexane. However, it was shown in Chapter 4 that the original phenomena on which the concept of "window effect" was based may not be real (see also [Magalhães, Laurence and Conner, 1996; Cavalcante, Eic and Ruthven, 1995]). No solid interpretation for the results with *trans*-1,4-dimethylcyclohexane was presented.

The objective of this work was to re-examine this system, in order to obtain further insight into the observed phenomena. A simultaneous thermal analyzer (STA)

was employed, allowing for the measurement of heats of adsorption in addition to the diffusivities. A comprehensive interpretation of the results was attempted, based on qualitative concepts of Transition State Theory.

5.2 Theory

In this work, most diffusivities have been determined gravimetrically. For diffusion in a parallel-side slab, the fractional mass uptake is described by [Crank, 1975]

$$\frac{m-m_0}{m_\infty-m_0} = 1 - \frac{8}{\pi^2}\sum_{n=0}^{\infty}\frac{1}{(2n+1)^2}\exp\left(\frac{-(2n+1)^2\pi^2 Dt}{h^2}\right) \qquad (5.1)$$

where h is the slab's thickness and D the diffusion coefficient. At short times, Equation 5.1 can be replaced by a simpler expression:

$$\frac{m-m_0}{m_\infty-m_0} = 4\left(\frac{Dt}{\pi h^2}\right)^{0.5} \qquad (5.2)$$

According to Equation 5.2, D can be computed from the slope of the initial linear portion of plot of fractional uptake versus square root of time. This is the method most commonly employed in estimating diffusivities from gravimetric measurements. However, Balik [1996] has recently proposed a variation with some interesting advantages. One starts by recognizing that another asymptotic representation of Equation 5.1 can be obtained for long times, by considering only the first term in the series:

$$\frac{m-m_0}{m_\infty-m_0} = 1 - \frac{8}{\pi^2}\exp\left(\frac{\pi^2 Dt}{h^2}\right) \tag{5.3}$$

Equation 5.1 can then be approximated by:

$$\frac{m-m_0}{m_\infty-m_0} \approx \phi(x)\, f_{st}(x) + [1 - \phi(x)]\, f_{lt}(x) \tag{5.4}$$

where $x = Dt/h^2$, $f_{st}(x)$ and $f_{lt}(x)$ are given by Equations 5.2 and 5.3 respectively, and $\phi(x)$ is a continuous step function:

$$\phi(x) = \frac{1}{1 + \exp\left(\frac{x - a}{b}\right)} \tag{5.5}$$

$\phi(x)$ changes from 1 to 0 very rapidly in the neighborhood of $x = a$, making it the ideal weighing function for Equation 5.4. The parameters a and b are chosen so that the errors of Equation 5.4 are minimized. Values of $a = 0.05326$ and $b = 0.001$ were shown to give optimum results. Note that the best value for a will depend on the particular geometry of the adsorbent particle. Equation 5.4 is a relatively simple analytical expression that can be used for numerically fitting the experimental uptake data to the theoretical model. Balik has proved the success of this technique (called the *hybrid 1-term method*) in the analysis of diffusion of small molecules in polymer thin films. One advantage lies in the fact that all the data is used in the fit, and good results may be obtained even when large data scattering is present. In the traditional method, the linear portion of the uptake vs. $t^{0.5}$ plot can be very small and difficult to identify. In addition, m_∞ can be included as a fitting parameter in the hybrid 1-term method, and therefore exact knowledge of the final loading is unnecessary. Finally, a graphical representation of Equation 5.4 is practically indistinguishable from the complete solution

(Equation 5.1). This significantly simplifies the final comparison of the data to the model fit.

Another experimental technique used in this study was zero length chromatography (ZLC). This was developed in the late 80's by Eic and Ruthven [1988]. It has been successfully applied to various zeolite/adsorbate systems [Ruthven and Eic, 1991; Voogd et al., 1991; Hufton and Ruthven, 1993; Brandani and Ruthven, 1995] and can now be considered a reliable method for diffusivity measurements. The carrier gas flows through a small sample bed (only a few milligram are used), containing initially a low constant concentration of adsorbate. After adsorption equilibrium is attained in the sample, pure carrier gas is flown, and an FID detector monitors the concentration of adsorbate in the outlet stream, as it is desorbed from the sample. A mathematical model for the measured concentration as a function of time can be derived for a parallel-sided slab of thickness [Eic and Ruthven, 1988]:

$$\frac{C}{C_0} = \frac{L}{2} \sum_{n=1}^{\infty} \frac{\exp\left(\frac{-\beta_n^2 Dt}{h^2}\right)}{\beta_n^2 + L(L+1)} \tag{5.6}$$

where the parameter L is defined as:

$$L = \frac{1}{4} \frac{F \rho_s h^2}{m_s K D} \tag{5.7}$$

and β_n is given by the roots of:

$$\beta_n \tan(\beta_n) = L \tag{5.8}$$

For long times, only the first time of the series becomes significant and Equation 5.6 can be simplified to:

$$\ln\left(\frac{C}{C_0}\right) = \ln\left(\frac{2L}{\beta_1^2 + L(L+1)}\right) - 4\frac{\beta_1^2 Dt}{h^2} \qquad (5.9)$$

The values of D and L can therefore be computed from the slope and intercept of a plot of $\ln(C/C_0)$ versus time.

Because of the small amount of sample employed, and the fact that the carrier gas flows directly through the sample, the ZLC method minimizes extra-crystalline mass and heat transfer resistances, which may affect conventional gravimetric measurements, especially for rapidly diffusing systems.

5.3 Experimental

5.3.1 Materials

The silicalite used in these study was synthesized by A.W. Peters at W.R. Grace, following the procedure described by Müller et al. [1989]. Scanning electron micrographs show that the crystals are coffin-shaped and have a relatively narrow size distribution. The dimensions are (thickness × width × length): 8.9 × 9.4 × 39.0 μm.

The zeolite was calcined at 450 °C for 12 hr. under air flow. Before use, each sample was activated in the experimental apparatus at 500 °C for 12 hr. under dry helium flow. Heating ramps were never above 10 °C/min.

All adsorbates were obtained from Aldrich Chemical Company (purities > 99%), except for *trans*-1,4-dimethylcyclohexane, which was obtained from Fluka Chemika (purity > 98%).

5.3.2 Apparatus and Procedures

Most of the experimental work was performed with a simultaneous thermal analyzer (Rheometrics STA 625). A schematic of the experimental setup is shown in Figure 5.1. This apparatus combines a microgravimetric balance (TGA) with 0.5 μg maximum resolution and a differential scanning calorimeter (DSC) with 5 μW maximum sensitivity. Gravimetric and calorimetric data can be collected simultaneously from a single sample. Approximately 10 mg of zeolite were used in each experiment, spread as thinly as possible in the sample pan (about 1 cm in diameter). The runs were conducted under high purity helium flow (40 - 60 cm^3 $min.^{-1}$, typically). The adsorbate was introduced in the gas stream via a bubbler. The concentration in the gas phase could be varied by changing the relative flow rates of the bubbler and diluent streams and the bubbler's temperature. The STA apparatus was interfaced with a personal computer for data acquisition and control, using native Rheometrics' hardware and software. The mass flow controllers and valve associated with the gas streams were also interfaced with the same computer, using a μMAC 4000 A/D board.

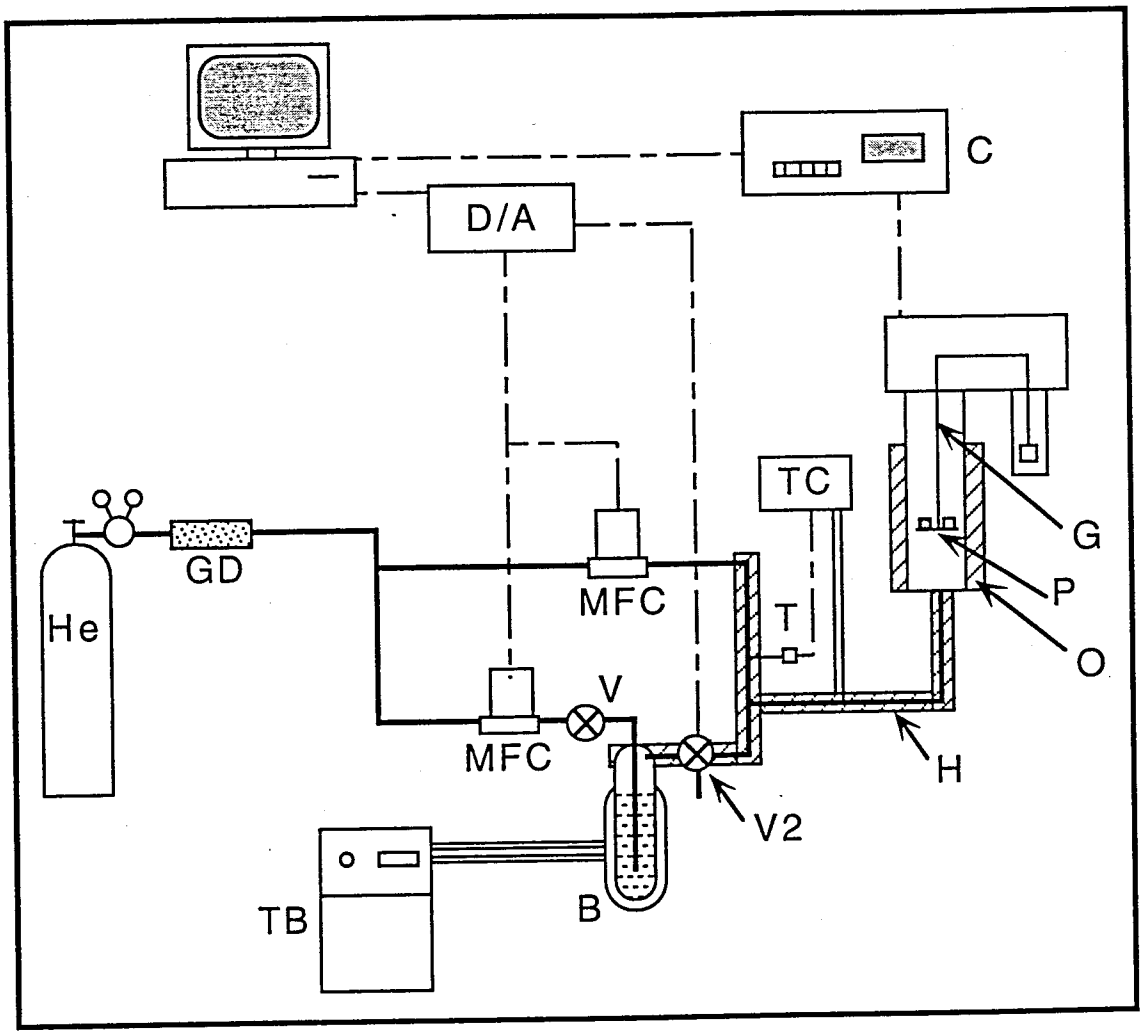

Figure 5.1 Setup of STA apparatus. B = bubler with adsorbate; C = STA's control unit; G = TGA hangdown assembly; GD = gas drier; H = heating tape; MFC = mass flow controler; O = STA's oven; P = DSC heat flux plate with sample and reference pans; T = thermocouple; TB = thermostatic bath with circulation; TC = temperature controler for region H; V = valve; V2 = two way valve.

The ZLC experiments were based on a typical setup [Kärger and Ruthven, 1992] (see Figure 5.2). A Hewlett Packard 5790A gas chromatograph equipped with a FID detector was employed. The sample (about 2 mg) was held in place by two stainless steel frits in a 1/8 in. Swagelock union. 1/16 in. tubing was always used if possible, in

order to minimize dead time effects. The carrier gas was high purity helium. All data acquisition and device control was again done with a personal computer, using a μMAC 1050 A/D board.

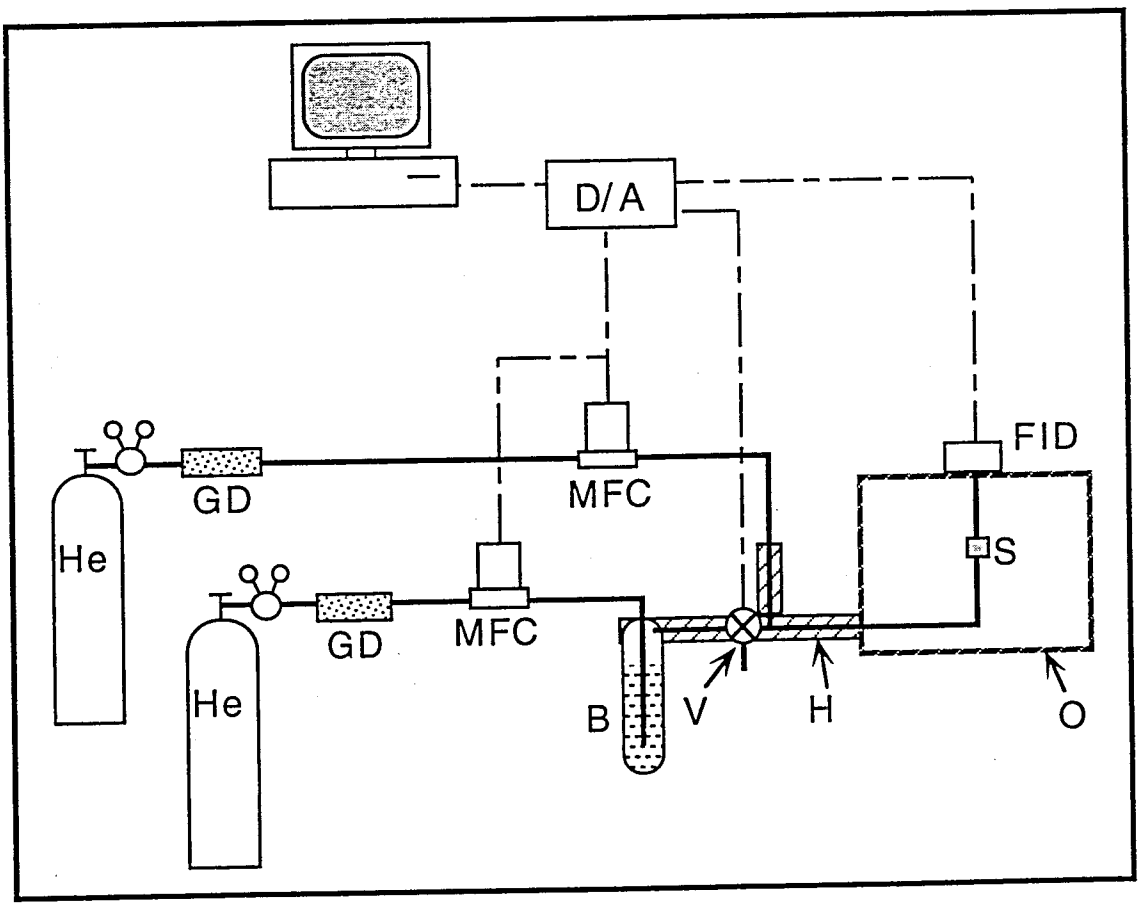

Figure 5.2 Setup of ZLC apparatus. B = bubbler with adsorbate; FID = flame ionization detector; GD = gas drier; H = heating tape; MFC = mass flow controler; O = GC's oven; S = sample; V = two way valve.

5.4 Results

5.4.1 STA experiments

The STA apparatus collects gravimetric and calorimetric data simultaneously. Figure 5.3 shows a typical set of data for adsorption of methylcyclohexane in silicalite. The heats of sorption are given by the integral area of the heat flow curve, while the diffusion coefficients are estimated from the gravimetric uptake data.

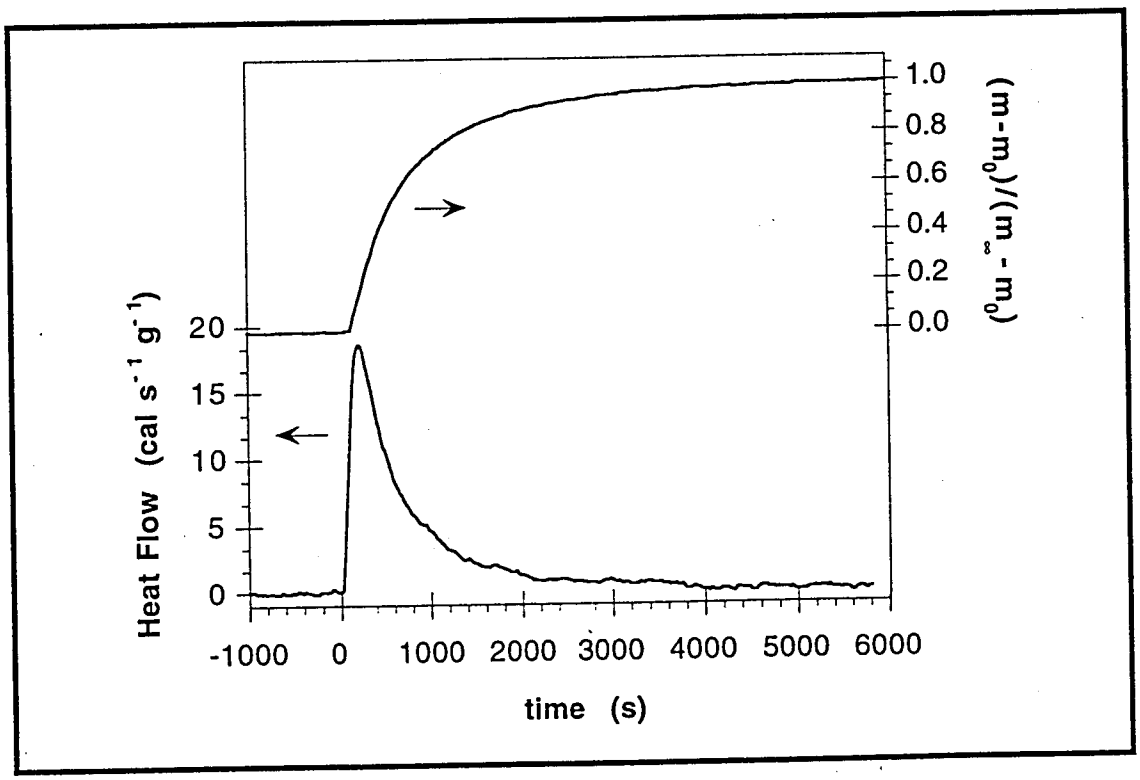

Figure 5.3 Gravimetric and calorimetric data obtained for methylcyclohexane at 150 °C.

The hybrid 1-term method described above was used in the computation of the diffusion coefficients. Some representative uptake curves are shown in Figure 5.4. It

can be seen that the theoretical model gives a very good representation of the data over the entire time range of measurement. This, together with the fact that different sample amounts (between 10 and 20 mg) gave consistent results, indicates that no extraneous mass or heat transfer effects affected the measurements.

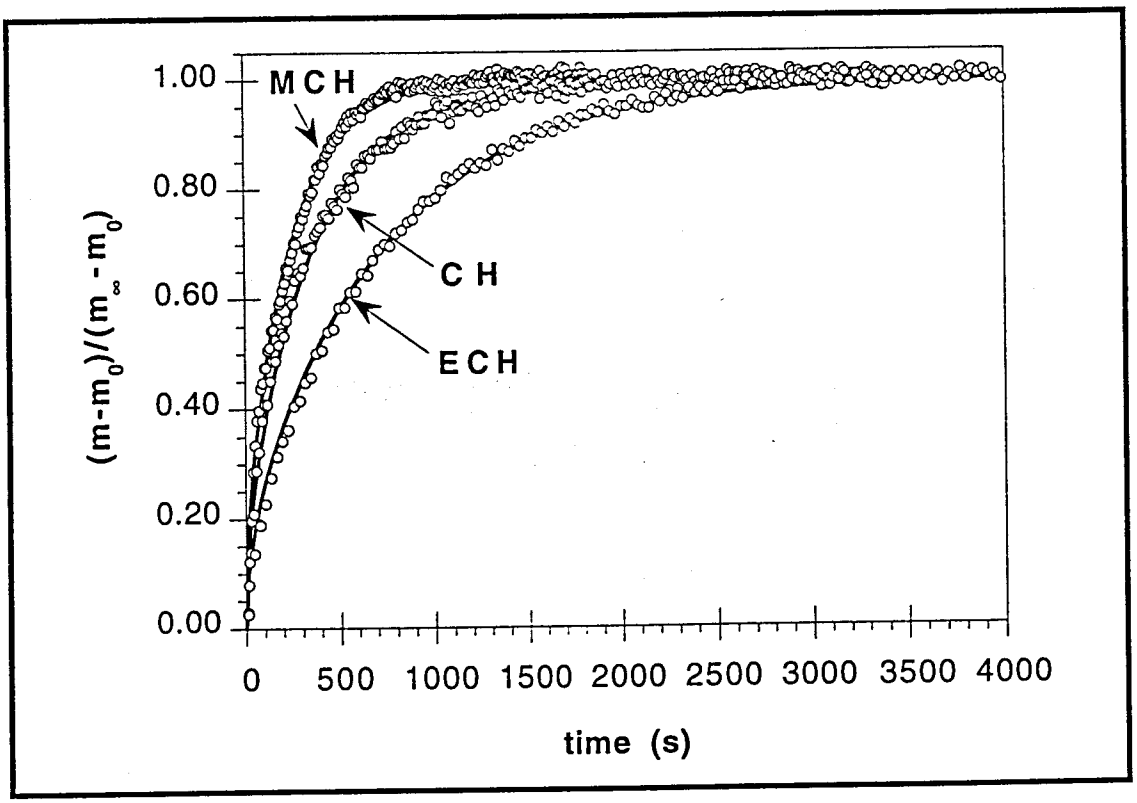

Figure 5.4 Typical gravimetric uptake curves for adsorption of cyclohexane (CH), methylcyclohexane (MCH) and ethylcyclohexane (ECH) at 200 °C. The solid lines are the fits of the diffusion model (Equation 5.1).

A maximum loading capacity of about 4 molecules per unit cell was observed for all adsorbates. In order to detect a possible dependence of the diffusivity with concentration, small sorption steps were performed at different zeolite loadings. There was good agreement between desorption and adsorption curves. The computed

diffusivities for cyclohexane (CH), methylcyclohexane (MCH) and ethylcyclohexane (ECH) are shown in Figure 5.5. No apparent dependencies with loading are observed. This is consistent with the results of Cavalcante and Ruthven [1995] for diffusion of cyclohexane in silicalite.

In Figure 5.6, the average diffusivities for each temperature are plotted versus 1/T. The data is well represented by an Eyring type expression ($D = A \exp(-E_a/RT)$). The values obtained for CH in this work are quite close to the results of Cavalcante and Ruthven [1995]. The data of Chon and Park [1988] are also plotted in Figure 5.6. Our results show the same relative trend in the diffusivities of the three adsorbates (MCH > CH > ECH), but the values are about one order of magnitude larger. It is important to note that those authors used very small crystals in the experiments (less than 1 μm thick). Under these conditions, extraneous effects may become significant. This fact was also discussed by Cavalcante and Ruthven, who indeed observed a difference of about one order of magnitude in the measured diffusivities of CH with sets of large and small crystals.

The heats of adsorption measured for CH, MCH and ECH at different loadings are shown in Figure 5.7. Adsorption and desorption measurements gave consistent results. A slight increase in the heats of adsorption with loading is apparent. This may be attributed to increasing adsorbate-adsorbate interactions. The isosteric heats measured by Cavalcante and Ruthven for CH show a similar trend, but were about 10% lower.

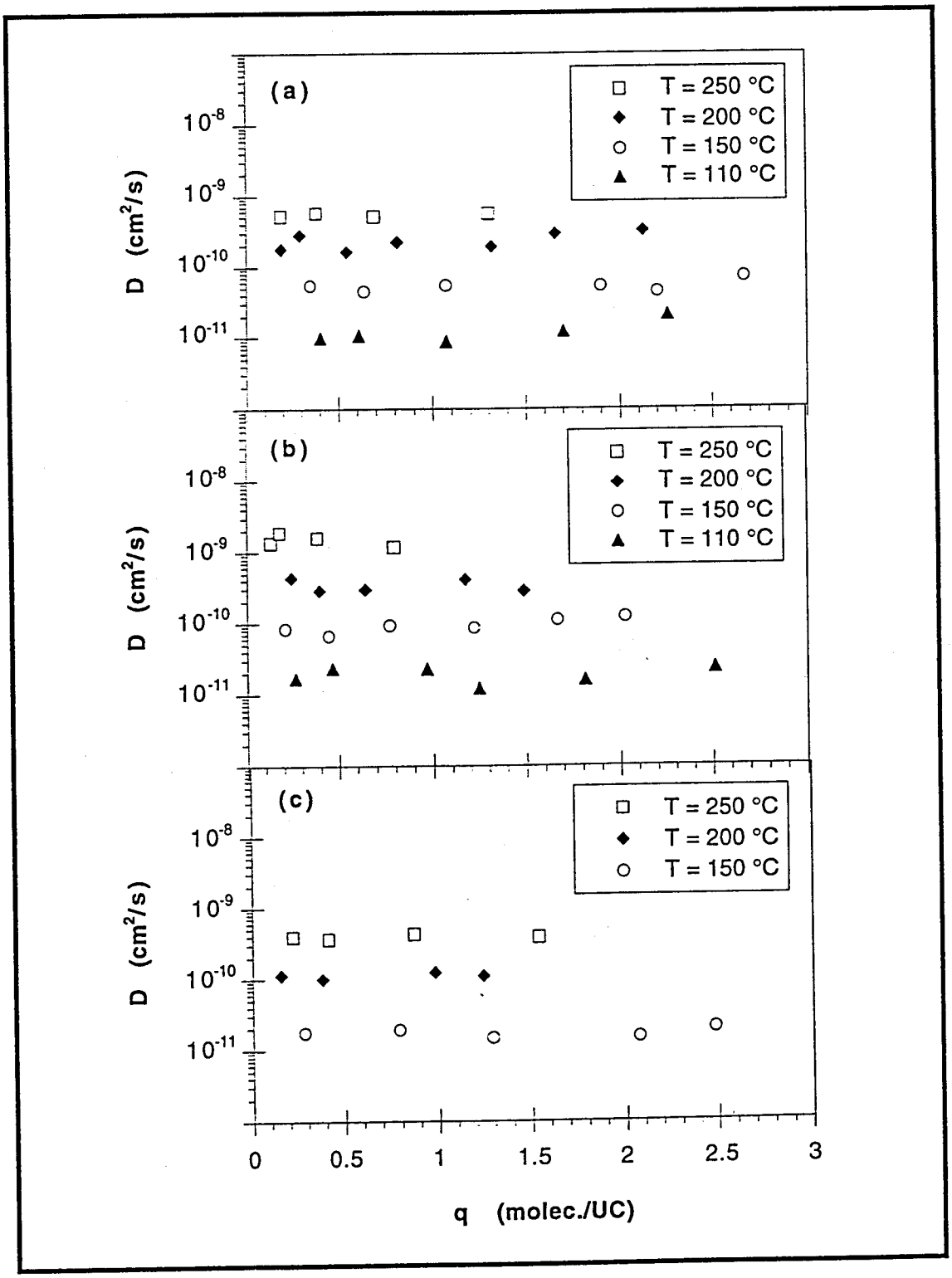

Figure 5.5 Diffusivities as a function of loading for a) cyclohexane, b) methylcyclohexane and c) ethylcyclohexane.

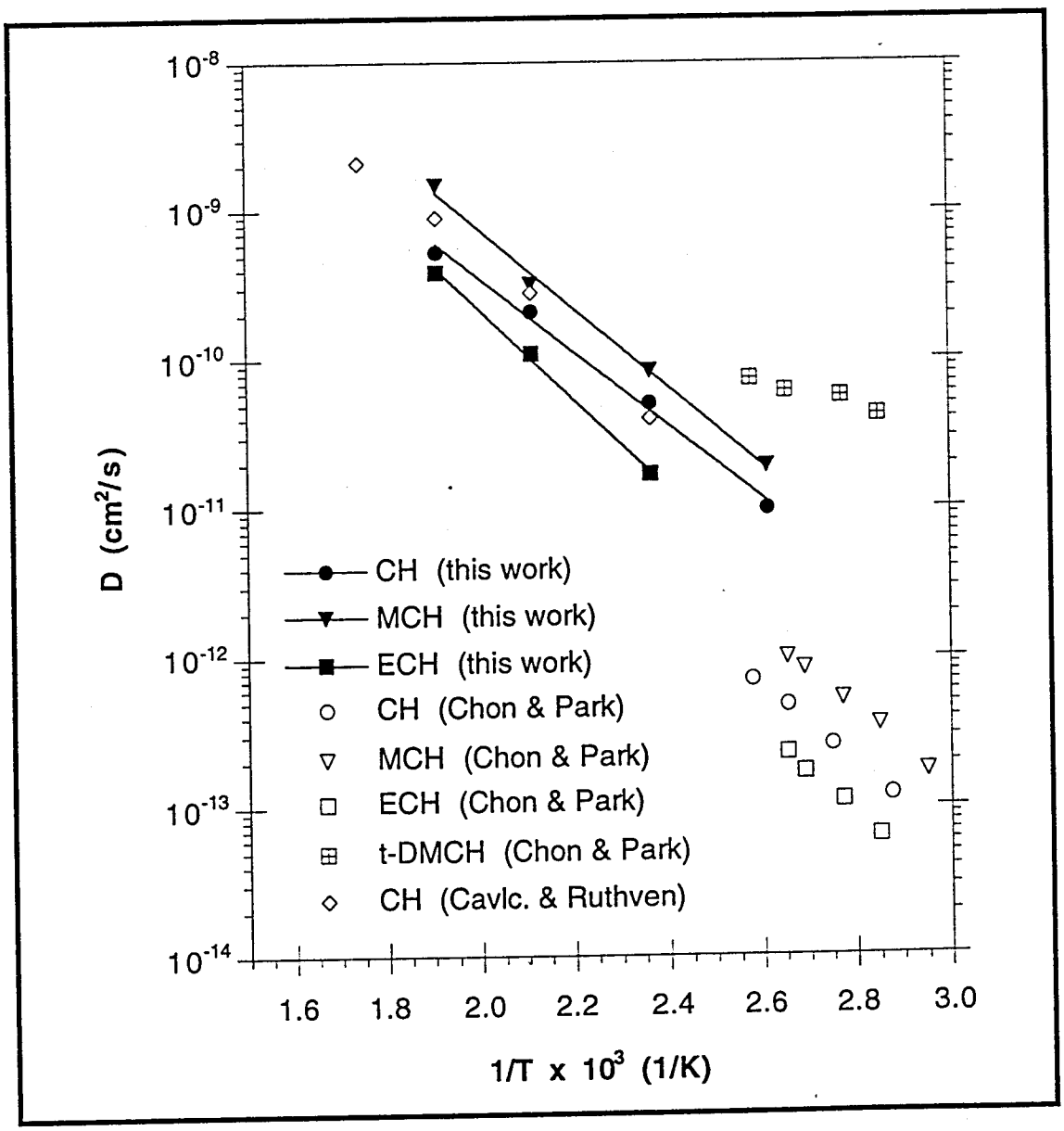

Figure 5.6 Arrhenius plots of diffusivities measured gravimetrically. Results of Chon and Park [1988] and Cavalcante and Ruthven [1995] are also shown.

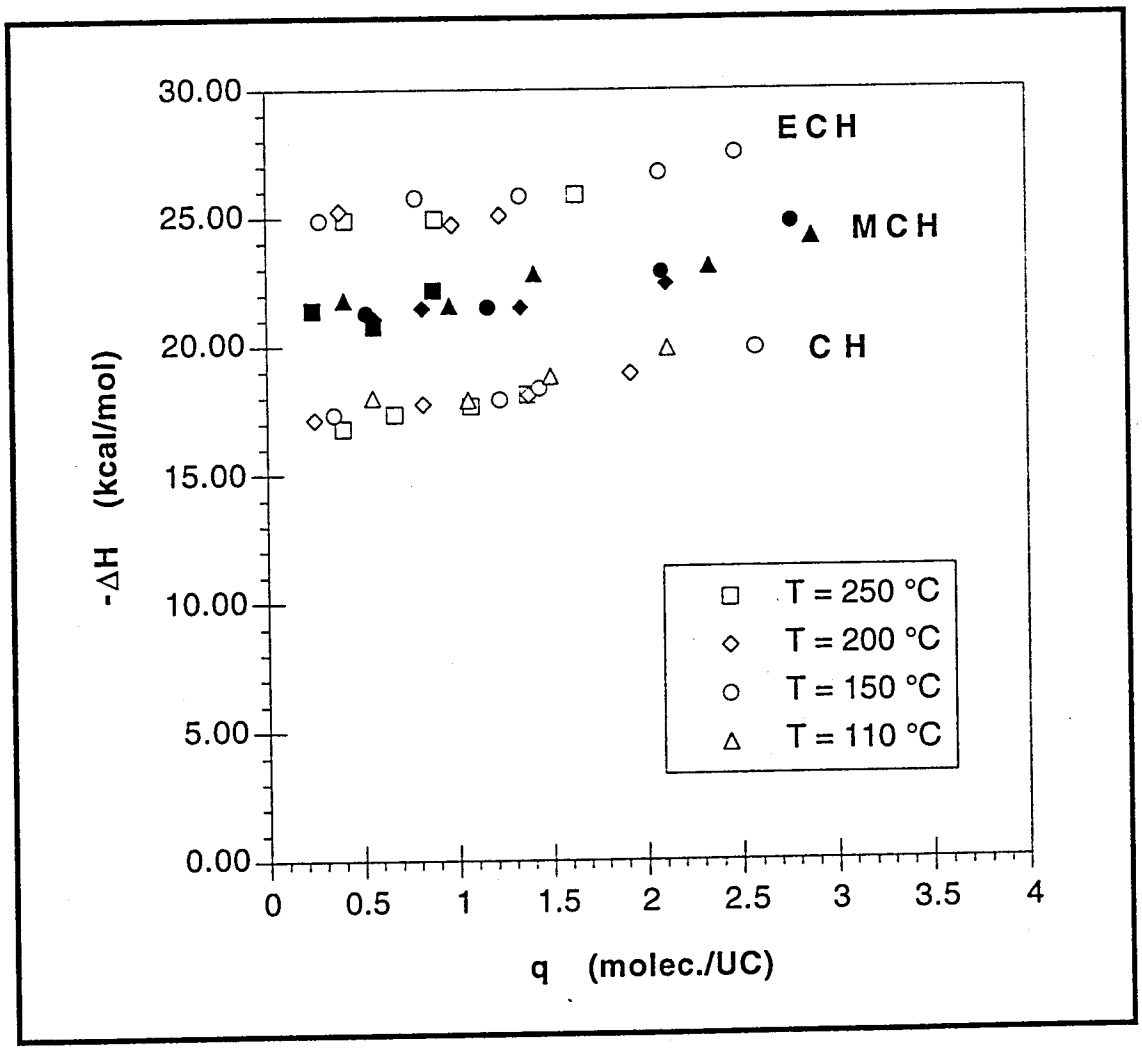

Figure 5.7 Heats of sorption as a function of loading.

5.4.2 ZLC experiments

We observed that *trans*-1,4-dimethylcyclohexane (*t*-DMCH) indeed diffuses significantly faster than the other adsorbates studied. Because the time scale of the gravimetric measurements would now be much shorter, intrusion of extra-crystalline resistances is possible, and the method cannot be used with confidence. We therefore used ZLC in the measurements for *t*-DMCH. The nature of this technique minimizes these extraneous effects. To test the consistency of the two methods, ZLC measurements for CH were also performed.

Some representative experimental data is shown in Figure 5.8, for both CH and *t*-DMCH. The theoretical diffusion model, also plotted, describes the data well. The values computed for the parameter L were always sufficiently large ($L > 50$) to warrantee that the process was not equilibrium-controlled [Brandani and Ruthven, 1995]. The Arrhenius plot of the measured diffusivities is shown in Figure 5.9. There is reasonable agreement between the CH diffusivities measured with the two techniques. The diffusivities measured for *t*-1.4-DMCH are more than one order of magnitude larger than for CH. Also shown in Figure 5.9 are the results for *cis*-1,4-dimethylcyclohexane (*c*-DMCH), measured gravimetrically.

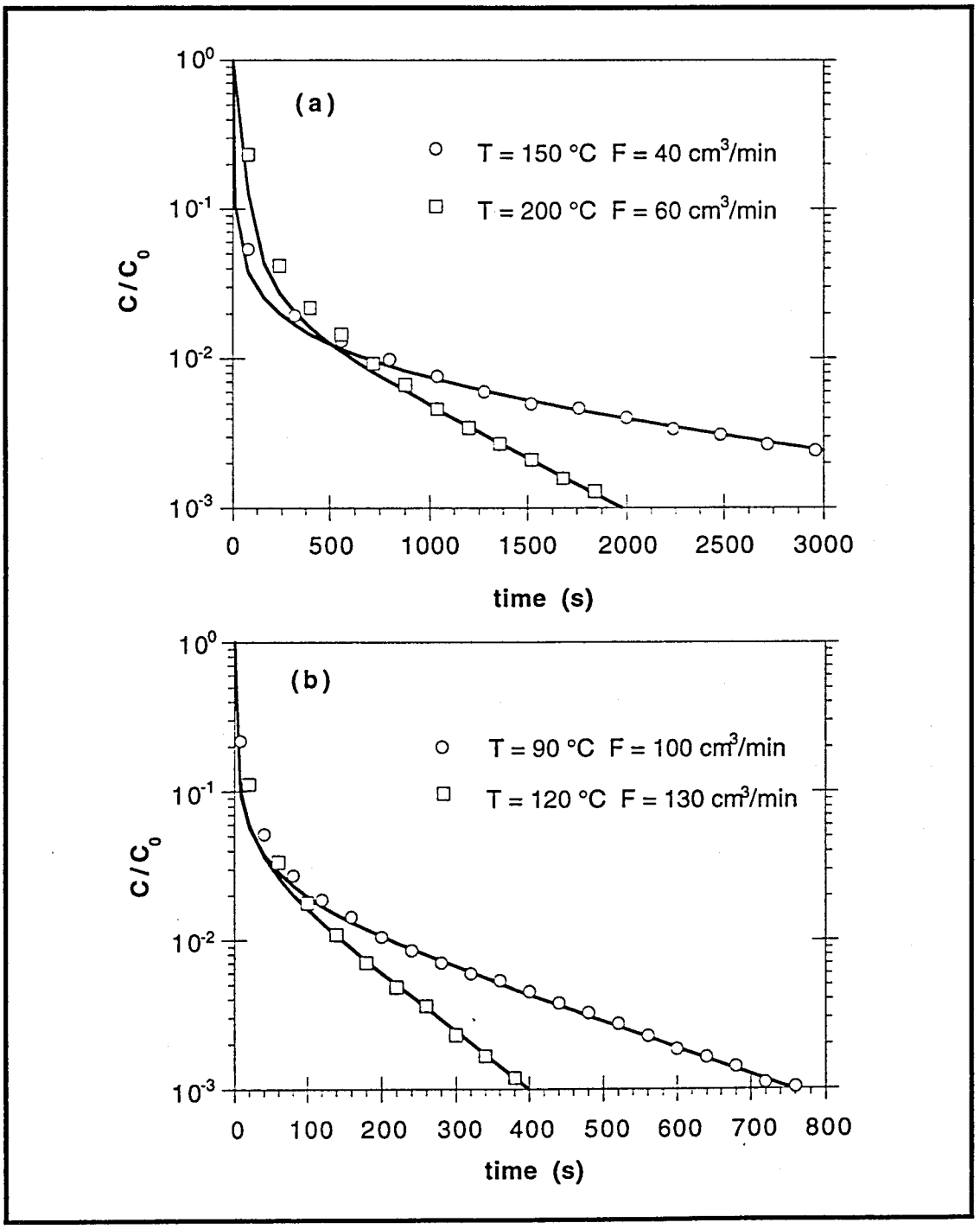

Figure 5.8 Typical experimental ZLC curves for a) cyclohexane and b) *trans*-1,4-dimethylcyclohexane.

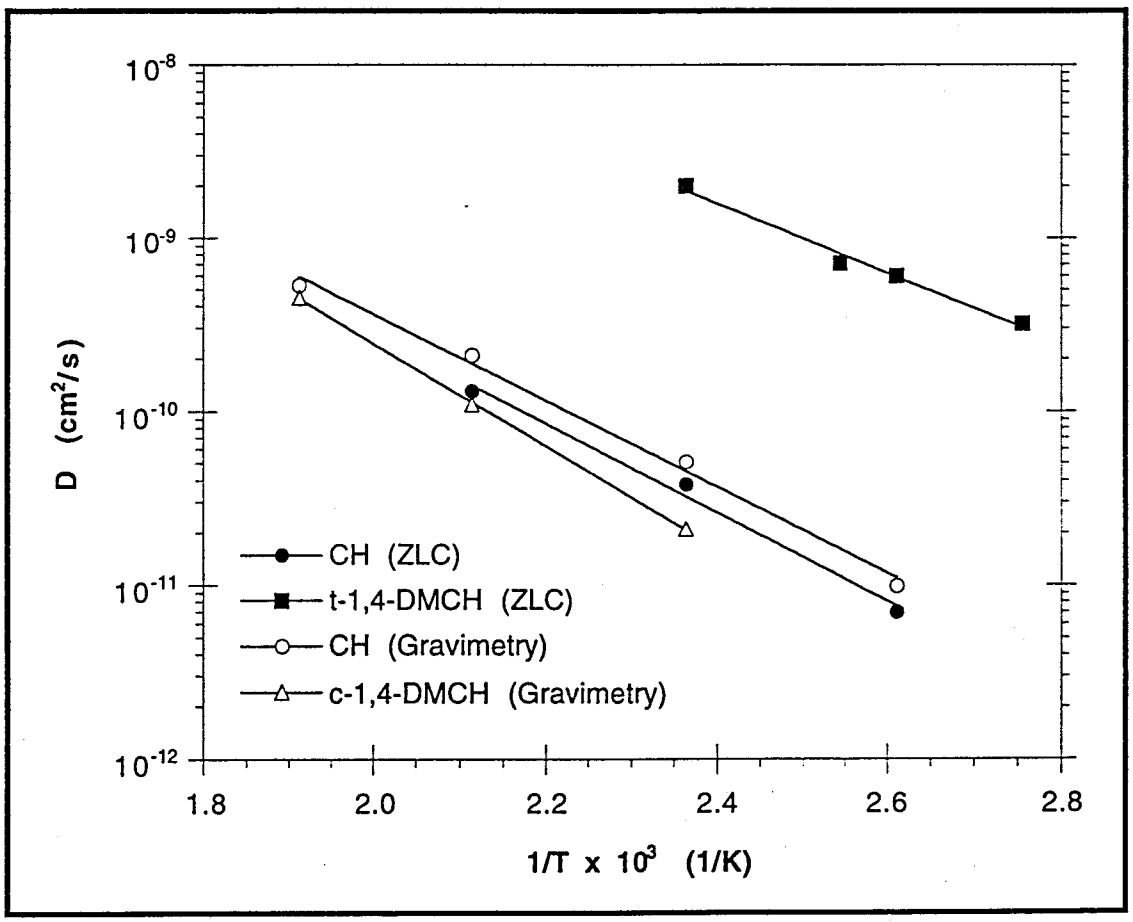

Figure 5.9 Arrhenius plots of diffusivities measured with the ZLC technique for cyclohexane (CH) and *trans*-1,4-dimethylcyclohexane (*t*-DMCH). Gravimetric measurements for CH and *cis*-1,4-dimethylcyclohexane (*c*-DMCH) are also shown.

The activation energies computed from the Arrhenius plots for all adsorbates are shown in Table 5.1. The activation energy obtained for CH in this work agrees well with those from prior studies. We observe an increasing trend in E_a with the length of the alkyl group, similar to the results of Chon and Park. There is however significant discrepancy for *t*-DMCH. One must again note that these authors used smaller crystals, and their measurements may have been masked by extra-crystalline mass or heat transfer

resistances. This would be particularly pertinent for a relatively fast diffusing adsorbate such as *t*-DMCH.

Table 5.1 Activation energies for diffusion of cyclohexane and alkyl-cyclohexanes in silicalite.

	E_a (kcal/mol)		
	this work	Chon and Park [1988]	Cavalcante and Ruthven [1995]
Cyclohexane	11.5	12.1	12.8
Methylcyclohexane	12.2	11.7	
Ethylcyclohexane	13.8	12.9	
n-Propylcyclohexane		13.2	
n-Butylcyclohexane		15.8	
n-Pentylcyclohexane		20.0	
t-1,4-Dimethylcyclohexane	9.3	5.7	
c-1,4-Dimethylcyclohexane	13.4		

5.5 Discussion

The following trend in the diffusion rates was observed in this work: *t*-DMCH >> MCH > CH > ECH, *c*-DMCH. Two main questions arise: why does *t*-DMCH have a much higher diffusivity than any of the other molecules, and why does MCH diffuse somewhat faster than CH? We shall try to develop a general reasoning that will allow for a satisfactory interpretation of these results.

The framework of silicalite is composed of two intersecting channel systems: straight channels (slightly elliptical, diameters 5.1 and 5.7 Å) and zigzag channels (nearly circular, 5.4 Å diameter). The channel intersections form a spherical "cavity" with a diameter of about 8.7 Å [Xiao and Wei, 1992]. The straight channels are oriented perpendicularly to the crystal's larger surface (*i.e.*, along the crystal thickness direction). We believe that diffusion of cyclohexane and alkyl-cyclohexanes occurs mainly along these channels. This assumption is supported by the fact that, in our work and in the work of Chon and Park [1988] and of Cavalcante and Ruthven [1995], the one-dimensional diffusion model for a parallel-sided slab gives the best fit of the experimental sorption curves. If diffusion along the zigzag channels were significant, a cylindrical or spherical diffusion model would probably give the best fit. A similar analysis, performed in detail by Ruthven and co-workers [Eic and Ruthven, 1988], indicated that also aromatic adsorbates diffuse preferentially along the straight channels of silicalite. Müller and Conner [1993] used in situ X-ray diffraction and FTIR during adsorption of cyclohexane and also concluded that CH does not access the zigzag channels.

Diffusion in zeolites can be viewed as an activated process. Transport along the zeolite framework involves activated "jumps" of the diffusing molecule between adjacent equilibrium adsorption sites. The size of the cyclohexane molecule can be characterized in terms of a kinetic diameter of 6.0 Å (from Breck [1974]) or 5.7 Å (from the Wilke and Lee method [Reid, Prausnitz and Poling, 1987]). However, the methylcyclohexanes are even larger (in length), to greater than 9Å for the ethyl- or dimethyl-cyclohexanes. Considering the dimensions of the framework, it is clear that the equilibrium sites will correspond to the ring being positioned at channel intersections. This is in agreement with the measured maximum adsorption capacities of

4 molecules per unit cell, corresponding precisely to one molecule per intersection [Chon and Park, 1988; Cavalcante and Ruthven, 1995; Müller and Conner, 1993]. The same is valid for the alkyl-cyclohexanes. The alkyl group will be accommodated so that interactions with the framework are maximized. Due to the small cross-sectional diameter of the alkyl group, it may be at least partially inserted (adsorbed) in the channel while the cyclohexane ring lies in the intersection. The transitional jumps will involve passage of the molecules through the channels, where they will suffer strong repulsions from the walls, due to the ring's large dimensions.

This visualization of the diffusion process will be useful in the interpretation of the experimental results. In Figure 5.10 are shown the values of the measured heats of adsorption ($-\Delta H$), and computed diffusional activation energies (E_a) and pre-exponential factors (A). The heat of adsorption reflects the intensity of the attractive interactions of the molecule with the framework at the equilibrium state. The increase in $-\Delta H$ in the sequence CH - MCH - ECH (Figure 5.10a) is certainly due to an increase in favorable interactions associated with the presence of the alkyl group (in a similar way toluene has been shown to have a higher heat of sorption than benzene, also in silicalite [Thamm, 1987]). In addition, the longer and more flexible the alkyl, the higher must the adsorption strength. *t*-DMCH, however, shows a somewhat lower heat of adsorption than ECH, despite both molecules possessing the same number of carbon atoms. The ethyl group in ECH may be more strongly adsorbed (maybe adsorbed deeper into the channel) than the two methyl groups in opposite ends of the ring in *t*-DMCH. Interestingly, *c*-DMCH exhibits the lowest heat of adsorption. The position of the two methyl groups in the *cis* configuration impairs the molecule's interaction with the zeolite walls. Due to this steric effect, the ring itself is less strongly adsorbed at the intersection.

The activation energy (Figure 5.10b) is associated with the height of the potential energy barrier involved in the passage through the transition state, between adjacent equilibrium sites. The magnitude of the barrier depends on the relative energy levels at the equilibrium and transition states. The increase of activation energy with the length of the alkyl group observed both in this work (ECH > MCH > CH) and in Chon and Park's (see Table 5.1) can be related to the increase in adsorption strength. In the ground (equilibrium) state, ECH is at a "deeper" potential energy well than CH. When the molecule passes through the channel, the energy level is essentially determined by the repulsions exerted on the ring, and the presence of the alkyl has little effect. Therefore, ECH has an higher energy barrier for diffusion. More puzzling is the fact that *t*-DMCH has the lowest activation energy of all the molecules studied, while its heat of adsorption is close to that of MCH. Therefore, its lower E_a has to be attributed to a more favorable passage through the channels. Why does the *trans* configuration facilitate this process so significantly? Detailed molecular potential simulations would be able to provide further insight. On the other hand, the high value of E_a measured for *c*-DMCH can be interpreted in terms of a very difficult passage through the channels, due to its less favorable configuration.

The energy relationships are illustrated schematically in Figure 5.11a. The relative location of the energy levels at equilibrium is given by the values of the heats of adsorption and the heights of the energy "jumps" are proportional to the activation energies.

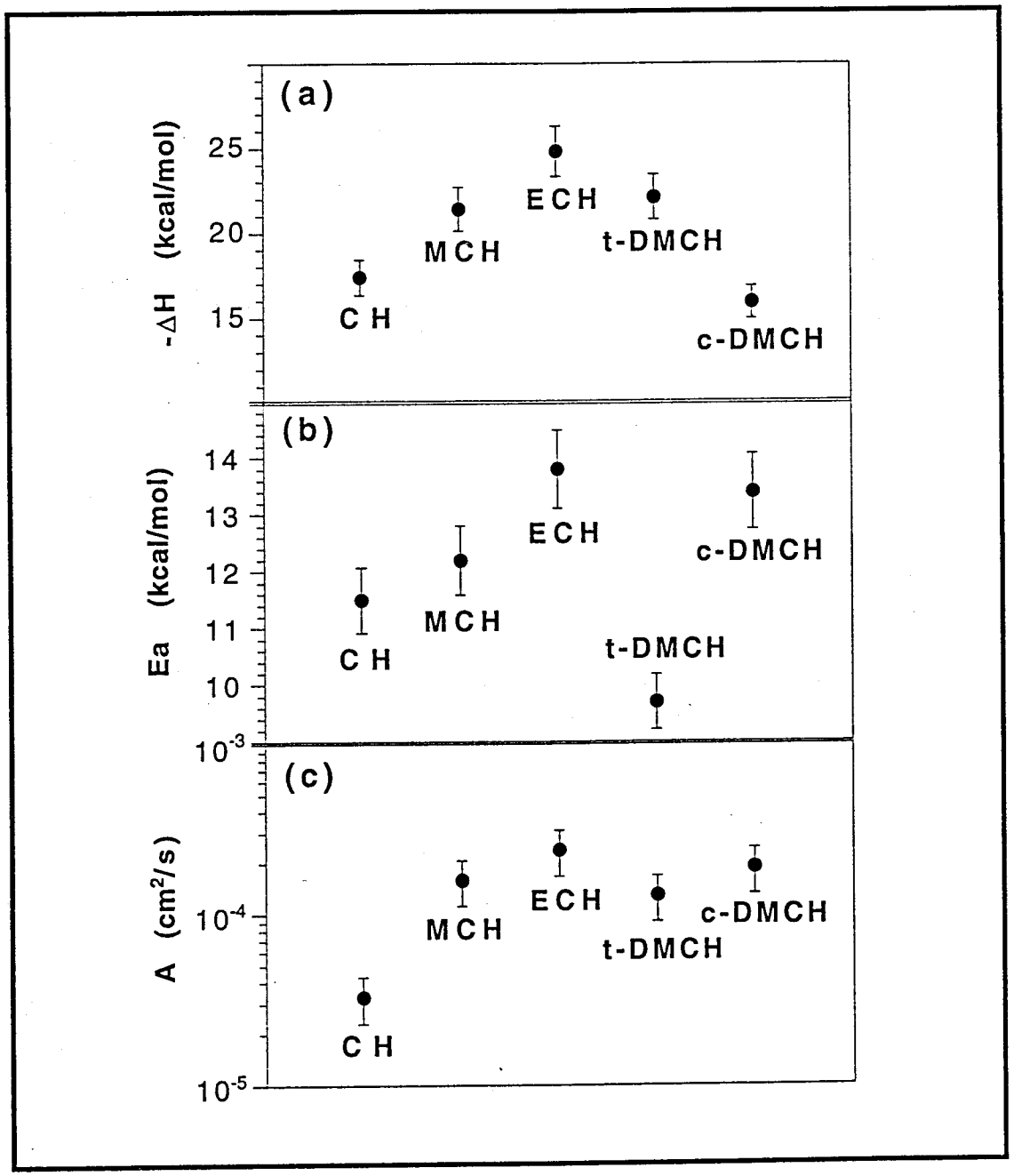

Figure 5.10 Computed values of a) heats of sorption (-ΔH), b) activation energies (E_a) and c) pre-exponential factors (A) for all the adsorbates studied. Rough error estimates are also shown.

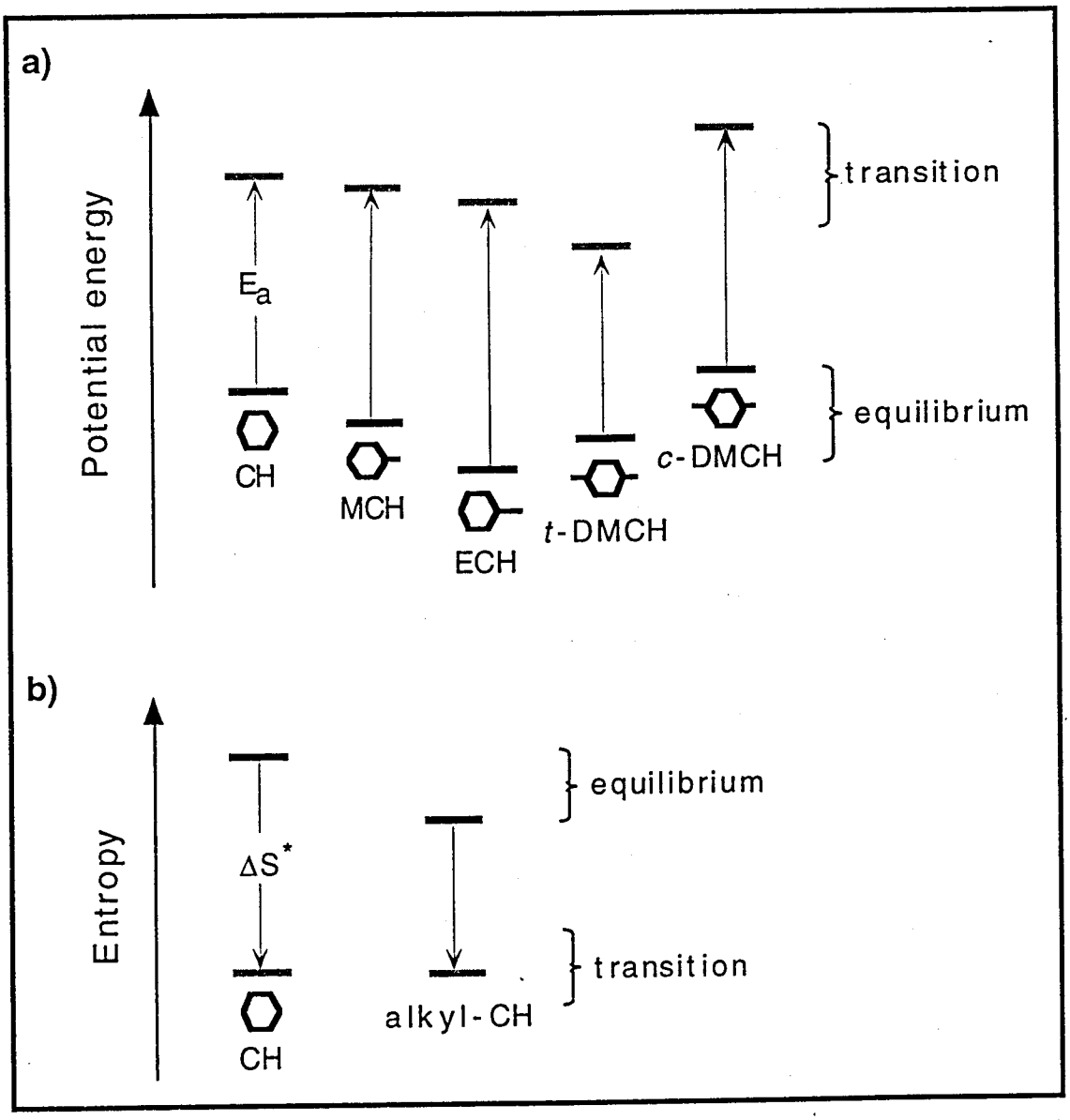

Figure 5.11 Schematic mapping of a) potential energy and b) entropy levels in the equilibrium and transition diffusional states.

The higher diffusivity of MCH in relation to CH is not associated with a lower activation energy, but with a higher pre-exponential factor (A). It seems that, for the sequence CH - MCH - ECH, there is an increase in activation energy simultaneously with an increase of the pre-exponential factor (see Figures 10b and 10c). This suggests the existence of a *compensation effect*. According to this theory, a correlation between activation energy and transition entropy is expected, in related processes, because they are effectively interdependent. In other words, an increase of the activation energy may require an increase of the entropy of transition. Justifications of this effect, as well as references to its occurrence in many fields of study, have been analyzed by Conner et al. [Conner and Schwarz, 1987; Conner, 1982]] and in references presented therein. An "isokinetic" relationship is often experimentally observed, viz.:

$$\ln A = \ln b + a E_a \qquad (5.10)$$

where a and b (related to the "isokinetic" temperature) are constants. A plot of the values of ln A versus E_a obtained in this work is shown in Figure 5.12. A linear relationship is not evident and, thus, compensation may exist but an isokinetic temperature is not evident. All the alkyl-cyclohexanes have relatively similar values for A, while cyclohexane falls outside this group, showing a lower pre-exponential factor. A compensation effect might be present, but the dominant influence may be those which affect the entropy of transition, which is common to the alkyl-cyclohexanes.

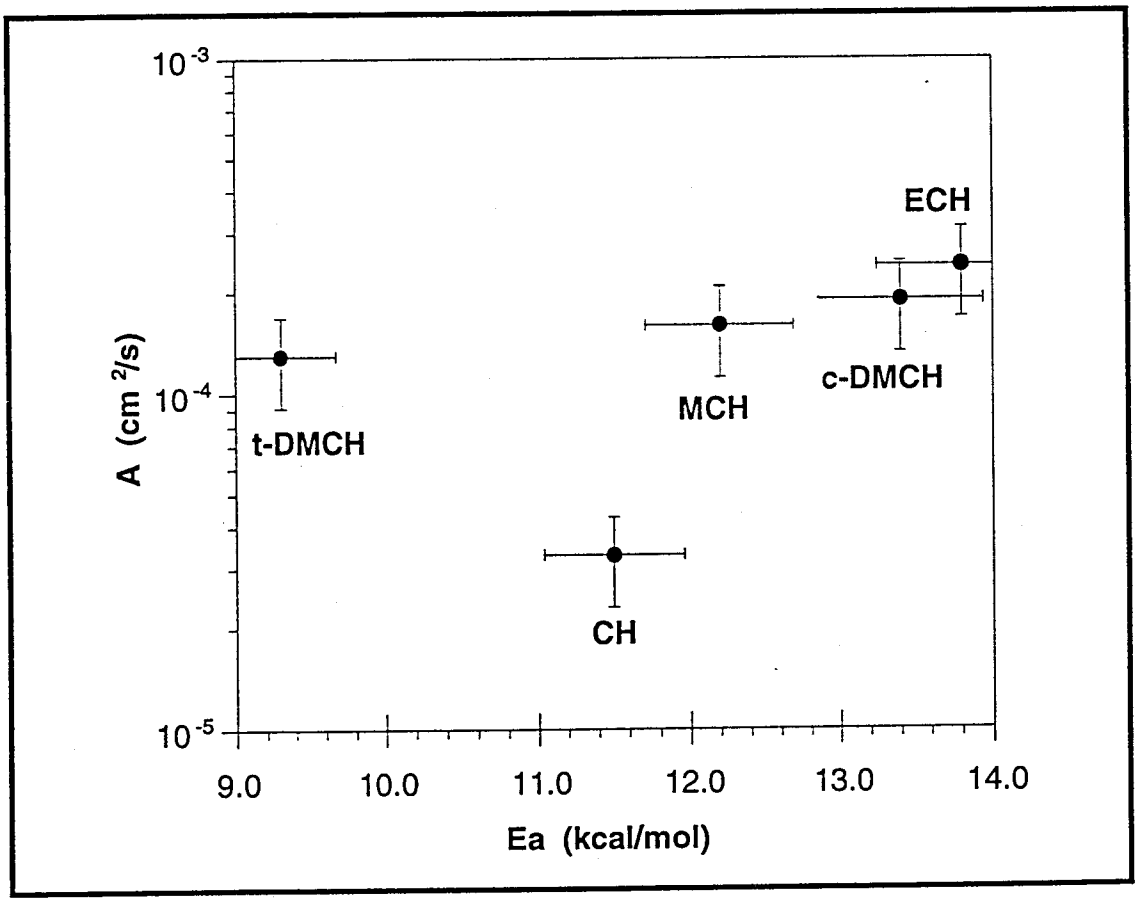

Figure 5.12 Pre-exponential factors (A) ploted versus activation energies (E_a) for all the adsorbates studied.

Qualitative arguments from Transition State Theory can provide an interpretation for this problem. The diffusion coefficient can be expressed following Eyring's theory of rate processes [Glasstone, Laidler and Eyring, 1941]:

$$D = \lambda^2 \frac{kT}{h} \exp\left(\frac{\Delta S^*}{R}\right) \exp\left(\frac{-E_a}{RT}\right) \tag{5.11}$$

The "pre-exponential" factor A is then a function of ΔS^*, the difference in molecular entropy between the transition and equilibrium states. This can be detailed in terms of the partition functions for the two states [Hill, 1986; Ruthven and Derrah, 1972; Kärger and Ruthven, 1992] (low adsorbate concentration and negligible adsorbate-adsorbate interaction is assumed):

$$D_x = \frac{\lambda_x^2}{2}\frac{kT}{h}\frac{1}{q_x}\frac{q^*}{q}\exp\left(\frac{-V_{0x}}{kT}\right) \qquad \text{with} \quad \frac{q^*}{q} = \frac{q_y^* q_z^* q_{rot}^* q_{int}^*}{q_y q_z q_{rot} q_{int}} \qquad (5.12)$$

Where the following partition functions have been introduced: translational (q_x, q_y, q_z), rotational (q_{rot}) and internal vibration (q_{int}). The superscript * designates the transition state. x is the direction of diffusion and V_{0x} the height of the energy barrier for passage, along x, to a neighboring site. When crossing the channel, a molecule will be significantly more restrained than when it resides at the intersection. There is therefore a loss of translational and rotational degrees of freedom. The more significant the difference in entropy between the equilibrium and transition states, the lower will be the ratio q^*/q in Equation 5.12, or the entropic term $\exp(\Delta S/R)$ in Equation 5.11 (recall that $\Delta S^* < 0$). It seems reasonable to assume that, at the equilibrium state, CH is at an higher entropy level than the alkyl-cyclohexanes. It is not clear whether cyclohexane is actually able to rotate in the intersection, but it will certainly have more degrees of freedom than the molecules with alkyl groups which may, as noted before, be partially adsorbed into the channel. On the other hand, the entropy at the transition state must be close for all molecules, since all should be similarly restricted when crossing the channel (the constriction of the ring being the determining factor). Consequently, CH must have the lowest pre-exponential factor, in agreement with the experimental results (Figure 10c). Figure 11b illustrates these considerations. This entropic effect is apparently

responsible for the higher diffusivity of MCH in relation to CH. For ECH, however, the increase in activation energy is overwhelming, causing the diffusivity to decrease.

The phenomena described above is a case of *intracrystalline partitioning*, as introduced by Xiao and Wei [1992]. In their study of diffusion of n-paraffins in zeolite 5A, they have shown quantitatively that differences in rotational degrees of freedom, induced by different molecular lengths, can have a very significant effect on the pre-exponential factors.

Recall that the cyclohexane ring can be in either boat or chair conformations, and the chair conformer is probably favored in the transition state due to its lower profile (cross section). Indeed, the chair conformation is favored in the gas phase by ~ 5 kcal/mole for cyclohexane and ~ 3.6 kcal/mole for the 1,4-*trans*-dimethylcyclohexane[26]. The methyl (or ethyl) groups will also tend to retain the molecules in the chair conformer as they will lead (or follow) the molecule through the straight channels. Indeed, the C8 cycloalkanes are larger in longest dimension than the channel intersections. This may contribute to the entropic constrainment of the alkylcyclohexanes at the channel intersections.

The significantly higher diffusivity of *t*-DMCH in relation to CH is due to the combined effects of lower activation energy and favorable entropic effect (higher pre-exponential factor). It is important to note that an apparently similar phenomena is exhibited with diffusion of *p*-xylene and benzene in silicalite. According to the recent results of Rees and co-workers [Rees, 1994; Shen and Rees, 1993], using a frequency response technique, the diffusion coefficient for *p*-xylene in the straight channels is two orders of magnitude greater than for benzene. The activation energy is 25% lower for *p*-

xylene and the pre-exponential factor is about one order of magnitude higher. The parallel between the two cases is evident.

5.6 Conclusions

The trend in the diffusivities observed by Chon and Park was reproduced in this work. The measured heats of adsorption and activation energies allowed for a mapping of the potential energies of the adsorbates at the equilibrium and transition diffusional states. A better understanding of the observed relative diffusion rates can be obtained this way. *Trans*-1,4-dimethylcyclohexane seems to go through a relatively low energy barrier when crossing the channels, thus having a significantly lower activation energy than the other molecules. The *cis* isomer of dimethylcyclohexane can only be adsorbed in a strained configuration (reducing the net enthalpy of adsorption) and, further, does not easily diffuse easily between channel intersections as it does not easily adopt the favorable chair configuration in this restricted environment. The ethylcyclohexane is the most strongly adsorbed due to the ability of the ethyl to interact with the zeolite pore walls. In addition to potential energy barriers, entropic factors also seem to play a role for transport in this system. The alkyl-cyclohexanes are more restricted at the channel intersections than cyclohexane, which favors diffusion. This entropic effect may be responsible for the greater diffusivity of methylcyclohexane in relation to cyclohexane.

An interesting aspect of diffusion in zeolites is suggested by this study. Diffusion in zeolites (and other porous networks) is certainly dictated by two factors: the difference in energies between equilibrium and transition states; and the difference between the entropic constraints on the diffusing species in these two states. If, in a set of adsorbates, the energy and entropy of the transition states are similar, some species

may be more strongly adsorbed due to their ability to interact with the surface, and simultaneously assume a more restricted adsorbed state within the zeolite framework. There would, thus, be a connection between an improved ability of a molecule to maximize its interaction with the surface (increasing the heat of adsorption at the equilibrium state) and a decrease in the difference in entropy between the equilibrium and transition states. Since the entropy difference is a negative quantity, this would result in a compensation between the availability (activation energy) and accessibility (transition entropy) of diffusion in zeolites. This compensation is somewhat unconventional in that the dominant differences between these systems involve differences in the equilibrium states and not differences in the transition states.

CHAPTER 6

CONCLUSIONS

Some essential conclusions of this work can be summarized as follows:

- Due to the very high adsorption capacity of zeolite crystals, transport through the gas phase in a particle bed can become the limiting step, relative to intra-crystalline diffusion. Close analysis of the bed dimensions, adsorption capacity, and gas and solid-phase diffusion coefficients is necessary before advancing any predictions relative to the nature of the controlling mass transport phenomena.

- A simple semi-quantitative model, based on two dimensional segregation of gas and solid phase transports, can be successfully applied to model transport in a bed of zeolite crystallites. The effectiveness of the model is confirmed by its success in describing ^{129}Xe NMR concentration probing experiments for the system benzene/ZSM-5.

- Transport in zeolite crystals can be strongly affected by the presence of external (non-diffusional) mass transfer resistances, or surface barriers. In this case, the transport parameters can still be extracted from conventional gravimetric uptake experiments, by using a method based on the fit of a detailled transport model to the temporal moments of the experimental data.

- In the studied transport of *n*-paraffins in zeolite T, the surface barrier may be associated with a non-instantaneous adsorption equilibrium at the surface. The magnitude of this resistance is strongly dependent on the local slope of the adsorption isotherm, and thus on zeolite loading. The intra-crystalline diffusivities are also significantly concentration dependent. As a consequence, the external resistance is limiting at low loadings, while closer to saturation intra-crystalline diffusion controls the global mass transfer process.

- No evidence was found of the "window effect" reported by Gorring for diffusion of *n*-paraffins in zeolite T. The computed diffusivities decrease with the chain length of the *n*-paraffin, for carbon numbers between 7 and 12.

- Intra-crystalline diffusion cannot be assumed to depend merely on average molecular size. More subtle geometric/configurational aspects play an important role, since they affect both the sorbate-framework interactions and the sorbate's degrees of freedom at the equilibrium and transition diffusional states.

- The simultaneous estimation of heats of sorption and activation energies, using a STA apparatus, allows for the mapping of the relative potential energies at the equilibrium and transition states. In this way, differences in diffusion rates of different sorbates can be more easily interpreted.

- The transition entropy for diffusion may be a significant parameter in intra-crystalline diffusion. Favorable entropic effects, induced by particular adsorbate sizes or geometries, can be described according to basic Transition State Theory.

But some questions relative to mass transport in zeolitic systems remain unanswered. For example, no new insights were obtained relative to the dependence of diffusivities on concentration. Why do systems like *n*-paraffins in zeolite T exhibit a strong concentration dependence, while the diffusivities cyclohexanes in silicalite seem independent on occupancy? Does the chemical potential driving force argument provide a consistent explanation for this? And what is the reasoning for the relatively low activation energy of *trans*-dimethylcyclohexane in silicalite? To what point are the cyclohexanes restricted at the channel intersections? Is there an "orientation" effect associated to the presence of alkyl groups in the ring? Are entropic effects also significant in other systems?

It is clear that mere accumulation of data on diffusion coefficients will not supply further insights into these problems. Work with other scientific tools is essential to complete our understanding. Detailed molecular simulations and spectroscopic studies may supply the complementary information needed.

APPENDICES

APPENDIX A

CONCEPTS OF TRANSITION STATE THEORY APPLIED TO DIFFUSION IN ZEOLITES

A.1 General Treatment

Zeolitic diffusion can be described by an analog of Eyring's Transition State Theory (or "absolute rate theory") [Ruthven and Derrah, 1972; Kärger et al., 1980]. In general, treating diffusion as a rate process, this theory implies that the diffusion coefficient can be expressed by [Glasstone, Laidler and Eyring, 1941]:

$$D = \lambda^2 \frac{kT}{h} \exp\left(\frac{\Delta S^*}{R}\right) \exp\left(\frac{-\Delta H^*}{RT}\right) \qquad (A.1)$$

where ΔS^* and ΔH^* are the molar entropy and enthalpy differences between the transition (activated) and equilibrium states. The experimental activation energy is related to ΔH^* by:

$$E_a = \Delta H^* + RT - p\Delta v^* \qquad (A.2)$$

where Δv^* is the change in molar volume between the two states and is assumed to be zero. Substituting A.2 in A.1 we get:

$$D = \lambda^2 e \frac{kT}{h} \exp\left(\frac{\Delta S^*}{R}\right) \exp\left(\frac{-E_a}{RT}\right) \qquad (A.3)$$

Let us now try to apply these concepts to the specific situation of molecular diffusion in a zeolite. The molecule occupies lower potential sites (equilibrium positions) in the framework. It may acquire sufficient energy to overcome the potential barriers that surround it and "jump" to another adjacent low potential site. This jump implies passing through a state of maximum potential, the transition state. The exact location in the zeolitic framework of the equilibrium and transition states will depend on several geometric, energetic and conformational factors. In simple terms we can say that a "small" molecule will have a more negative (attractive) potential at the channels and a higher potential (still negative but with lower absolute value) at the cages. Thus, its equilibrium state will be at the channels. A "larger" molecule will eventually suffer repulsions in the channels (positive potential) and will have an attractive (negative) potential at the cages. The equilibrium site is now at the cages. These concepts are supported by experimental evidence, both from molecular dynamics simulations and experimental molecular localization. It is however important to recall that we are considering only systems with moderate interactions between the diffusing molecule and the framework atoms. Otherwise the molecule would be strongly adsorbed in localized sites of the framework and the potential barrier for diffusion would be associated with the strength of the adsorption interactions and not with the structural and geometric factors referred to above. The description of the statistical thermodynamical treatment follows.

The random walk model gives for diffusion in the x direction:

$$D_x = f_x \frac{l_x^2}{2\tau_x} = f_x \frac{l_x^2}{2} \nu_x \qquad \text{(A.4)}$$

where l_x is the jump distance, $\frac{1}{\tau_x} = \nu_x$ is the jump frequency and $f_x = \frac{\nu_x}{\nu_x + \nu_y + \nu_z}$ is the probability for the jump to occur in the x direction.

The jump frequency can be obtained from the concepts of Eyring's absolute rate theory and statistical thermodynamics. The following result can be derived [Hill, 1986; Kärger and Ruthven, 1992]:

$$D_x = f_x \frac{l_x^2}{2} \frac{kT}{h} P_{yzr} \frac{1}{q_x} \exp\left(-\frac{V_{0x}}{kT}\right), \qquad P_{yzr} = \frac{q_y^* q_z^* q_{rot}^*}{q_y q_z q_{rot}} \qquad (A.5)$$

where q_x, q_y and q_z are translational partition functions and q_{rot} is a rotational partition function. The superscript * designates the activated state. Notice that P_{yzr} corresponds to the entropy factor in Equation A.3, while V_{0x} (the potential barrier in the x direction) is equivalent to E_a, the activation energy.

We must now define the x-component of the Hamiltonian function, necessary for the derivation of the translational partition function q_x:

$$H_x = \frac{1}{2m} p_x^2 + \phi(x) \qquad (A.6)$$

where p_x is the molecular momentum in the x-direction and $\phi(x)$ is the potential. $\phi(x)$ is defined as a sinusoidal potential:

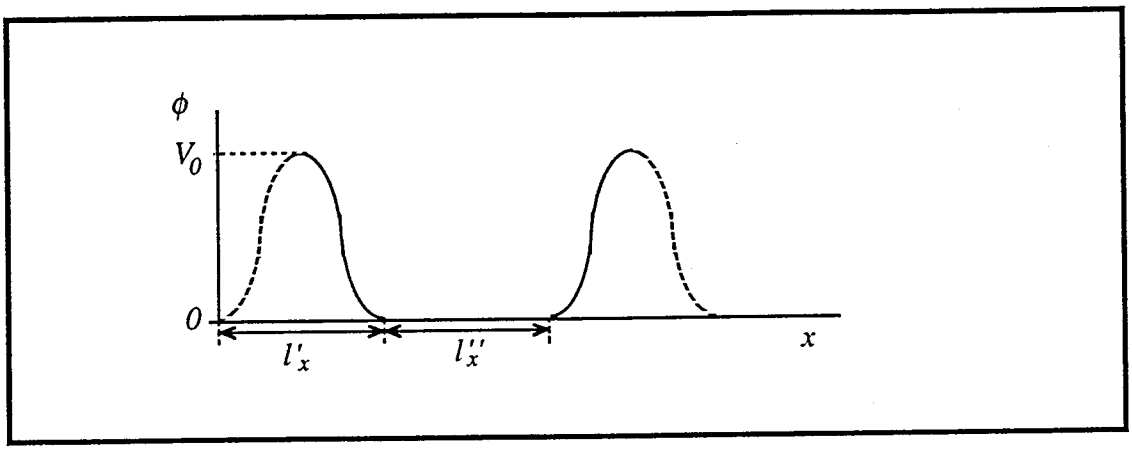

Figure A.1 Sinusoidal potential $\phi(x)$.

note that l'_x and l''_x depend on the specific dimensions and geometry of the molecule but $l_x = l'_x + l''_x$ (distance between adjacent potential maxima) is related only to the zeolitic framework.

q_x can then be obtained from:

$$q_x = \frac{(2\pi mkT)^{1/2}}{h}\int_0^{l_x} \exp\left(\frac{\phi(x)}{kT}\right)dx \qquad (A.7)$$

Substituting the final result into A.5 we get:

$$D_x = f_x\, l_x^2 \left(\frac{kT}{8\pi m}\right)^{1/2} P_{yzr}\, \frac{1}{l'_x \exp\left(-\frac{V_{0x}}{2kT}\right) I_0\left(\frac{V_{0x}}{2kT}\right) + l''_x}\, \exp\left(-\frac{V_{0x}}{kT}\right) \qquad (A.8)$$

Notice that in the limit $V_{0x} \rightarrow 0$ (no potential barriers) and with $P_{yzr} = 1$

Equation A.8 is reduced to:

$$D_x = \text{const.} \times \left(\frac{T}{m}\right)^{1/2} \qquad (A.9)$$

which corresponds to the temperature and molecular weight dependences characteristic of Knudsen diffusion regime.

As before, we can now consider some limiting situations. If $\frac{V_{0x}}{kT} >> 1$ and $l''_x \rightarrow 0$:

$$D_x = f_x \, l_x \left(\frac{V_{0x}}{8m}\right)^{1/2} P_{yzr} \exp\left(-\frac{V_{0x}}{kT}\right) \qquad (A.10)$$

This result, with f_x and P_{yzr} unity, is equivalent to the expressions derived by Chihara et al. [1978] and Kärger et al. [1980] using an analogy to Einstein's model of a monatomic crystal [Hill, 1986]. This would simply imply substituting the following results in Equation A.5:

$$q_x = \frac{kT}{h\nu_x} \quad \text{and} \quad \nu_x = \left(\frac{V_{0x}}{2ml_x^2}\right)^{1/2} \qquad (A.11)$$

It is easy to see that the molecule would indeed obey the premises of Einstein's model under the conditions imposed (i.e., the molecule is vibrating in the minimum of a potential surface with steep incline). This situation may be associated, as suggested by Kärger, to a large pore zeolite in which the repulsive potentials molecule-channel become less important than the molecule-adsorption site (localized atom or set of atoms) interactions. Thus the relevant diffusion "jump" does not occur between cages but between "sites" defined in terms not related to zeolitic geometry.

On the other hand, if $\frac{V_{0x}}{kT} >> 1$ and $l''_x > 0$ then:

$$D_x = f_x \frac{l_x^2}{l''_x}\left(\frac{kT}{8\pi m}\right)^{1/2} P_{yzr} \exp\left(-\frac{V_{0x}}{kT}\right) \qquad (A.12)$$

This result, with f_x and P_{yzr} unity, is now equivalent to the one derived by Xiao and Wei [1992a] assuming a square potential:

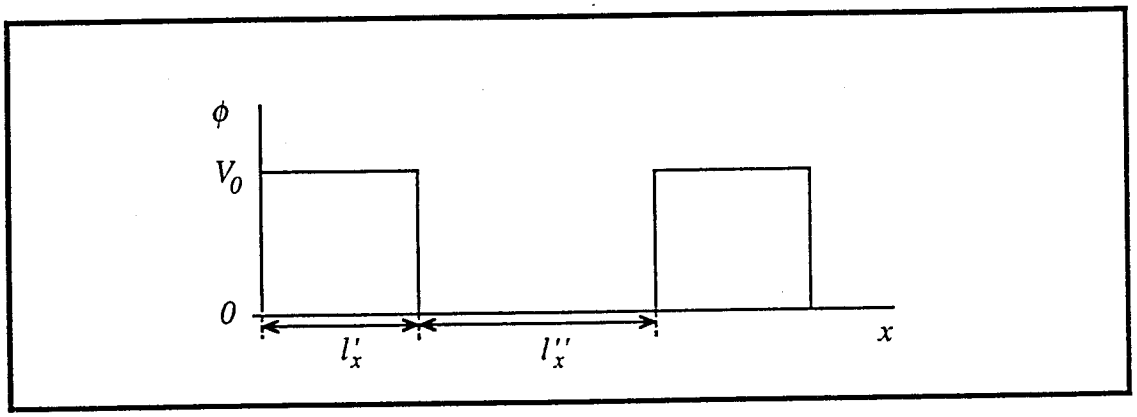

Figure A.2 Square potential $\phi(x)$.

Once again it is easy to realize how our initial model will become almost equivalent to this one under the imposed conditions.

Some attention must now be payed to the factor P_{yzr} or, in other words, the partitioning effects. We shall always consider that the equilibrium site is located in the cage.

A.2 Translational partitioning

Lets assume that the cage is closed in the y and z directions. This defines a "particle in a box" model for these directions. The molecule can move freely in a certain extension but, as it approaches the walls, it will suffer strong repulsions. The potential profile can be visualized in a simplified way as:

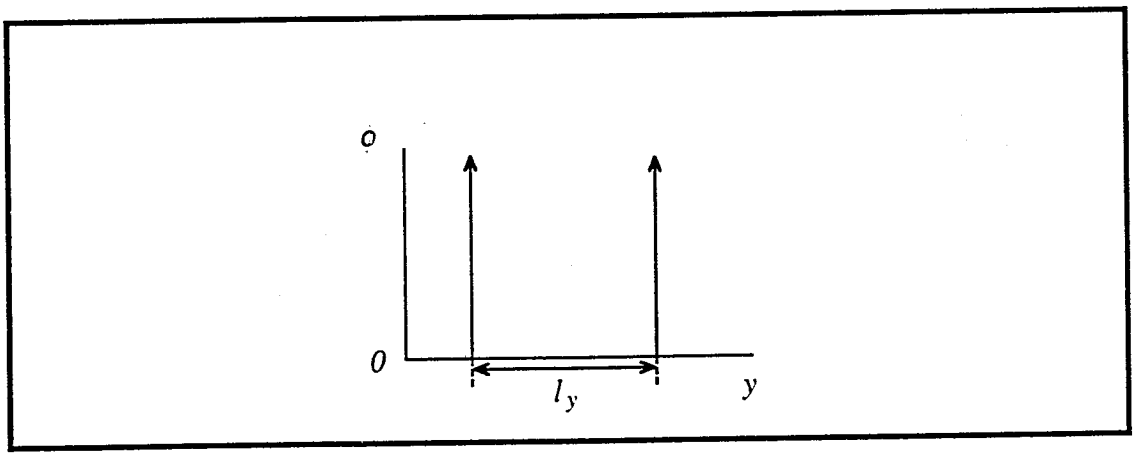

Figure A.3 "Particle in a box" potential $\phi(y)$.

We can then show that:

$$q_y = \frac{(2\pi mkT)^{1/2}}{h} l_y \qquad \text{(A.13)}$$

The same model can be applied to the transition state, in the channel (we expect $l_y^* < l_y$):

$$q_y^* = \frac{(2\pi mkT)^{1/2}}{h} l_y^* \qquad \text{(A.14)}$$

and thus:

$$P_{yzr} = \frac{l_y^* l_z^* q_{rot}^*}{l_y l_z q_{rot}} \qquad \text{(A.15)}$$

and from A.10:

$$D_x = f_x l_x \left(\frac{l_y^* l_z^* q_{rot}^*}{l_y l_z q_{rot}}\right)\left(\frac{V_{0x}}{8m}\right)^{1/2} \exp\left(-\frac{V_{0x}}{kT}\right) \qquad \text{(A.16)}$$

If, on the other hand, the cage is also open in the y and z directions, then one can assume a potential profile for $\phi(y)$ (and $\phi(z)$) similar to the sinusoidal potential $\phi(x)$. This means that there is a finite repulsion force as the molecule approaches the border of the cage, corresponding to a channel in the y direction (see Figure A.4).

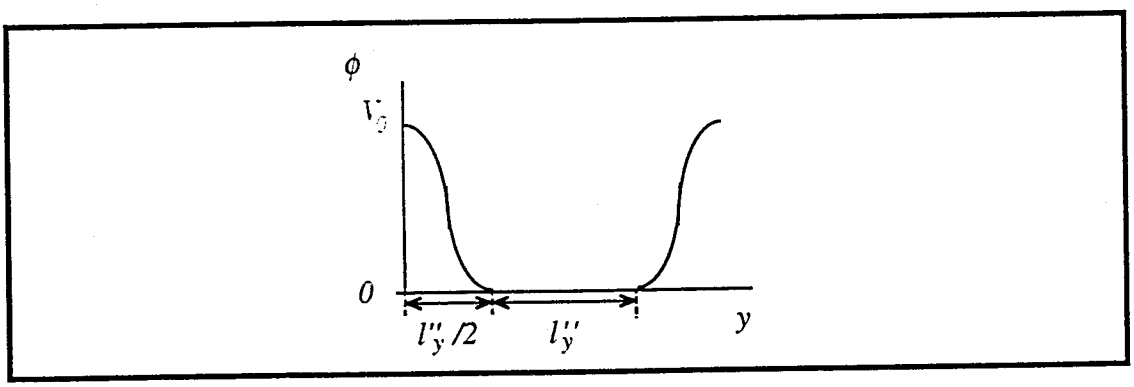

Figure A.4 Sinusoidal potential $\phi(y)$.

The translational partition function for the y direction becomes (when $\frac{V_{0y}}{kT} >> 1$ and $l''_y \rightarrow 0$):

$$q_y = \frac{(2\pi mkT)^{1/2}}{h} l_y \left(\frac{\pi V_{0y}}{kT}\right)^{-1/2} \qquad (A.17)$$

q^*_y is supposed to remain the same as in A.2.2. Substituting in Equation A.9, with $V_{0y} = V_{0x}$ and $l''_x \rightarrow 0$ and still considering cage closed in z direction:

$$D_x = f_x l_x \frac{l_y^* l_z^*}{l_y l_z} \frac{q_{rot}^*}{q_{rot}} \left(\frac{\pi}{8mkT}\right)^{1/2} V_{0x} \exp\left(-\frac{V_{0x}}{kT}\right) \qquad (A.18)$$

If the cage is also open in the z direction, and following the same reasoning:

$$D_x = f_x l_x \frac{l_y^* l_z^*}{l_y l_z} \frac{q_{rot}^*}{q_{rot}} \frac{\pi}{kT} \left(\frac{1}{8m}\right)^{1/2} (V_{0x})^{3/2} \exp\left(-\frac{V_{0x}}{kT}\right) \qquad (A.19)$$

If the equilibrium site is located at the channel and the activated state at the cage then, according to our simple model, the expressions previously derived for q_y (and q_z) should now be used for q_y^* (and q_z^*) and vice versa. This would result in different dependencies of the pre-exponential factors on V_0. However, in this case, the existence of relatively large channels and cages implies that the potential profile associated to this structural factors is less pronounced and the interaction potentials between the molecule and specific sites (atoms) in the framework are the most important. This may result in complex potential profiles inside the cage (and the channel) that cannot be reduced to a simple potential barrier as described by our simple model. Thus, we shall not analyze this case in more detail, at least in this phase of the work.

A.3 Rotational partitioning

This effect is due to the fact that a molecule may be able to rotate freely or partially in the cage but not in the channel (see figure A.5).

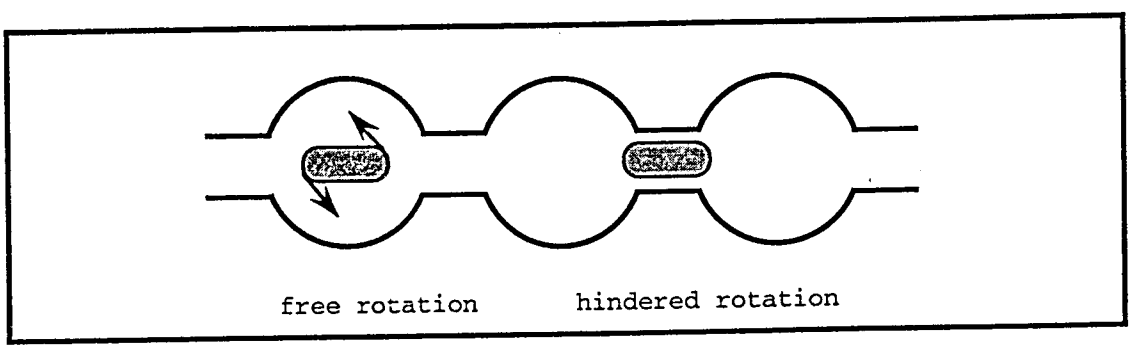

Figure A.5 Rotational partitioning.

If free rotation (or no rotation) occurs both in the cage and the channel then the rotational partition functions q_{rot} and q_{rot}^* will be identical and the ratio q_{rot}/q_{rot}^* in P_{yzr} will become unity. If, however, rotation in the channel is hindered then:

$$\frac{q_{rot}^*}{q_{rot}} = \prod_{\text{axis of hindered rot.}} \left(\frac{8\pi^2 I_i kT}{\sigma h^2}\right)^{1/2} \qquad \text{(A.20)}$$

where $I_i = \sum_n m_n r_{ni}^2$ is the moment of inertia for rotation in direction i and σ is the symmetry number ($\sigma(H_2O) = 2$, $\sigma(NH_3) = 3$, $\sigma(CH_4) = 12$)

This form of the rotational partition functions is based on the "ellipsoid of inertia" representation of the molecular rotation (see, for example, Hill [1960]) for a detailed description).

Xiao and Wei [1992] noted the importance of rotational partitioning effects on the diffusion of n-paraffins in 5A. This zeolite has large cages and narrow channels. Thus, linear paraffins, below a certain chain length, will be able to rotate in the cage around two axis (both perpendicular to the chain axis). Rotation in the channel will be however impossible. In this case A.19 becomes:

$$\frac{q_{rot}^*}{q_{rot}} = \left(\frac{8\pi^2 I kT}{\sigma h^2}\right)^{-1} \qquad \text{(A.21)}$$

Above a certain length the molecule will also not be able to rotate in the cage, and the partitioning effect disappears. These authors estimated the ratio q_{rot}/q_{rot}^* should be about $8*10^{-3}$ for propane and $3*10^{-3}$ for n-butane. These implies that the pre-

exponential factor of the smaller n-paraffins can be three orders of magnitude lower than for the longer ones! This is confirmed by experimental measurements. For other zeolites, like ZSM-5, in which the diameter of the cage and the channel are not so different they consider the rotational partitioning to be unimportant.

APPENDIX B

BROWNIAN MOTION IN A PERIODIC POTENTIAL

The classical theory of Brownian motion describes the continuous process of diffusive motion due to intermolecular collisions. According to the Stokes-Einstein equation:

$$D = k\,T\,B \qquad B = \frac{1}{3\pi\sigma\eta} \tag{B.1}$$

where B is the mobility, η the friction coefficient and σ the particle diameter.

On the other hand, activated diffusion is more accurately described as a "jump process", with the diffusing particles jumping in each step from one equilibrium site to another. From the rate theory we have:

$$D = A\exp\left(\frac{-\Delta G^*}{kT}\right) = A\exp\left(\frac{\Delta S^*}{k}\right)\exp\left(\frac{-E_a}{kT}\right) \qquad A = \lambda^2\nu \tag{B.2}$$

where ΔG^* is the free energy barrier associated to the activation process, ΔS^* the entropy change, E_a the activation energy, ν the jumping frequency and λ the jump length.

Both models can be applied to diffusion in liquids if the appropriate corrections are introduced. However, it is clear that the simple Brownian motion model cannot describe an activated diffusion process like diffusion in zeolites. But we can consider at

an intermediate case, between continuous Brownian motion and "step jump" activated diffusion: Brownian motion in a periodic potential field. This model was developed by Festa and d'Agliano [1978]. The only application of their result to zeolitic diffusion was presented by Nitsche and Wei (1991) in order to describe Gorring's "window effect". Despite the fact that this work has shown that there is no evidence of an window effect actually existing, the approach developed by Nitsche and Wei deserves some attention, being one of the few theoretical treatments of diffusion in zeolites. Here we analyze their model in some detail, starting with its application in a more general context, and ending with the particular case of diffusion of long molecules, as studied by those two authors.

The transport equation of a particle undergoing Brownian motion is given by the Fokker-Planck equation. When the dissipative forces are large enough this can be reduced to the Smoluchowski equation (one dimensional case):

$$\frac{\partial \rho}{\partial t} = \frac{\partial}{\partial x}\left\{D^*(x)\left[\frac{\partial \rho}{\partial x} + \frac{\rho}{kT}\frac{dV(x)}{dx}\right]\right\} \qquad (B.3)$$

where $V(x)$ is the potential and $\rho(x,x_0,t)$ is the probability density of finding the particle in position x at time t, if it was in x_0 at time $t = 0$.

When the potential is given by a periodic function of x, $V(x) = \phi(x)$ (with period l) the following expression for the diffusion coefficient was derived by Festa and d'Agliano [1978] (and later rederived by Weaver [1979] using a simpler mathematical method):

$$D(L) = \frac{l^2}{\int_0^l D^*(x)\exp\left(\frac{\phi(x)}{kT}\right)dx \int_0^l \exp\left(\frac{-\phi(x)}{kT}\right)dx} \qquad (B.4)$$

In the special case when D^* is not a function of x:

$$D(L) = D^* \frac{l^2}{\int_0^l \exp\left(\frac{\phi(x)}{kT}\right) dx \int_0^l \exp\left(\frac{-\phi(x)}{kT}\right) dx} \qquad (B.5)$$

It is clear that D^* is the value of the diffusivity when ϕ = constant. In the original development D^* was given by Equation B.1.

There have been suggestions for the use of this remarkably simple result in different fields. Some examples are: diffusion of ions in polyelectrolyte solutions; solute transport within biological membranes; superionic conductors; atomic migration in crystals. The extension to zeolitic diffusion is tempting. The fact that the result seems to be limited to a Brownian process should not condition this approach. Paraphrasing Nitsche and Wei [1991]: "[...] an analogy exists between these two distinct processes [zeolitic and Brownian diffusion], because thermal vibrations of the lattice introduce a stochastic element into the otherwise deterministic trajectory of the hydrocarbon, not unlike that in Brownian diffusion". We furthermore note that the Smoluchowski equation is not restricted to the description of Brownian movement. It can be used in other stochastic processes since it is essentially a "phenomenological tool for describing the fluctuation of physical quantities" [Doi and Edwards, 1986].

Let us then proceed with the zeolitic approach. We assume that the periodic potential $\phi(x)$ is given by the following wave:

$$\phi(x) = \frac{V_0}{2}\left[1-\cos\left(\frac{2\pi x}{l'}\right)\right], \quad 0 < x < l'$$

$$\phi(x) = 0, \quad l' < x < l'+l'' = l \qquad (B.6)$$

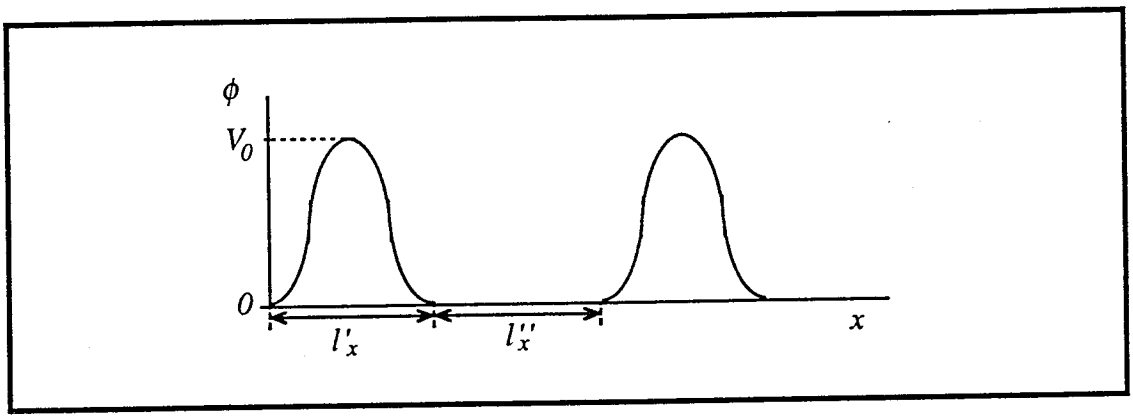

Figure B.1 Sinusoidal potential $\phi(x)$.

The region where $\phi(x) = 0$, with length l", corresponds to the "equilibrium site" (location of lower potential) of the molecule in the zeolite framework. It may be either the zeolite's cages or channels, depending on the molecular dimensions. The length of this region is determined by the characteristics of the framework and the molecule. For instance, if the molecule assumes a lower potential at the cage and this is large compared to the molecular size, then l" will be relatively large (the molecule can move in an extension l" without suffering the repulsion from the channels). A larger molecule in the same cage would be "stuck" between the repulsion regions of the channels (potential peaks in figure B.1) and l" would be lower. In reality the potential profile is not uniform within the cage. There may be several potential maxima and minima in this region. However we assume that the amplitude of these variations is negligible in comparison to the much higher potentials that the molecule will present at the channels. Substituting B.6 in B.5 and integrating, we get:

$$D = D^* \frac{(l'+l'')^2}{\left[\frac{l'}{2\pi}\exp\left(\frac{V_0}{2kT}\right) I_0\left(-\frac{V_0}{2kT}\right) + l''\right]\left[\frac{l'}{2\pi}\exp\left(-\frac{V_0}{2kT}\right) I_0\left(\frac{V_0}{2kT}\right) + l''\right]} \qquad (B.7)$$

If $\frac{V_0}{2kT} >> 1$ then:

$$D = D^* \frac{(l'+l'')^2}{\left[\frac{l'}{2\pi}\frac{1}{\sqrt{2\pi\frac{V_0}{kT}}}\exp\left(\frac{V_0}{kT}\right) + l''\right]\left[\frac{l'}{2\pi}\frac{1}{\sqrt{2\pi\frac{V_0}{kT}}} + l''\right]} \qquad (B.8)$$

Notice that if $V_0 = 0$ in (B.8) (negligible potential barrier) then $D = D^*$. It seems therefore obvious to identify in our model D^* with the Knudsen diffusion coefficient, since we know that this is the diffusional regime that characterizes the transport in small pore of a molecule not subjected to potential barriers:

$$D^* = \frac{4}{3} r \left(\frac{2kT}{\pi m}\right)^{1/2} \qquad (B.9)$$

where r is the pore radius and m the molecule's mass.

We can consider now two limiting cases, having present what was previously said about the significance of l".

Case 1: $l'' \sim l'$

$$D = D^* 4(2\pi)^{3/2}\sqrt{\frac{V_0}{kT}}\ \exp\left(\frac{V_0}{kT}\right) \qquad (B.10)$$

Case 2: $l'' \rightarrow 0$

$$D = D^* (2\pi)^3 \frac{V_0}{kT}\ \exp\left(\frac{V_0}{kT}\right) \qquad (B.11)$$

The result depends on the shape assumed for the potential. If, for instance, $\phi(x)$ is a "square potential":

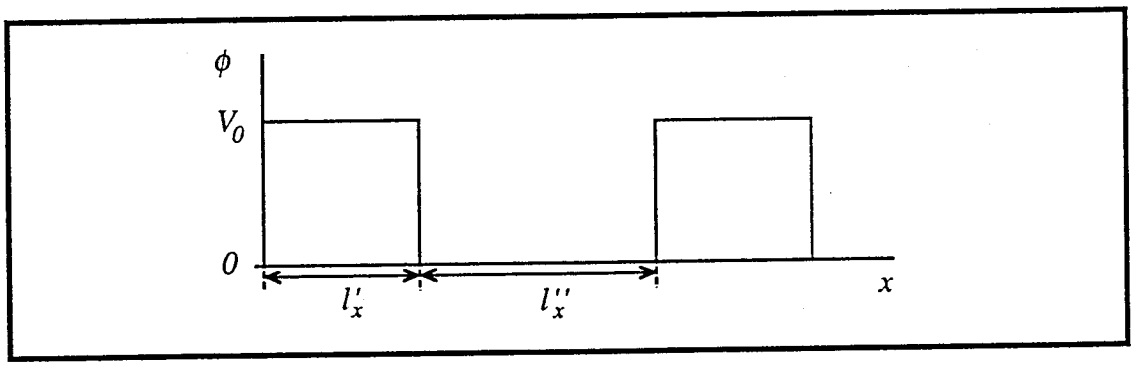

Figure B.2 Square potential $\phi(x)$.

then we will have the result:

$$D = D^* \frac{(l'+l'')^2}{\left[l' \exp\left(\frac{V_0}{kT}\right) + l''\right]\left[l' \exp\left(\frac{-V_0}{kT}\right) + l''\right]} \qquad (B.12)$$

Furthermore, when $\frac{V_0}{2kT} >> 1$, the previous equation becomes (with $l'' > 0$):

$$D = A\frac{(l'+l'')^2}{l'\,l''} \exp\left(-\frac{V_0}{kT}\right) \qquad (B.13)$$

Nitsche and Wei used the theory specifically in order to develop a quantitative model for Gorring's data on the "window effect" (see Section 2.5). The framework connectivity is ignored, and the diffusion process is assumed to be uni-directional. From Equation B.4 the diffusion coefficient is given by:

$$D(L) = D^* \frac{l^2}{\int_0^l \exp\left(\frac{\Psi(x,L)}{kT}\right) dx \int_0^l \exp\left(\frac{-\Psi(x,L)}{kT}\right) dx} \qquad (B.14)$$

where L is the molecular chain length and $\Psi(x.L)$ is the potential of the molecule when the beginning of the chain is in position x. Nitsche and Wei assumed that the molecule behaves like a rigid rod and $\Psi(x,L)$ can be computed from:

$$\Psi(x,L) = \int_x^{x+L} \phi(x')dx' \qquad (B.15)$$

$\phi(x')$ is the potential energy associated to the element dx' at position x' and is assumed to be a square potential (Figure B.3).

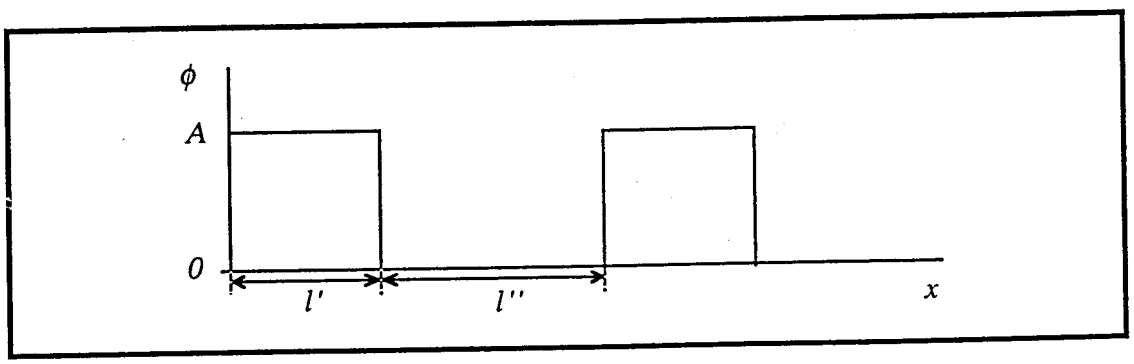

Figure B.3 Square potential $\phi(x')$.

The parameter l' corresponds to the length of the Erionite's channel and l'' to the cage.

We can then obtain $\Psi(x,L)$ from B.15:

$$H(L) = A\alpha(L)$$

$$0 < L < l' \Rightarrow \quad \alpha = L \quad \beta = l'-L \quad \gamma = l''-L$$

$$l' < L < l'' \Rightarrow \quad \alpha = l' \quad \beta = L-l' \quad \gamma = l''-L$$

$$l'' < L < l \Rightarrow \quad \alpha = l-L \quad \beta = L-l' \quad \gamma = L-l''$$

$$l < L < l+l' \Rightarrow \quad \alpha = L-l \quad \beta = l+l'-L \quad \gamma = 2l-L-l' \qquad \text{(B.16)}$$

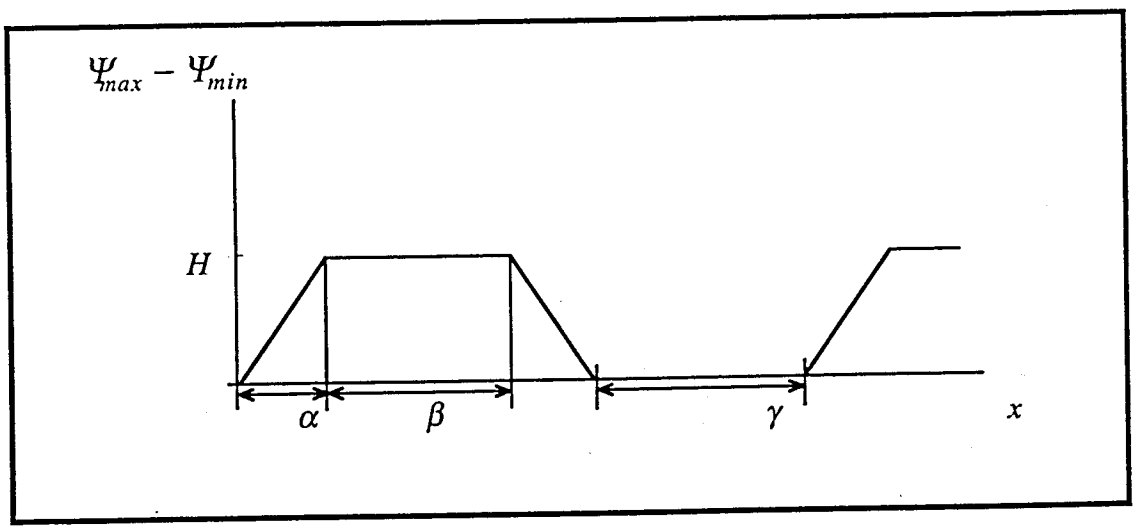

Figure B.4 $\Psi(x,L)_{max} - \Psi(x,L)_{min}$ as function of the molecular position, x.

An expression for D(L) can now be derived:

$$D(L) = D^* l^2 \frac{1}{\gamma + \beta \exp\left(\frac{H}{kT}\right) + \frac{2kT}{A}\left[\exp\left(\frac{H}{kT}\right)-1\right]} \times$$

$$\times \frac{1}{\gamma + \beta \exp\left(-\frac{H}{kT}\right) - \frac{2kT}{A}\left[\exp\left(-\frac{H}{kT}\right)-1\right]} \qquad \text{(B.17)}$$

In the special case when $\frac{H}{kT} >> 1$, Equation B.17 can be simplified according to the interval where L lies, originating Eyring type equations ($D = A \exp(-E_a/RT)$). For example:

$$0 < L < l' \Rightarrow D(L) = A \frac{l^2}{\beta\gamma} \exp\left(-\frac{H}{kT}\right) \qquad (B.18)$$

This last analysis was not actually done by Nitsche and Wei, but it is an important complement to their approach. Notice that, for any L, the "activation energy" is given by $H(L) = A\alpha(L)$. When $L = l$ we see from B.16 that $\alpha = 0$ and $H = 0$. Then the diffusivity will have a maximum value. Parameter l, we recall, is the period of $\phi(x')$, i.e. the period of the framework structure. Thus, a molecule with a length equal to the periodicity (or a integer multiple of the periodicity) of the zeolite's framework will have zero activation energy. Actually, the activation energy will vary periodically with L, with minima located at multiples of l. This fact constitutes the basis for the explanation of the diffusional behavior observed in the "window effect". Ruckenstein and Lee [1976] had already used this idea in a qualitative justification of Gorring's results. They recognized that the potential of a molecule with length l is independent of the position of the molecule in the linear channel. Since there are no potential barriers to overcome the diffusion process will show no activation energy. In a longer molecule, only the fraction (L - l) will contribute for the potential. They have called this phenomena "resonant diffusion".

In order to complete the mathematical treatment we must figure which values of l' and l" to use in the model. Nitsche and Wei, based on the paraffins' chain lengths and the Erionite framework's dimensions, identified $l = l' + l"$ with the carbon number $N = 12$ and l" with $N = 8 - 10$. We are now left with two parameters in Equation B.17:

D^* and A (the height of the barrier in $\phi(x')$). We shall assume that A is inversely proportional to the square root of the molecular weight ($D^* = b/m^{1/2}$), according to the Knudsen diffusion limit described in before. Nitsche and Wei chose the values of b and A based on the best possible fitting of the diffusivity values measured by Gorring. The resulting plot can be seen in figure B.5. The values of D(L) computed from the simplified Eyring type expressions like B.18 are also shown. The pre-exponential factors, A, and activation energies, E_a, obtained from the simplified expressions were plotted in figures B.6 and B.7, together with the corresponding Gorring's results.

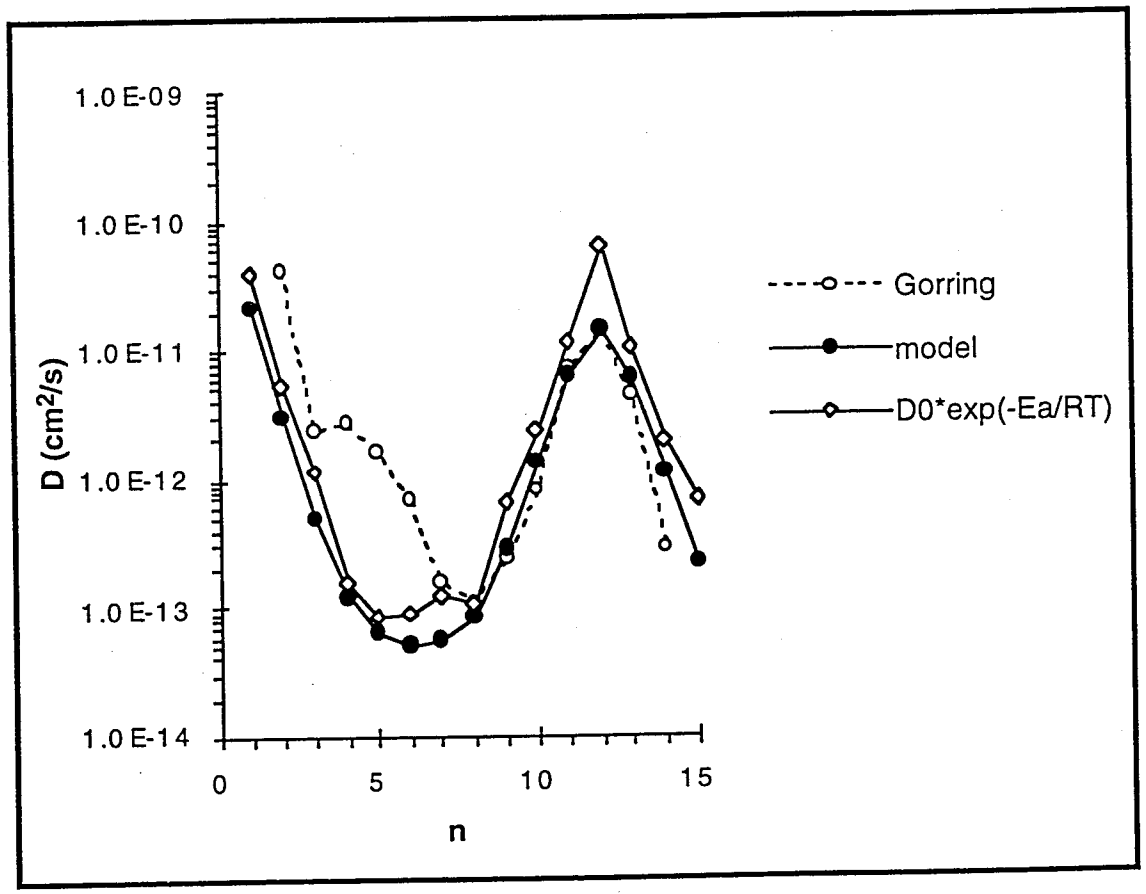

Figure B.5 Diffusivities of n-paraffins in zeolite T. Comparison between Gorring's data (T = 300 °C) and results from the model (Equation B.17). Results from the model's simplified Eyring type expressions (like B.18) are also shown. The following critical chain length values were used: l = 12, l' = 4, l'' = 8. The model's parameters b and A were fitted in order to minimize the difference $|D(n)_{model} - D(n)_{exp}|$.

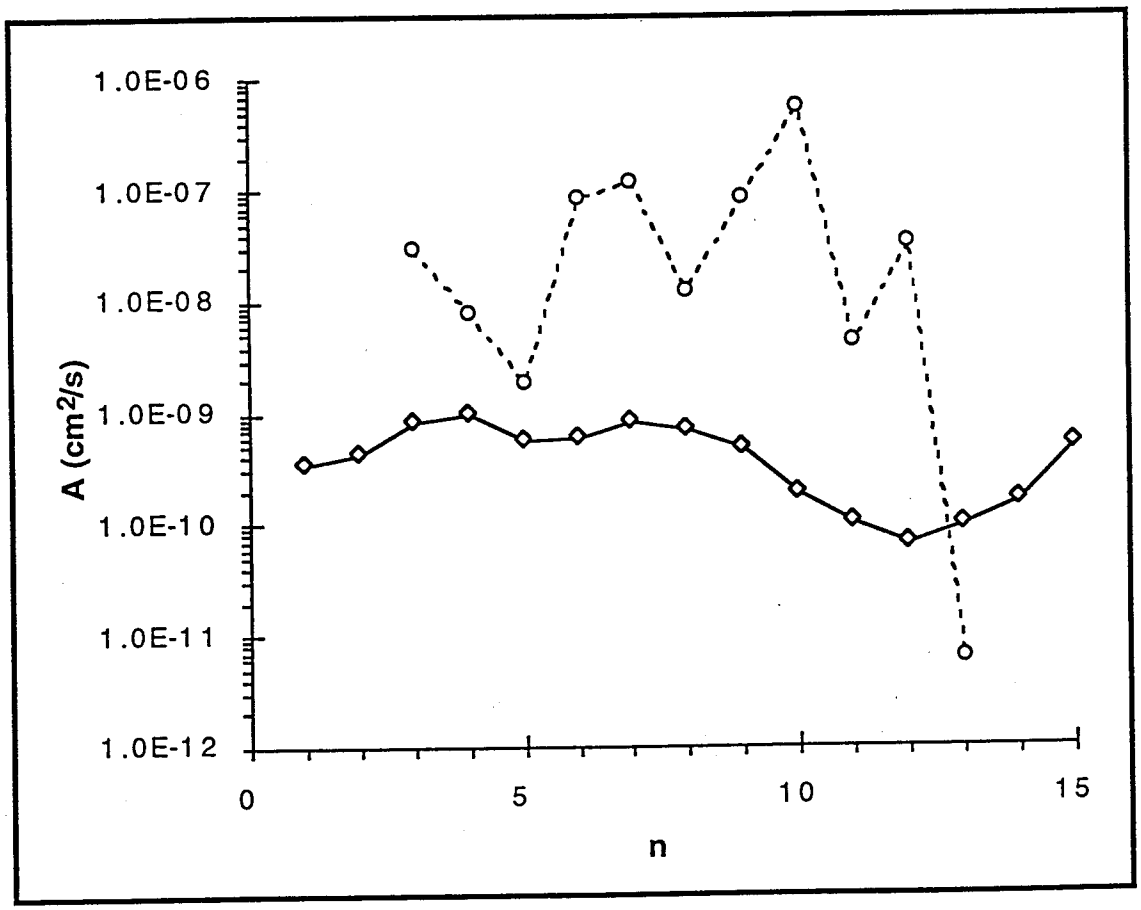

Figure B.6 Comparison between the pre-exponential factors, A, measured by Gorring and the values obtained from the simplified Eyring type expressions. Same conditions as in figure B.5.

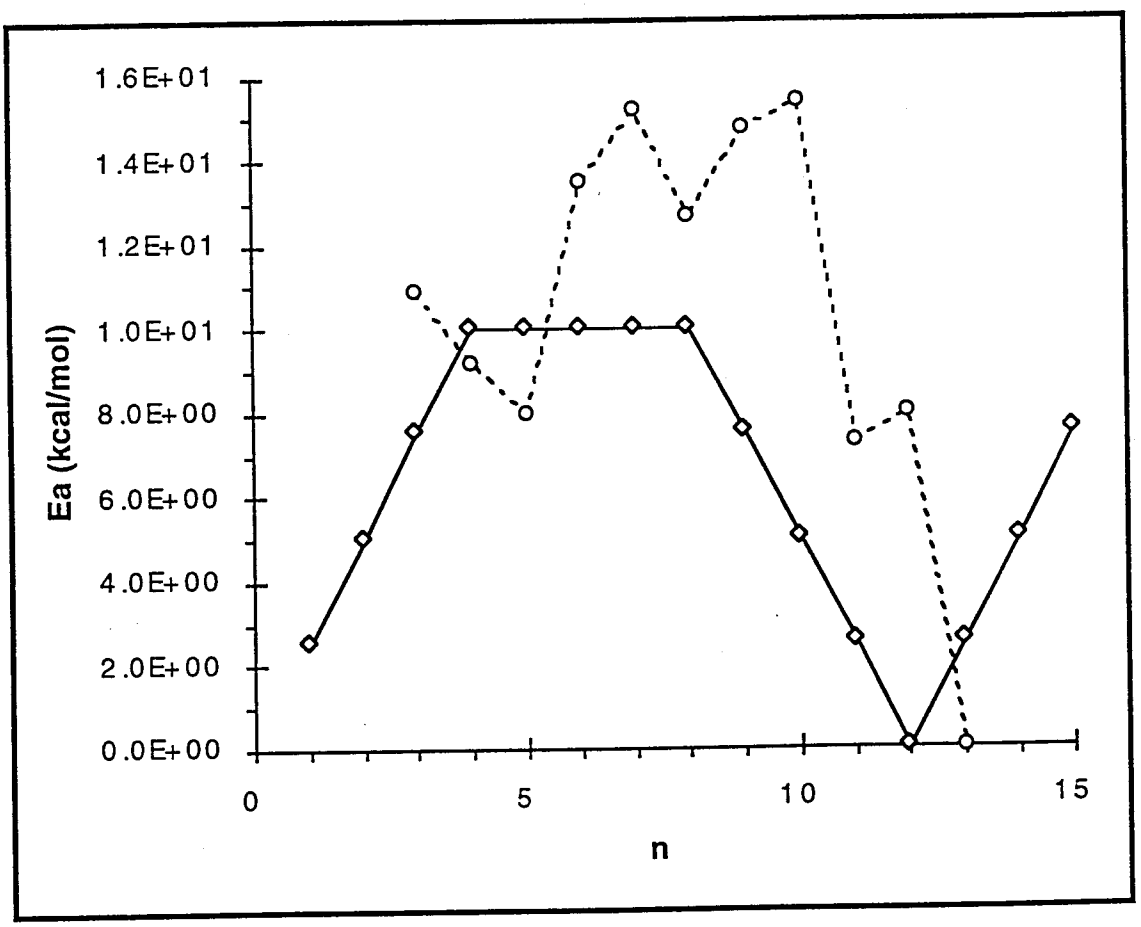

Figure B.7 Comparison between the activation energies, Ea, measured by Gorring and the values obtained from the simplified Eyring type expressions. Same conditions as in figure B.5

APPENDIX C

DRIFTS STUDIES ON CYCLOHEXANE ADSORBED IN SILICALITE

C.1 Introduction

Diffuse reflection infrared Fourier transformed spectroscopy (DRIFTS) is a very useful technique in many situations where traditional spectroscopic techniques fail. This is the case of turbid, colloidal or powder systems where light-scattering phenomena cause significant energy loss.

Some previous work [Müller and Conner, 1993] used DRIFTS to study possible modifications of the ZSM-5 lattice upon adsorption of *p*-xylene and cyclohexane. Our objective is now to obtain information on the state of the adsorbed cyclohexane, as a complement to the diffusional and calorimetric studies presented in Chapter 5. Some preliminary experimental results are shown and discussed next.

C.2 Experimental Setup

The zeolite sample used in these studies was Silicalite, supplied by W.R. Grace. The crystals presented the typical coffin-like shape, with dimensions $9.9 \times 9.4 \times 39.0$ μm. It is the same sample that was employed in the work described in Chapter 5.

The sample was calcined and mixed with ground KBr (mixture about 5% in weight). The measurements were performed with a Mattson Cygnus spectrometer equipped with a TGS detector, at a resolution of 1 cm^{-1} and 16 scans/spectrum. A praying-mantis mirror assembly and a gas cell were used for the DRIFTS setup.

C.3 Results and Discussion

Figure C.1 shows a spectra obtained for unloaded silicalite. H_2O and CO_2 peaks are visible, since it was not possible to close the cell to dry the sample in situ (due to the low sensitivity of the TGS detector). The shape of the spectrum agrees well with published work for Silicalite [Zecchina et al., 1992a and 1992b; Wang et al., 1990; Miecznikowski and Hazuna, 1987]. The peak assignments indicated in the figure were based on the literature information.

For the runs with adsorbed cyclohexane, the sample (previously dried) was first saturated with cyclohexane at room temperature in a sealed vial. At the start of the experiment, the vial was opened and the sample rapidly placed in the cell's sample cup, therefore initiating the desorption of cyclohexane. Scanning started immediately after that. Figures C.2-C.5 show the obtained spectra at different wavenumber ranges and scan times:

scan #1: right after loading cell

scan #2: 75 min. after loading cell

scan #3: 145 min. after loading cell

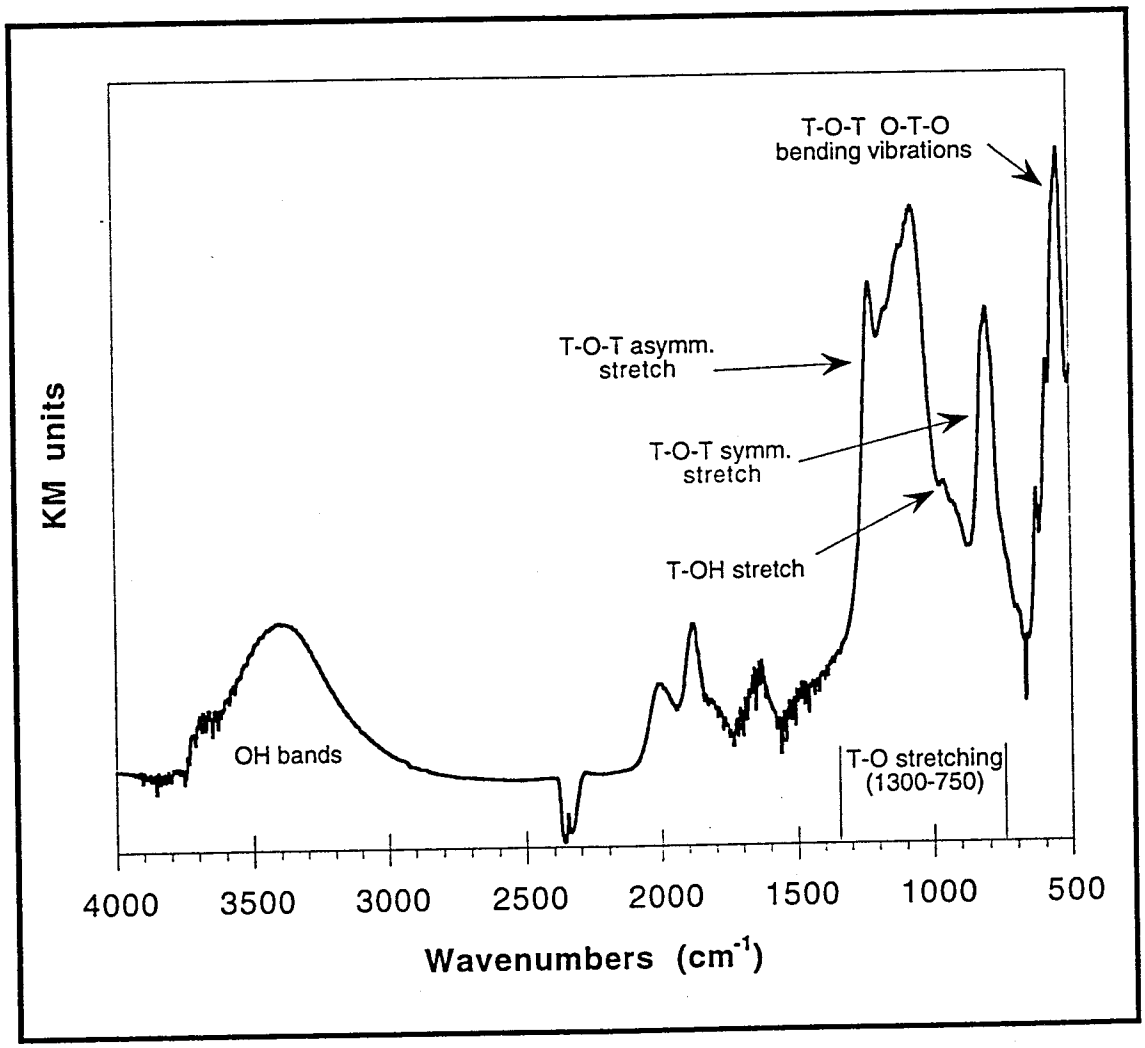

Figure C.1 DRIFTS spectrum (in Kubelka-Munk units) obtained for Silicalite at room temperature.

Figure C.2 shows the wavenumber range corresponding to OH bands and the most intense cyclohexane bands (3800-2800 cm^{-1}). There seems to be a shift of the OH bands towards high wavenumbers as cyclohexane is desorbed, but this may be just associated with the loss of water (the spectrometer's chamber is purged with dry air throughout the experiment).

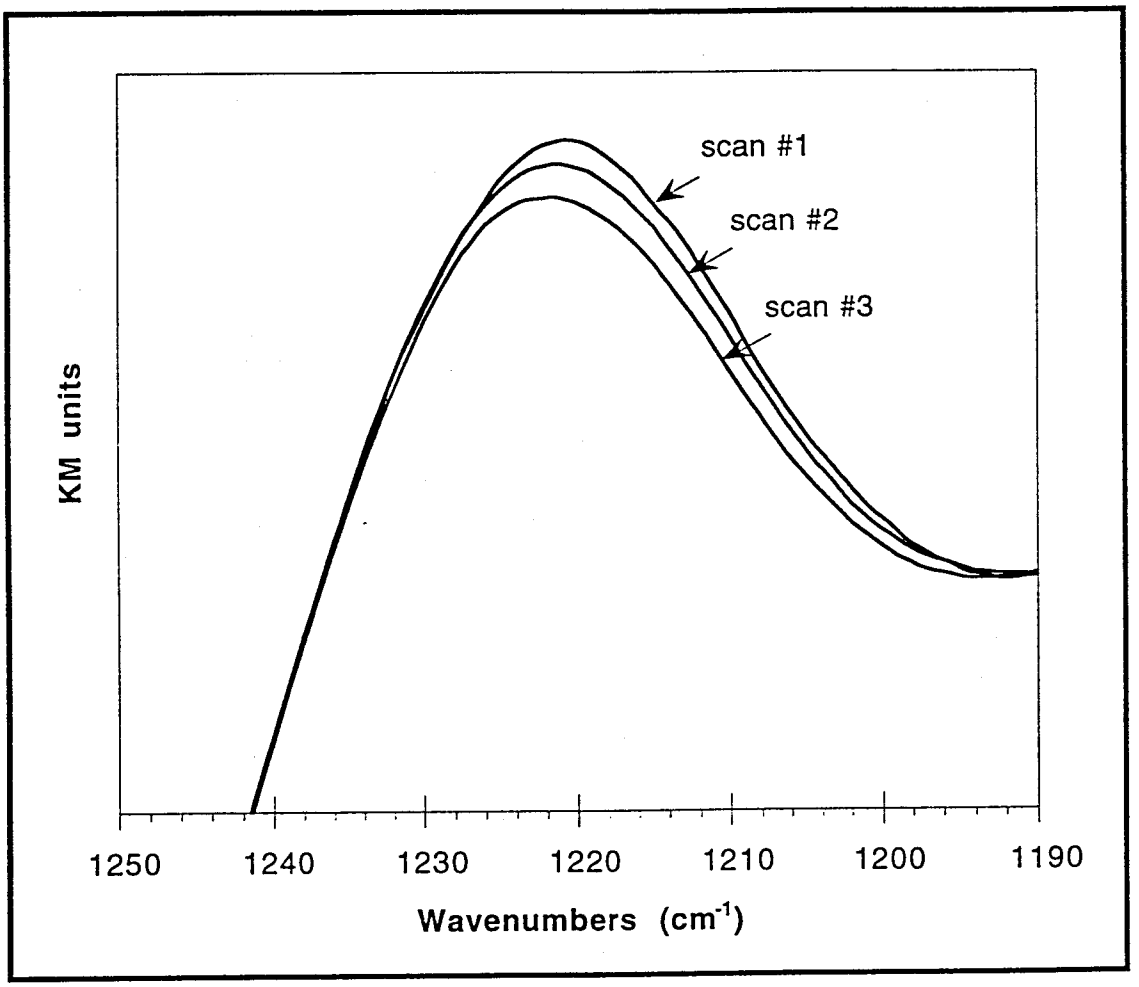

Figure C.2 Portion of the DRIFTS spectra obtained during desorption of cyclohexane from Silicalite.

Figure C.3 shows in greater detail the cyclohexane bands. These are located at about 2933 and 2852 cm^{-1}, which agrees well with the literature assignments for, respectively, the asymmetric and symmetric CH_2 stretches [Takahashi et al., 1964; Rounds, 1978]. These are by far the strongest bands in the cyclohexane's spectrum (see Aldrich database) and, indeed, no other adsorbate bands are visible in the full spectrum of the loaded sample. Wang et al. [1990] also found only C-H stretch bands in the adsorption of benzene on ZSM-5. Interestingly, they report a 3 cm^{-1} shift in a 3092 cm^{-1} band for different loading levels. No apparent shift is visible in this work for

the cyclohexane bands, though. It must, however, be noted that desorption of cyclohexane from silicalite is not complete at room temperature. There was no apparent reduction in the intensity of the cyclohexane bands for scans performed after scan #3. I estimate about 70% of the initial amount remains adsorbed at this point. A "clean" spectrum was only obtained again after heating the sample above 100 °C. Only a step adsorption experiment could indicate whether there is any shift in these bands as loading changes from zero to saturation.

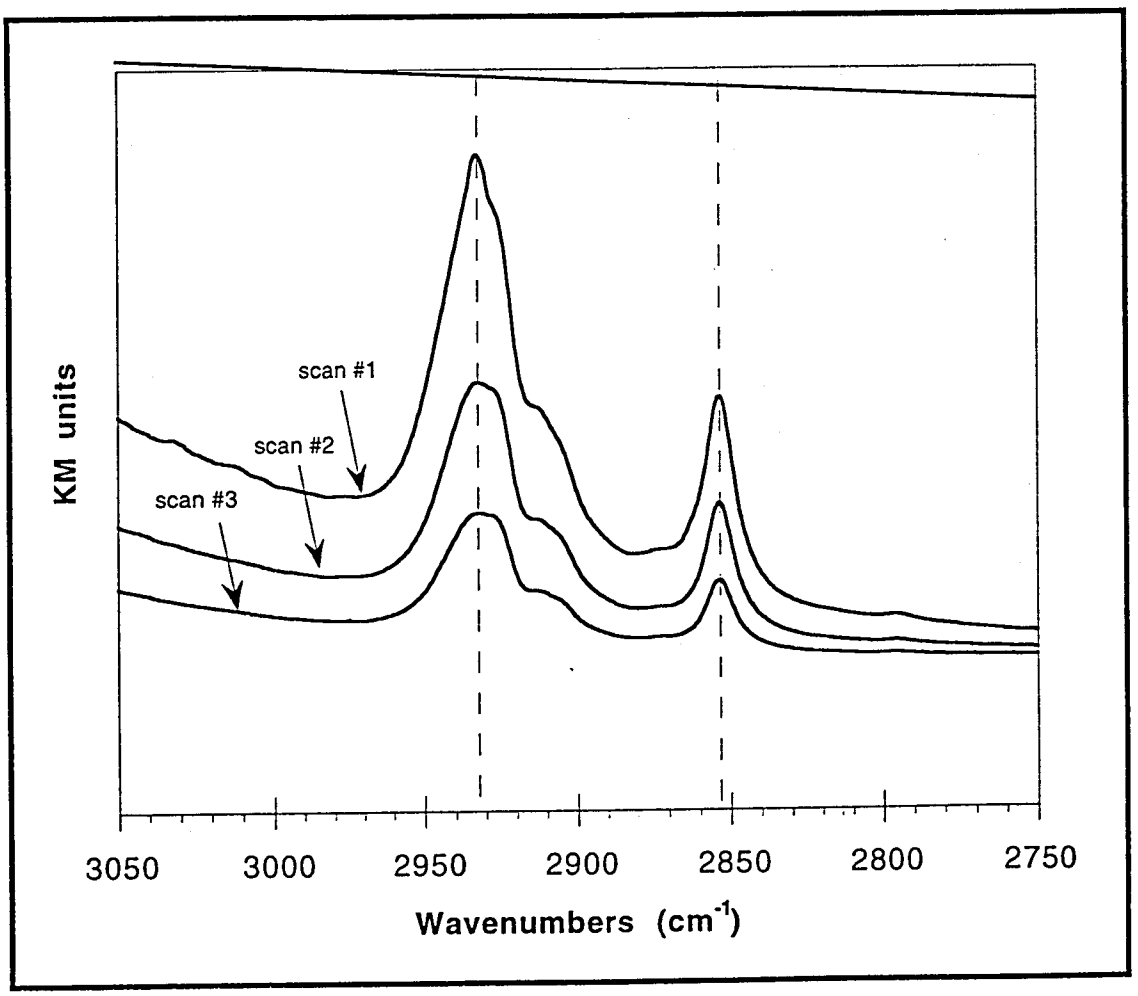

Figure C.3 Portion of the DRIFTS spectra obtained during desorption of cyclohexane from Silicalite.

Figure C.4 shows the portion of the silicalite spectrum corresponding to T-O-T asymmetric stretching. There is a small shift of about 2 cm^{-1} as cyclohexane is desorbed. Wang et al. [1990] report a shift of 8 cm^{-1} between zero loading and saturation (with benzene) in this same band (see figure 3 in their paper).

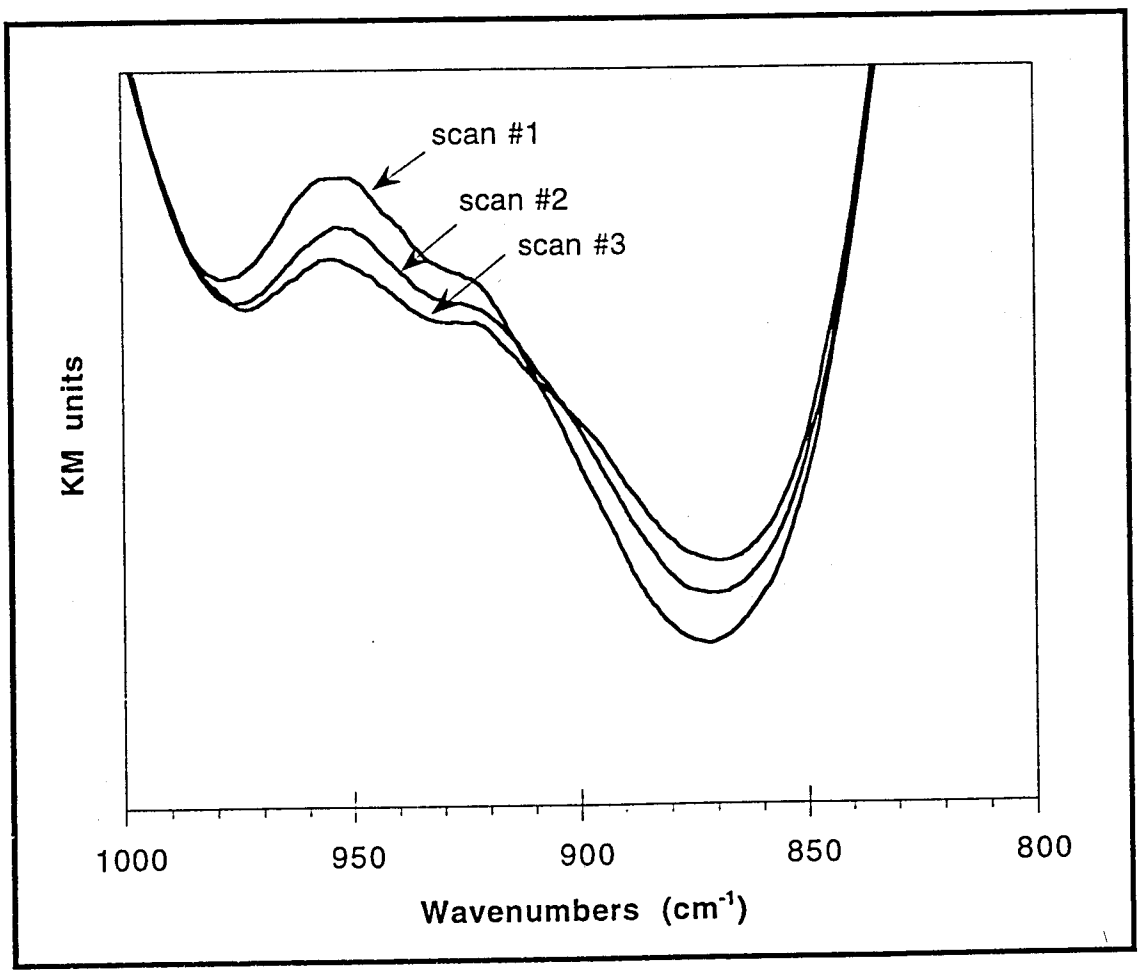

Figure C.4 Portion of the DRIFTS spectra obtained during desorption of cyclohexane from Silicalite.

Finally, Figure C.5 shows the small T-OH stretch bands [Zecchina et al., 1992a]. A small shift is apparent.

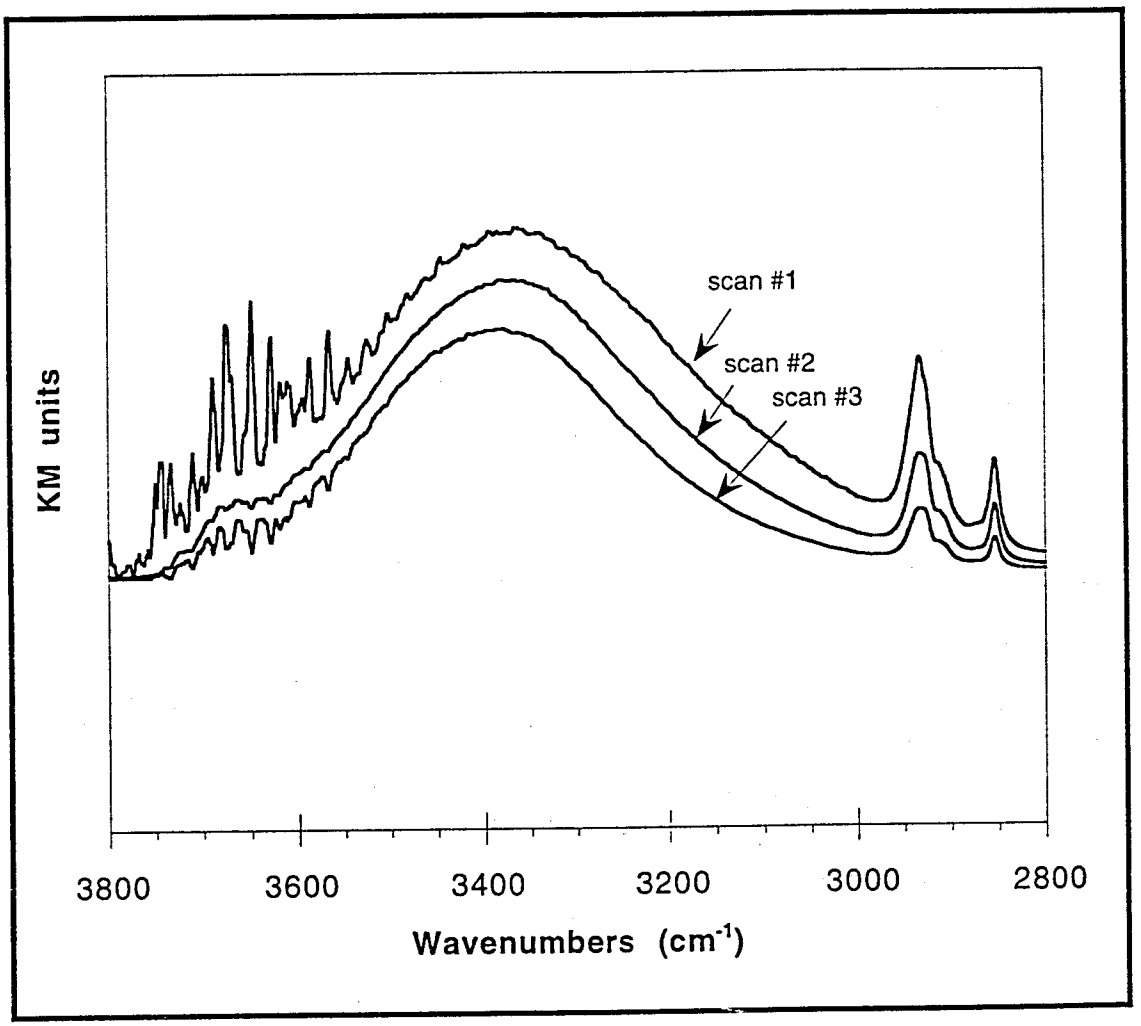

Figure C.5 Portion of the DRIFTS spectra obtained during desorption of cyclohexane from Silicalite.

As mentioned before, in addition to the more intense CH_2 stretch bands, no other cyclohexane bands were detected. Also, no other modifications in the sample spectrum were visible as cyclohexane desorbed, besides the ones described before.

APPENDIX D

MODELING OF TRANSPORT IN CHROMATOGRAPHIC SYSTEMS

The use of the gas pulse chromatography (GPC) technique for determination of diffusion coefficients has diminished significantly in the last years, due to the development of other methods, more versatile and easier to implement, like ZLC (see Chapter 5). The theoretical approach behind GPC is still presented here, howerver, as an exercise that may be a useful reference in future work.

It is necessary to obtain a mathematical model that describes all the phenomena involved in the transport process. This model allows us to obtain analytical expressions for the transformed concentration at column outlet and the moments of the elution response. These will be used in the parameter estimation from the experimental data.

Lets first describe the model. The system consists of a chromatographic column packed with spherical *pellets*. These are formed by zeolite *crystals* bound together by an inert binder. This structure generates a bimodal pore structure: micropores in the crystals and macropores in the voids between the crystals that form a pellet.

The main assumptions are the following:

- Linear adsorption isotherm in the region of operation.

- Negligible thermal effects caused by adsorption.

- Significant adsorption occurs only in the micropore surfaces.

- Constant intraparticle diffusivities.

- The size distribution of zeolite crystals and pellets can be adequately described in terms of average sizes.

- Effects of non-plug flow are adequately described by an axial dispersion coefficient.

- Crystal mass balance:

$$D_c\left(\frac{\partial^2 q}{\partial r_c^2} + \frac{2}{r_c}\frac{\partial q}{\partial r_c}\right) = \frac{\partial q}{\partial t} \qquad (D.1)$$

With initial and boundary conditions:

$$q\,(r_c, r_p, z, 0) = 0 \qquad (D.2)$$

$$\frac{\partial q}{\partial r}(0, r_p, z, t) = 0 \qquad (D.3)$$

$$q\,(R_c, r_p, z, t) = K_c\, C_p\,(r_p, z, t) \qquad (D.4)$$

- Pellet mass balance:

$$D_p\left(\frac{\partial^2 C_p}{\partial r_p^2} + \frac{2}{r_p}\frac{\partial C_p}{\partial r_p}\right) = \frac{\partial C_p}{\partial t} + \frac{1-\varepsilon_p}{\varepsilon_p}\frac{\partial \bar{q}}{\partial t} \qquad (D.5)$$

where:

$$\bar{q}\,(r_p, z, t) = \frac{3\,\varepsilon_c}{R_c^3} \int_0^{R_c} r^2\, q\, dr_c \qquad (D.6)$$

The initial and boundary conditions for D.6 are:

$$C_p\,(r_p, z, 0) = 0 \qquad (D.7)$$

$$\frac{\partial C_p}{\partial r_p}\,(0, z, t) = 0 \qquad (D.8)$$

$$\frac{3\,k_f}{R_p}[C\,(z,t) - \varepsilon_p\, C_p\,(R_p, z, t)] = \frac{\partial \bar{Q}}{\partial t} \qquad (D.9)$$

with:

$$\bar{Q}\,(z, t) = \frac{3\,(1-\varepsilon_p)}{R_p^3} \int_0^{R_p} R^2\, \bar{q}\, dr_p + \frac{3\,\varepsilon_p}{R_p^3} \int_0^{R_p} r_p^2\, C_p\, dr_p \qquad (D.10)$$

- Column mass balance:

$$D_{ax} \frac{\partial^2 C}{\partial z^2} - \frac{v_s}{\varepsilon} \frac{\partial C}{\partial z} = \frac{\partial C}{\partial t} + \frac{1-\varepsilon}{\varepsilon} \frac{\partial \bar{Q}}{\partial t} \qquad (D.11)$$

The initial and boundary conditions for D.11 are:

$$C\,(z, 0) = 0 \qquad (D.12)$$

$$C\,(0, t) = C_0\, \delta(t) \qquad (D.13)$$

$$\lim_{z \to \infty} C(z, t) = 0 \qquad (D.14)$$

The expression for the Laplace transform of the exiting concentration is:

$$\tilde{C}(L,s) = \exp\left(\frac{L_d}{L}\tau\ s\right) \exp\left[\frac{1}{2\ \varepsilon\ \gamma^2}\left(1 - \sqrt{1 + 4\ \varepsilon^2\ \Psi^2}\right)\right] \qquad (D.15)$$

where:

$$\Psi^2 = \gamma^2\left[\tau\ s + 3\ \frac{1-\varepsilon}{\varepsilon}\ \frac{\Psi_p \coth(\Psi_p) - 1}{\beta_p^2\ \frac{1}{\varepsilon_p} + \xi_f\ (\Psi_c \coth(\Psi_c) - 1)}\right] \qquad (D.16)$$

$$\Psi_p^2 = \beta_p^2\left[\tau\ s + 3\ \frac{1-\varepsilon_p}{\varepsilon_p}\ \frac{\Psi_c \coth(\Psi_c) - 1}{\frac{\beta_c^2}{K_c}\ \frac{1}{\varepsilon_c^2}}\right] \qquad (D.17)$$

$$\Psi_c^2 = \beta_c^2\ \tau\ s\ \frac{1}{\varepsilon_c} \qquad (D.18)$$

and the nondimensional parameters were defined as:

$$\beta_c^2 = \frac{R_c^2\ v_s}{D_c\ L} \qquad \beta_p^2 = \frac{R_p^2\ v_s}{D_p\ L}$$

$$\xi_f = \frac{R_c\ v_s}{k_f\ L} \qquad \gamma = \frac{D_{ax}}{v_s\ L} \qquad \tau = \frac{L}{v_s} \qquad (D.19)$$

This result is equivalent to the one derived by Hsu and Haynes [1981].

In order to analyze the effect of some parameters on the shape of the response peaks, several time domain solutions were computed from Equation D.15 using a Fast Fourier Transform algorithm for the numerical inversion. The results are summarized in Figure D.1.

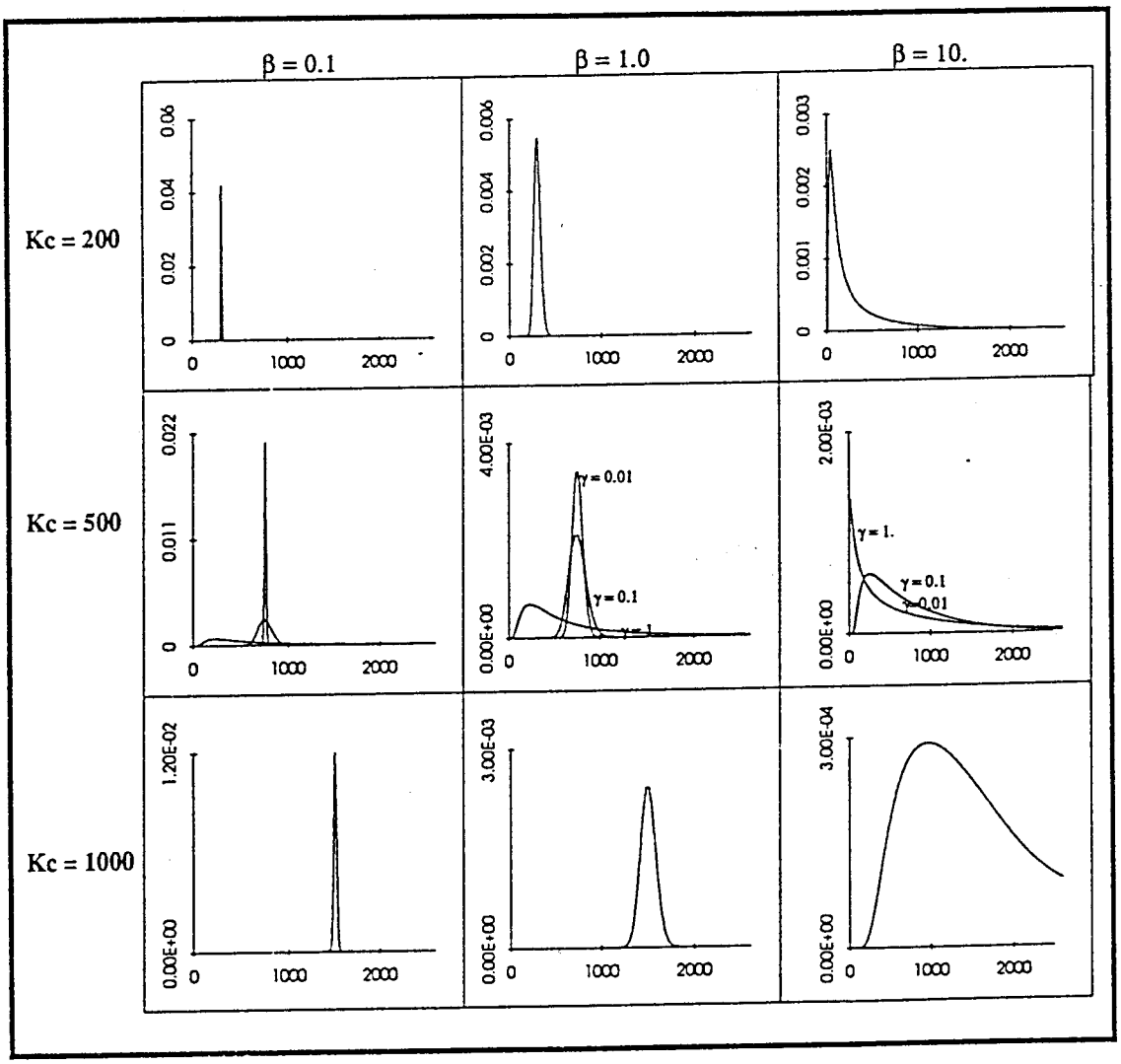

Figure D.1 Response peaks computed obtained by numerical inversion of Equation D.11. The pellets were assumed monodisperse (micropores only) and the external film resistance neglected. $\gamma = 0.01$ unless otherwise indicated. β in the figure refers to β_c in the model.

The moments of the response peak are obtained from:

$$m_n = (-1)^n \lim_{s \to 0} \frac{d^n \tilde{C}(L,s)}{ds^n} \tag{D.20}$$

The mean and variance of the residence time distribution are related to the moments by:

$$\mu = \frac{m_1}{m_0} \tag{D.21}$$

$$\sigma^2 = \frac{m_2 - m_1^2}{m_0} \tag{D.22}$$

and the following expressions can be derived [Sarma and Haynes, 1973; Shah and Ruthven, 1977; Hufton and Danner, 1990]:

$$\frac{\mu}{L} = \frac{1}{v_s}\left\{[\varepsilon + (1-\varepsilon)\,[\varepsilon_p + (1-\varepsilon_p)\,\varepsilon_c\,K_c]]\,f_2 + \frac{L_d}{L} f\right\} \tag{D.23}$$

$$\frac{\sigma^2 v_s}{2L} = \frac{\varepsilon D_{ax}}{v_s^2}\left\{[\varepsilon + (1-\varepsilon)\,[\varepsilon_p + (1-\varepsilon_p)\,\varepsilon_c\,K_c]]^2\,f_2^2\,f_1 + \frac{L_d}{L} f^2\right\} +$$

$$+ (1-\varepsilon)\left\{\frac{[\varepsilon_p + \omega\,(1-\varepsilon_p)\,\varepsilon_c\,K_c]^2\,R_p}{3\,k_f} + \frac{[\varepsilon_p + (1-\varepsilon_p)\,\varepsilon_c\,K_c]^2\,R_p^2}{15\,\varepsilon_p\,D_p} + \frac{(1-\varepsilon_p)\,\varepsilon_c\,K_c\,r_c^2}{15\,D_c}\right\} f_2 \tag{D.24}$$

where the following pressure drop correction factors were introduced [Chiang, Dixon and Ma, 1984a]:

$$f_1 = \frac{9}{8} \frac{[(P_{in}/P_{out})^2 - 1]\ [(P_{in}/P_{out})^4 - 1]}{[(P_{in}/P_{out})^3 - 1]^2} \tag{D.25}$$

$$f_2 = \frac{2}{3} \frac{(P_{in}/P_{out})^3 - 1}{(P_{in}/P_{out})^2 - 1} \tag{D.26}$$

$$f = \frac{P_{in}}{P_{out}} \tag{D.27}$$

The strategy for computing the model's parameters (D_c, K_c, D_p, k_f, D_{ax}, $\frac{L}{L_d}$) involves a sequence of experimental steps in order to obtain initial estimates from the mean and variance of the response peaks (Equations D.21 and D.22). This procedure is summarized in Table D.2.

Set A is performed with a bed of nonporous particles ("sand") with the same average size as the zeolite sample. This will give us information about the system's dead volume and axial dispersion in the column. We will attempt to correlate D_{ax} with v_s according to relationships available in the literature [Edwards and Richardson, 1968; Wakao and Funazkri, 1978]. The general form of this correlation is:

$$D_{ax} = a\, D_m + \frac{b\, v_s}{1 + \frac{c}{v_s}} \tag{D.28}$$

where D_m is the molecular diffusion coefficient. Notice that if we have a monodisperse system (micropores only) then an alternative to the use of sand we can perform experiments with a compound of large diameter, such that it cannot penetrate the micropores. One example is iso-butane in zeolite 5A.

Set B is divided in two subsets. First (*BI*) the micropores are blocked by previously saturating and condensing in them an adequate compound. This way the

diffusant under study will diffuse only in the macropores and D_p can be estimated. In order to do this, however, we must estimate the external film mass transfer coefficient, k_f. We can use the following correlation [Wakao and Funazkri, 1978]:

$$Sh = 2 + 1.1\ Sc^{1/3}\ Re^{0.6} \tag{D.29}$$

or:

$$\frac{k_f\ 2\ R_p}{D_m} = 2 + 1.1 \left(\frac{\nu}{D_m}\right)^{1/3} \left(\frac{2\ R_p\ v\ \varepsilon}{\nu}\right)^{0.6} \tag{D.30}$$

The following set (*BII*) is performed with free access to the micropores. Now K_c and D_c can be determined.

Set C is an alternative to set B, in which different pellet sizes are employed, allowing for the estimation of the macropore and micropore diffusivities without having to block the micropores.

The model and the derived equations can be easily transformed in order to describe a monodisperse system in which each pellet consists of one single crystal. The analysis would in this case be simpler since we do not have to estimate the macropore mass transfer parameters.

Some useful descriptions of experimental setups and procedures can be found in the literature [Ruthven and Kumar, 1979; Hsu and Haynes, 1981; Chiang, Dixon and Ma 1984b; Hyun and Danner, 1985; Fu, Ramesh and Haynes 1986; Hufton and Danner 1991].

Table D.2 Sequence of experimental runs for determination of the model's parameters. μ and σ^2 are obtained from Equations D.21 and D.22. See text for details.

Set A (bed of "sand")	Set BI (blocked micropores)	Set C (varying R_p)
$\frac{\mu}{L}$ vs. $\frac{1}{v_s} \rightarrow \frac{L_d}{L}$	$\frac{\sigma^2}{\mu^2}L$ vs. $v_s \rightarrow D_p$	$\frac{\mu}{L}$ vs. $\frac{1}{v_s} \rightarrow K_c$
$\frac{\sigma^2 v_s^3}{2L}$ vs. $v_s \rightarrow D_{ax}(v_s)$	$\downarrow$	$\frac{\sigma^2}{\mu^2}L$ vs. $v_s \rightarrow$ slope S_1
	Set BII (unblocked µpores)	S_1 vs. R_p^2 $\downarrow$ slope $S_2 \rightarrow D_p$ intersection $I_2 \rightarrow D_c$
	$\frac{\mu}{L}$ vs. $\frac{1}{v_s} \rightarrow K_c$	
	$\frac{\sigma^2}{\mu^2}L$ vs. $v_s \rightarrow D_c$	

The estimates obtained from the moments of the response peaks can be improved using a Fourier domain fitting of the model to the experimental data. The objective function is defined as:

$$F_{obj} = \int_0^\infty \{ [Re_{exp}(\omega) - Re_{theo}(\omega)]^2 + [Im_{exp}(\omega) - Im_{theo}(\omega)]^2 \} \, d\omega \qquad (D.31)$$

which, according to Parseval's theorem, is mathematically equivalent to a least squares fitting in the time domain. $Re_{exp}(\omega)$ and $Im_{exp}(\omega)$ are the real and imaginary parts of the response peak transformed into the frequency domain. $Re_{theo}(\omega)$ and $Im_{theo}(\omega)$ are

computed from Equation D.15 replacing s with iω. A Levenberg-Marquardt algorithm should be used for the fitting. The parameter values obtained from the moments should be used as first estimates

BIBLIOGRAPHY

Abramowitz, M. and I. A. Stegun, *Handbook of Mathematical Functions* (Dover, New York) (1965).

Arnould, D. and R. L. Laurence, "Solute Diffusion in Polymers by Capillary Column Inverse Gas Chromatography" in *Inverse Gas Chromatography* , Lloyd, D. R., H. P. Schreiber and T. C. Ward Ed. (American Chemical Society, Washington, D. C.), pp. 87-106 (1989).

Ash, R. and R. M. Barrer, "Mechanisms of Surface Flow", *Surface Sci.*, **8**, 461-466 (1967).

Aust, E., K. Dahlke and G. Emig, "Simulation of Transport and Self-Diffusion in Zeolites with Monte Carlo Method", *J. Catal.*, **115**, 86-97 (1989).

Balik, C. M., "On the Extraction of Diffusion Coefficients from Gravimetric Data for Sorption of Small Molecules by Polymer Thin Films", *Macromolecules*, **29**, 3025-3029 (1996).

Barrer, R. M. and D. L. Peterson, "Kinetics of n-Paraffin Sorption in the Natural Zeolite Erionite", *J. Phys. Chem.*, **68**, 3427-3429 (1964).

Barrer, R. M. and W. Jost, "A Note on Interstitial Diffusion", *Trans. Faraday Soc.*, **45**, 928-930 (1949).

Barrer, R. M., "Flow into and through Zeolite Beds and Compacts", *Langmuir*, **3**, 309-315 (1987).

Barrer, R. M., "Migration in Crystal Lattices", *Trans. Faraday Soc.*, **37**, 590-599 (1941).

Barrer, R. M., "Sorption by Zeolites Part II: Kinetics and Diffusivities" in *Zeolites: Science and Technology. NATO ASI Series*, Alcabideche, Portugal, pp. 261-288 (1983)

Bennett, J. M. and J. A. Gard, "Non-identity of the Zeolites Erionite and Offretite", *Nature*, **214**, 1005-1006 (1967).

Beschmann, K., G. T. Kokotailo and L. Riekert, *Chem. Eng. Process.*, **22**, 223 (1987).

Brandani, S. and D. M. Ruthven, "Analysis of ZLC Desorption Curves for Liquid Systems", *Chem. Engng. Sci.*, **50**, 2055-2059 (1995).

Breck, D. W., *Zeolite Molecular Sieves* (John Wiley & Sons, New York), page 507 (1974a).

Breck, D. W., *Zeolite Molecular Sieves* (John Wiley & Sons, New York), page 48 (1974b).

Breck, D. W., *Zeolite Molecular Sieves* (John Wiley & Sons, New York) (1974).

Bülow, M. and P. Struve, "Experimental Evidence of The Influence of Sorption-heat Release Processes on the Sorption Kinetics of Benzene in NaX Zeolite Crystals", *J. Chem. Soc., Faraday Trans. I*, **80**, 813-822 (1984).

Bülow, M., "Molecular Mobility of Single Components and Mixtures on Zeolites" in *Chemistry of Microporous Crystals; Proceedings of the International Symposium on Chemistry of Microporous Crystals* , (Elsevier, Tokyo), pp. 199-212 (1991).

Bülow, M., P. Struve and L. V. C. Rees, "Investigation of the Gaseous Phase Diffusion and Liquid Phase Self-diffusion of n-Decane on NaCa-A Zeolites", *Zeolites*, **5**, 113-117 (1985).

Bülow, M., P. Struve and S. Pikus, "Influence of Hydrothermal Pretreatment on Zeolitic Diffusivity Detected by Comparative Sorption Kinetics and Small-Angle X-Ray Scattering Investigations", *Zeolites*, **2**, 267-270 (1982).

Bülow, M., P. Struve, C. Redszus and W. Schirmer, "Sorption Kinetics of n-Decane on MgA Type Zeolites of different Crystal Size" in *Proceedings of the Fifth International Conference on Zeolites*, Naples, pp. 580-591 (1980)

Bülow, M., P. Struve, G. Finger, C. Redszus, *et al.*, "Sorption Kinetics of n-Hexane on MgA Zeolites of Different Crystal Sizes", *J. C. S. Faraday I*, **76**, 597-615 (1980).

Cavalcante, C. L. and D. Ruthven, "Adsorption of Branched and Cyclic Paraffins in Silicalite. 2. Kinetics", *Ind. Eng. Chem. Res.*, **34**, 185-191 (1995).

Chen, N. Y., "Offretite-T-Erionite Catalytic Characterization" in *Proceedings of the Fifth International Congress on Catalysis*, Miami Beach, Fla., pp. 1343-1351 (1972)

Chen, N. Y., S. J. Lucki and E. B. Mower, "Cage Effect on Product Distribution from Cracking ober Crystalline Aluminosilicalite Zeolites", *J. Catal.*, **13**, 329-332

Chiang, A. S., Dixon, A. G., Ma, Y. H.,, 'The Determination of Zeolite Crystal Diffusivity by Gas Chromatography - I. Theory' , *Chem. Engng. Sci.*, **39**, 1451. (1984a)

Chiang, A. S., Dixon, A. G., Ma, Y. H. , 'The Determination of Zeolite Crystal Diffusivity by Gas Chromatography - II. Experimental' , *Chem. Engng. Sci.*, **39**, 1461-1468 (1984b)

Chihara, K., M. Suzuki and K. Kawazoe, "Interpretation for the Mocropore Diffusivities of Gases in Molecular-Sieving carbon", *J. Coll. Interface Sci.*, **64**, 584-587 (1978).

Chmelka, B. F., J. V. Gillis, E. E. Petersen and C. J. Radke, "Transport of Aromatic Molecules in NaY Zeolite Powders", *AIChE J.*, **36**, 1562-1568 (1990).

Chon, H. and D. H. Park, "Diffusion of Cyclohexanes in ZSM-5 Zeolites", *J. Catal.*, **114**, 1-7 (1988).

Choudhary, V. R. and D. B. Akolekar, "Evaluation of Sorbate/Reactant Shape-Selectivity of Zeolites by GC Pulse Techniques", *J. Molec. Cat.*, **60**, 172-188 (1990).

Choudhary, V. R. and D. B. Akolekar, "Shuttlecock-Shuttlebox Model for Shape Selectivity of Medium-Pore Zeolites in Sorption and Difusion", *J. Catal.*, **117**, 542-548 (1989).

Choudhary, V. R. and K. R. Srinivasan, "Desorptive Diffusion of Benzene in H-ZSM-5 under Catalytic Conditions Using Dynamic Sorption/Desorption Technique", *J. Catal.*, **102**, 316-327 (1986).

Choudhary, V. R., V. S. Nayak and A. S. Mamman, "Diffusion of Straight- and Branched-Chain Liquid Compounds in H-ZSM-5 Zeolite", *Ind. Eng. Chem. Res.*, **31**, 624-628 (1992).

Conner, W. C. and J. A. Schwarz, "A Consistent Theoretical Framework for Analysis of Diverse Rate Processes", *Che, Eng. Comm.*, **55**, 129-138 (1987).

Conner, W. C., "A general Explanation for the Compensation Effect: The Relationship between ΔS^* and Activation Energy", *Journal of Catalysis*, **78**, 238-246 (1982).

Crank, J., *The Mathematics of Diffusion* (Clarendon Press, Oxford) (1975).

Derouane, E. G., 'The Energetics of Sorption by Molecular Sieves: Surface Curvature Effects' , *Chem. Phys. Lett.*, **142**, 200-204 (1987a)

Derouane, E. G., André, J. M., 'A Simple van der Waals Model for Molecule-Curved Surface Interactions in Molecular-Sized Microporous Solids' , *Chem. Phys. Lett.*, **137**, 336-340 (1987b)

Derouane, E. G., Andre, J. M., Lucas, A. A., 'Surface Curvature Effects in Physisorption and Catalysis by Microporous Solids and Molecular Sieves' , *J. Catal.*, **110**, 58-73 (1988a)

Derouane, E. G., et al. , 'Diffusion of Alkanes in Molecular Sieves. Evidence of Confinement Effects.' , *App. Cat.*, **40**, L1-L10 (1988b)

Doi, M. and S. F. Edwards, *The Theory of Polymer Dynamics* (Oxford University Press, New York) (1986).

Dubinin, M. M., I. T. Erashko, O. Kadlec and V. I. Ulin, "Kinetics of Physical Adsorption by Carbonaceous Adsorbents of Biporous Structure", *Carbon*, **13**, 193-200 (1975).

Edwards, M. F., Richardson, J. F., 'Gas Dispersion in Packed Beds' , *Chem. Engng. Sci.*, **23**, 109-123 (1968)

Eic, M. and D. Ruthven, "A New Experimental Technique for Measurement of Intracrystalline Diffusivity", *Zeolites*, **8**, 40-45 (1988).

Eliel, E. L., *Stereochemistry of Carbon Compoumds*, (McGraw-Hill Inc.), New York, (1962) pp. 204-216.

Festa, R. and E. G. d'Agliano, "Diffusion Coefficient for a Brownian Particle in a Periodic Field of Force", *Physica*, **90A**, 229-244 (1978).

Fraissard, J. and T. Ito, *Zeolites*, **8**, 350 (1988).

Froment, G. F. and K. B. Bischoff, *Chemical Reactor Analysis and Design* (John Wiley & Sons, New York) (1990).

Garcia, S. F. and P. B. Weisz, "Effective Diffusivities in Zeolites 1. Aromatics in ZSM-5 Crystals", *J. Catal.*, **121**, 294-311 (1990).

Garcia, S. F. and P. B. Weisz, "Effective Diffusivities in Zeolites. 2. Experimental Appraisal of Effective Shape-Selective Diffusivity in ZSM-5 Catalysis", *J. Catal.*, **142**, 691-6967 (1993).

Garg, D. R. and D. M. Ruthven, "The Effect of the Concentration Dependence of Diffusivity on Zeolitic Sorption Curves", *Chem. Eng. Sci.*, **27**, 417-423 (1972).

de Gennes, P.-G., *Scaling Concepts in Polymer Physics* (Cornell University Press, London) (1979).

Glasstone, S., K. J. Laidler and H. Eyring, *The Theory of Rate Processes* (McGraw-Hill Book Company, New York) (1941).

Gorring, R. L., "Diffusion of Normal Paraffins in Zeolite T", *J. Catal.*, **31**, 13-26 (1973).

Guo, C.-J., O. Talu and D. T. Hayhurst, "Phase Transition and Structural Heterogeneity; Benzene Adsorption on Silicalite", *AIChE J.*, **35**, 573-578 (1989).

Haynes, H. W., "The Determination of Effective Diffusivity by Gas Chromatography. Time Domain Solutions.", *Chem. Eng. Sci.*, **30**, 955-961 (1975).

Hill, T. L., *An Introduction to Statistical Thermodynamics* (Dover Publications, New York) (1986).

Hufton, J. R. and R. P. Danner, "Chromatographic Study of Alkanes in Silicalite:

Hsu, L.-K. P. and H. W. Haynes, "Effective Diffusivity by The Gas Chromatography Technique: Analysis and Application to Measurements of Diffusion of Various Hydrocarbons in Zeolite NaY", *AIChE Journal*, **27**, 81-91 (1981).

Kärger, J. and D. M. Ruthven, "On the Comparison Between Macroscopic and N.M.R. Measurements of Intracrystalline Diffusion in Zeolites", *Zeolites*, **9**, 267-281 (1989).

Kärger, J. and D. Ruthven, *Diffusion in Zeolites and other Microporous Solids* (John Wiley & Sons, New York), chapter 9 (1992a).

Kärger, J. and D. Ruthven, *Diffusion in Zeolites and other Microporous Solids* (John Wiley & Sons, New York), page 235 (1992b).

Kärger, J. and D. Ruthven, *Diffusion in Zeolites and other Microporous Solids* (John Wiley & Sons, New York), page 393 (1992c).

Kärger, J., "A Study of Fast Tracer Desorption in Molecular Sieve Crystals", *AIChE J.*, **28**, 417 (1982).

Kärger, J., H. Pfeifer, M. Rauscher and A. Walter, "Self-diffusion of n-Paraffins in NaX Zeolite", *J. C. S. Faraday I*, **76**, 717-737 (1980).

Kärger, J., H. Pfeifer, M. Rauscher, M. Bülow, *et al.*, "Comparative NMR and Uptake Studies os Molecular Transport of Ethane in 5A Zeolites after Different Sample Pretreatment", *Z. phys. Chemie*, **262**, 567-576 (1981).

Kärger, J., H. Pfeifer, R. Richter, H. Fürtig, *et al.*, "NMR Study of Mass Transfer in Granulated Molecular Sieves", *AIChE J.*, **34**, 1185-1189 (1988).

Kärger, J., H. Pfeifer, R. Seidel and B. Staudte, "Investigation of Surface Barriers on CaNaA type Zeolites by Combined Application of the N.M.R. Tracer Desorption Method and X-ray Photoelectron Spectroscopy", *Zeolites*, **7**, 282-284 (1987).

Kärger, J., M. Bülow, V. I. Ulin, A. M. Voloshchek, *et al.*, "On the Importance of Dimension Variation in Determining the Limiting Steps in Adsorption Kinetics", *J. Chem. Tech. Biotechnol.*, **32**, 376-381 (1982).

Kocirik, M. and A. Zikánová, "The Analysis of the adsorption Kinetics in Materials with Polydisperse Pore Structure", *Ind. Eng. Chem. Fund.*, **13**, 347-350 (1974).

Kocirik, M. and A. Zikánová, "The Statistical Moments Method for the Calculation of the Coefficients of Radial Diffusion from Kinetic Measurements", *Z. Phys. Chem. (N. F.)*, **71**, 311-319 (1970).

Kondis, E. F. and J. S. Dranoff, "Kinetics of Isothermal Sorption of Ethane on 4A Molecular Sieve Pellets", *Ind. Eng. Chem, Process Des. Develop.*, **10**, 108-114 (1971).

Krishna, R., "Multicomponent Surface Difusion of Adsorbed Species: A Description Based on the Generalized Maxwell-Stefan Equations", *Chem. Eng. Sci.*, **45**, 1779-1791 (1990).

Kumar, R., R. C. Duncan and D. M. Ruthven, "A Chromatographic Study of Diffusion of Single Components and Binary Mixtures of Gases in 4A and 5A Zeolites", *Can. J. Chem. Eng.*, **60**, 493-499 (1982).

Kutner, R., "Chemical Diffusion in the Lattice Gas of Noninteracting Particles", *Phys. Lett.*, **81A**, 239-240 (1981).

Kärger, J. and D. M. Ruthven, "Diffusion in Zeolites", *J. Chem. Soc., Faraday Trans. I*, **77**, 1485 (1981).

Kärger, J. and D. Ruthven, *Diffusion in Zeolites and other Microporous Solids* (John Wiley & Sons, New York) (1992).

Kärger, J., H. Pfeifer, M. Rauscher and A. Walter, "Self-diffusion of n-Paraffins in NaX Zeolite", *J. C. S. Faraday I*, **76**, 717-737 (1980).

Kärger, J., H. Pfeifer, T. Wutscherk, S. Ernst, J. Weitkamp and J. Fraisard, "Direct Observation of Intracrystalline Transport Diffusion in Zeolites by Xenon-129 NMR", *J. Phys. Chem.*, **96**, 5059-5063 (1992).

Li, J.-M. and O. Talu, "Effect of Structural Heterogeneity on Multicomponent Adsorption: Benzene and p-Xylene on Silicalite." in *Proc. IVth Int. Conf. on Fundamentals of Adsorption.*, Kyoto, pp. 373-380 (1992)

Magalhães, F. D., R. L. Laurence and W. C. Conner, "Transport of n-paraffins in Zeolite T", *AIChE J.*, **42**, 68-86 (1996).

Meier, W. M. and D. H. Olson, *Atlas of Zeolite Structure Types* (Butterworth-Heinemann, (1992).

Mentzen, B. F., "Characterization of Guest Molecules Adsorbed on Zeolites of Known Structure by Combined X-Ray Powder Profile Refinements and Conventional Difference-Fourier Techniques. Part I - Localization of the Benzene Molecule in a Pentazil Type Zeolite", *Mat. Res. Bull.*, **22**, 337-343 (1987).

Micke, A., M. Bülow and M. Kocirik, "A Nonequilibrium Surface Barrier for Sorption Kinetics of p-Ethyltoluene on ZSM-5 Molecular Sieves", *J. Phys. Chem.*, **98**, 924-929 (1994).

Miecznikowski, A. and J. Hazuna, "Infrared and Raman studies of ZSM-5 and silicalite-1 at room, liquid nitrogen and helium temperatures.", *Zeolites*, **7**, 249-254 (1987).

Müller, J. A. and W. C. Conner, "Cyclohexane in ZSM-5. 1. FTIR and X-ray Studies", *J. Phys. Chem.*, **97**, 1451-1454 (1993).

Müller, U., A. Brenner, A. Reich and K. K. Unger, "Significant Parameters in the Synthesis of Large Alkaline-Free MFI-Type Zeolites and AFI-Type Aluminophosphates" in *ACS Symposium Series - Zeolite Synthesis* , Occelli, M. L. and H. E. Robson Ed. (ACS, Washington), pp. chap. 24 (1989).

Nayak, V. S. and J. B. Moffat, "Sorption and Diffusion in Heteropolyoxometalates", *J. Coll. Interface Sci.*, **120**, 301-311 (1987).

Nayak, V. S. and J. B. Moffat, "Sorption and Diffusion of Alcohols in Heteropoly Oxometalates and ZSM-5 Zeolite", *J. Phys. Chem.*, **92**, 7097-7102 (1988).

Nitsche, J. M. and J. Wei, "Window Effects in Zeolite Diffusion and Brownian Motion over Potential Barriers", *AIChE J.*, **37**, 661-670 (1991).

Palekar, M. G. and R. A. Rajadhyaksha, "Sorption on Zeolites - I", *Cem. Eng. Sci.*, **40**, 1085-1091 (1985).

Paravar, A. and D. T. Hayhurst, "Direct Measurement of Diffusivity for Butane across a Single Large Silicalite Crystal" in *Proceedings of the Sixth International Conference on Zeolites* , Olson, D. H. and A. Bisio Ed. (Butterworths, Reno, NV), pp. 217-224 (1983).

Qureshi, W. R. and J. Wei, "One- and Two-Component Diffusion in Zeolite ZSM-5. I. Theoretical", *J. Catal.*, **126**, 126-146 (1990).

Rees, L. V. C., "Exciting New Advances in Diffusion of Sorbates in Zeolites and Microporous Materials" in *Zeolites and Related Microporous Materials. Studies in Surface Science and Catalysis* , Weitkamp, J., H. G. Kared, H. Pfeifer, *et al.* Ed. (Elsevier Science, (1994).

Reid, R. C., J. M. Prausnitz and B. E. Poling. *The Properties of Gases and Liquids* (McGraw-Hill, New York) (1987).

Riekert, L., "Rates of Sorption and Diffusion of Hydrocarbons in Zeolites", *AIChE J.*, **17**, 446-454 (1971).

Riekert, L., "Sorption, Diffusion, and Catalytic Reaction in Zeolites", *Adv. Catal.*, **21**, 281-321 (1970).

Riekert, L., "Transport of Mass and Heat in Porous Adsorbents", *Chem. Eng. Process.*, **26**, 59-62 (1989).

Rounds, T. C. and H. L. Strauss, "Vibrational Spectrospcopy of the Medium Rings" in *Vibrational Spectra and Structure* , Durig, J. R. Ed. (Elsevier, New York), pp. 237-268 (1978).

Ruckenstein, E. and P. S. Lee, "Resonant Diffusion", *Phys. Lett.*, **56A**, 423-424 (1976).

Ruckenstein, E., A. S. Vaidyanathan and G. R. Youngquist, "Sorption by Solids with Bidisperse Pore Structures", *Chem. Eng. Sci.*, **26**, 1305-1318 (1971).

Ruthven, D. M. and I. H. Doetsch, "Diffusion of SF6 in 13X Zeolite", *J. C. S. Faraday I*, **72**, 1043-1050 (1976).

Ruthven, D. M. and K. F. Loughlin, "Correlation and Interpretation of Zeolitic Diffusion Coefficients", *Trans. Faraday Soc.*, **67**, 1661-1671 (1971).

Ruthven, D. M. and K. F. Loughlin, "Correlation and Interpretation of Zeolitic Diffusion Coefficients", *Trans. Faraday Soc.*, **67**, 1661-1671 (1971).

Ruthven, D. M. and K. F. Loughlin, "The Sorption and Diffusion of n-butane in Linde 5A Sieve", *Chem. Eng. Sci.*, **26**, 1145-1154 (1971).

Ruthven, D. M. and K. F. Loughlin, "The Sorption and Diffusion of n-butane in Linde 5A Sieve", *Chem. Eng. Sci.*, **26**, 1145-1154 (1971).

Ruthven, D. M. and L.-K. Lee, "Kinetics of Nonisothermal Sorption in Molecular Sieve Crystals", *AIChE J.*, **26**, 16-23 (1981).

Ruthven, D. M. and M. Eic, "Intracrystalline Diffusion in Zeolites" in *Perspectives in Molecular Sieve Science* , Flank, W. H. and T. E. Whyte Ed. pp. 362-375 (1988).

Ruthven, D. M. and R. I. Derrah, "Transition State Theory of Zeolitic Diffusion", *J. Chem. Soc. Faraday Trans. I*, **68**, 2332-2343 (1972).

Ruthven, D. M., "Diffusion of Oxygen and Nitrogen in Carbon Molecular Sieve", *Chem. Eng. Sci.*, **47**, 4305-4308 (1992).

Ruthven, D. M., "Intracrystalline Diffusion in Zeolites and Carbon Molecular Sieves", *AIChE Symp. Series*, **80**, 21-33 (1984).

Ruthven, D. M., A. Vavlitis and K. Loughlin. "Diffusion of n-Decane in 5A Zeolite Crystals", *AIChE J.*, **28**, 840-841 (1982).

Ruthven, D. M., K. F. Loughlin and K. A. Holborow, "Multicomponent Sorption Equilibrium in Molecular Sieve Zeolites", *Chem. Eng. Sci.*, **28**, 701-709 (1973).

Ruthven, D. M., *Principles of Adsorption and Adsorption Processes* (John Wiley & Sons, New York), chapter 5 (1984).

Ruthven, D. M., *Principles of Adsorption and Adsorption Processes* (John Wiley & Sons, New York) (1984).

Ruthven, D. M., R. I. Derrah and K. F. Loughlin, "Diffusion of Light Hydrocarbons in 5A Zeolite", *Can. J. Chem.*, **51**, 3514-3519 (1973).

Ruthven, D. M., R. I. Derrah and K. F. Loughlin, "Diffusion of Light Hydrocarbons in 5A Zeolite", *Can. J. Chem.*, **51**, 3514-3519 (1973).

Ruthven, D., M. Eic and E. Richard, "Diffusion of C8 Aromatic Hydrocarbons in Silicalite", *Zeolites*, **11**, 647-653 (1991).

Sacerdote, M., F. Bosselet and B. F. Mentzen, "The MFI(ZSM-5)/Sorbate systems. Comparison between Structural, Theoretical and Calorimetric Results. Part II - the MFI/Benzene System.", *Mat. Res. Bull.*, **25**, 593-599 (1990).

Sarma, P. N. and H. W. Haynes, "A Model for the Application of gas Chromatography to Measurements of Diffusion in Bidisperse Structured Catalysts", *AIChE Journal*, **19**, 1043-1046205-217 (1973).

Shah, D. B., D. T. Hayhurst, G. Evanina and C. J. Guo, "Sorption and Difusion of Benzene in HZSM-5 and Silicalite Crystals", *AIChE J.*, **34**, 1713-1717 (1988).

Shah, D. B. and D. M. Ruthven, "Measurement of Zeolitic Diffusivities and Equilibrium Isotherms by Chromatography", *AIChE J.*, **23**, 804-809 (1977).

Shen, D. and L. V. C. Rees, "Adsorption and Diffusion of n-Butane and 2-Butyne in Silicalite-I", *Zeolites*, **11**, 684-689 (1991).

Shen, D. and L. V. C. Rees, "Diffusion of Benzene, p-Xylene and their Mixture in Silicalite-1 usinga Frequency Response Technique" in *9th international Zeolite Conference*, Montreal, pp. 45-54 (1993)

Shen, D., L. V. C. Rees, J. Caro, M. Bülow, B. Zibrowius and H. Jobic, "Diffusion of C4 Hydrocarbons in Silicalite-1", *J. C. S. Faraday Trans.*, **86**, 3943-3948 (1990).

Springuel-Huet, M.-A., A. Nosov, J. Kärger and J. Fraissard, "129XE NMR Study of the Bed Resistance to Molecular Transport in Assemblages of Zeolite Particles", *J. Phys. Chem.*, **100**, 7200-7203 (1996).

Takahashi, H. and T. Shimanouchi, "Infrared Spectrum and Normal Vibrations of Cyclohexane", *J. Mol. Spectrosc.*, **13**, 43-53 (1964).

Talu, O., C. Guo and D. T. Hayhurst, "Heterogeneous Adsorption Equilibria with Comparable Molecule and Pore Sizes", *J. Phys. Chem.*, **93**, 7294-7298 (1989).

Thamm, H., "Adsorption Site heterogeneity in Silicalite: a Calorimetric Study", *Zeolites*, **7**, 341-346 (1987).

Thamm, H., "Calorimetric Study on the State of Aromatic Molecules Sorbed on Silicalite", *J. Phys. Chem.*, **91**, 8-11 (1987).

Thamm, H., "Sorption of Strongly Polar Moleculas on Silicalite. Calorimetric Evidence for the Formation of Associates in the Sorbed Phase.", *J. Phys. Chem.*, **92**, 193-196 (1988).

Theodorou, D. and J. Wei, "Diffusion and Reaction in Blocked and High Occupancy Zeolite Catalysts", *J. Catal.*, **83**, 205,224 (1983).

Transport Properties", *AIChE J.*, **39**, 962-974 (1993).

Tsikoyannis, J. G. and J. Wei, "Diffusion and reaction in High-Occupancy Zeolite Catalysts - I. A Stochastic Theory", *Chem. Eng. Sci.*, **46**, 233-253 (1990).

Tsikoyannis, J. G. and J. Wei, "Diffusion and reaction in High-Occupancy Zeolite Catalysts - II. Experimental", *Chem. Eng. Sci.*, **46**, 233-253 (1990).

Vavlitis, A. P., D. M. Ruthven and K. F. Loughlin, "Sorption of N-Pentane, N-Octane, and N-Decane in 5A Zeolite Crystals", *J. Coll. Interface Sci.*, **84**, 526-531 (1981).

Voogd, P., H. Bekkum, D. Shavit and H. W. Kouwenhoven, "Effect of Zeolite Structure and Morphology on Intracrystalline n-Hexane Diffusion in Pentasil Zeolites studied by the Zero-length Column Method", *J. Chem. Soc. Faraday Trans.*, **87**, 3575-3580 (1991).

Wang, P. W., T. Yu, B. A. Garland and E. M. Eyring, "Benzene in Zeolite ZSM-5 Studied by Diffuse Reflectance Infrared Spectroscopy", *Appl. Spectrosc.*, **44**, 1070-1073 (1990).

Weaver, D. L., "Some Exact Results For One-Dimensional Diffusion with Absorption", *Phys. Rev. B*, **20**, 2558-2561 (1979).

Wei, P. B., "Zeolites - New Horizons in Catalysis", *Chemtech*, **3**, 498-505 (1973).

Weisz, P. B., "Zeolites - New Horizons in Catalysis", *Chemtech*, **3**, 498-505 (1973).

Xiao, J. and J. Wei, "Diffusion Mechanism of Hydrocarbons in Zeolites I: Theory", *Chem. Eng. Sci.*, **47**, 1123-1141 (1992).

Xiao, J. and J. Wei, "Diffusion Mechanism of Hydrocarbons in Zeolites I: Theory", *Chem. Eng. Sci.*, **47**, 1123-1141 (1992).

Xiao, J. and J. Wei, "Diffusion Mechanism of Hydrocarbons in Zeolites II: Analysis of Experimental Observations", *Chem. Eng. Sci.*, **47**, 1143-1159 (1992).

Yucel, H. and D. M. Ruthven, "Diffusion in 5A Zeolite", *J. C. S. Faraday I*, **76**, 71-83 (1980).

Zecchina, A., S. Bordiga, G. Spoto, L. Marchese, G. Petrini, G. Leofanti and M. Padovan, "Silicalite Characterization. 1. Structure, Adsorptive Capacity, and IR Spectroscopy of the Framework and Hydroxil Modes", *J. Phys. Chem.*, **96**, 4985-4990 (1992).

Zecchina, A., S. Bordiga, G. Spoto, L. Marchese, G. Petrini, G. Leofanti and M. Padovan, "Silicalite Characterization. 2. IR Spectroscopy of the Interaction of CO with Internal and External Hydroxil Groups", *J. Phys. Chem.*, **96**, 4991-4997 (1992).

Zikánová, A., M. Bülow and H. Schlodder, *Zeolites*, **7**, 115 (1987).